

Luminescent Cyclometallated Pt(II) Complexes for Cellular Imaging

Thesis submitted for the degree of
Doctor of Philosophy
at the University of Leicester

by

Nada Mofadi Alatawi



Department of Chemistry
University of Leicester

2019

Abstract

The photoluminescence properties of cyclometallated platinum(II) complexes make them potential candidates for use in a range of applications such as triplet harvesting agents in OLEDs, as photosensitizers, and in solar cells. Also, the strong luminescence of these complexes gives them much potential for use in chemosensing applications and as bioimaging agents. This final topic is an area of increasing study as a result of the diverse and tuneable excited states of such molecules, and their advantages over conventional organic emitters such as reduced photobleaching and long luminescence lifetimes allowing time-resolved imaging to be performed. This research project aimed to develop luminescent polyamine appended Pt(II) complexes to target and image synaptic vesicles. Polyamines are frequently found in high concentrations in cancer cells which have an up-regulated polyamine transport system (PTS). The exploration of PTS as a vector to selectively target live cells to understand the cellular uptake is an important aspect of research for this project.

Intensely luminescent cyclometallated platinum(II) complexes have been prepared containing N[^]C[^]N-coordinating ligands, based on 1,3-di(2-pyridyl)benzene, 1,3-di(1,2,3-triazole)benzene and 2-(3-(1,2,3-triazol)phenyl)pyridine derivatives. Tridentate ligand functionalisation has been employed to obtain complexes that features either one of or a combination of hydrophilic and lipophilic groups. Substitution of the chloride ancillary ligand for pyridine or alkyne derivatives has been achieved. A variety of synthetic strategies were employed in the synthesis of the proligands, for which the main strategies involve either one of or a combination of metal catalysed cross-coupling and click reactions. A series of monodentate ligands with an alkyne functionality were synthesised *via* different methods such as amine or PEG alkylation, amide coupling and reductive amination of a Schiff base. All the ligands and Pt(II) complexes were characterised by ¹H and ¹³C NMR spectroscopy, mass spectrometry and X-ray analysis. 1,3-di(2-pyridyl)benzene based Pt(II) complexes are intensely luminescent, in their own right, with significantly high quantum yields and lifetimes ($\Phi = 0.039-0.13$), ($\tau = 0.50-0.85 \mu\text{s}$). Whereas, 1,3-di(1,2,3-triazole)benzene -type cyclometalated Pt(II) complex, the high energy of the π^* orbitals of the 1,2,3-triazole units resulted in the absence of detectable emission; this was attributed to an inadequate energy separation between the emissive state and the d-d states. However, when formally replacing only one pyridine ring in Pt(II) complexes of 1,3-di(2-pyridyl)benzene ligands by a 1,2,3-triazole, an intense green emission could be achieved ($\Phi = 0.09$, $\tau = 0.85 \mu\text{s}$) in aerated DCM. Finally, Substitution of the chloride ancillary ligand for pyridine led to further blue-shifts, whereas alkyne substitution led to red-shifts.

Dedication

Dedicated to my mother and the memory of my father, a fantastic man who passed away during my study.

Acknowledgments

Working in the department over the last few years has been a really fun experience. While the chemistry has been interesting, there are also many people who have made the day to day work much more enjoyable and ultimately possible to whom I would like to say 'thank you'. Firstly, I would like to express my sincere gratitude to my fabulous supervisor Dr Mark Lowe for his help, guidance, support and encouragement throughout my studies; particularly for long chemistry discussions which have been one of the most enjoyable aspects of this project. In addition, I would like to thank my second supervisor Prof. David L Davies for his help and support.

Secondly, a massive thank you goes out to Mick Lee for keeping things running smoothly in the lab and in getting me such fine mass spectra. Huge thanks also to Dr Gerry Griffith for his invaluable knowledge of NMR spectroscopy. Thanks also to Kuldip Singh for X-Ray structures. I also would like to thank Dr Andrew Hudson for help with measuring lifetimes.

Members of the Lowe group, both past and present, have been a great source of support, and friendship; thank you to Vicki, Adil, Sarab, Adhit, Lucy, and Joanna. Thank you also to all the friends who have made tea breaks and lunch trips so much fun.

Last but by no means least, I am very grateful to my family and friends for all their love and support. I am deeply grateful to my parents for all the encouragement and guidance given throughout my life. I would not be who I am today if not for them. I also wish to thank my dearest two sisters Najod and Raneem for their support and love. And most of all a very special thanks goes to my husband and love of my life, Hussain, for keeping things going and for always showing how proud he is of me and always knew how to make me smile. The last word goes for Lana, Bker and Hatim my kids, who have been the light of my life and who have given me the extra strength and motivation to get things done.

Nada

Table of Contents

Abbreviations	IX
Chapter 1	1
1 Introduction.....	2
1.1 Luminescence.....	2
1.2 Luminescent Transition Metal Complexes.....	5
1.3 Polyamines.....	12
1.3.1 Polyamine Synthesis and Metabolism.....	13
1.3.2 Polyamine Transport	15
1.3.3 Polyamines co-ordinated to Transition Metals.....	17
1.4 The Role of Luminescence in Cellular Studies	20
1.4.2 Applications of Metal-Ligand Complexes in Imaging Studies.....	21
1.4.2.1 Cellular Imaging.....	21
1.5 Synaptic Vesicles.....	23
1.5.1 Synaptic Vesicle Cycle	24
1.5.2 Different Modes of Exocytosis and Endocytosis.....	25
1.5.3 Full fusion.....	25
1.5.4 Kiss-and-run	26
1.6 Synaptic Vesicles Imaging	28
1.7 Summary	32
1.8 Aims and Objectives.....	33
1.9 Thesis Outline	34
Chapter 2	35
2.1 Ligand Synthesis Overview.....	36
2.2 Synthesis of Pro-Ligands	37
2.2.1 Synthesis of Boc-protected Putrescine (1a).....	37
2.2.2 Synthesis of TFA-protected Putrescine (3a) ⁹⁴	38
2.2.3 Synthesis of tri-Boc-protected Spermine (4a).....	39
2.3 Tri-dentate N [^] C [^] N ligands synthesis	40
2.3.1 Cross-coupling Reactions	40
2.3.2 Ligand Synthesis	41
2.3.3 Ligands Prepared via Stille Cross-Coupling.....	41
2.3.4 Ligand prepared via Negishi Cross-Coupling.....	43
2.3.5 Sonogashira Coupling Reactions.....	44
2.3.6 The Click Reaction.....	48

2.3.7	<i>Synthesis of HL9</i>	50
2.3.8	<i>Alkyne Hydrogenation</i>	51
2.4	<i>Spectroscopic Characterisation of Tri-dentate N⁺C⁺N ligands</i>	52
2.4.1	<i>NMR Spectroscopy</i>	52
2.4.2	<i>X-ray Crystal Structure</i>	59
2.5	<i>Synthesis of Ancillary Ligands</i>	60
2.5.1	<i>Polyamines and PEG Alkynes Synthesis</i>	61
2.5.2	<i>Synthesis of Putrescine Alkyne (9a)</i>	61
2.5.3	<i>Synthesis of PEG alkyne 10a</i>	62
2.5.4	<i>PEG Alkyne Hydroxyl Group Protection</i>	63
2.5.5	<i>Reductive Amination</i>	65
2.5.6	<i>Amide Coupling Reaction</i>	67
2.6	<i>Spectroscopic Characterisation of Ancillary Ligands</i>	70
2.6.1	<i>NMR Spectroscopy</i>	70
2.7	<i>Conclusion</i>	71
	Chapter 3	72
3	<i>Synthesis of Platinum Complexes</i>	73
3.1	<i>Complexation to Pt(II)</i>	73
3.2	<i>Substitution of the Ancillary Chloride with Alkyne or Pyridine ligands</i>	78
3.2.1	<i>Synthesis of Pyridine Substituted Pt(II) Complexes</i>	79
3.2.2	<i>Synthesis of Alkyne Substituted Pt(II) Complexes</i>	80
3.3	<i>Amide Coupling on PtLnCl Complexes</i>	83
3.4	<i>Deprotection of the Amino Groups on Pt(II) Complexes</i>	84
3.5	<i>Spectroscopic Characterisation of Complexes</i>	86
3.5.1	<i>NMR Spectroscopy</i>	86
3.5.2	<i>Mass Spectrometry</i>	91
3.5.3	<i>X-ray Crystal Structures</i>	93
3.5.3.1	<i>Crystal Structures of Pt(II) Complexes</i>	93
3.5.3.2	<i>Pt(IV) Complex Structure of PtL12Cl₃</i>	96
3.5.3.3	<i>Crystal Packing</i>	97
3.6	<i>Concluding remarks</i>	98
	Chapter 4	99
4	<i>Photophysical Properties</i>	100
4.1	<i>Absorbance</i>	100
4.2	<i>Emission</i>	103

4.3	<i>Excimeric Emission</i>	107
4.4	<i>Luminescence Quantum Yields and Lifetime Measurements</i>	108
4.4.1	<i>Quantum Yield and Lifetime of PtLnCl Complexes</i>	110
4.5	<i>Ancillary Ligand Substitution</i>	114
4.5.1	<i>Cl Substitution for PtL7Cl</i>	114
4.5.2	<i>Cl Substitution for PtL1Cl</i>	115
4.6	<i>Concluding Remarks</i>	117
Chapter 5		118
5	<i>Conclusions and Scope for Future Work</i>	119
5.1	<i>General Conclusions</i>	119
5.2	<i>Future Direction</i>	121
5.2.1	<i>Cytotoxicity</i>	121
5.2.2	<i>Cellular Studies</i>	121
5.2.3	<i>Modification of the Tridentate N[^]C[^]N Ligand</i>	121
5.2.4	<i>Potential Applications</i>	124
Chapter 6		127
6	<i>Experimental</i>	128
6.1	<i>Material and instrument</i>	128
6.2	<i>Synthesis of Pre-ligands;</i>	130
6.2.1	<i>Tert-butyl (4-aminobutyl)carbamate (1a).</i> ⁹³	130
6.2.2	<i>Tert-butyl (4-(2,2,2-trifluoroacetamido)butyl)carbamate (2a).</i> ⁹⁴	130
6.2.3	<i>N-(4-aminobutyl)-2,2,2-trifluoroacetamide (3a).</i> ⁹⁴	131
6.2.4	<i>Tert-butyl(4-((3-aminopropyl)(tert-butoxycarbonyl)amino)butyl)(3-((tert-butoxycarbonyl)amino)propyl) carbamate (4a).</i> ¹⁵⁸	132
6.2.5	<i>2-(4-Hexylphenyl)ethynyl) trimethylsilane (5a).</i> ¹⁰³	133
6.2.6	<i>1-Ethynyl-4-hexylbenzene (6a).</i> ¹⁰³	133
6.2.7	<i>Methyl 3-bromo-5-(pyridin-2-yl)benzoate (7a)</i>	134
6.2.8	<i>Methyl 3-(pyridin-2-yl)-5-((trimethylsilyl)ethynyl)benzoate (8a)</i>	135
6.2.9	<i>1,3-dibromo-5-(phenylethynyl)benzene (2).</i> ¹⁵⁹	135
6.3	<i>Synthesis of Mono-ligands</i>	136
6.3.1	<i>Tert-butyl (4-(prop-2-yn-1-ylamino)butyl)carbamate (9a).</i> ¹¹⁶	136
6.3.2	<i>2-(2-(2-(prop-2-yn-1-yloxy)ethoxy)ethoxy)ethan-1-ol (10a).</i> ¹²⁰	137
6.3.3	<i>2,2,3,3-tetramethyl-4,7,10,13-tetraoxa-3-silahexadec-15-yne (11a)</i>	137
6.3.4	<i>2,5,8,11-tetraoxatetradec-13-yne (12a).</i> ¹²⁰	138
6.3.5	<i>Tert-butyl(4-((tert-butoxycarbonyl)(3-((pyridinylmethyl)amino)propyl) amino)butyl)(3-((tert-butoxycarbonyl)amino)propyl)carbamate (13a)</i>	139

6.3.6	<i>Tert-butyl (4-(tert-butoxycarbonyl) (3-(tert-butoxycarbonyl) amin)propyl) amino)butyl(3-(4-(trimethylsilyl)ethynyl)benzamido) propyl)carbamate (14a)</i>	140
6.3.7	<i>4-ethynyl-N-(3-(2,2,2-trifluoro-N-(4-(2,2,2-trifluoro-N-(3-(2,2,2-trifluoro acetamido)propyl)acetamido)butyl)acetamido)propyl)benzamide (15a)</i>	141
6.4	<i>Synthesis of Tridentate-ligands</i>	142
6.4.1	<i>1,3-Di(2-pyridyl)benzene (HL1).¹⁶⁰</i>	142
6.4.2	<i>1-Bromo-3,5-bis(2-pyridinyl)benzene (HL2).⁹⁷</i>	143
6.4.3	<i>Methyl-3,5-di(2-pyridyl)benzoate (HL3).⁹⁷</i>	144
6.4.4	<i>2,2'-(5-(phenylethynyl)-1,3-phenylene)dipyridine (HL4)</i>	145
6.4.5	<i>2,2'-(5-((4-hexylphenyl)ethynyl)-1,3-phenylene)dipyridine (HL5)</i>	146
6.4.6	<i>2,2'-(5-(oct-1-yn-1-yl)-1,3-phenylene)dipyridine (HL6)</i>	147
6.4.7	<i>1,3-bis(1-butyl-1H-1,2,3-triazol-4-yl)benzene (HL7)</i>	147
6.4.8	<i>di-tert-butyl(1,3-phenylenebis(1H-1,2,3-triazole-4,1-diyl))bis(butane4,diyl) dicarbamate (HL8)</i>	148
6.4.9	<i>Methyl 3-(1-butyl-1H-1,2,3-triazol-4-yl)-5-(pyridin-2-yl)benzoate (HL9)</i>	149
6.4.10	<i>2,2'-(5-phenethyl-1,3-phenylene)dipyridine (HL10)</i>	150
6.4.11	<i>2,2'-(5-(4-hexylphenethyl)-1,3-phenylene)dipyridine (HL11)</i>	151
6.4.12	<i>2,2'-(5-octyl-1,3-phenylene)dipyridine (HL12)</i>	152
6.4.13	<i>3,5-di(pyridin-2-yl)benzoic acid (HL3')</i>	152
6.4.14	<i>3,5-di(2pyridine-2-yl)-N-(4-(2,2,2-trifluoroacetamido)butyl)benzamide (HL13)</i>	153
6.5	<i>Synthesis of PtLCl Complexes</i>	154
6.5.1	<i>General Procedures</i>	154
6.5.2	<i>Synthesis of PtL1Cl Complex.⁹⁷</i>	155
6.5.3	<i>Synthesis of PtL2Cl Complex.⁹⁷</i>	155
6.5.4	<i>Synthesis of PtL3Cl Complex.⁹⁷</i>	156
6.5.5	<i>Synthesis of PtL10Cl Complex</i>	156
6.5.6	<i>Synthesis of PtL11Cl Complex</i>	157
6.5.6	<i>Synthesis of PtL12Cl Complex</i>	158
6.5.7	<i>Synthesis of PtL12Cl₃ Complex</i>	158
6.5.8	<i>Synthesis of PtL6^aCl Complex</i>	159
6.5.9	<i>Synthesis of PtL3^aCl Complex.¹⁵⁷</i>	160
6.5.10	<i>Synthesis of PtL3^{NHS}Cl Complex.¹⁵⁷</i>	160
6.5.11	<i>Synthesis of PtL3^{1a}Cl Complex</i>	161
6.5.12	<i>Synthesis of PtL3^{4a}Cl Complex</i>	162
6.5.13	<i>Synthesis of PtL7Cl Complex</i>	163
6.5.14	<i>Synthesis of PtL9Cl Complex</i>	163

6.5.15	<i>Synthesis of PtL9^aCl Complex.</i>	164
6.5.16	<i>Synthesis of PtL9^{1a}Cl Complex.</i>	165
6.6	<i>Synthesis of PtLII Complex.</i>	166
6.7	<i>Synthesis of Cationic Complexes</i>	166
6.7.1	<i>Synthesis of PtL9^{1a}Cl_d</i>	166
6.7.2	<i>Synthesis of PtL3^{1a}Cl_d</i>	167
6.7.3	<i>Synthesis of PtL3^{4a}Cl_d</i>	168
6.7.4	<i>Synthesis of PtL7Py</i>	169
6.7.5	<i>Synthesis of PtL1-13a</i>	169
6.8	<i>Neutral Pt(II) complexes</i>	170
6.8.1	<i>Synthesis of PtL7C≡CPh</i>	170
6.8.2	<i>Synthesis of PtL1-12a</i>	171
6.8.3	<i>Synthesis of PtL1-14a</i>	172
7	References	173
8	Appendix	180
8.1	<i>X-ray Crystallography Data</i>	181

Abbreviations

Bio

ADP	Adenosine diphosphate
APAO	Acetyl polyamine oxidase
ATP	Adenosine triphosphate
ATPase	Adenosine triphosphatase
AZ	Antizyme
CME	Clathrin mediated endocytosis
CPP	Cell penetrating peptide
DAM	Decarboxylated-S-Adenosyl Methionine
DNA	Deoxyribonucleic acid
Gpc-1	Glypican-1
GTP	Guanosine-5'-triphosphate
GFP	Green Fluorescence protein
HDAC	Histone deacetylase
HER2	Human epidermal growth factor receptor 2
HSPG	Heparan sulfate proteoglycan
MTA	5'-deoxy, 5'-methylthioadenosine
NO	Nitric Oxide
ODC	Ornithine Decarboxylase
PTS	Polyamine transport system
PTD	Protein transduction domain
RNA	Ribonucleic acid
mRNA	Messenger ribonucleic acid
tRNA	Transfer ribonucleic acid
rRNA	Ribosomal ribonucleic acid
siRNA	Short interfering RNA
SAM	S-Adenosyl Methionine
SAMO	S-Adenosyl Methionine Decarboxylase
SLC	Solute carriers
SMO	Spermine oxidase
SMRT	Silencing mediator of retinoic acid & thyroid hormone receptor
SPDS	Spermidine synthase

SPECT	Single photon emission computed tomography
SPMS	Spermine synthase
SSAT	Spermine/Spermidine acetyl transferase
SV	Synaptic Vesicle
FF	Full Fusion
KR	Kiss and Run
RRP	Ready Releasable Pool
NMJ	Neuromuscular Junction

NMR

bd	broad doublet
bs	broad singlet
d	doublet
dd	doublet of doublets
ddd	doublet of doublet of doublets
dt	doublet of triplets
m	multiplet
s	singlet
q	quartet
quin	quintet
t	triplet
td	triplet of doublets
COSY	correlated spectroscopy
HMBC	heteronuclear multiple bond correlation
HSQC	heteronuclear single quantum correlation
NMR	nuclear magnetic resonance
NOE	nuclear Overhauser effect
NOESY	nuclear Overhauser effect spectroscopy
ppm	parts per million
δ	delta (NMR Chemical Shift)
J	coupling constant H_z

Chemical

acac	anion of pentane-2,4-dione
ACOH	Acetic acid
bipy	2,2'-bipyridine
bipy-tBu ₂	4,4'-di-tert-butyl-2,2'-bipyridine
Boc	tert-Butoxy carbonyl
Boc-ON	2-(tert-butoxycarbonyloxyimino)-2-phenylacetonitrile
DAB	Diaminobenzidine
DCM	dichloromethane
DMSO	dimethylsulfoxide
DMF	N,N-Dimethyl formamide
EtOAc	Ethyl Acetate
EtOH	Ethanol
iPr	isopropyl
MeCN	Acetonitrile
MeOH	Methanol
Phen	1, 10- phenanthroline
Py	pyridine
pht	1,2,3-phenyltriazole
ppy	2-phenylpyridine put putrescine
spd	spermidine
spm	spermine
TFA	Trifluoroacetic acid
THF	Tetrahydrofuran
TMS	Tetramethylsilane

Techniques

CCD	Charge- Coupled Device
CuAAC	Copper(I)-catalysed Azide –Alkyne Cycloaddition
ECL	Electrochemiluminescence
HPLC	high performance liquid chromatography
IR	infra-red

MW	microwave
MS	mass spectroscopy
MRI	Magnetic resonance imaging

Others

Abs	Absorbance
au	Arbitrary Units
CFSE	Crystal Field Splitting Energy
eq	Equivalent
F	Fluorescence Intensity
fs	femtosecond
g	gram
HOMO	Highest Occupied Molecular Orbital
I	Intensity
I ₀	Incident radiant power
IL	Intra Ligand
ISC	Inter System crossing
k	Rate of Non-Radiative Decay
M	Molar (mol dm ⁻³)
<i>m/z</i>	mass to charge Ratio
MC	metal-Centred
mg	milligram
min	minute
ml	milliliter
MLCT	Metal to ligand charge transfer
mM	millimolar(mol dm ⁻³)
mol	mole
nm	nanometer
P	Partition coefficient
s	second
t _{1/2}	half time
TCSPC	Time-Correlated Single Photon Counting

t_R	Retention Time
Γ	Rate of Radiative Decay
ε	Extinction Coefficient
η	Refractive Index
λ_{em}	Emission Wavelength
λ_{ex}	Excitation Wavelength
μM	Micromolar ($\mu mol dm^{-3}$)
τ	Fluorescence life time
Φ	Fluorescence quantum yield

Chapter 1

1 Introduction

The ability of certain compounds to emit light provides a vital tool in chemistry since in many cases the characteristics of the emitted radiation are sensitive to the molecular environment. Emissive molecules, therefore, are widely used as reporters for many processes.^{1,2} The diverse photophysical properties of transition metals with aromatic chelating ligands such as polypyridyls or their cyclometallated analogues have led to their use in many areas involving the absorption and emission of light.^{3,4,5} Such compounds often display strong, long-lived emission and thus are well suited to roles in sensing. More recently, in addition to their use in chemosensing applications, these metal complexes are becoming more common in cellular studies and bioimaging.^{6,7}

1.1 Luminescence

One of the most sensitive spectroscopic techniques, luminescence was first described by the Irish scientist Sir George Gabriel Stokes. Since then, luminescence has become one of the most powerful and extensively utilised tools in diverse fields including cell biology, physiology, and related areas of the biomedical sciences.^{8,9}

Photoluminescence is the light produced from a substance when it is stimulated by photon of light. This is often described as a “cold light emission” as it does not come from a hot source such as an incandescent light bulb. A molecule can be excited by the absorption of energy in the form of electromagnetic radiation resulting in the promotion of an electron to a higher energy level (S_1 or S_2), which can return to the ground state (S_0) by a number of routes with emission of light such as fluorescence, phosphorescence and delayed fluorescence described as radiative processes, demonstrated by the classical Jablonski diagram (Figure 1.1).¹⁰

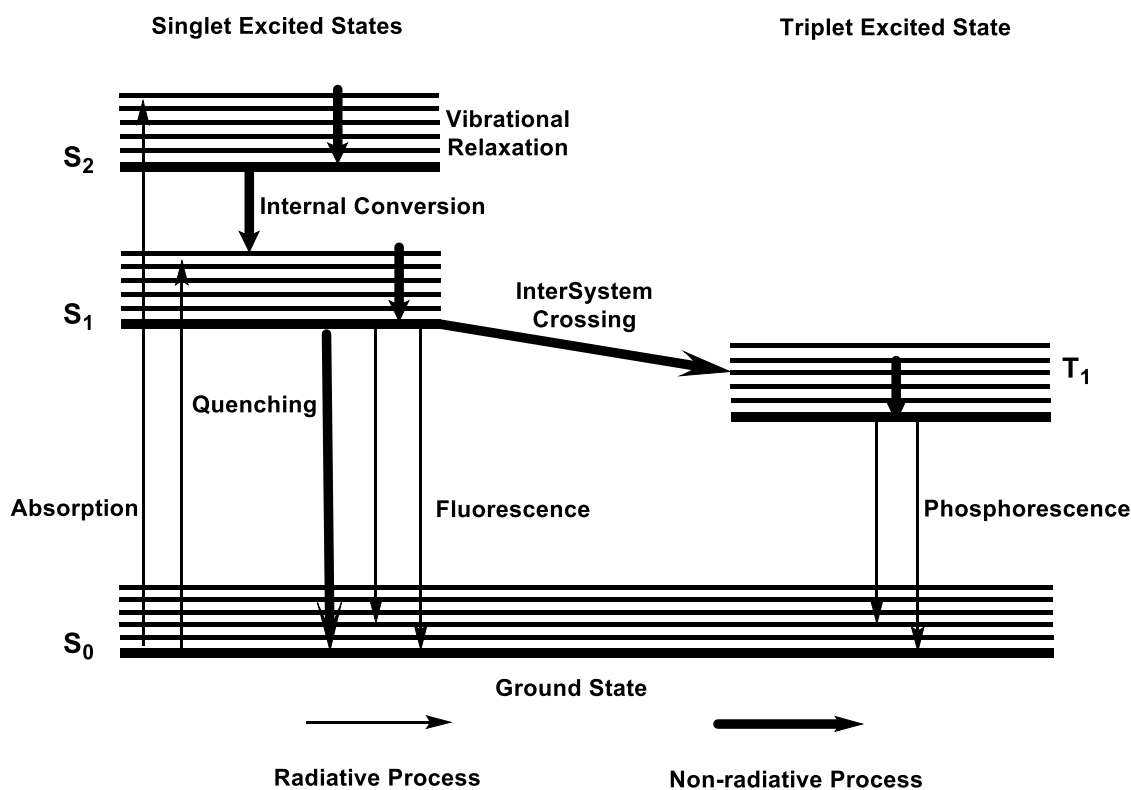


Figure 1.1: Jablonski energy diagram illustrating the photochemical processes from absorption to emission of light.

In luminescence, there are intermediate processes between absorption and emission of light such as vibrational relaxation, internal conversion and inter-system crossing (Figure 1.1) which exceed the period of electromagnetic oscillation and as a result luminescence loses correlation between phases of absorbed and emitted light in contrast to reflected light, where a phase correlation is always observed.¹¹ The time taken between absorption of energy (10^{-15} s) and re-emission of light energy is determined by the lifetime of excitation states. Based on these experimental observations, two main types of luminescence are described – fluorescence and phosphorescence. The distinction between the two depends on the nature of the excited states, singlet (S_1 or S_2) or triplet (T_1) (Figure 1.2). Though ground state is always described as a singlet state (S_0), excited states are determined by their spin multiplicity, defined by their total spin angular momentum, S (Figure 1.2). The emission of a photon is very rapid (10^{-9} - 10^{-7} s), if the electron decays from S_1 to S_0 directly as this is a spin allowed process and is known as fluorescence. Excitation from ground state (S_0) to the excited triplet state (T_1) is spin forbidden, therefore, T_1 state is only populated through a non-radiative process termed as inter-system crossing, involving the electronic spin conversion (Figure 1.1). The emission from T_1 state is

described as phosphorescence, which is also spin forbidden. Phosphorescence occurs with lower energy (longer wavelength) relative to fluorescence and lasts long after the excitation i.e. 10^{-3} - 10^2 s due to its spin forbidden nature. Apart from these radiative processes, the excited molecules in S_1 state can also lose energy through certain non-radiative processes (loss of energy as heat to the surroundings) e.g. internal conversion and quenching.

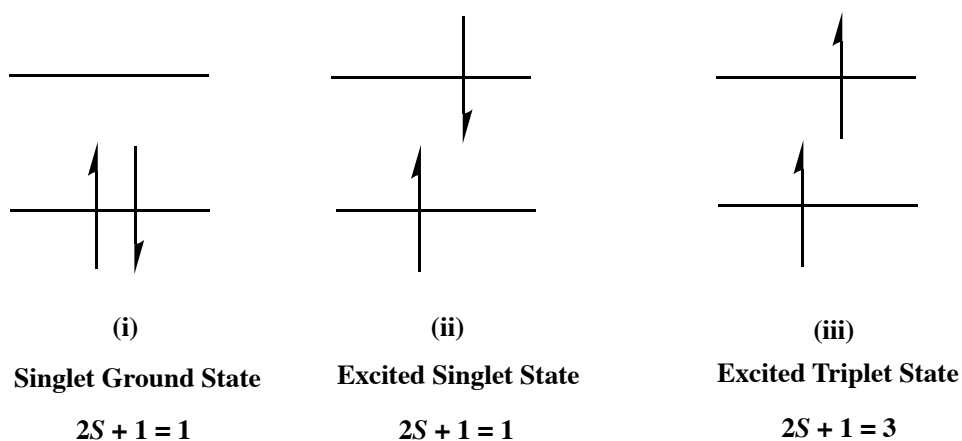


Figure 1.2: Electronic configurations for energy states.

During luminescence, when a molecule is excited *via* absorption of light, the average photon energy of the luminescent light is usually smaller than that of the incident light and therefore, emission is observed at a longer wavelength. The shift of the luminescent emission band compared with the absorption band, due to the non-radiative deactivation processes, arising from the same electronic transition is described as Stokes Shift named after Sir George Gabriel Stokes. Stokes shift is always positive if it is demarcated through the absorption and emission band maxima for a given electronic transition. A large Stokes shift helps to isolate the excitation and emission wavelengths.

The emission quantum yields⁸ and lifetimes¹² are the most important selection criteria for fluorophores in luminescence spectroscopy. The quantum yield (Φ) is described as the ratio of photons absorbed to photons emitted through emission. Consequently, the quantum yield describes the probability of the excited state being deactivated by luminescence rather than by other non-radiative processes. According to Equation 1.1, the quantum yield can be described by two rate constants, radiative decay constant, k_r , comprising the emission, and non-radiative

decay constant, k_{nr} , involving all possible competing deactivation processes, such as internal conversion, intersystem crossing and/or intra- and inter-molecular quenching. For an efficient emission process, k_r should be larger than k_{nr} .

$$\Phi = \frac{k_r}{k_r + k_{nr}} \quad \text{Equation 1.1}$$

The emission lifetime of the excited state is the average time a molecule spends in the excited state before emitting a photon. As quantum yields are found very challenging to measure with absolute accuracy, therefore, emission lifetimes are given more importance, because their measurements are more robust due to their dependence on the intensity of excitation not on the concentration of fluorophores. Based on these properties, some desirable key features of luminescence which make them particularly attractive for biological applications are: the exquisite sensitivity of emission, detection wavelength range of visible light (compatible with the study of many intracellular structures) and fast time scale of light emission (\sim nanosecond to microsecond timescale), so that rapidly changing events can be monitored in real time. The design of functionalised luminescent molecules bearing the above mentioned features has progressed rapidly over the past few decades and is discussed further.

1.2 Luminescent Transition Metal Complexes

Owing to the interesting photo-physical properties of the luminescent transition metal complexes, they have attracted much attention due of their varied applications in many fields, including biological systems, luminescent sensors,^{13,14} biological labels^{15,16} and fluorescent probes.¹⁷ In particular, these applications have focussed on a few crucial d^6 and d^8 2nd and 3rd row transition metals e.g. Re(I), Ru(II), Os(II), Pt(II), Rh(III) and Ir(III), co-ordinated with combinations of relatively strong ligand-field poly-pyridyl and/or organic ligands. Some of the archetypal metal complexes are shown in Figure 1.3. These metal complexes exhibit a range of desirable luminescent properties comprising long emission life times (0.1 to $> 100 \mu\text{s}$), high quantum yields (0.01 to nearly 1) and large Stokes shifts. Long-lived luminescent emission helps to distinguish the ubiquitous background fluorescence of bio-molecules ($\tau = \sim \text{ns}$) from the emission of the metal complex ($\tau = \sim \mu\text{s}$), *via* delaying the process of emission before detection.

already present inside the cell and also offers the potential for lifetime based sensing and imaging.¹⁸

In transition metal complexes four types of transitions could be observed; $d-d$, $d-\pi^*$, $\pi-\pi^*$ and $n-\pi^*$, and $\pi-d$:

- i) $d-d$ transition states - these are generated *via* metal-centred (MC) transitions. This type of an excited state arises when an electron is transferred from a lower d orbital to an upper d orbital.
- ii) $d-\pi^*$ transition states - these are generated *via* metal-to-ligand charge transfer (MLCT) transitions. These are formed when a metal centred d electron is transferred to a ligand anti-bonding π^* orbital.
- iii) $\pi-\pi^*$ and $n-\pi^*$ transition states - these are generated *via* intra-ligand transitions. Electrons are transferred from a π bonding or non-bonding orbital to a higher anti-bonding π orbital.
- iv) $\pi-d$ transition states - these are generated *via* ligand-to-metal charge (LMCT) transfer transitions. Electrons are transferred from a ligand centred π orbital to a metal centred d orbital.

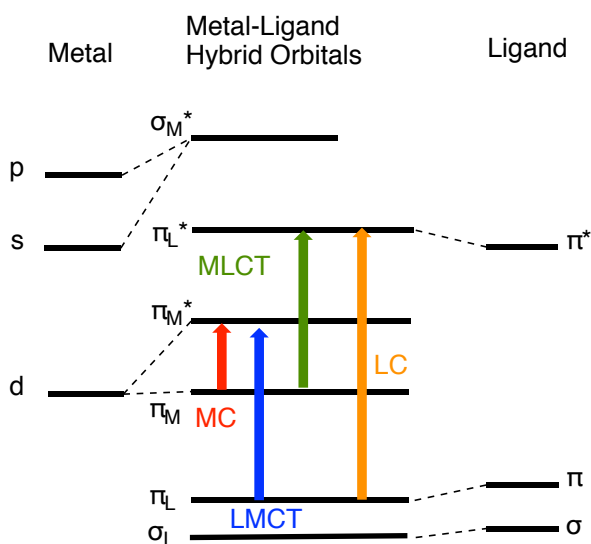


Figure 1.4: A schematic diagram illustrating the MC, LC, MLCT and LMCT transitions of transition metal complexes.

As noted previously, transition metal complexes tend to show phosphorescence emission as they facilitate spin orbit coupling (SOC) followed by inter-system crossing (ISC). Hence, observation of fluorescence in these materials is rare. However, a number of reports on fluorescent emissive metal complexes are available in the literature.¹⁹

Up until the late 1980s, there were no reports on luminescent square planar Pt complexes due to the high rates of non-radiative decay. As a result of crystal field stabilisation, Pt complexes tend to highly prefer a square planar geometry. In square planar geometries the unoccupied $d_{x^2-y^2}$ orbital lies high in energy and is strongly anti-bonding. Populating this orbital involves elongation of Pt-ligand bonds and hence severe distortion of the metal complex. This promotes non-radiative decay of metal centred ($d-d$) excited states to the ground state at the isoenergetic intersection point of the potential energy surfaces (Figure 1.5). Even if other excited states such as LC ($\pi-\pi^*$) or MLCT ($d-\pi^*$) reside at lower energies than $d-d$ states, and if the latter states are thermally accessible, this results in adverse effects/non-radiative decay processes.

In order to overcome this problem, ligands with low lying excited states or those with high electron donor capacities are used. These being strong field ligands, they further raise the $d-d$ excited state up in energy making this a thermally non-accessible state. Hence this results in reduced non-radiative decay and enhanced luminescence of Pt complexes.

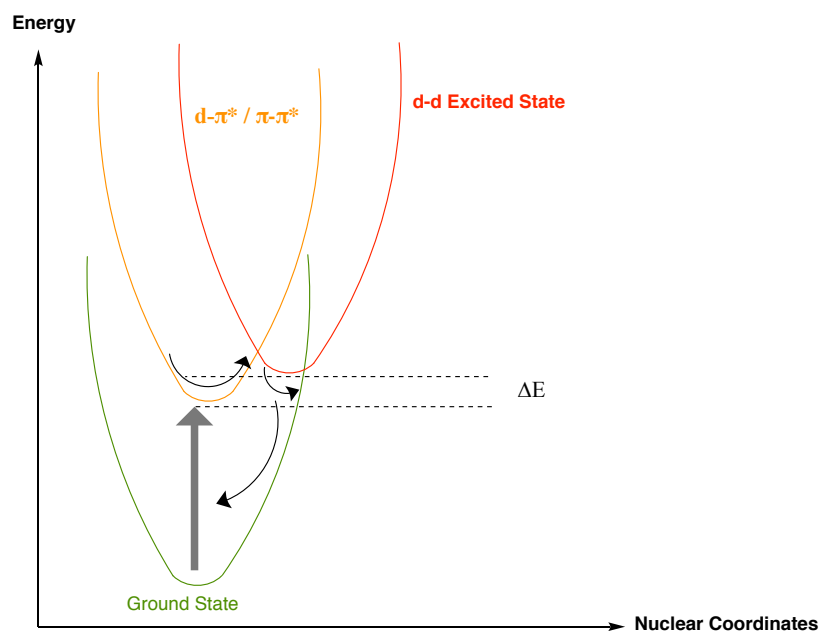


Figure 1.5: Potential energy surface of the $d-d$ excited state in Pt(II) complexes which is displaced relative to the ground state. Thick arrow represents absorption and thin ones indicate vibrational relaxation and non-radiative decay.

Though Pt(II) complexes can rarely acquire octahedral geometry like Re(I), Ru(II) and Ir(III), in general, being a d^8 metal ion, these differ from the complexes of other elements - and always acquire a stable and rigid 4-coordinate square planar geometry as opposed to the distorted octahedral complexes of the d^6 metal ions. Two common ligands bpy (2,2'-bipyridine) and tpy (2,2':6',2''-terpyridine), are studied extensively in this context.²⁰ Owing to the synergistic combination of σ -donating nitrogen atoms and π -accepting heterocycles, coupled with the favourable formation of 5-membered chelating rings, the complexes of these ligands characteristically have high stability with respect to metal ion dissociation.⁴ Moreover, the square planar geometry is given more importance from the point of view of interactions with the biological molecules and intrinsic bio-localisation within the cell.²¹

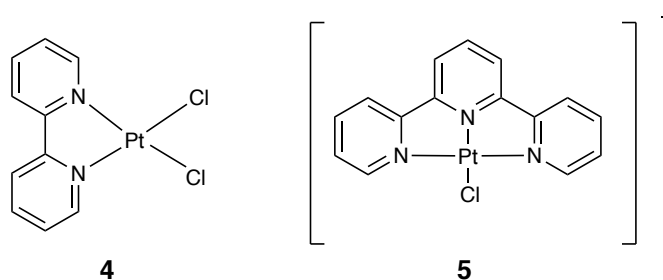
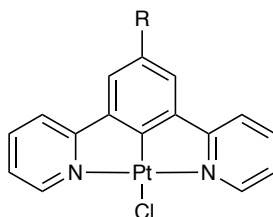


Figure 1.6: Example structures of bi- and tri-dentate Pt(II) complexes.

Analogous to earlier mentioned complexes i.e. **1**, **2** and **3**, a range of bi- and tri-dentate platinum(II) complexes, such as $[Pt(bpy)Cl_2]$ **4**, $[Pt(tpy)Cl]^+$ **5**, were synthesised,²² but these are usually either non-emissive or only very weakly luminescent at room temperature. This is attributed to the presence of low-lying MC ($d-d$) excited states, which are rigorously distorted compared to the ground state and therefore lead to efficient non-radiative decay.²³ In order to increase the ligand field strength and raise the energy of the deactivating $d-d$ states alternative routes have been adopted such as replacing the polypyridyl ligand by a cyclometallating analogue. Cyclometallation offers certain advantages; firstly, the strong σ -donating character of the metallated aryl ring helps to raise the energy of the metal-centred deactivating $d-d$ states such that they can participate to a greater extent in the excited state. This will promote ISC and hence the radiative rate constants are increased.²⁴ Also the majority of platinum complexes,

have a limited absorption in the visible region and to overcome this problem the majority of the researches in the area employ two-photon excitation to populate the emissive excited state.^{24,25} This also offers a number of advantageous features including the reduction of phototoxicity to biological samples, the lowering of scattering, and the inherent capability of optical sectioning.²⁶



- 6a** **R = H**
6b **R = -CH₂-NH₃⁺ Cl⁻**

Figure 1.7: Common cyclometallated Pt(II) complexes incorporating a strong field tri-dentate ligand.

Therefore, related to the cyclometallated Ir(III) complex **3**, the most extensively studied archetypal system of Pt(II) is complex (**6a**) (Figure 1.7), incorporating a strong field tri-dentate cyclometallated ligand has been developed and studied widely.^{27,28} Though bidentate cyclometallated ligands e.g. 2-phenylpyridine (ppy) have been considered mostly for this purpose, owing to their strong luminescent nature, these complexes are potentially susceptible to a distortion away from square planarity towards a D_{2d} geometry in the excited state, which facilitates non-radiative decay, causing a limitation on the luminescence efficiency. The use of tri-dentate ligands can lead to more rigid complexes and hence to brighter emission. In particular, complex **6a** has a luminescence quantum yield of 0.6 in dilute DCM solution at room temperature. Hence, tridentate ligands were considered for this research study and are discussed thereafter.

Williams and co-workers worked extensively in this area, to gain deeper insights into the behaviour of platinum complexes and test their applicability inside different type of cells.^{29,30} They reported highly emissive and photo-stable Pt(II) complexes **6a,b** (Figure 1.7) and demonstrated that the green luminescent complexes possess microsecond lifetimes and

emission quantum yields of up to 70% in degassed organic solvents which is quite high for Pt(II) complexes in general. They reported that even after a short incubation time of 5 minutes, both of the complexes **6a,b** are internalized in a range of live cell lines including normal human dermal fibroblast (HDF), neoplastic C8161 and CHO, with negligible up to low toxicity. They employed NIR two photon excitation to these complexes because of their low absorption in the visible region. The exceptional long lifetime of the excited state of the complexes allowed them to apply a time-gated technique to eliminate background fluorescence or emission coming from other cell labels.

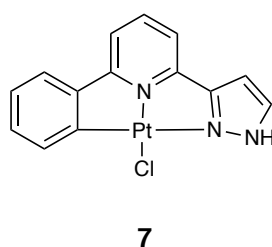


Figure 1.8: C[^]N[^]N Pt(II) complex.

Changing the position of the cyclometallated ring from central to a lateral position in the ligand, yields complexes with very different spectroscopic properties as cited in recent reviews and papers.^{31,32} The general trend described reduced emission quantum yields, accompanied by shorter excited state lifetimes. Lam and co-workers reported a Pt(II) complex (**7**) incorporating a new tridentate cyclometallating ligand 2-phenyl-6-(1H-pyrazol-3-yl)pyridine.²⁵ Complex **7** exhibits intense green emission (500-520 nm) under ambient conditions with a quantum yield of 0.09 and emission lifetime of 0.57 μ s. HeLa and NIH3T3 cells were incubated with complex **7** for various time durations (0–60 minutes); however, only a 5 minute exposure time allowed more than 95% of the cells to exhibit green luminescence but no clear images of the localization of the complex have been reported. The author claimed that the two-photon-induced luminescence of the complex **7** was retained after live cell internalization and can be observed *via* two-photon confocal microscopy. Complex **7** was described to have low toxicity which is consistent with that observed by Botchway *et al.*²⁹

Another approach to improve the luminescence properties of Pt(II) complexes is the substitution of the weak field ligand, i.e. chloride, with a strong field ligand such as alkynyl or CN⁻.^{33,34} Yam and co-workers widely explored the substitution of Cl⁻ with alkynyl ligands,

which led to a larger $d-d$ orbital splitting and hence raising of the energy of the non-emissive $d-d$ ligand field excited state. The author claims that this results in emission which arises from the triplet excited state, including metal to ligand charge transfer (MLCT) [$d\pi(\text{pt}) \rightarrow \pi^*(\text{tpy})$] and some ligand to ligand charge transfer (LLCT) [$\pi(\text{C}\equiv\text{C}) \rightarrow \pi^*(\text{tpy})$] character.

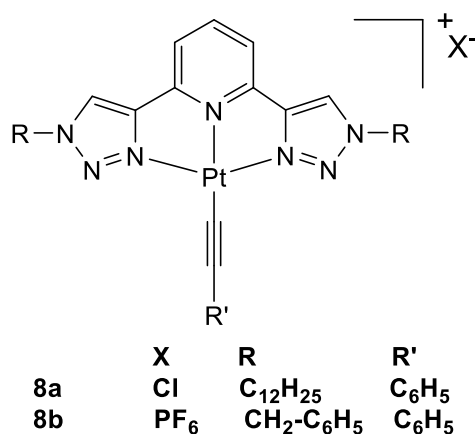


Figure 1.9: A range of cationic Pt(II) complexes.

Yam *et al.* reported a range of cationic Pt(II) complexes including **8a** and **8b** incorporating a new ligand based on a bis-triazole moiety.³⁵ Both of the complexes were found to be emissive bearing large Stokes shifts. The emission lifetimes within the microsecond range were indicative of an origin of triplet parentage. The author claimed that the emission predominantly originated from MLCT excited state character.

In conclusion, owing to intriguing spectroscopic and photo-physical properties, square-planar d^8 Pt(II) complexes, have been widely explored and still have a lot of potential to investigate their applications further in the area of biological fields including as antitumor drugs and imaging of synapse vesicles.

1.3 Polyamines

Polyamines are ubiquitous small basic molecules present in all living cells and play multiple essential roles in mammalian physiology. Even though the first polyamine, spermine, was discovered over 330 years ago by microscopic observations of human semen,³⁶ they have received significant attention in the past 30 years for their involvement in a large number of cellular processes, and the area had been widely reviewed.^{37,38} Polyamines are low molecular weight aliphatic polycations and thus one of their main features is to interact with the negatively charged molecules such as DNA, RNA and proteins. They are thought to be involved in

multiple roles such as gene transcription and translation, DNA stabilization, signal transduction, cell-cell interactions, cell growth, survival and proliferation, membrane stability, functioning of ion channels and receptor-ligand interactions, consequently, their intracellular concentrations are tightly regulated.³⁹ At physiological pH the amines are protonated and hence seem to exert their role through ionic interactions, due to their unique structural feature of regularly spaced positive charges which is distinct from point charges associated with metal ions.⁴⁰

1.3.1 Polyamine Synthesis and Metabolism

Three most abundant and naturally occurring polyamines are putrescine (1,4-diaminobutane), spermidine (1,8-diamino-4-aza-octane) and spermine (1,12-diamino-4,9-diazadodecane) (Figure 1.10), which are present in almost every living cell and in many every day foods such as broccoli, cauliflower, citrus fruits and meat etc. These are part of a very tightly regulated polyamine metabolic pathway and their levels are maintained by a combination of synthesis, catabolism and transport; a number of comprehensive reviews and papers are available in this context.^{40,41,42,43}

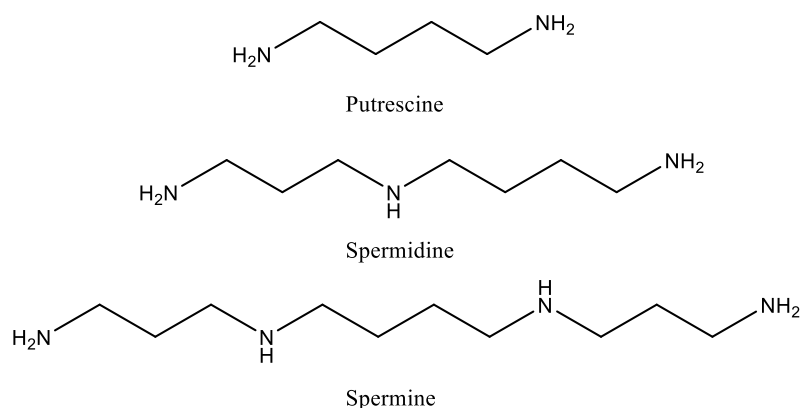


Figure 1.10: Chemical structures of naturally occurring polyamines.

There are three major sources of polyamines that occur in organisms: food intake, cellular synthesis and microbial synthesis in the gut. With regard to the bio-synthesis of polyamine

occurring in the cytoplasm of cells, polyamines are synthesised from the amino acids L-arginine, L-ornithine and L-methionine (Figure 1.11). Initially, L-ornithine is produced from L-arginine by the mitochondrial enzyme arginase, which is then decarboxylated by ornithine decarboxylase (ODC) to produce putrescine in the rate determining step. In parallel to putrescine production, S-adenosine-L-methionine is produced from L-methionine, which is further decarboxylated by S-adenosine methionine decarboxylase (SamDC) to produce decarboxy-S-Adenosine methionine. Spermidine and spermine are further synthesised from putrescine by the sequential addition of n-propylamino groups from decarboxy-S-Adenosine methionine and a transferase enzyme (spermidine synthase SpdS or spermine synthase SpmS). The transferase enzyme catalyses the transfer of the n-propylamino group to the primary amine groups of putrescine or spermidine, to produce spermidine and spermine, respectively (Figure 1.11).⁴⁰

The higher polyamines spermidine and spermine can be reconverted back to the shorter polyamine i.e. putrescine, *via* the involvement of a rate limiting enzyme of polyamine catabolism described as cytosolic spermidine/spermine acetyl transferase (SSAT) (Figure 1.11).⁴⁴ SSAT acetylates both spermine and spermidine to produce N-acetyl spermine and N-acetyl spermidine respectively, which then move into peroxisome, where they are oxidized by polyamine oxidase (PAO) and release acetaminopropanal and hydrogen peroxide (H₂O₂) as by-product of this oxidation. The production of H₂O₂ induces SSAT; however, this can also cause oxidative stress to the cell resulting in apoptosis i.e. programmed cell death.⁴⁰ This has encouraged the researchers to think about the dual role of polyamines, i.e. decrease in the polyamine levels hinders with the cell growth and proliferation while high levels of polyamines appear to be toxic and may be responsible for cell death. Their precise role is yet to be understood fully.³⁷ In the light of their fundamental significance, it is vital to maintain the intracellular level of polyamines within a very narrow range.

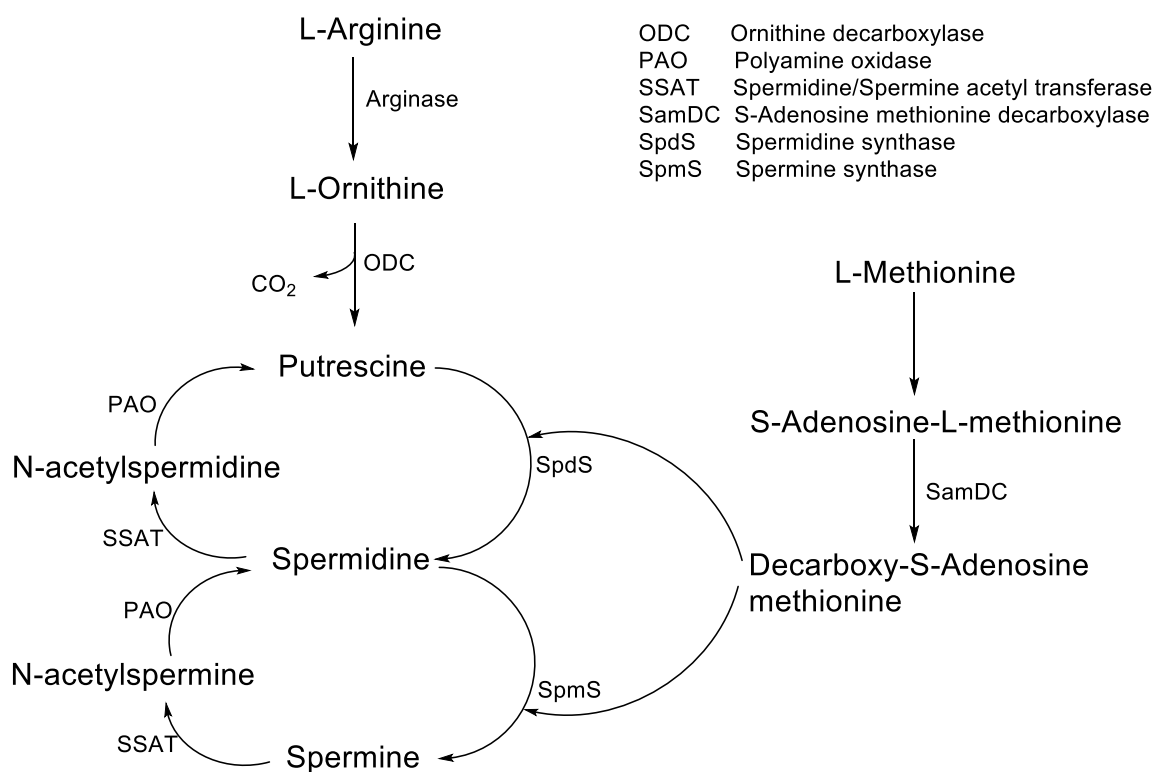


Figure 1.11: A schematic representation of polyamine metabolism including biosynthesis and interconversion.⁴⁵

1.3.2 Polyamine Transport

As discussed in the previous section, in addition to the biosynthesis of polyamines in the mammalian cells, they are found to be capable of taking up polyamines from the extracellular medium. The uptake and excretion of the naturally occurring polyamines i.e. putrescine, spermidine and spermine by mammalian cells are fundamental parts of the cellular systems which regulate the intracellular concentrations of these biogenic amines according to needs. For the process of uptake of polyamines by cells, a system has been described named as the polyamine transport system (PTS). As described earlier, polyamines play an important role in cell proliferation and differentiation; hence, PTS can be correlated to diseases characterised by rapid and uncontrolled cell growth e.g. cancer(s). It is believed that subduing the amount of polyamine within the tumour cells would starve the cell and will eventually lead to apoptosis.⁴⁶ This describes the importance of PTS and evaluates the need to study/understand PTS in detail.

Though polyamines are a part of the diet consumed by mammals, the bio-availability of these is still unknown and the PTS is currently poorly understood at the bio-chemical level.^{40,45,47} Mutated cell lines lack the ability to uptake the polyamines from the surroundings, but these are capable of releasing polyamines. This indicates that similar to the uptake of polyamines, another transport system exists and is described for the efflux from the cells, this is also considered to explore the applications of polyamines in biological field. A transporter gene from a mammalian cell line is still not isolated and is a matter of further investigation.⁴⁸

The PTS is not very specific and can transport a number of related chemical substrates including paraquat **4**,⁴⁹ mapacrine **5**,⁴⁷ methylglyoxalbisguanylhyazone (MGBG) **6**,⁴⁰ and synthetic drugs conjugated with a polyamine.^{48,50} Polyamines tagged with fluorescent molecules are known to be transported through PTS and have been localized in discrete vesicles.⁵¹

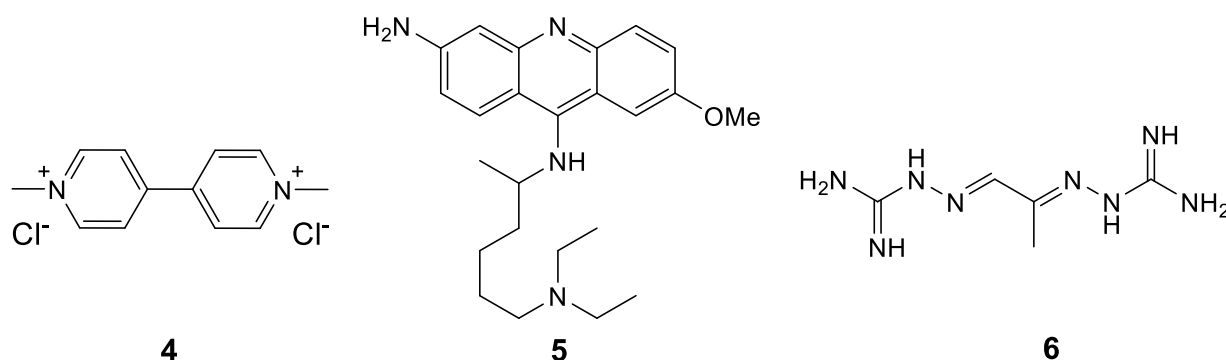


Figure 1.12: Chemical structures of paraquat **4**, mapacrine **5** and methylglyoxalbisguanylhyazone (MGBG) **6**.

As mentioned above, PTS is not specific to the transport of natural polyamines,^{52,53} and allows the transport of tagged polyamines with the chemotherapeutic agents and/or polyamines coordinated to fluorophores, hence, the tumour cells can uptake both the natural and structurally modified polyamines from the extra-cellular medium through the PTS.⁵⁴ A range of studies have been carried out to investigate the PTS including a range of polyamines varying in size of anti-cancer agent, the number and spacing of charges and the length of polyamine tail.⁵⁵ Wang *et al.* described the efficient uptake of N(1)-(9-anthracenylmethyl)homospermidine (4,4-triamine) conjugate by Chinese hamster ovary (CHO) and murine melanoma B16 screens.^{55,56} N(1)-(9-anthracenylmethyl)homospermidine (4,4-triamine) conjugate has also been investigated to induce apoptosis in several cell lines.

Though, the PTS has not yet been described at molecular level, but it is found that PTS is dependent on temperature and concentration of polyamines.⁵⁷ The PTS also requires energy for its functioning. In general, most cells have two transport systems: the first is described as the sodium dependent channel, and although it is capable of transporting all three polyamines, this has a preference for the transport of putrescine; the second one is a sodium independent channel for the transport of higher polyamines i.e. spermine and spermidine.^{17,58,59} This suggests that there should be two different mechanisms for the polyamine transport. The first one is described as receptor-mediated endocytosis model, in which polyamines bind to heparin sulphate on a molecule of glypican-1, a membrane-associated protein, before being taken into the cell by endocytosis. Inside the cell, polyamines are released from glypican-1 by NO-mediated oxidation within the endosome.⁶⁰ It was claimed that heparin sulphate side chain of glypican-1 can sequester spermidine and the uptake was dependent on nitric oxide synthase (NOS₂). Secondly, the other model of polyamine uptake is defined as a process in which polyamines are imported into the cell *via* a polyamine transporter that requires an electronegative membrane potential followed by rapid sequestration through vesicular antiporters into polyamine-sequestering vesicles (PSV).⁵¹ This is evident from another study that the cell surface heparin sulphate proteoglycans have been involved in polyamine transport, and the uptake of polyamines was blocked by a single chain variable fragment anti-heparin sulphate antibody.⁶¹ In 2008, a caveolin-regulated system was reported to transport polyamines in colon cancer cells. Phosphorylation of caveolin-1 at Tyr14 has further improved the activity of this system.⁶²

In conclusion, polyamines are the ubiquitous small basic molecules found in the cell and perform several roles inside the cells. Hence, it is very important to regulate their concentration within the limits *via* bio-synthesis, degradation and a polyamine transport system (PTS). The PTS is not specific and hence can be exploited for applications in treating many diseases such as cancer(s).

1.3.3 Polyamines co-ordinated to Transition Metals

Since the serendipitous discovery of cisplatin (7) to oncology as an anti-cancer drug, Pt(II) compounds have been intensively studied with a view to develop the improved anti-cancer agents.⁶³ As discussed previously, in particular, poly-nuclear polyamine metal complexes have received much attention, since they were found to yield DNA adducts and too often circumvent acquired cisplatin resistance. Generally, in the treatment of malignant formations, metal-

polyamine complexes have had an enormous impact. Their activity is mainly relied on specific interactions with DNA, leading to blocking of replication and inhibition of transcription; with treated cells ultimately undergoing apoptosis i.e. cell death.

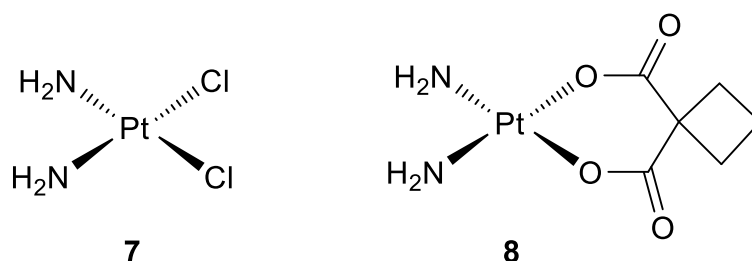


Figure 1.13: Cisplatin (**7**) and carboplatin (**8**) – Archetypal platinum complexes with demonstrated antitumor activity.

The importance of Pt-based anticancer agents is demonstrated by the fact that they are presently used in 50 to 70% of all chemotherapeutic treatments administered to cancer patients. The anti-tumour agents cisplatin (**7**) and carboplatin (**8**) (Figure 1.13) have high cytotoxic effects against a variety of tumour types, particularly against epithelial cancers, testicular, ovarian, head and neck, oesophagus, cervix, bladder carcinomas as well as lymphomas.^{64,65} However, the usage of cisplatin (**7**) and related drugs such as second generation carboplatin (**8**) and third generation oxaliplatin (**9**) is restricted, owing to their dose-limited detrimental side effects such as nephrotoxicity and hepatotoxicity. These became less popular due to their potential to acquire resistance upon prolonged administration and their lack of efficacy against many cancer types, specifically metastatic ones.

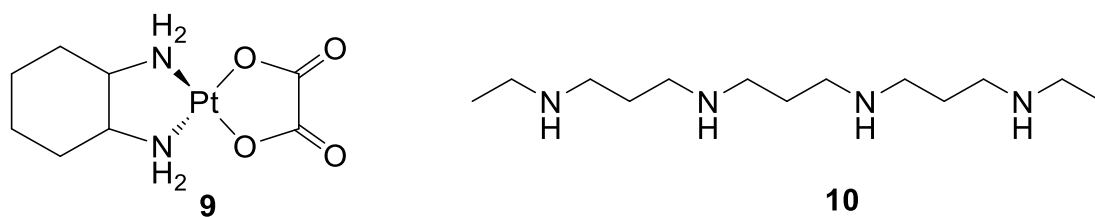


Figure 1.14: Oxaliplatin (**9**) and diethylnorspermine (**10**).

According to a study carried by Hector and co-workers, it was claimed that cisplatin (**7**) and oxaliplatin (**9**) can induce SSAT more efficiently than diethylnorspermine (**10**), which is considered as a potent inducer of SSAT.⁶⁶ Furthermore, in combination the two compounds produce a synergistic induction of SSAT and polyamine depletion that exhibits superior cytotoxicity than either agent alone.⁶⁷

Early studies on the new generation dinuclear bis-platinum or trinuclear tris-platinum complexes (Figure 1.15) have suggested that these are more potent than cisplatin against murine leukemia cells, murine solid tumour cells and had good activity against cisplatin resistant cell lines.⁶⁸ This has encouraged more research into multi-nuclear platinum complexes co-ordinated to polyamines (similar to **11-19**) to investigate and deploy them in the treatment of cancers. Additionally, the cytotoxic potency of these polyamine-bridged complexes is austere regulated by their structural characteristics, which renders these compounds more interesting for investigation. These complexes are expected to display a higher cytotoxicity due to more severe DNA damage. The naturally occurring polyamines putrescine, spermidine, spermine and their N-alkylated counterparts, have been used as bridging ligands in these multi-nuclear complexes that leads to distinctive and very effective interactions with DNA. For example, BBR3464, **12**, is said to interact with DNA through electrostatic interactions and hydrogen bonding to increase its affinity for DNA and form adducts through each of its terminal, monofunctional platinum chloride moieties.⁶⁹

In conclusion, the development of platinum based polyamine anticancer agents has acquired much attention owing to their importance in treatment with a view to enhance and extend cytotoxic activity with a minimal side effects and a target-directed tailored drug design with an emphasis on the controlled delivery.

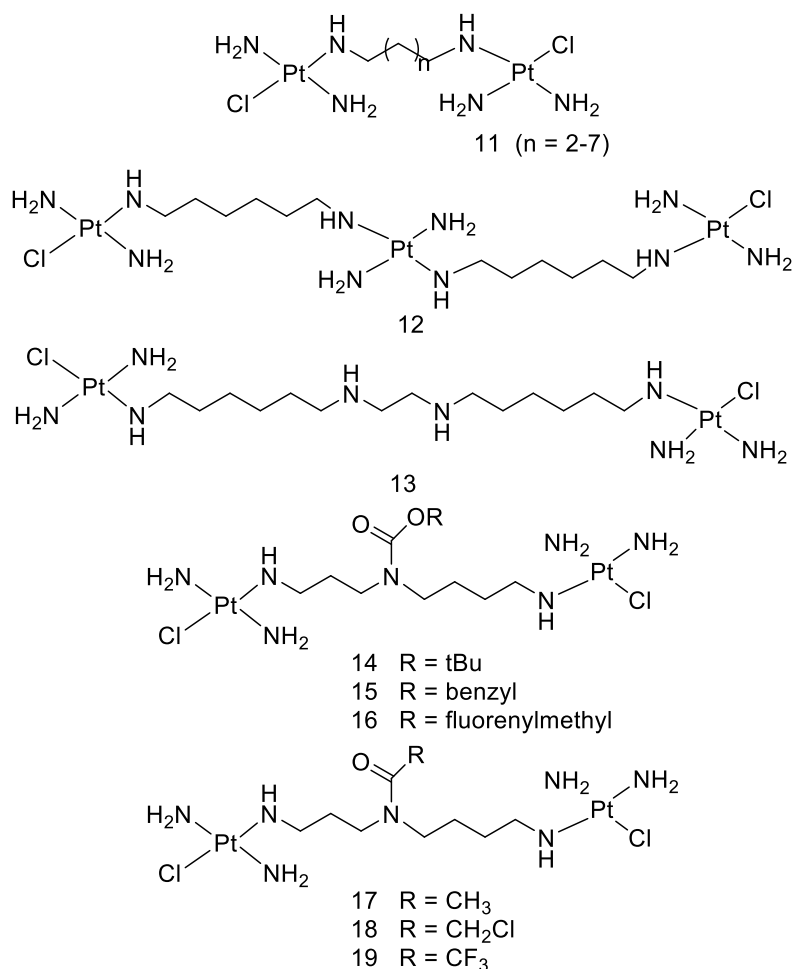


Figure 1.15: Dinuclear and trinuclear Pt-polyamine complexes with significant antitumor activity.

1.4 The Role of Luminescence in Cellular Studies

Microscopy is well established in studies of the cellular environment and as a non-invasive technique is vital in exploring the behaviour of cells without disturbing their function. The introduction of fluorescent cellular probes and the associated use of fluorescence microscopy can provide the opportunity to study in more detail specific sub-cellular structures by using probes which display specific cellular localisation. It is also possible, through the design of fluorescent probes that are responsive to their environment, to investigate the biological processes at work within the cell.

1.4.1 Applications of Metal-Ligand Complexes in Imaging Studies

1.4.1.1 Cellular Imaging

As discussed previously, a range of transition metal complexes display properties suitable for their applications in biological systems. These have been employed for cell imaging owing to their attractive photo-physical properties and the area has been widely studied and still has a scope to investigate further.⁶ This is important to consider that the metal complexes used for cellular imaging should have high cellular uptake, low toxicity and able to internalise and localise inside the cell.

So far, organic fluorophores which are highly conjugated heterocyclic compounds, have been given considerable importance for the cellular imaging investigations due to their high extinction coefficients and high quantum yields, but these molecules are greatly susceptible to photo-bleaching, have small Stokes shifts and short lifetimes.⁶ Therefore, these molecules often suffer from the problem of background interference from other fluorescent bio-molecules present within the cell.

To explore the area further, robust fluorophores having high quantum yields and long emission life-times are often sought which are capable of targeting different cell organelle to understand the biological functions in detail. Different research groups have focussed on developing fluorophores incorporating the desirable photo-physical properties, based on various sides of chemistry including quantum dots, lanthanides complexes and transition metal complexes. Quantum dots⁷⁰ and lanthanide complexes⁶ exhibit strong luminescence and claim long lifetimes and high quantum yields but both of these suffer from a common limitation of high cellular toxicity. Lanthanide complexes also suffer from a problem of direct excitation and hence, require an additional antenna chromophore to excite the lanthanide *via* resonance energy transfer (RET).

Transition metal complexes have abundant potential for applications in cellular imaging due to attractive photo-physical properties, easier cellular uptake and relatively lower cytotoxicity. Moreover, the longer emission lifetimes of these complexes relative to most organic fluorophores, allows them to be employed for lifetime imaging microscopy. Re-based complexes are the most commonly studied in this context.^{71,72} Coogan *et al.* reported a range of Re-complexes (**20a-g**) (Figure 1.17) and tested their applications in cell imaging.⁷² To understand the toxicity and cellular uptake of the metal complexes, they synthesised a

combination of cationic, neutral and anionic complexes bearing lipophilic and hydrophilic properties. The author claimed that cellular toxicity is highly dependent on the choice of ligand. The neutral complex **20a** showed high toxicity which was attributed to the easy substitution of chloride by donor groups present on bio-molecules. All cationic complexes (**20b-e**) showed good cellular uptake and low toxicity (except **20e**, only at low concentration). Compound **20e** showed high toxicity at the moderate concentrations. The cationic complexes were observed throughout the cells concentrating mainly in membranes and membrane structures in the cytoplasm. Lastly, anionic complexes (**20f,g**) were found to be least toxic among all others and accumulated in the digestive vacuoles by phagocytosis.

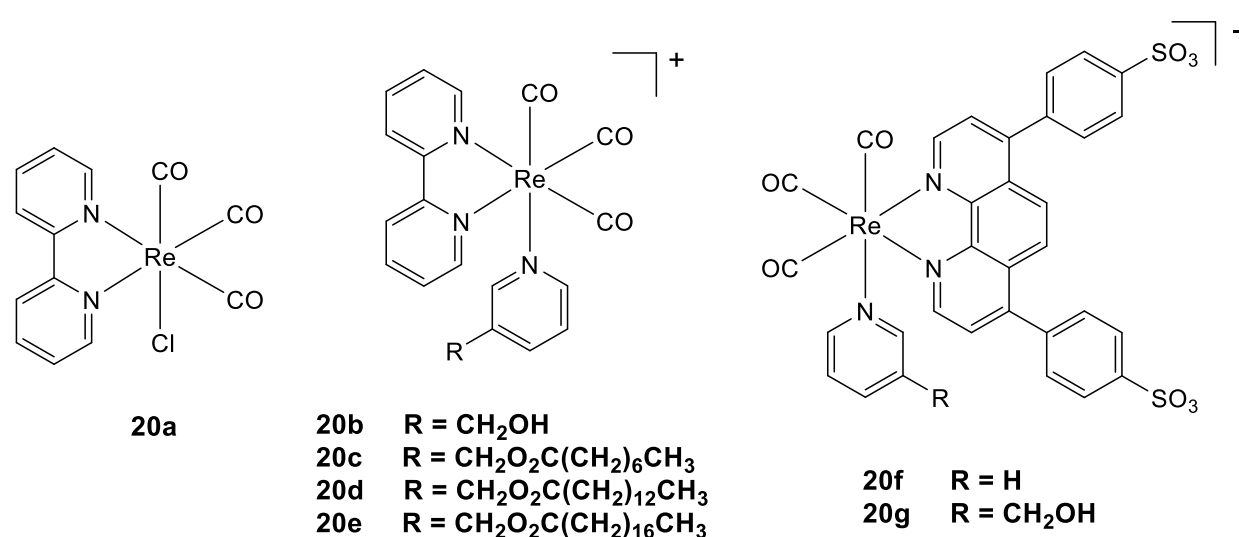


Figure 1.17: Structures of a range of Re-complexes (**20a-g**).

To improve the cellular uptake and reduce cellular toxicity in transition metal complexes, a variety of approaches have been tested successfully. Among all, the most common approach is to incorporate some biological molecules in the ligand system, for *e.g.* a biotin moiety to exogenous species,⁷³ or the inclusion of estradiol molecule.⁷⁴ As described previously, cancer cells possess a specific PTS to sustain their fast proliferation and therefore, polyamines have been recognised as targeting vectors for cancer cells. Therefore, this project will focus on the inclusion of polyamines linked ligands coordinated to transition metals, specifically Pt(II) and explore them for cell imaging and hence will be discussed further to explore their effects on cellular uptake and localisation.

1.5 Synaptic Vesicles

Chemical synapses are specific confluences at the junctions of neurons within the central nervous system, through which neurons signal to each other across the synaptic cleft *via* releasing specialised neurotransmitter molecules such as amino acids, peptides and some ions. This involves a sequence of steps described in (Figure 1.18).

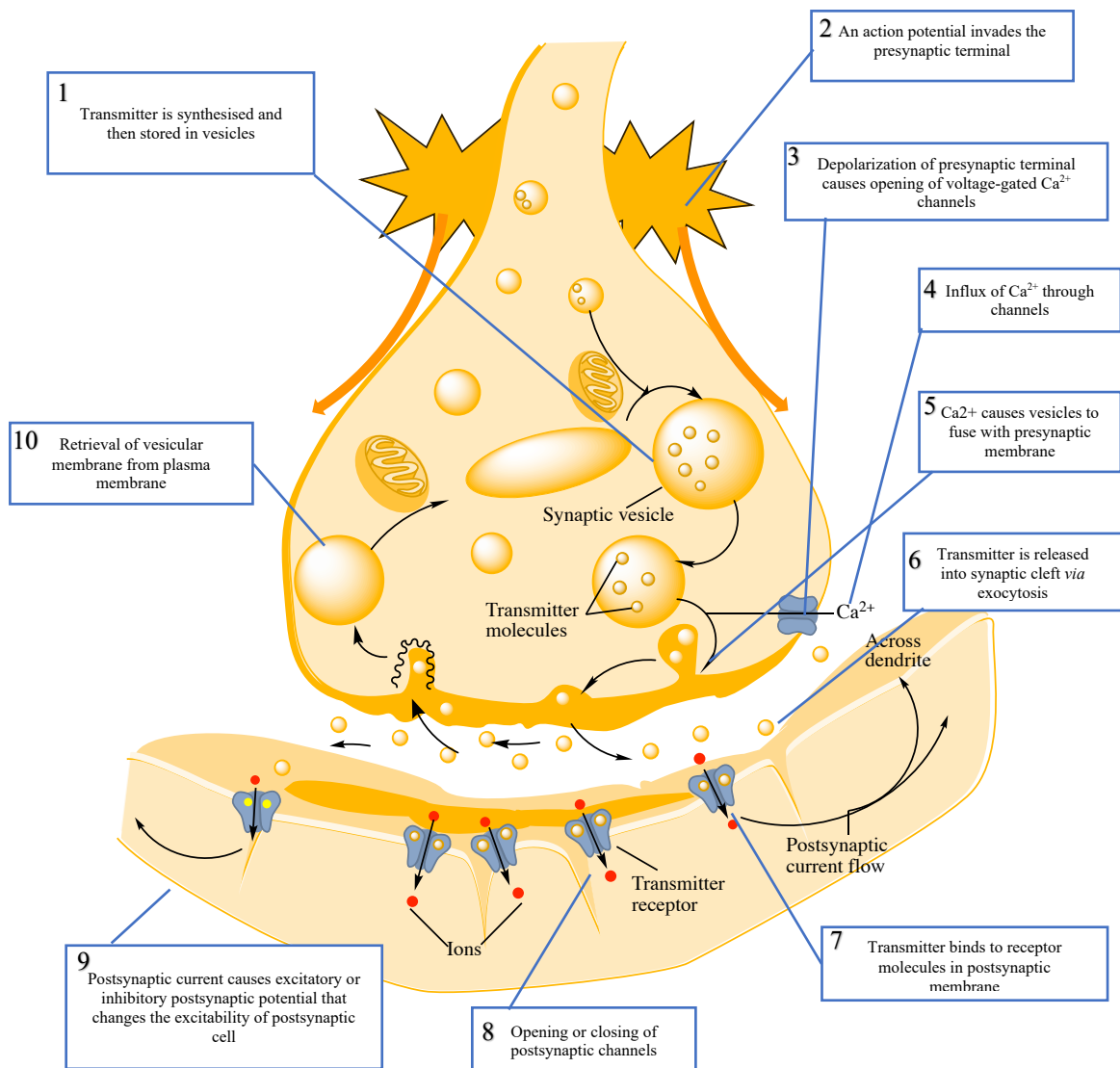


Figure 1.18: A proposed sequential representation of events involved in transmission at a typical chemical synapse.⁷⁵

1.5.1 Synaptic Vesicle Cycle

The synapses formed by neurons are independently regulated. The major event in the synaptic vesicle cycle is exocytosis by membrane fusion. The presynaptic boutons contain numerous synaptic vesicles filled with neurotransmitter. On arrival of an action potential, the predocked vesicles at the active zone undergo a Ca^{2+} -dependent fusion at the active zone resulting in neurotransmitter release through the formation of a fusion pore. Fusion pores help regulate the rate and the amount of release of neurotransmitter. The exocytosed vesicles are then retrieved *via* endocytosis for refilling the neurotransmitter and are also docked and primed for re-release.⁷⁶ These observations indicate that synaptic vesicle membrane is recycled within the presynaptic terminal *via* the sequence summarized in (Figure 1.19).

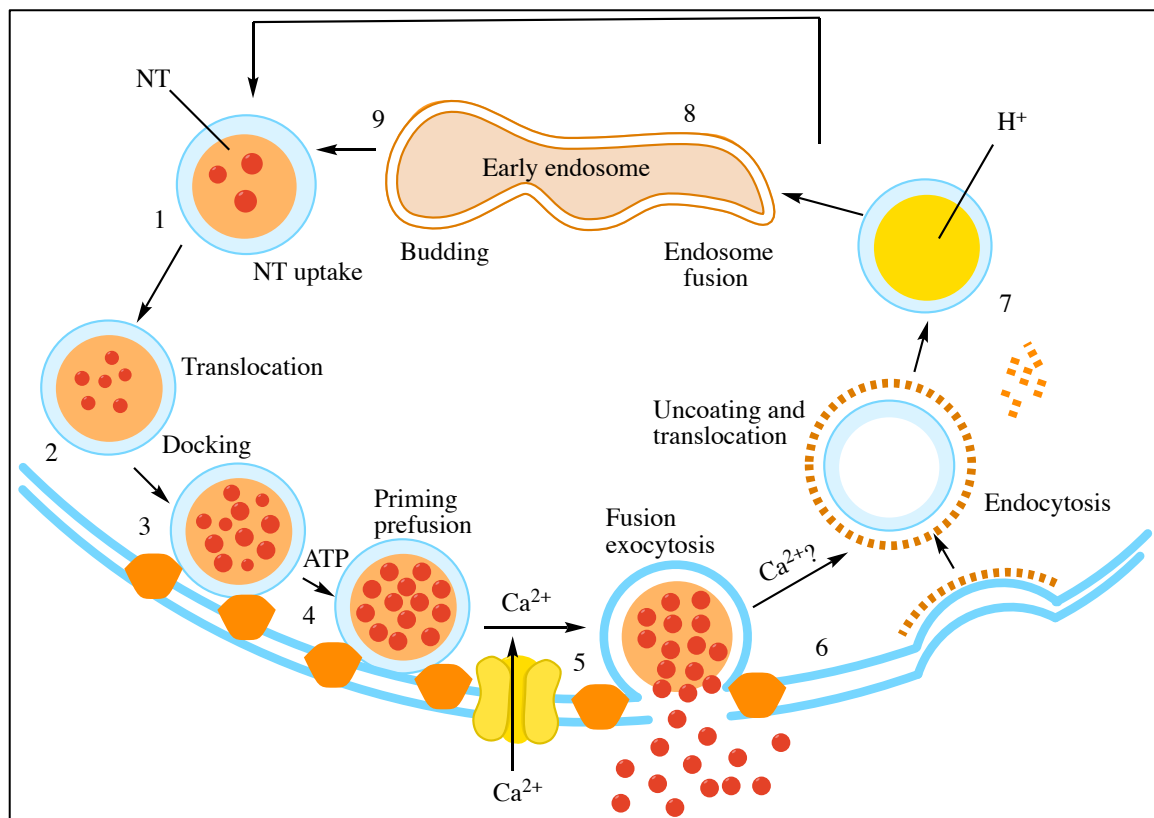


Figure 1.19: Figure shows events that orchestrate neurotransmitter release at the synapse (full fusion): 1) Synaptic vesicles are filled with neurotransmitter using specific transporters in the synaptic vesicle membrane. This process is ATP dependent. 2) The synaptic vesicles are moved to the active zone 3) They are then docked at the active zone 4) and primed for fusion event 5) On arrival of an action potential, there is an influx of calcium through the opening of the voltage gated calcium channels that triggers the fusion of the synaptic vesicles to the plasma membrane for release of transmitter release 6) The vesicles then move away from the active zone and gathered in coated pits for endocytosis 7) The coated vesicles begin to acidify and the clathrin coat is removed by a chaperone 8) The endocytosed vesicles are then fused with an early endosome for sorting and reconstitution 9) with synaptic vesicle then ready for re-use.⁷⁷

1.5.2 Different Modes of Exocytosis and Endocytosis

This conventional model only takes into account the full fusion mode of exocytosis when in fact, there are two forms of exocytosis: full fusion (FF) and Kiss-and-run (KR).

1.5.3 Full fusion

Full fusion was initially described in 1973 by Heuser and Reese at the frog neuromuscular junction.⁷⁸ In this mode, the synaptic vesicles manifest a complete aqueous continuity between vesicle lumen and external medium and full lipid continuity vesicle membrane and plasma membrane, causing near- instantaneous neurotransmitter release at the active zone as shown in (Figure 1.20).⁷⁹ The collapsed membrane then moves away from the active zone and is retrieved by clathrin-mediated endocytosis, slow recycling *via* endosomal compartments or bulk endocytosis. This process has also been implicated in central nervous system terminals.⁸⁰

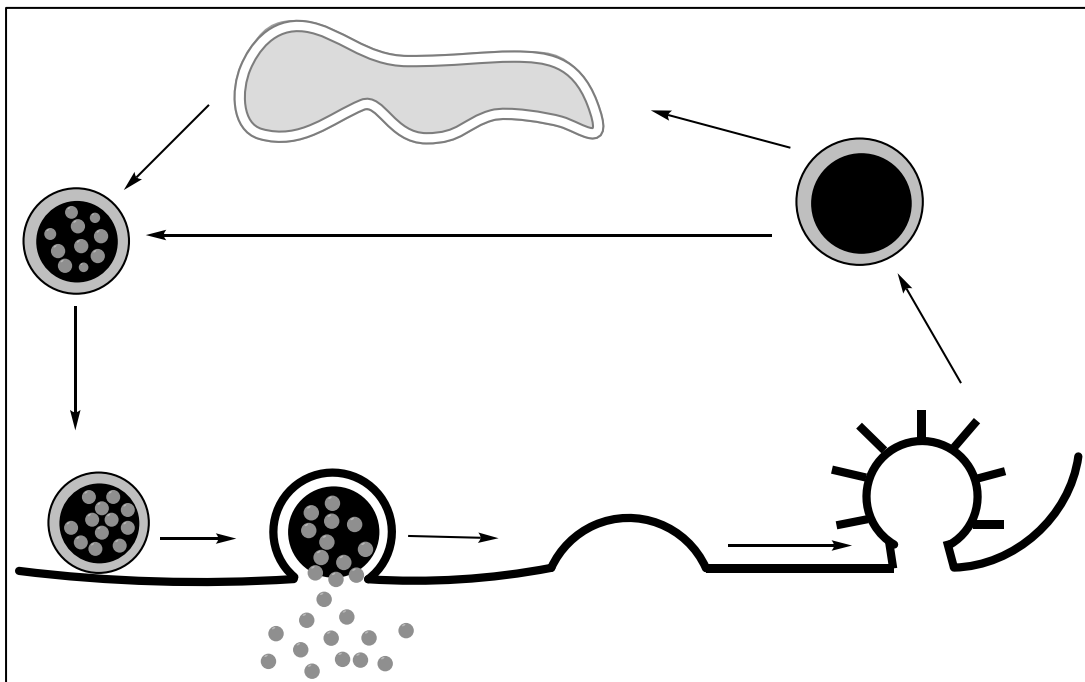


Figure 1.20: Schematic diagram showing release of neurotransmitters from synaptic vesicles *via* a full fusion mechanism. The synaptic vesicles then diffuse laterally and are retrieved *via* clathrin-mediated endocytosis or endosomal recycling.⁸¹

This process would put tremendous pressure on the ready releasable pool (RRP) vesicles to maintain a speedy and efficient exocytosis process because the endocytosed vesicles would have to quickly return to the interior and then through the following endocytosis steps in quickly and be primed and ready for release in order to maintain the signal downstream, this would mean that the vesicles race back and forth and in the process restore the complement of proteins and lipids required for release; a quick exocytosis process called kiss-and run helps solve the dynamic dilemma of the RRP vesicles allowing them to release the neurotransmitter and help maintain the signal.

1.5.4 Kiss-and-run

KR or non-classical mode of fusion was also discovered in 1973 by Ceccarelli and colleagues at the frog neuromuscular junction (NMJ).⁷⁸ KR results in the formation of a transient pore for release of neurotransmitter, without complete loss of identity of synaptic vesicles and cessation of this would occur by closing of the fusion pore. Thus, the synaptic vesicles are available for rapid re-use.

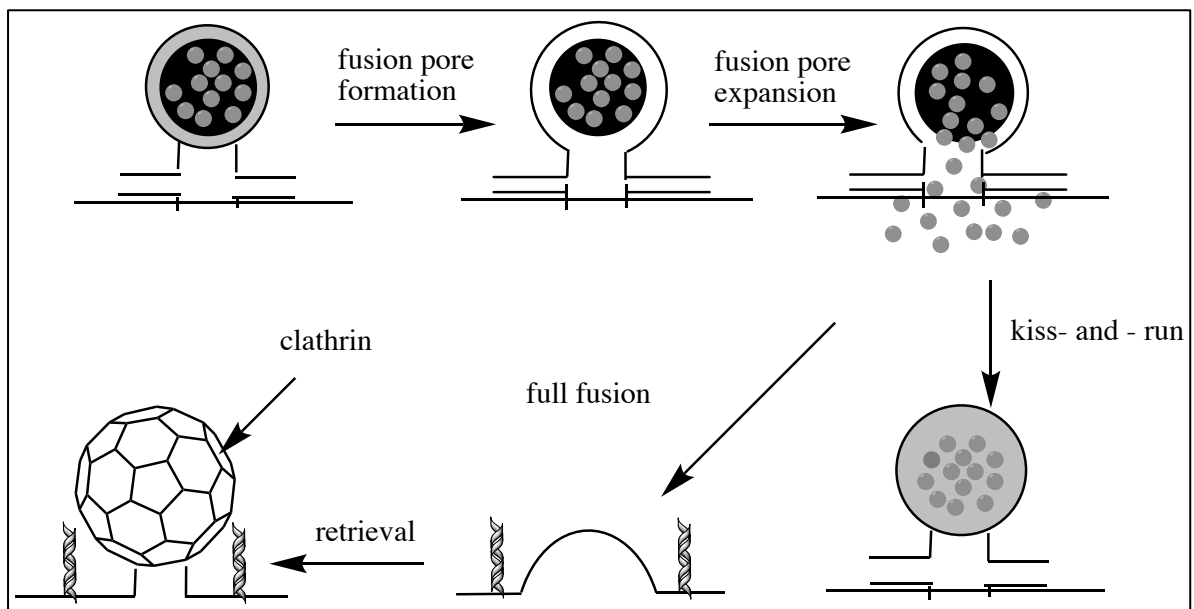


Figure 1.21: Diagrammatic representation of the comparison between kiss-and run and full fusion.⁸²

Harata *et al.*, have proposed that KR helps to conserve the resources during periods of stimulation and this ensures that the synapses are ready for high frequency firing with a full quota of fusion-competent vesicles.⁷⁹ These processes co-exist in nerve terminals with frequency of stimulation being the deciding factor. KR and FF are at variance with each other (as shown in Figure 1.21) on various factors like lack of lipid and protein continuity when the synaptic vesicle fuses with the plasma membrane or vesicle location after fusion. KR still remains a debatable concept. Harata *et al.*, have shown the prevalence of KR in the hippocampal cells by using bromophenol blue to quench the incompletely released FM dye, **21**.⁷⁹ Harata *et al.*, have performed capacitance measurements at giant synapses to demonstrate the prevalence of KR while Zhong *et al.*, have used recycling of quantum dots in synaptic vesicles technique to show KR.⁸³ KR mode of exocytosis involves the endocytic stage where the fusion pore closes.⁷⁹

Ashton *et al.*, have shown that a switch in the mode of exocytosis can be brought about by modulating $[Ca^{2+}]_i$ and protein phosphorylation.⁸⁴ Strong stimulation of nerve terminals causes the RRP to undergo KR while the RP fuses *via* FF.

In synapses at a given time period, the number of vesicles undergoing exocytosis can surpass the reserve of precursor synaptic vesicles delivered from the cell body. Thus, to the balance the demand and supply of vesicles, nerve terminals have developed efficient endocytic ways for recapturing and reusing membranes that have fused with the plasma membrane for neurotransmitter release. Electrophysiological studies using extracellular endocytic tracers performed at the frog NMJ by Heuser, Reese, Ceccarelli and colleagues have given rise to two schools of thought: one holding that vesicles acquire tracers directly *via* a reversible exo/endocytic sequence in which they consistently maintain their biochemical identity during transient continuity with plasma membrane, the other that synaptic vesicles acquire tracers indirectly *via* the formation of clathrin coated vesicles which are spatially and temporally separate from exocytosis and reverse a temporary loss of vesicles' individual identity upon merger with plasma membrane.⁷⁸ Depending on the intensity of stimulation at various synapses the time taken for endocytosis can vary.⁸⁵ There are in fact four different forms of synaptic vesicles endocytosis: clathrin mediated endocytosis, KR (mentioned earlier), bulk endocytosis/ activity dependent bulk endocytosis and ultrafast endocytosis.

In conclusion, Neurons are involved in the fast transmission of electrical signals and can sustain high rates of synaptic transmission without draining the amount of synaptic vesicles. This process involves a highly efficient local endocytotic recycling of synaptic vesicle membranes, which can be used again and again in exo- endocytotic cycles. The means of such rapid vesicular recycling of synaptic vesicles are still under-explored and further research is required to understand this thoroughly.⁸⁶

1.6 Synaptic Vesicles Imaging

The understanding of morphology and chemical composition of synapses can help to explore the structural basis for synaptic function.⁸⁷ In order to understand the properties and functioning of the synaptic pools, it is vital to describe the ultra-structure of the synaptic vesicles.^{86,88} This suggests that electron microscopy along with the fluorescence microscopy can be used as a strong tool to provide better resolution micrographs and can help to explore the area further. Current studies rely on the use of organic lipophilic styryl dyes such as FM-143FX (**21**) for fluorescence microscopy. These dyes are used to stain the synaptic vesicles which are capable of binding to the membrane and be internalised upon induction of endocytosis. For the application of electron microscopy to this work, 3, 3'-diaminobenzidine (DAB), **22** is added, which is capable of undergoing polymerisation due to photo-activation in the presence of **21**. OsO₄ will adhere to the precipitate of polymerisation product and hence provide the electron density for the electron microscope.⁸⁸ In literature, fluorescent dye FM-143 is described to be used in the study and visualisation of clathrin-mediated or bulk endocytosis from the presynaptic membrane using fluorescence microscopy.⁸⁹

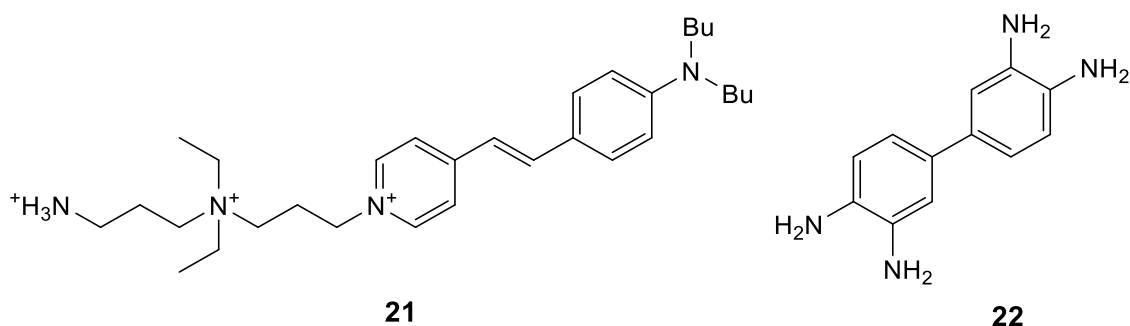


Figure 1.22: FM-143FX (**21**) and 3, 3'-diaminobenzidine (DAB), (**22**).

As this is an upcoming area, consequently, there are not many examples in the literature. A previous member of the Lowe/Cullis group developed some Ir(III) based polyamine conjugates including complex **23** and tested them successfully for targeting and imaging of synaptic vesicles.⁹⁰ Iridium was chosen for the study owing to its adequately electron rich density and anticipated to provide contrast in electron microscopy images. Electron dense iridium allows the accumulation of the complex and hence eliminates the need for treatment with DAB before performing the electron microscopy, as well as avoiding the use OsO₄ which is toxic in nature. Moreover, iridium based complexes can be excited using a multiphoton system which eliminates the use of harmful UV radiations for excitation.

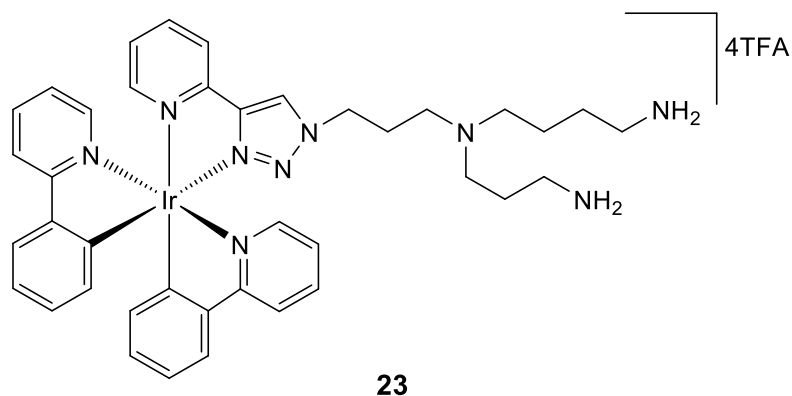


Figure 1.23: Ir(III) based polyamine conjugates complex **23**.

The preliminary results on polyamine appended Ir(III) complex **23** showed their potential to be employed for multiphoton fluorescence imaging and it is anticipated that in future, these metal-based probes will replace the currently used organic dyes e.g. **21**. However, these require further work to establish these metal-complexes in the field of imaging. While performing initial tests on complex **23**, it was shown to visualise putative presynaptic terminals after treatment with excess potassium chloride to change the membrane potential and induce endocytosis (Figure 1.24 and 1.25). This is potentially due to its adherence to the cell membrane bearing negative charge through electrostatic interactions with the cationic polyamine tail. Further studies are required to define the localisation of **23**, so as to develop similar conjugates as fluorescent probes of synaptic function.

As discussed earlier in introduction section, Pt(II) complexes have high quantum yields and allows the application of two photon excitation in the NIR region, hence, these complexes can be considered as bio-compatible. Though complex **23** has shown promising preliminary results in synaptic imaging, it was felt that these complexes needed to be more lipophilic in nature so as to enhance cellular uptake. While this line is being investigated by another member of the group, similar to polyamine appended Ir(III) systems, Pt(II) complexes will be considered to study as a part of this project and lipophilic alkyl chains will be introduced *via* the triazole in the N[^]C[^]N ligand so as to improve the lipophilicity. Synthesis of these Pt(II) complexes will be discussed ahead in results and discussion section.

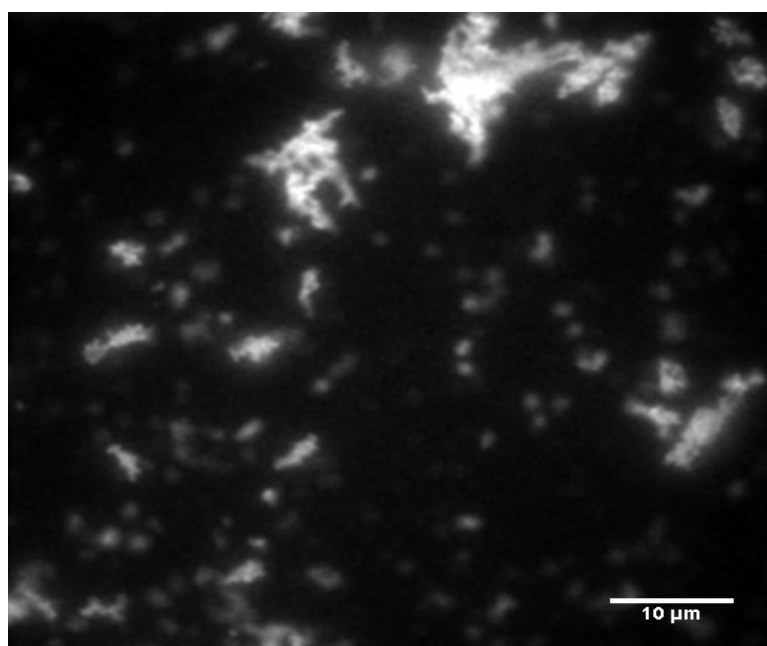


Figure 1.24: Image of primary neuronal cultures harvested from E17 rats incubated with **23** showing incorporation into putative terminal synaptic vesicles. Excitation at 350 nm, emission monitored above 505 nm, 60x objective.⁹⁰

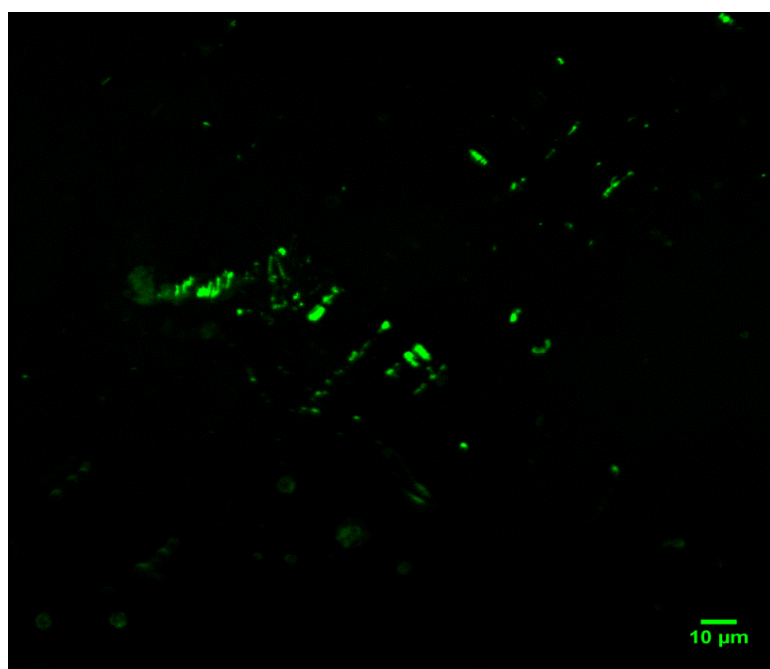


Figure 1.25: Multiphoton image of primary neuronal cultures harvested from E17 rats incubated with **23** showing incorporation into putative terminal synaptic vesicles. Excitation at 710 nm with a 500-550 nm emission filter.⁹⁰

1.7 Summary

A brief overview has been given of the role of second and third row transition metals in photochemical and photophysical applications, with particular reference to complexes containing cyclometallating ligands. The utility and tenability of such complexes has been discussed.

The role of the transition metal complexes in cellular studies has also been explored. Many biologically significant molecules have been conjugated to transition metal complexes of varying structure and function, and in all cases the conjugation does not nullify the function of either the biological or the chemical moiety.

The conjugation of biologically relevant molecules is nothing new, and what has been discussed here does not intend to demonstrate all the examples of such conjugations, but to show that this area of research is growing and can prove potentially valuable from a clinical perspective in terms of improving the selectivity or efficiency of current imaging as well as the development of new molecules for similar applications.

In conclusion, owing to intriguing spectroscopic and photo-physical properties of square-planar d^8 Pt(II) complexes, these have been widely explored and still have a lot of potential to explore their applications further in the area of biological fields as imaging of synapse vesicles.

1.8 Aims and Objectives

The synthesis of the targeted polyamine tagged Pt(II) complex is the overall objective, but earlier aims are more exploratory. In the first instance it is important to discover if such metal complexes can be made followed by considering the ease of synthesis *via* comparing conventional heating *vs* microwave heating.

The main aim of this project is to synthesise Pt(II) complexes **PtLnCl** incorporating two individual fragments, firstly, a metal-based luminescent probe for cellular imaging which can assist in understanding the localisation of the complex and secondly, a polyamine tail as a targeting vector for more selective delivery inside the cell for imaging purpose. This approach also includes incorporating a greasy group within the Pt(II) complex **PtLnCl** to augment the lipophilicity of the complex which is considered as a key for the interaction with the surface of the neuronal cells.

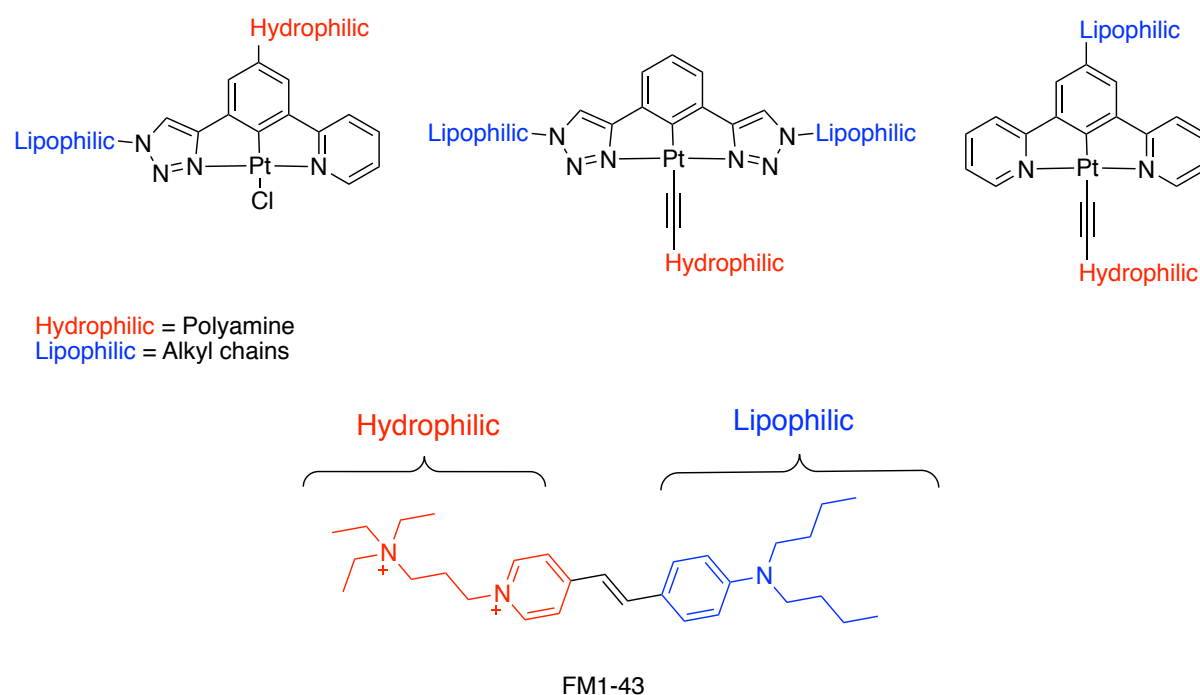


Figure 1.26: The Primary target complexes.

The desired Pt(II) complexes (Figure 1.26) have features such as that resemble FM1-43FX dye in term of structure and function. Lipophilic alkyl chains or the polyamine can be introduced *via* the cyclometallated N[^]C[^]N ligands, that can be synthesized by either one of or a combination of a cross-coupling and click reactions. Another approach to incorporate a polyamine or a lipophilic group into Pt(II) complexes is the substitution of chloride with an

ancillary ligand containing one of these functionalities. As previously discussed, the substitution of the weak field ligand, *i.e.* chloride, with a strong field ligand such as an alkynyl ligand will improve the luminescence properties of Pt(II) complexes. Thus, a series of ligands with an alkyne functionality will be synthesised *via* different methods such as amine or PEG alkylation, amide coupling and reductive amination of a Schiff base. Once these complexes were synthesised, photophysical properties of these complexes were studied. Combining the hydrophilic and hydrophobic features with Pt(II) could potentially yield complexes suitable as dyes for staining synaptic vesicles by both light and electron microscopy.

1.9 Thesis Outline

Chapter 1 presents an introduction to polyamines and luminescent of transition metal complexes and an overview about their application. Chapter 2 discusses the synthesis of the two types of ligands that will be able to cyclometalate or coordinate with Pt(II) metal centre to produce the desired complexes. The synthesis of the tridentate N[^]C[^]N ligands involved either one of or a combination of a cross-coupling and click reactions. Monodentate ligands which were prepared by different methods such as direct alkylation, reductive amination and amide coupling reactions.

Chapter 3 describes the synthesis of Pt(II) complexes with three different types of cyclometalated ligands: 1,3-di(2-pyridyl)benzene, 1,3-di(1,2,3-triazole)benzene and 2-(3-(1,2,3-triazol)phenyl)pyridine derivatives. In addition, the effects of the introduction of alkyne or pyridine ligands into the coordination sphere of platinum were explored. The synthesis of pyridine and alkyne substituted Pt(II) complexes were also discussed in this chapter.

Chapter 4 discusses the photophysical properties of Pt(II) complexes and presents comparison in terms of effect of the change in the structure of the tridentate N[^]C[^]N ligand or in terms of the effect of the electron donating group on the photophysical properties. The photophysical properties including absorption, emission wavelengths, luminescent quantum yields and lifetimes of the generated Pt(II) complexes were discussed in details. Chapter 5 gives some overview to the whole thesis as well as a scope to future directions. Chapter 6 presents the experimental part for all ligand and complexes synthesis. Finally, Chapter 7 presents the appendix for HPLC and X-ray crystallography.

Chapter 2

2 Ligand Syntheses and Characterisation

2.1 Ligand Synthesis Overview

The primary aim of the project is to synthesise and fully characterise platinum(II) complexes, incorporating variously functionalised N[^]C[^]N ligands. This approach allows for the incorporation of two individual fragments; firstly, a polyamine tail as a targeting vector for selective delivery inside the cell; secondly, a lipophilic group with the aim of augmenting the lipophilicity of the complex, which is considered as a key to the imaging of synaptic vesicles. A number of synthetic strategies have previously been employed in the synthesis of such ligands, for which the main strategies involve either one of or a combination of a cross-coupling and click reactions (Figure 2.1). Each strategy has its own merits and disadvantages, which will be discussed in turn.

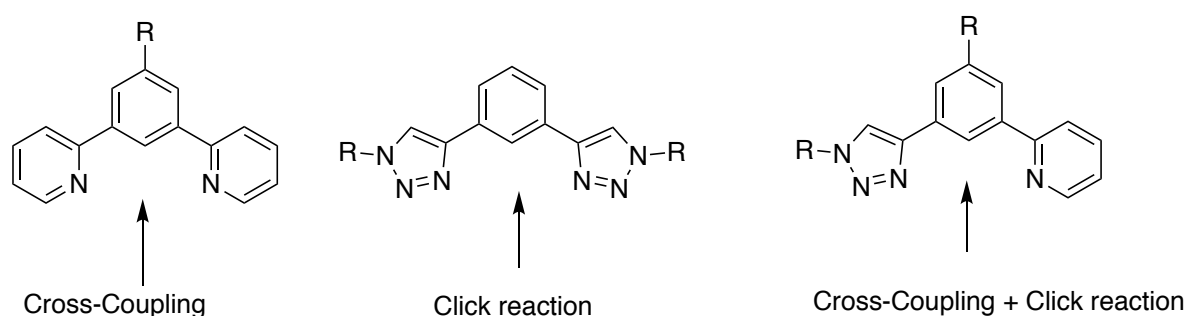
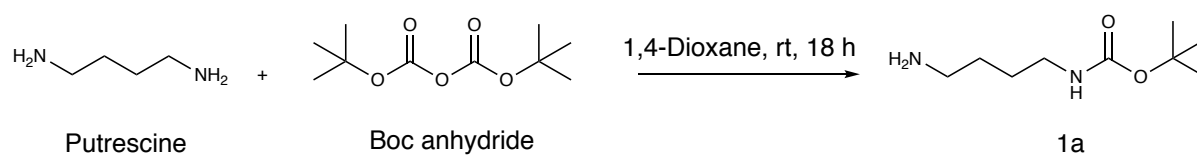


Figure 2.1: The routes that have been adopted to prepare N[^]C[^]N ligands systems.

2.2 Synthesis of Pro-Ligands

2.2.1 Synthesis of Boc-protected Putrescine (1a)

The tert-butoxycarbonyl (Boc) group is a frequently used protecting group for amines since it is tolerant to a wide range of reaction conditions, easy to introduce and can be removed cleanly afterwards.⁹¹ The Boc group is able to tolerate the reaction conditions for tandem diazotransfer/Cu(I)-catalysed azide-alkyne cycloaddition (CuAAC) which makes it ideal for the synthesis of the polyamine tagged ligands that will complex to platinum(II).



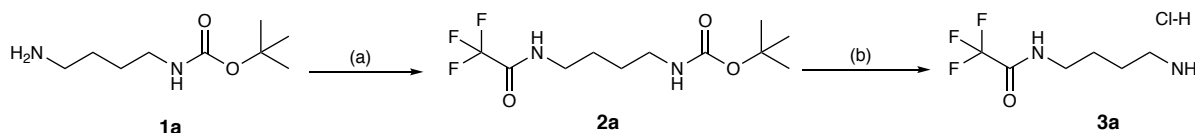
Scheme 2.1: Synthesis of N-Boc putrescine (**1a**).

Mono-protected putrescine was a prerequisite for the synthesis of N[^]C[^]N (**HL8** and **HL13**), mono-ligand (putrescine alkyne) (**9a**) and a precursor for TFA protected putrescine (**2a** and **3a**) (Scheme 2.1). In order to ensure the formation of mono-protected putrescine **1a**, two strategies were applied. Firstly, controlling the kinetics of the reaction was considered as a key to success of the reaction to ensure that only one of the two terminal amine groups was protected. Secondly, di-tert-butyl carbonate must be added very slowly to an excess of putrescine, whilst the reaction mixture is stirred rapidly in order to avoid localized high concentrations of di-tert-butyl carbonate, which may result in the formation of bis-protected putrescine.⁹¹ During the work up of the reaction, bis-protected putrescine was easily removed via filtration, due to its insolubility in water. The resulting pure product was isolated in a 57% yield and no further purification was required. A very high yield (95%) of Boc-putrescine has been quoted using anhydrous dioxane.⁹² Therefore, in order to improve the yield, anhydrous conditions could be applied in the future. The synthesis of the desired product was confirmed by MS and NMR spectroscopy analyses at high temperature (323-328 K) to resolve the spectra. The Boc groups on the polyamines can show slow rotation (on NMR timescale) about the carbonyl-nitrogen bond leading to two sets of signals. The carbon signals at room temperature appear as doublets. At higher temperatures the two signals coalesce into one signal as the rate of rotation on the

NMR timescale increases. Recording ^1H NMR spectra at higher temperature increases the resolution of the methylene signals by reducing the line broadening allowing signals to separate and resolve into multiplets.

2.2.2 Synthesis of TFA-protected Putrescine (**3a**)⁹³

To overcome issues raised during deprotecting the amine on the desired platinum complexes, where acidic conditions were required (see section 3.2.2 for further details), it was necessary to incorporate a base-labile protecting group, rather than the acid-labile *tert*-butoxycarbonyl (Boc) protecting group. Trifluoroacetyl (TFA) was selected as a suitable protecting group for this purpose due to its ease of installation, high stability under acidic and neutral conditions (pH 1-7; RT), and low steric influence.

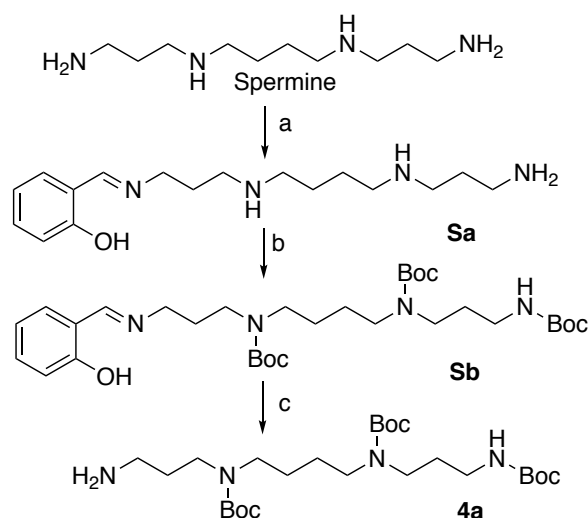


Scheme 2.2: Synthetic procedure for the preparation of TFA-protected putrescine (**3a**). Reagents and Conditions: (a) Ethyltrifluoroacetate, CHCl_3 , r.t, 24 hours, 95%; (b) 4 M HCl/dioxane, 0°C , 3 hours, 69%.

The terminal amine of **1a** was protected with a TFA protecting group upon treatment with ethyltrifluoroacetamide to afford compound **2a** in high yield (95%) (Scheme 2.2). Characterisation by ^1H , ^{13}C and ^{19}F NMR spectroscopy, as well as HRMS (ESI+) confirmed formation of **2a**; characterisation indicated complete conversion from the starting material, allowing the product to be carried through without further purification. Formation of **2a** was confirmed *via* a shift in the ^1H NMR signals corresponding to the methylene protons neighbouring the free amine group; upon TFA-protection a signal at 3.34 ppm was observed, integrating for two protons with a quartet-like splitting pattern (due to coupling with the adjacent NH and CH_2 protons); this is characteristic of a methylene resonance neighbouring an amino group bearing a strongly electron-withdrawing substituent. Further evidence suggested formation of the anticipated product; MS fragmentation gave a distinctive pattern indicative of the expected structure (MS (ESI+) 307 $[\text{M}+\text{Na}]^+$, 185 $[\text{M}-\text{Boc}+2\text{H}]^+$) and the ^{19}F NMR spectrum confirmed the presence of CF_3 (-76.1 ppm) in the product.

Following isolation of **2a**, the Boc protecting group was removed on treatment with 4 M HCl/dioxane to afford the TFA-protected polyamine (**3a**) as a pale yellow solid in good yield (69%). Comparisons of the ^1H NMR spectra of **3a** and **2a** confirmed complete conversion from the starting material had been achieved; the absence of singlet resonance at 1.40 ppm, corresponding to the nine equivalent protons of the $\text{C}(\text{CH}_3)_3$ group, indicated complete removal of the Boc-protecting group. Analysis by HRMS (ESI+) also indicated Boc-cleavage was complete after 3 hours, with a single molecular ion peak given with m/z 185, thus suggesting the TFA-protecting groups are left untouched under these conditions.

2.2.3 Synthesis of tri-Boc-protected Spermine (**4a**)



Reagents and Conditions: (a) 2-Hydroxybenzaldehyde, Na_2SO_4 , DCM/MeOH, 24 h, rt; (b) di-tert-butyl dicarbonate; $0\text{ }^\circ\text{C}$ -rt (c) $\text{CH}_3\text{ONH}_2/\text{Na}_2\text{CO}_3$ (41% yield after three steps)

Scheme 2.3: Synthetic procedure for the preparing of tri-Boc-protected spermine.

The synthesis of Tri-Boc-Spermine (**4a**) was previously described by Muth *et al.*⁹⁴ **4a** was synthesised directly from spermine using (1 equivalent) salicylaldehyde as shown in Scheme 2.3. The formation of the salicylimine, at the primary amine sites, allowed the easy introduction of Boc groups to the remaining three amine centres of spermine in situ to give **Sb**. Subsequent imine exchange of **Sb** with methoxyamine gave the desired tri-Boc-protected spermine **4a** in 41% yield after three steps. The synthesis of the desired product confirmed by MS and NMR spectroscopy analyses.

2.3 Tri-dentate N^C^N ligands synthesis

2.3.1 Cross-coupling Reactions

The most commonly used reaction to produce 1,3-di(2-pyridyl)benzene ligands is palladium-catalysed cross-coupling.^{95,96,97} In these reactions, carbon-carbon bond forming reactions can be performed by the combination of electrophilic carbon species such as aryl or vinyl halides and organometallic agents such as Grignard reagents and organoboron compounds. The method offers a route to larger, more functionalised ligands, allowing many of the ligand precursors to be prepared within a few steps from commercially available starting materials. It had previously been difficult to form C-C bond via classical synthetic reactions, without using metal catalysts. Subsequent to the development of cross coupling methods, substitution reactions to sp^2 carbon and sp carbon are easily accomplished. The mechanism of cross-coupling is determined by the nature of the “metalloaryl” species, which can be, for example, an aryl-stannane (Stille reaction), an aryl-zinc reagent (Negishi reaction) or an aryl-boronic acid/ester (Suzuki reaction). A generalised catalytic cycle is shown in (Figure 2.2).

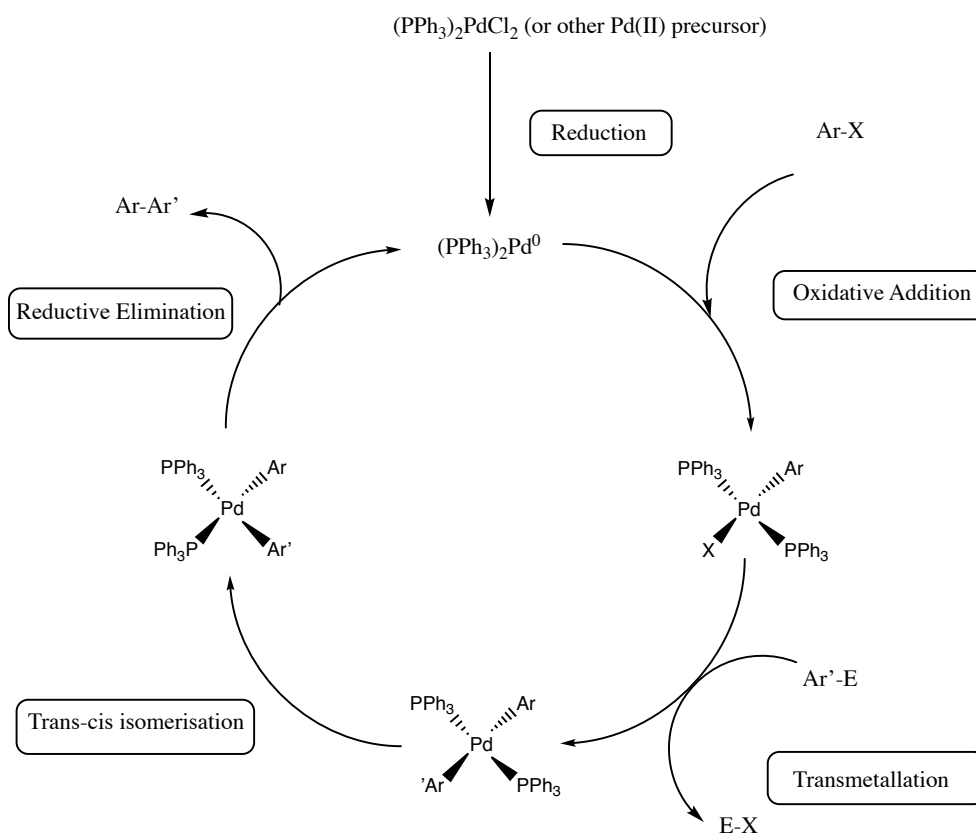
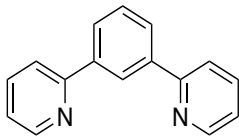
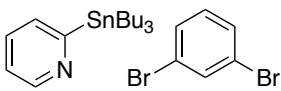
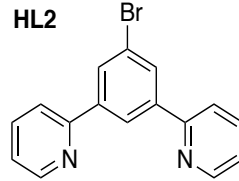
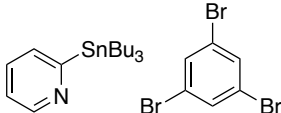
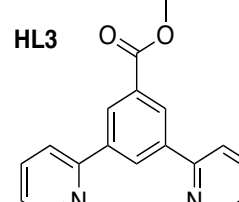
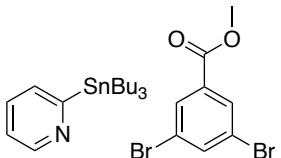


Figure 2.2: Proposed general catalytic cycle for palladium based cross-coupling reactions.⁹⁸ Here, $Ar-X$ represents an aryl halide or triflate and $E-Ar'$ represents the “metalloaryl” species.

2.3.2 Ligand Synthesis

The dipyridyl-benzene **HL1**, **HL2** and **HL3** ligands prepared during the project were all made via cross-coupling reactions, which involved either Negishi or Stille methodology (Table 2.1).

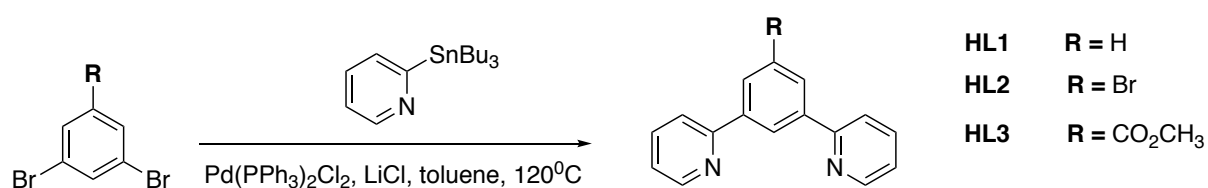
Table 2.1: The selection of tridentate ligands prepared herein, the reactive precursors, and the reaction conditions employed.

Ligand	Precursors	Synthetic procedure	Solvent	Catalyst	Yield (%)
HL1 		Stille	Toluene	$\text{Pd}(\text{PPh}_3)_2\text{Cl}_2$	78
HL2 		Stille Negishi	Toluene THF	$\text{Pd}(\text{PPh}_3)_2\text{Cl}_2$ $\text{Pd}(\text{PPh}_3)_4$	20 61
HL3 		Stille	Toluene	$\text{Pd}(\text{PPh}_3)_2\text{Cl}_2$	45

2.3.3 Ligands Prepared via Stille Cross-Coupling

The 1,3-di(2-pyridyl)benzene **HL1**, **HL2** and **HL3** were prepared via Stille cross-coupling reaction following a literature method.⁹⁹ The Stille reaction is a palladium-catalysed reaction for coupling an organo tin compound with a sp^2 -hybridised organo-halide. Trimethylstannyl or tributylstannyl compounds are commonly used, and, although trimethylstannyl compounds show higher reactivity compared with the butyl derivatives, the toxicity of the former is *ca.* 1,000 times higher than that of the latter. Therefore, the less toxic 2-(tributylstannyl)pyridine was used, typically 1.25 equivalents per aryl-halide bond, due to competitive formation of homo-coupled products.

Stille cross-coupling reactions utilised during the project involved a 2-tri-n-butylstannyl pyridine species and a 1,3-dibromo aryl species (Scheme 2.4), and were performed in dry toluene. Pd(PPh₃)₂Cl₂ was added as catalyst. Reactants were degassed using freeze-pump-thaw methodology, and the reactions were heated at 120°C under nitrogen for 24 h. An inert atmosphere was crucial to prevent oxidation (and deactivation) of the palladium catalyst and to minimise homo-coupling reactions between the stannanes, both of which would have a detrimental effect on the yield. LiCl was also added to increase the yield – the compound is thought to stabilise the intermediate complex formed after oxidative addition, accelerating the reaction.⁹⁹



Scheme 2.4: Stille cross-coupling reaction for **HL1**, **HL2** and **HL3**.

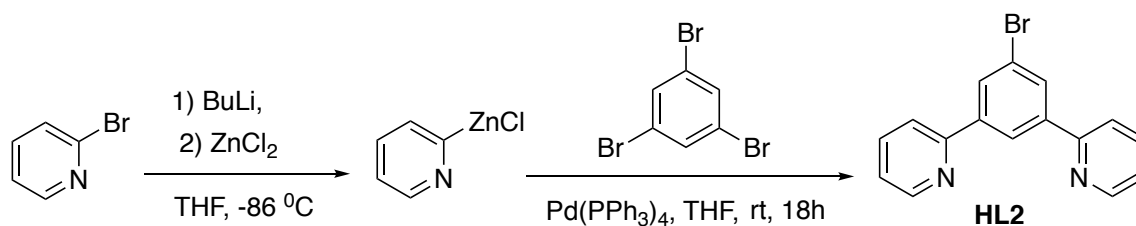
The reactions were found to generate a significant amount of waste material, which was removed from the desired product by lengthy work-up followed by SiO₂ column chromatography. Stannyl by-products can be notoriously difficult to remove – they are insoluble in water so cannot be simply washed out. KF was added during the work-up to form insoluble tri-n-butyltin fluorides, which are subsequently filtered from the product. Sometimes, however, some tin residues remained after the full work-up and column; since the desired products were generally insoluble in hexane, several washings with this solvent were usually sufficient to remove the excess tin by-products. 1-bromo-3-(2-pyridinyl)benzene and 1,3-dibromo-5-(2-pyridinyl) benzene “by-product” were isolated via a silica column chromatography and used by another member of the Lowe group to synthesise ligands for iridium coordination. Methyl 3-bromo-5-(pyridin-2-yl)benzoate, **HL3** by-product was isolated in 51% yield and modified to be used as precursor in the synthesis of **HL9** (Section 2.3.7).

The Stille reaction gave a wide range of yields, **HL1** and **HL3** were formed in moderate (45-78%) yield, Whereas **HL2** was produced in a poor yield (20%), due to the formation of the 1,3-dibromo-5-(2-pyridinyl) benzene “by-product” (in approximately 50% yield). In order to improve the yield of **HL2** Negishi cross-coupling was performed and found to be a much better choice to construct this type of ligand.

2.3.4 HL2 Ligand prepared via Negishi Cross-Coupling

Ligand **HL2** was prepared *via* Negishi cross-coupling reaction. The Negishi coupling reaction becomes a preferred chosen method mainly because of a few beneficial factors to organic synthesis which distinguish Negishi coupling from other cross coupling reactions. First, Negishi coupling proceeds with generally high efficiency, specifically high yields and high selectivity. Second, organozinc reagents are more reactive than tin and boron reagents and can tolerate more functional groups than Grignard reagents. Third, Negishi coupling often can be performed under mild conditions; unlike Suzuki and Stille couplings, cross coupling with organozinc reagents does not require base or other additives. Another useful feature of Negishi coupling is operational simplicity as the organozinc can be generated *in situ* and used directly in the subsequent cross coupling. Finally, unlike Stille coupling using highly toxic organostannanes, Negishi coupling with organozinc is more environmentally benign.

HL2 was prepared following a literature method.⁹⁵ The reaction required initial preparation of a pyridylzinc chloride species, which is then cross-coupled with a 1,3,5-tribromobenzene in the presence of Pd(PPh₃)₄ as a catalyst. Pyridylzinc chloride species are prepared *via* lithium-halogen exchange between 2-bromopyridine and ⁿBuLi at -78°C in THF, followed by nucleophilic substitution with ZnCl₂. **HL2** was successfully isolated in 61% yield (Scheme 2.5).



Scheme 2.5: Negishi coupling reaction for **HL2**.

The remaining bromine in **HL2** was used for further cross-coupling to introduce the requisite butyl group via Sonogashira coupling. This strategy will be discussed in more detail in the next section.

2.3.5 Sonogashira Coupling Reactions

A Sonogashira coupling is a palladium catalysed reaction for coupling a terminal sp hybridized carbon from an alkyne with a sp^2 carbon of an aryl or vinyl halide.¹⁰⁰ The reaction name arises from the discovery in 1975 by Sonogashira, Tohda, and Hagihara that this process could be performed easily at room temperature using a palladium source such as $PdCl_2(PPh_3)_2$ as catalyst, combined with a co-catalytic amount of CuI . The full reaction mechanism is still not completely understood, but the widely accepted mechanism follows the pathway shown below (Figure 2.3) which involves two catalytic cycles working in tandem to produce the final alkyne product.¹⁰⁰

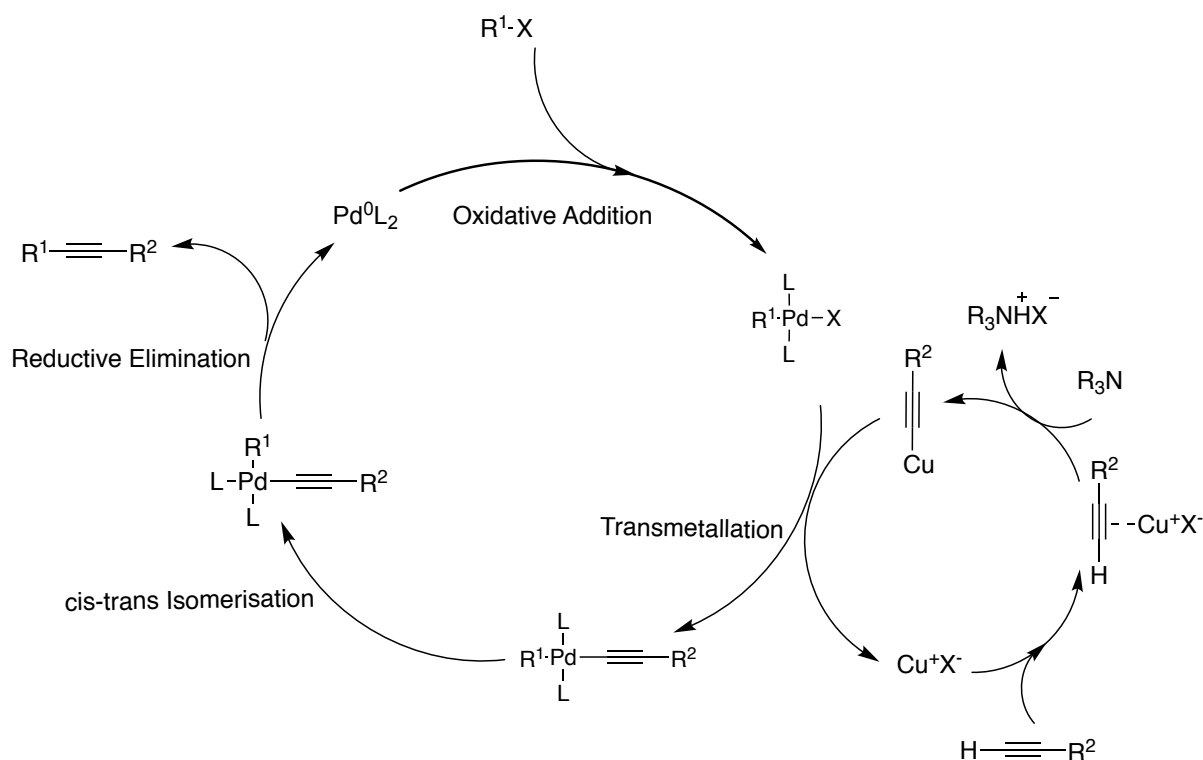
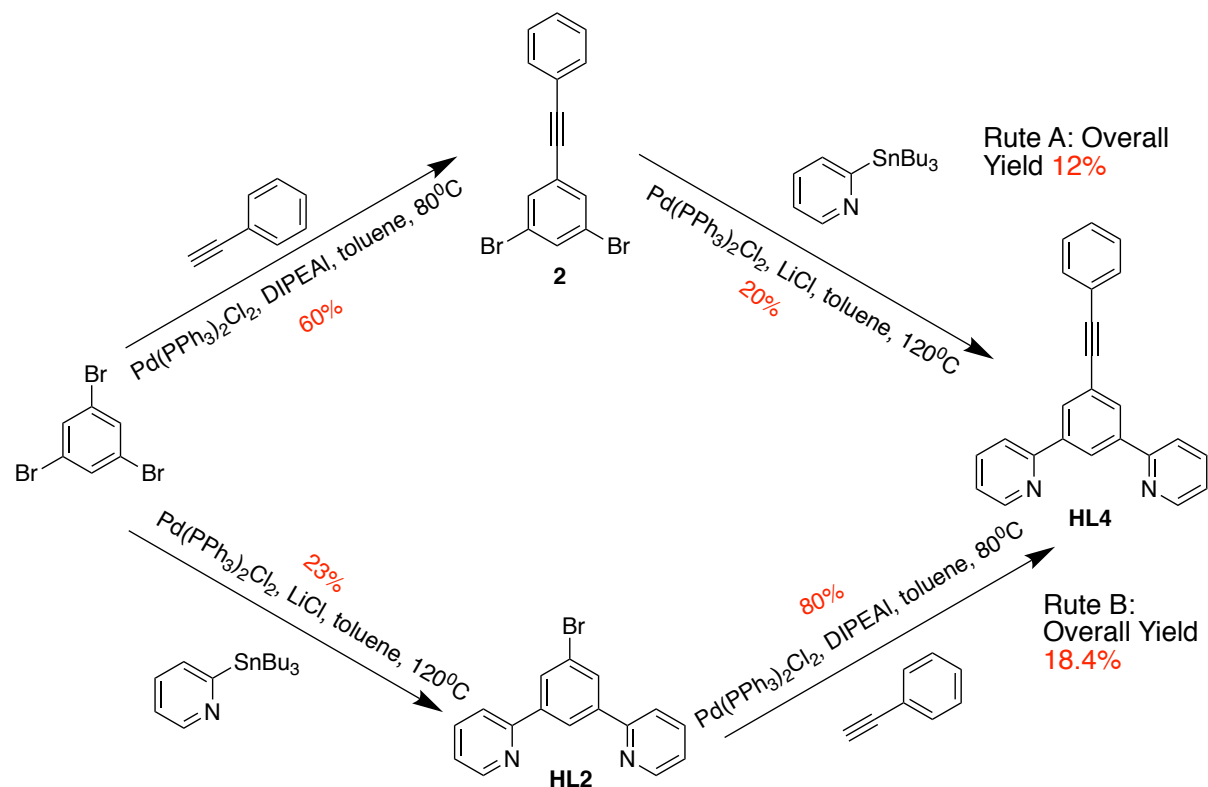


Figure 2.3: Proposed mechanism for the Sonogashira reaction.¹⁰⁰

From the key intermediate **HL2**, the substitution of the final bromine atom on the benzene ring could readily be achieved through Sonogashira cross-coupling reactions, (Scheme 2.6: Route B) to generate ligands **HL4**, **HL5**, and **HL6** (Scheme 2.7) using commercially available butyl alkyne or the synthesised 1-ethynyl-4-hexylbenzene. An alternative approach of mono-substituting the 1,3,5-tribromobenzene (**tbb**) starting material with the requisite lipophilic-group by Sonogashira coupling, prior to reaction with stannylpyridine, was also investigated and shown to be a less viable option, (Scheme 2.6: Route A).

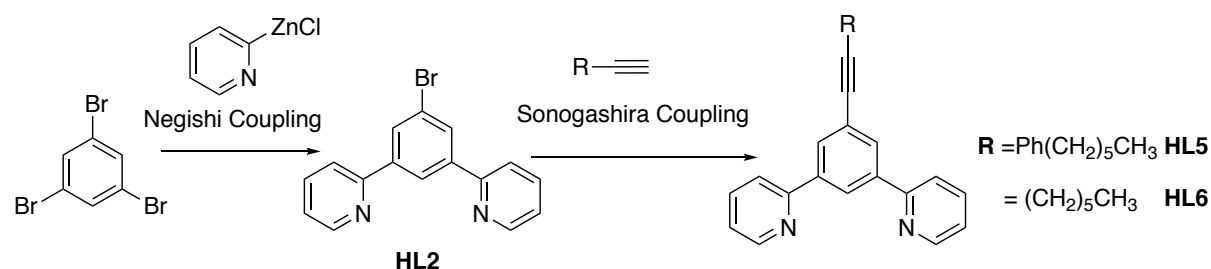


Scheme 2.6: Two synthetic routes through alternative Stille and Sonogashira couplings for the production of **HL4**.

The 5-alkyne substituted 1,3-dipyridylbenzene ligand **HL4** was synthesised from **tbb** using different systems of cross-coupling reactions. Two routes were investigated to generate **HL4** in relatively high yield. First route proceeded via the intermediate **HL2**, obtained by Stille-coupling of **tbb** with 2 equiv. of (tributylstannyl)-pyridine in dry toluene at 120°C, the remaining bromine atom is then available for further Sonogashira cross-coupling to introduce the required alkynal group (Scheme 2.6, route B). Second route proceeded by monosubstituting the **tbb** with one equivalent of the required lipophilic group using Sonogashira coupling in toluene at 80°C, the remaining two bromines are then substituted by two equivalents of 2-pyridyl group via Stille coupling (Scheme 2.6, route A). Route B, was thought to be the most

viable option to generate **HL4** and this method was also employed for the production of ligands **HL5** and **HL6**.

As discussed in Section 2.3.4, **HL2** was synthesised by Negishi coupling to generate a relatively high yield. Therefore, **HL5** and **HL6** were synthesised via route B starting from Negishi coupling followed by Sonogashira coupling (Scheme 2.7).

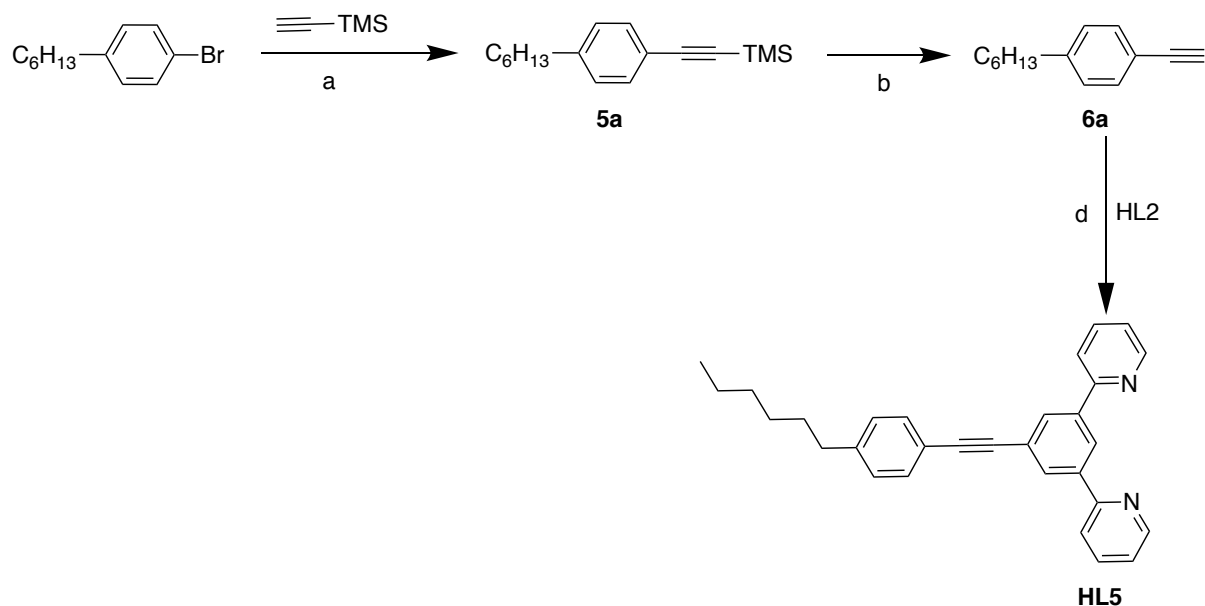


Scheme 2.7: General synthetic route for **HL5** and **HL6** ligands.

To enhance the lipophilicity of the ligands, a greasy substituent (alkyl chain), was inserted on the para position of the benzene ring. This was achieved by substituting the bromine in the intermediate **HL2** with either commercially available 1-octyne to give **HL6** or synthesised (1-ethynyl-4-hexylbenzene) to give **HL5**, both produced via Sonogashira cross coupling. An important note when preparing to carry out Sonogashira type reactions is the susceptibility of the reaction to be compromised in the presence of oxygen. This issue results from the copper catalyst and basic solvent allowing homo-coupling of two deprotonated alkyne molecules to form a 1,3-diyne; known as the ‘Hay coupling product’.¹⁰¹ To avoid this unwanted side reaction, all glassware must be thoroughly cleaned and dried in an oven before use, cooled in a desiccator and kept under nitrogen to avoid oxygen/moisture exposure within the reaction vessel.

HL6 was generated by reacting two equivalents of 1-octyne with one equivalent of **HL2** in toluene in the presence of Pd(PPh₃)₄ as a catalyst combined with CuI. The reaction mix was subjected to 3 cycles of a freeze-pump-thaw process to degas the reaction chamber in a Schlenk flask as the reaction vessel and left for 24 hr. at room temperature. Unfortunately, the conversion of the bromine was not achieved so the temperature was raised to 80°C and that provided the desired para-substituted product in a yield of 91%. TLC analysis showed the

reaction was incomplete after stirring at 80°C for 3 hr, however at 18 hr the presence of a single spot on the TLC plate demonstrated the completion of the reaction. After a Celite filtration to remove the palladium and copper, a silica plug was used to purify the product.



Scheme 2.8: The synthetic route of **HL5**: a) CuI, Et₃N, PdCl₂(PPh₃)₂, PPh₃, 18 h., in toluene at 70°C; b) K₂CO₃, in dry CH₃OH/ THF, 18h. r.t; d) CuI, DIPAE, Pd(PPh₃)₄, 18 h.; in toluene at 80°C.

HL5 was synthesised through palladium-catalysed Sonogashira coupling reaction of **HL2** with the corresponding acetylene derivatives (Scheme 2.8). **6a** was synthesised following a literature procedure and obtained as yellow oil in 87% yield.¹⁰² This was reacted with **HL2** following the same Sonogashira method used for **HL6** to give 2,2'-(5-((4-hexylphenyl)ethynyl)-1,3-phenylene) dipyridine **HL5**, in excellent yield (94%).

2.3.6 The Click Reaction

Using the term ‘click reaction’ indicates that the reaction occurs as a one pot synthesis, has a high thermodynamic driving force that drives it irreversibly to a high yield of a single product, and provides very few by-products.^{103,104} In this work, the term ‘click chemistry’ refers to a specific reaction involving a 1,3 cycloaddition of an azide to an alkyne, forming a 1,4 substituted 1,2,3 triazole. This is known as the copper(I) catalysed alkyne-azide cycloaddition (CuAAC reaction). Early work on this reaction was able to afford a mixture of 1,5 and 1,4 substituted products, but it was found that the addition of a copper(I) catalyst provided improvements on the true concerted cycloaddition which proceeded without a catalyst.¹⁰⁵ Two groups reported independently that a Cu(I) catalyst affords the 1,4 product alone, required a lower temperature and had a faster reaction rate.^{106,107} The reaction mechanism (Figure 2.4) was originally thought to involve only one copper atom; however, the recent interpretation, supported by isotope studies, is that two catalytic copper atoms are involved in this coupling.¹⁰⁸

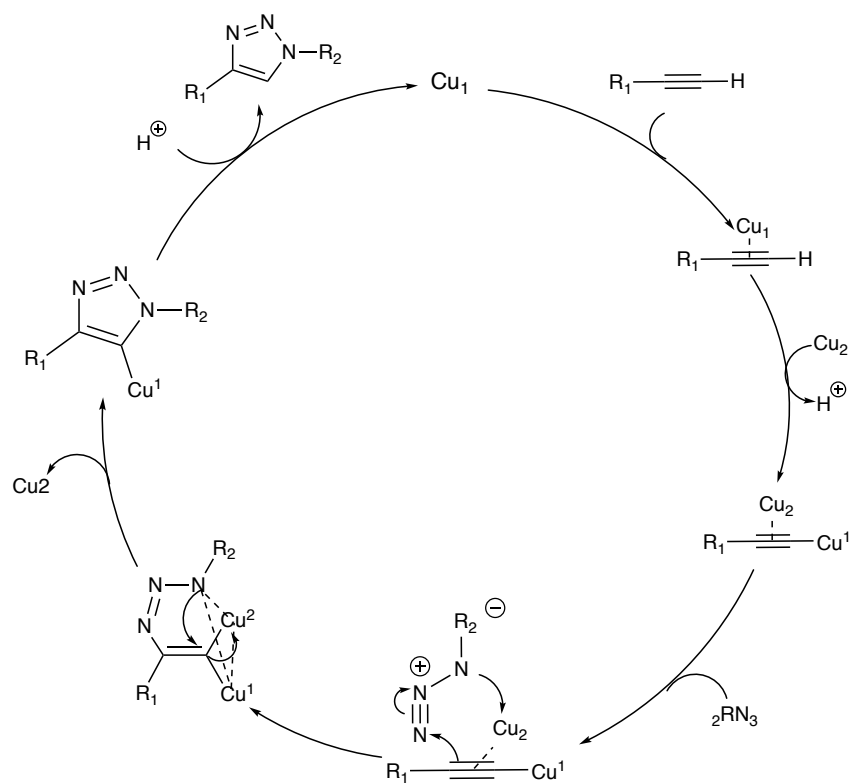
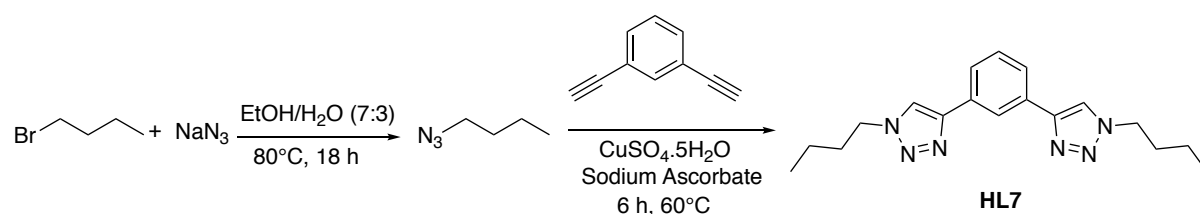


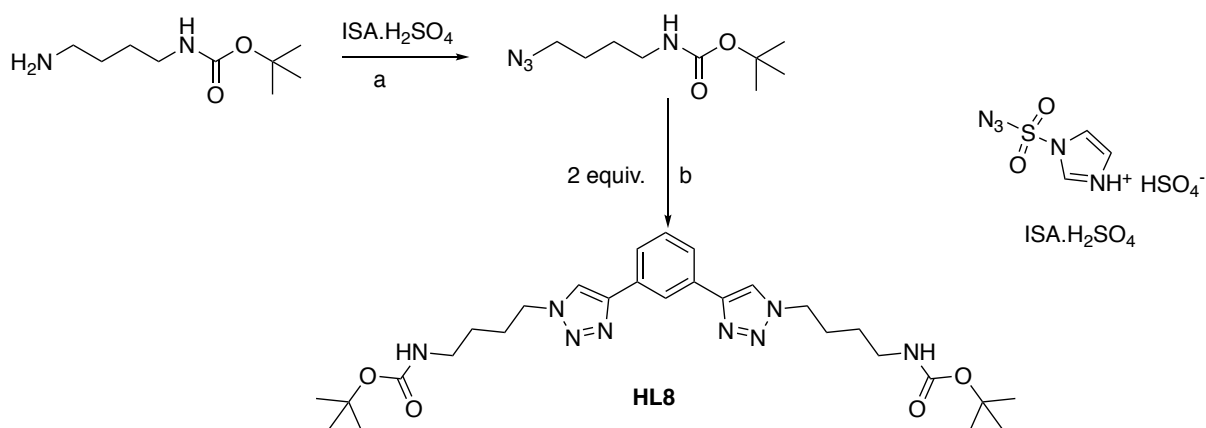
Figure 2.4: Reaction mechanism of the ‘click’ type reaction, better termed a copper(I)-catalysed azide-alkyne cycloaddition (CuAAC).¹⁰⁹

The **CuAAC** cycloaddition approach was used to synthesise polyamine based ligand **HL7**. Starting from bromobutane, the bromide can be easily substituted with azide functionality *in situ* (Scheme 2.9) by using sodium azide. *In situ* generation of azides is an important consideration as it avoids the need for isolation of potentially explosive and hazardous azides. The alkyne *i.e.* 1,3-diethynylbenzene was added to the reaction mixture along with $\text{CuSO}_4 \cdot 5\text{H}_2\text{O}$ and sodium ascorbate to generate the desired triazole ligands. The sodium ascorbate acts as the reductant in the reaction to reduce Cu(II) to Cu(I) , which acts as a catalyst for this reaction.¹¹⁰ The synthesis of the azide, followed by the triazole ligand is completed as a one-pot reaction, with good yield and good purity, showing the importance of click chemistry. **HL7** was prepared in moderate yield (54%) in high purity by recrystallisation from EtOAc/Hexane to give the title compound as a white solid.



Scheme 2.9: Synthetic route for **HL7**.

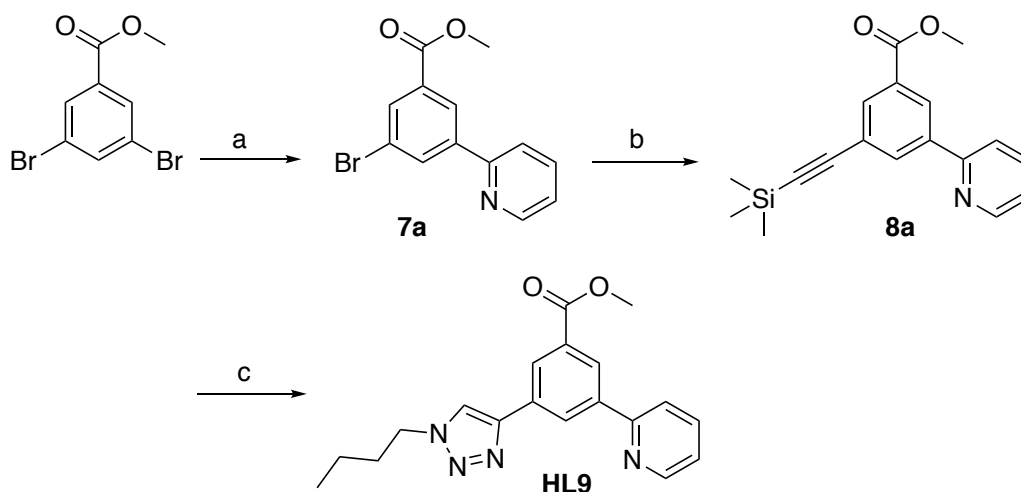
An alternative for synthesis of aryl triazoles was also explored. Using a catalytic diazotransfer reaction, the ligand can be prepared directly from a polyamine; however, protecting groups are needed to prevent azide formation at multiple sites (Scheme 2.10).¹¹¹ A diazotransfer agent is normally a sulfonyl azide which causes the interconversion of an amino to an azido group. The sulfate salt of imidazole sulfonyl azide (ISA) is chosen as a diazotransfer agent as this reagent has a longer shelf life and hence can be stored for long periods of time. Also, this is less sensitive to shock than its neutral form or other salts such as the hydrochloride.¹¹² Even so, caution must be taken when handling and storing the reagent to ensure there is no decomposition to give HN_3 .



Scheme 2.10: Reagents and conditions: (a) ISA.H₂SO₄, NaHCO₃, CuSO₄.5H₂O, MeOH/H₂O (3:1), rt, 1 hr; (b) 1,3-diethynylbenzene, NaAsc, 60°C, 18 hr, 57%.

2.3.7 Synthesis of HL9

The synthetic route to the asymmetric **HL9** features both a pyridine and 1,2,3-triazole ring. This required a sequence of Stille and Sonogashira-type cross-coupling reactions, followed by the cleavage of the trimethylsilyl (TMS) group, yielding the pyridine-function alised alkyne building block, which was readily converted into the N^CN- ligand *via* a (CuAAC) reaction (Scheme 2.11).

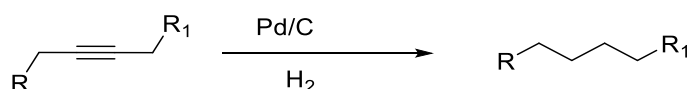


Scheme 2.11: Synthetic route to HL9. Reagents and conditions: (a) 2-tri-*n*-butylstannylpyridine, Pd(PPh₃)₂Cl₂, LiCl, toluene, reflux, 24h, 51%. (b) trimethylsilyl acetylene, Pd(PPh₃)₂Cl₂, PPh₃, Et₃N, THF, 48h, r.t. (c) K₂CO₃, (4:1, THF:H₂O), 1-Bromobutane, sodium azide, sodium ascorbate, CuSO₄.5H₂O 60°C for 72h.

7a was isolated as a side-product from the synthesis of **HL3** Stille coupling reaction with ($R_f = 0.75$) as a white solid (51%). The remaining bromine atom on the benzene ring was functionalized further by incorporating a butyl chain (greasy group), via a click reaction. **8a** was successfully synthesised by a Sonogashira coupling reaction and isolated in excellent yield 89% as orange oil. As previously established in the literature, the TMS-alkyne on **8a** must be deprotected to undergo a 1,3-dipolar cycloaddition.¹¹³ Thus, a one pot reaction of desilylation, and cycloaddition was performed in the presence of potassium carbonate, which acts as a base in the nucleophilic substitution reaction, as well as to remove the TMS from the alkyne. The desired compound was purified by column chromatography on silica gel (eluent: ether/DCM 20:80) to afford **HL9** as a sticky yellow oil in a yield of 30%.

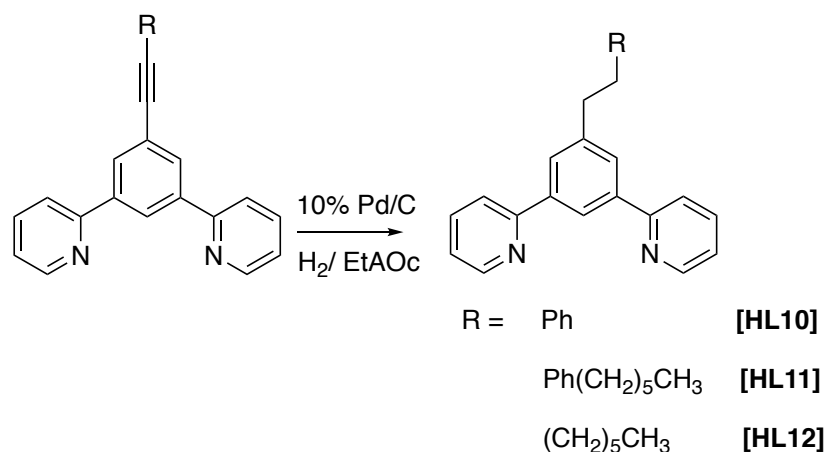
2.3.8 Alkyne Hydrogenation

The necessity of alkyne reduction on ligands **HL4**, **HL5** and **HL6** was raised to overcome obstacles with complexation of the ligands with K_2PtCl_4 ; issues arising from this include products with a mixture of ketone and alkyne based complexes (see Section 3.1 for details). Alkynes can be reduced using hydrogen in the presence of a metal catalyst such as palladium on activated charcoal (Pd/C) to give alkanes (Scheme 2.12).¹¹⁴



Scheme 2.12: Hydrogenation of an alkyne with Pd/C and H_2 to give the alkane.

HL10, **HL11** and **HL12** were all generated via a hydrogenation reaction of their corresponding substrates (Scheme 2.13). The reactions were performed in ethyl acetate in the presence of a 10% Pd/C catalyst, and under an atmosphere of hydrogen at 30°C for 48 h. Hence, Pd/C catalyst was added in excess amount to enhance the interaction of ligands and H_2 on the solvent surface. From a safety perspective, activated Pd/C is pyrophoric and thus safety caution must be taken during and after the reaction. Completion of the reaction was confirmed by MS and the desired products were isolated in quantitative yield without further purification.



Scheme 2.13: Hydrogenation reaction scheme for **HL10**, **11** and **12**.

2.4 Spectroscopic Characterisation of Tri-dentate N[^]C[^]N ligands

2.4.1 NMR Spectroscopy

All ligands **HL_n** (n = 1-12) were fully characterised by 2-D ¹H and ¹³C NMR spectroscopy and mass spectrometry. The aromatic region of the proton NMR spectra of the symmetric terdentate pyridyl-benzene ligands was generally straightforward to assign, due to the recurrence of certain trends in the NMR scale. (Figure 2.5) shows the generic numbering used for all symmetrical ligands prepared here – the pyridyl groups have been given priority over any substituent to aid comparison.

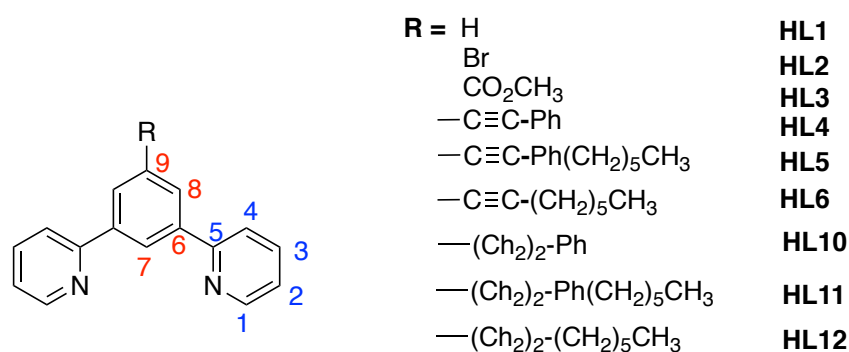


Figure 2.5: General numbering scheme of the symmetric terdentate ligands.

To describe the patterns observed in the proton NMR spectra of such ligands, it is easiest to start by describing trends observed in the precursors. For example, the proton NMR of 1,3-dibromobenzene consists of two triplets and a doublet in the aromatic region. The triplet at lowest frequency corresponds to proton H₉ and the triplet of highest frequency to H₇, which is confirmed by the relative magnitudes of the J-couplings. The doublet, which occurs in-between these resonances, corresponds to H₈, with a relative integration of two protons. Similarly, methyl 3,5-dibromobenzoate consists of one triplet which corresponds to H₇, one doublet H₈, both are in the aromatic region and one singlet CH₃ in the aliphatic region. In this molecule, H₉ has been replaced by carboxylate ester. In comparison, 1, 3, 5- tribromobenzene contains one singlet with a relative intensity of three protons, at 7.92 ppm only, which corresponds to H₈ and H₇. These patterns are carried through to the respective tridentate ligands.

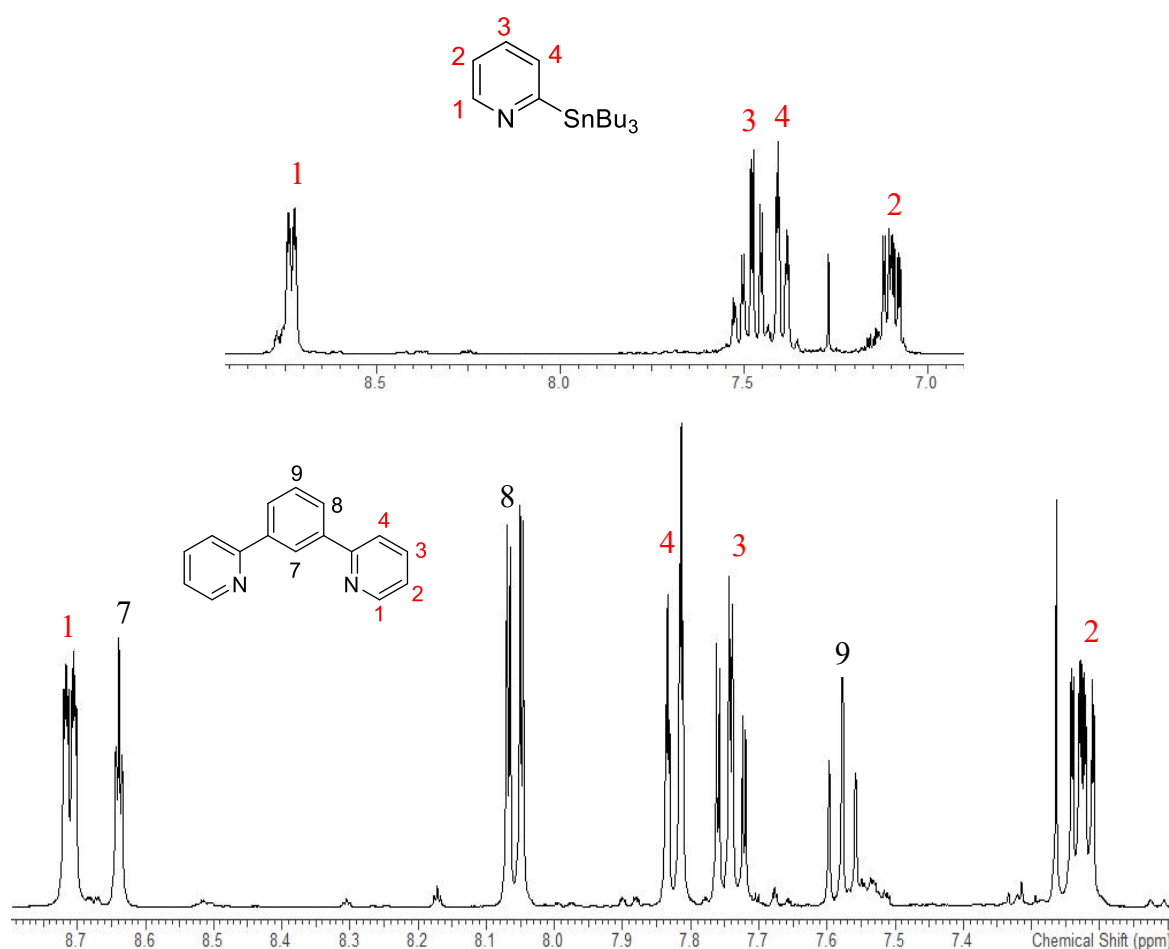


Figure 2.6: ¹H NMR spectra (CDCl₃, 400 MHz) of ligand precursor (2-tri-nbutylstannyl pyridine)(top) and the resultant terdentate ligand, 1,3-di(pyridin-2-yl)benzene (bottom).

The ^1H NMR spectra of 2-tri-*n*-butylstannylpyridine and 2-bromopyridine show a consistent trend of peak ordering, regardless of any additional substituent. H_2 always occurs at the lowest frequency, and H_1 always occurs at the highest frequency, with H_3 and H_4 peaks occurring somewhere in-between. This trend was carried through to the ligand (Figure 2.6), where COSY spectra and the J -splitting pattern were used in the assignments. In addition, the proton NMR spectra of tri-*n*-butylstannyl pyridine species showed satellites around the H_4 signal. Tin has three spin 1/2 nuclei (^{115}Sn , ^{117}Sn and ^{119}Sn) hence the satellites arise through J coupling to tin.

The NMR spectrum of **HL2** was also used for a comparison with **HL6**, **HL3** and **HL12** substituted ligands. The aromatic region of the proton NMR spectra of these ligands was nearly identical, as they show a consistent trend of peak ordering, regardless of any additional substituent. H_2 always occurs at the lowest frequency, and H_1 always occurs at the highest frequency, with H_3 , H_4 , H_7 and H_8 peaks occurring somewhere in-between. Upon substitution of the bromine by an alkyne group H_7 is notably shifted down field on **HL6** as well as the peak corresponding to H_8 (Figure 2.7).

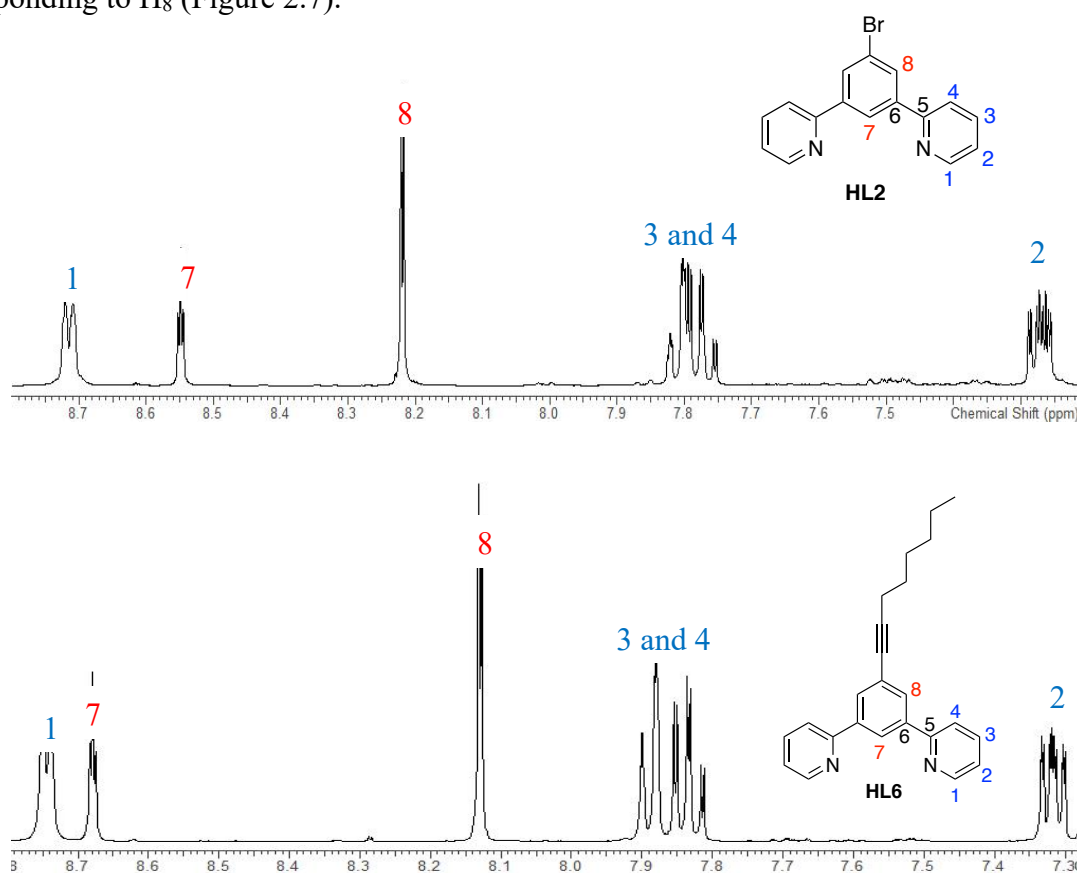


Figure 2.7: ^1H NMR spectra (CDCl_3 , 400 MHz) of ligand intermediate **HL2** (top) and the resultant terdentate ligand **HL6** (bottom).

For ligands containing an ethynyl benzene on the substituted H₉ position (**HL4**, **HL5**, **HL10** and **HL11**) extra peaks were observed in the aromatic region. Three extra peaks were detected for **HL4** and **HL10**, all of them appeared in between H₂ and (H₃ and H₄). Whereas, **HL5** and **HL11** proton NMR spectra show two extra peaks, which appear at lower frequency than H₂. However, H₁₃ proton peak on **HL5** appears at a higher frequency than H₂ and upon hydrogenation of the neighbouring alkyne, the H₁₃ proton peak moved to a lower shift as the protons become more shielded (Figure 2.8). Also, it can be clearly observed, two extra peaks on the aliphatic region appears which corresponds to the hydrogenated alkyne H₁₀ and H₁₁.

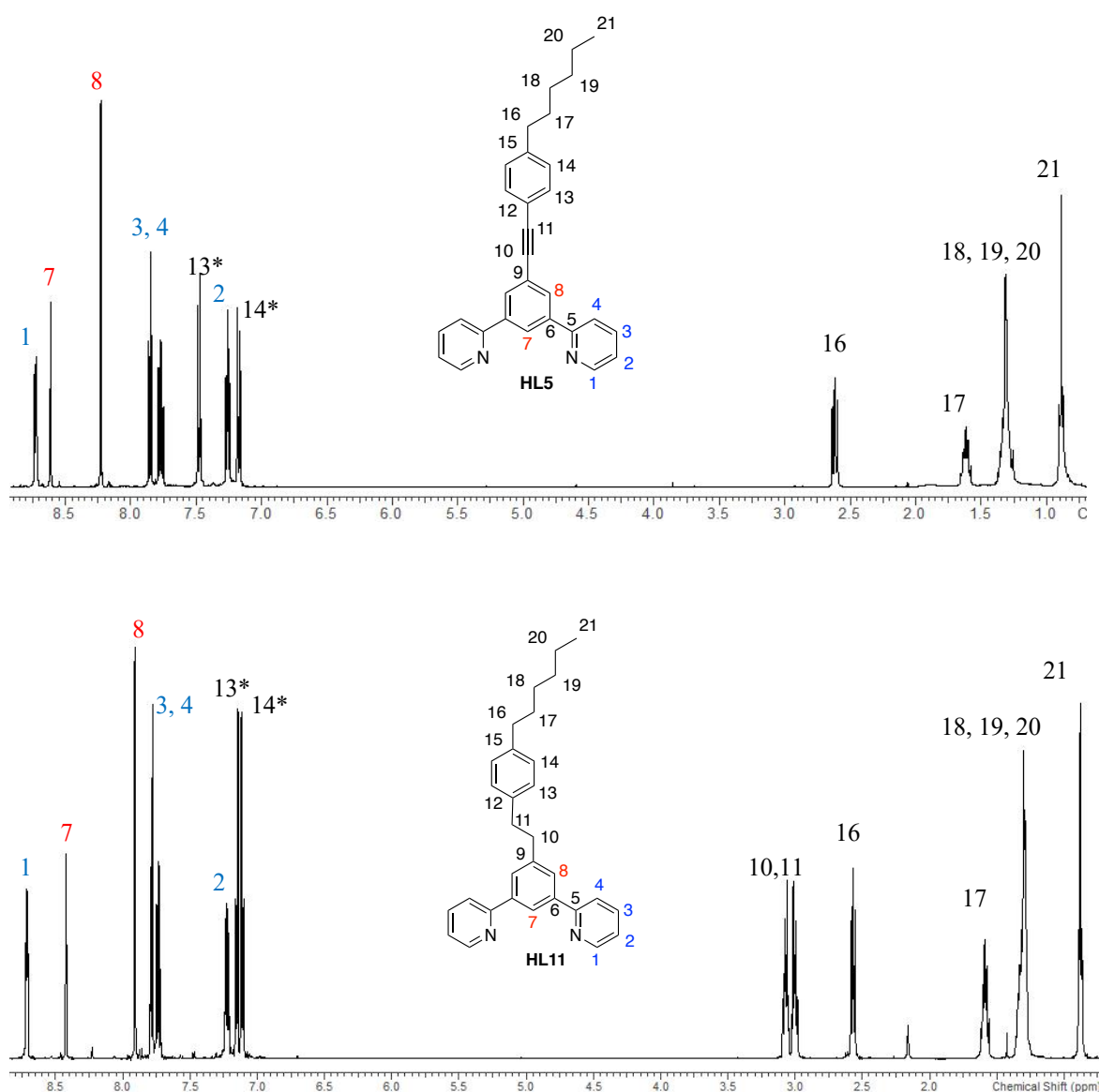


Figure 2.8: ¹H NMR spectra (CDCl₃, 400 MHz) of ligand **HL5** (top) and the resultant hydrogenated ligand **HL11** (bottom).

^{13}C NMR spectroscopy has been also used to confirm the alkyne hydrogenation of **HL4** and **HL5**. Two peaks corresponding to the alkyne C_{10} and C_{11} disappear upon hydrogenation (Figure 2.9) and are replaced by two peaks in the aliphatic region (not shown).

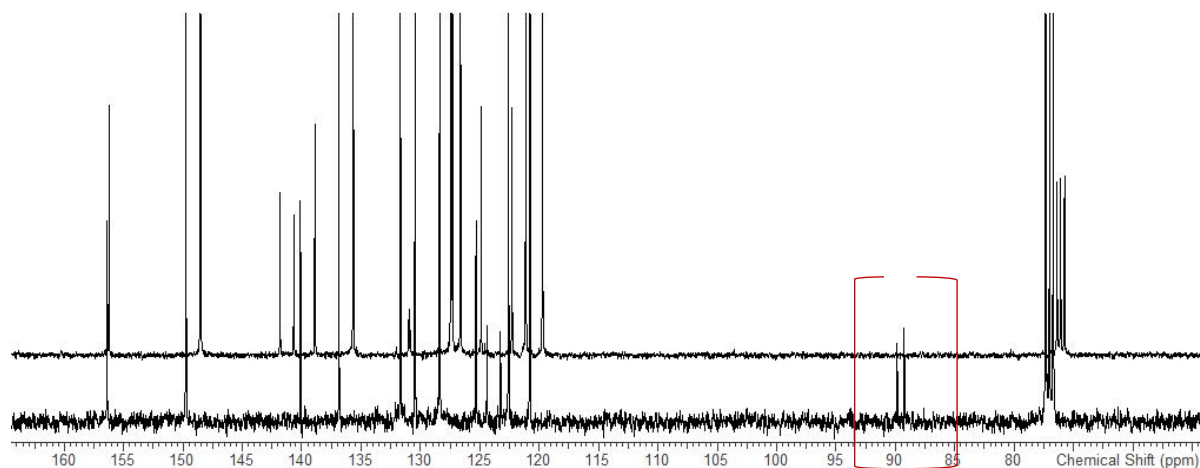


Figure 2.9: ^{13}C NMR spectra (CDCl_3 , 400 MHz) of the resultant hydrogenated ligand **HL11** (top) and ligand **HL5** (bottom).

HL7 and **HL8** were characterised by ^1H and ^{13}C NMR spectroscopy and ES-mass spectrometry. The ^1H aromatic region of **HL7** and **HL8** shows identical proton patterns which contain four peaks. The ^1H NMR spectrum of **HL8** and **HL7** displays a singlet at 7.9 ppm corresponding to H_6 , which confirms the formation of 1,2,3-triazole on both ends as shown in the (Figure 2.10). No alkyne C-H is observed, showing that all of the starting material was consumed, and the reaction has gone to completion. In **HL8** the integration of the protons shows that each signal for the butyl CH_2 groups integrate for 4 protons, which also indicates that the click reaction has occurred on the both ends of 1,3-diethynylbenzene, as does the fact that a spectrum of a symmetrical species is obtained.

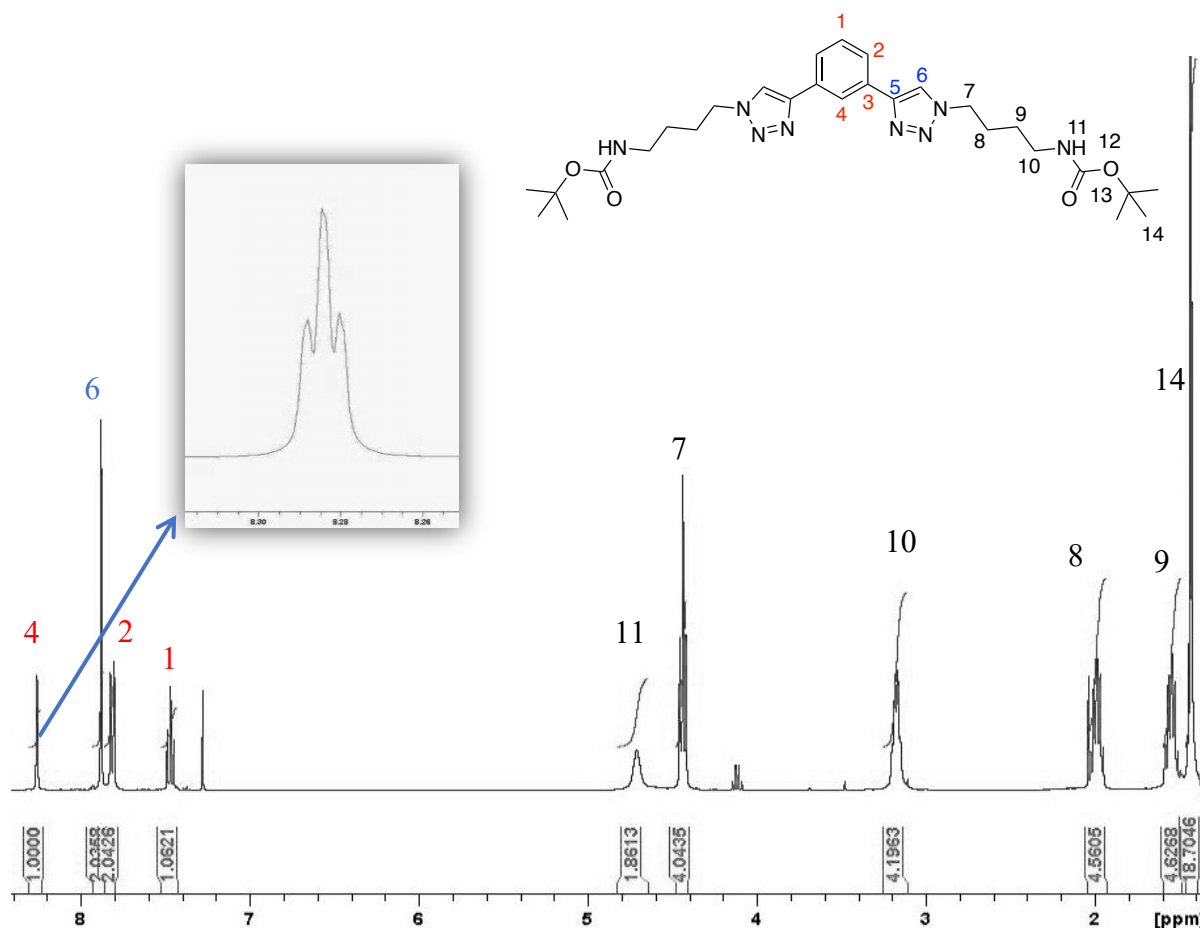


Figure 2.10: ^1H NMR spectra of **HL8** (CDCl_3 , 400 MHz).

In both **HL7** and **HL8**, H_4 (Figure 2.10) shows an interesting feature in the ^1H NMR spectrum. In contrast to a singlet as reported in the literature for **HL7**, this shows as a triplet with a small coupling constant ($J = 1.4 \text{ Hz}$).

The proton NMR spectrum of **HL9** was also similar to that of its precursors. **7a** and **8a** proton NMR spectra show a consistent trend of peak ordering, regardless of any additional substituent. H_2 always occurs at the lowest shift, and H_1 always occurs at the highest shift, with H_3 , H_4 , H_7 , H_9 and H_{11} peaks occurring somewhere in-between. This trend was carried through to the ligand (Figure 2.11). In addition to the former peaks, a singlet peak at 7.78 ppm corresponding to H_{15} was observed on **HL9** ^1H NMR spectra, which confirms the formation of 1,2,3-triazole as shown in Figure 2.11.

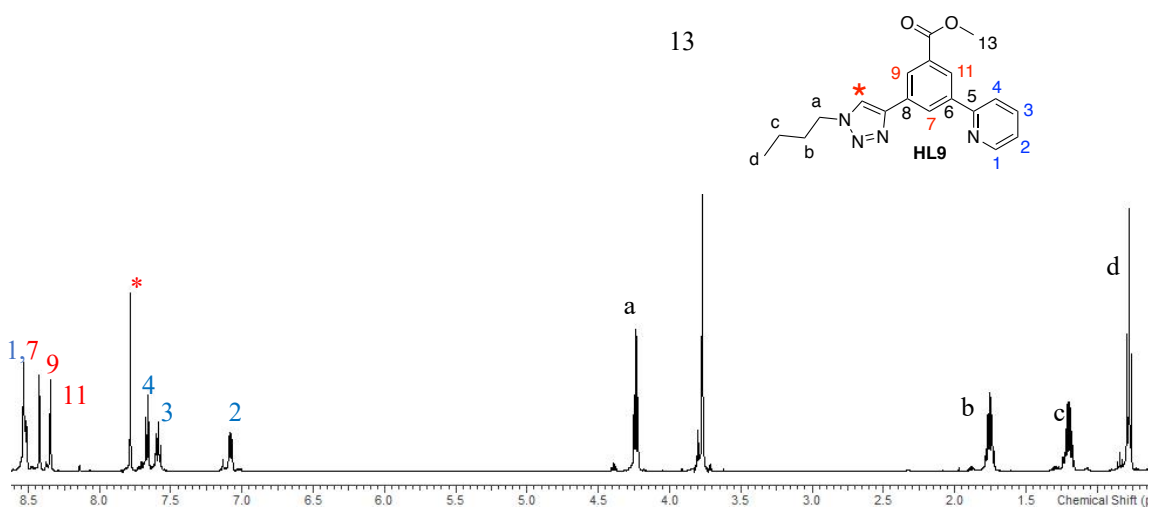
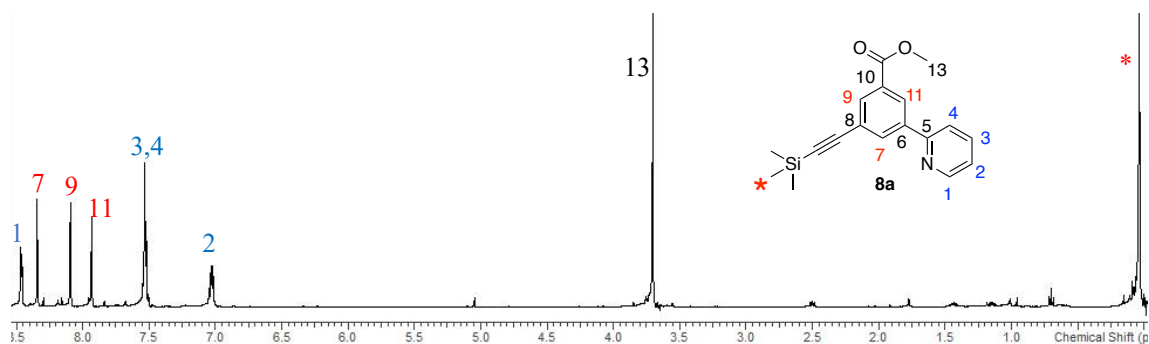
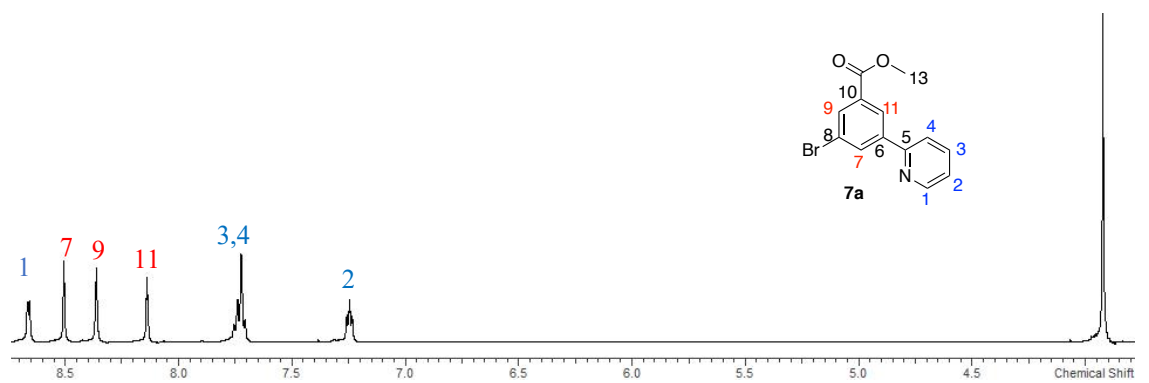


Figure 2.11: ^1H NMR spectra (CDCl_3 , 500 MHz) of precursor **7a** (top), precursor **8a** (middle), and the resultant ligand **HL19** (bottom).

2.4.2 X-ray Crystal Structure

Further, to investigate the structure, single crystals were grown by the slow diffusion of hexane in the solution of **HL7** in ethylacetate and the crystal structure is displayed in (Figure 2.12) including selected bond lengths (\AA) and angles ($^\circ$). The N1–N2 bond length (1.315 \AA) is shorter than the bond length of N2–N3 (1.350 \AA) in the same triazole ring. Due to the free rotation along C–C single bond, one of the triazoles is observed in the flipped position with respect to other.

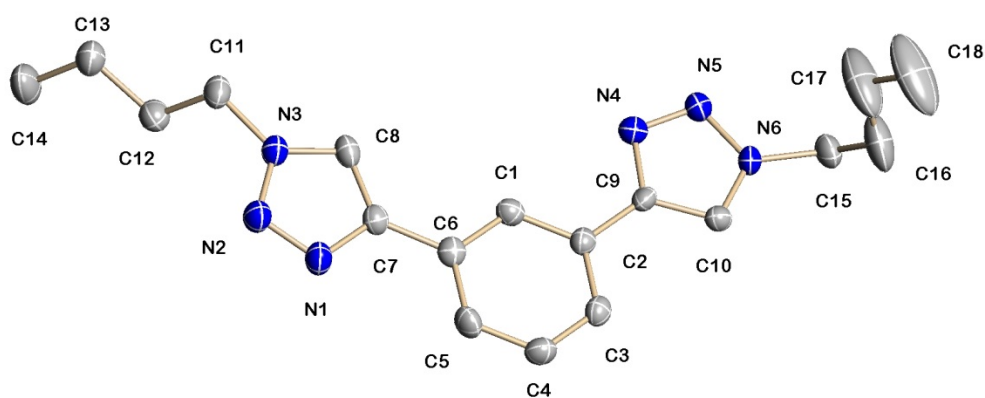


Figure 2.12: Crystal structure of **HL7**, N1–N2(1.315(3)) and N1–C7 (1.367(3)).

2.5 Synthesis of Ancillary Ligands

Another approach to incorporate a polyamine or a lipophilic group into Pt(II) complexes is the substitution of chloride with an ancillary ligand containing one of these functionalities. As previously discussed, the substitution of the weak field ligand, *i.e.* chloride, with a strong field ligand such as an alkynyl ligand will improve the luminescence properties of Pt(II) complexes. Thus, a series of ligands with an alkyne functionality were synthesised *via* different methods such as amine or PEG alkylation, amide coupling and reductive amination of a Schiff base (Figure 2.13). Furthermore, a substitution of the Cl with a pyridine functionalized mono dentate ligand was considered and will be discussed further in the next chapter.

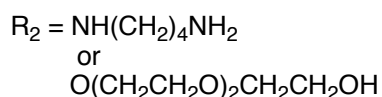
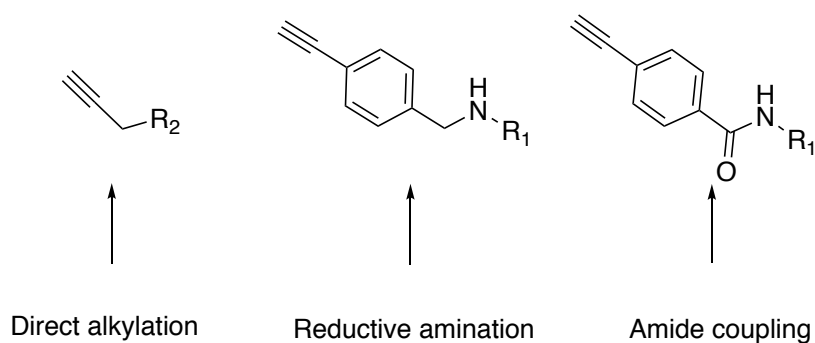
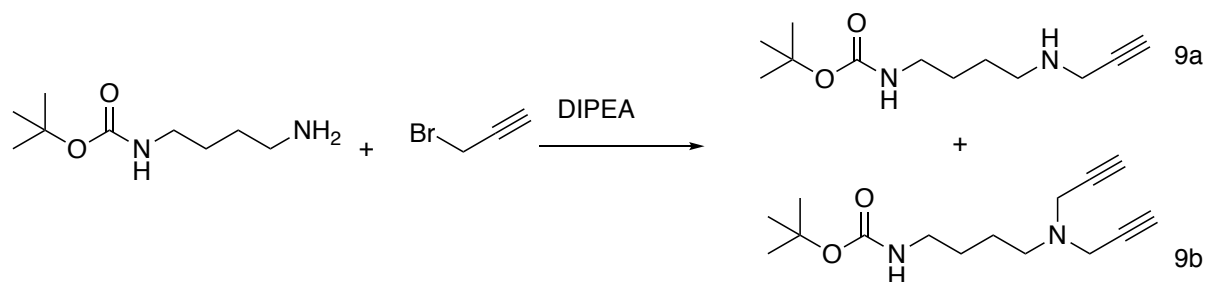


Figure 2.13: The methods that have been adopted to prepare mono ligands systems.

2.5.1 Polyamines and PEG Alkynes Synthesis

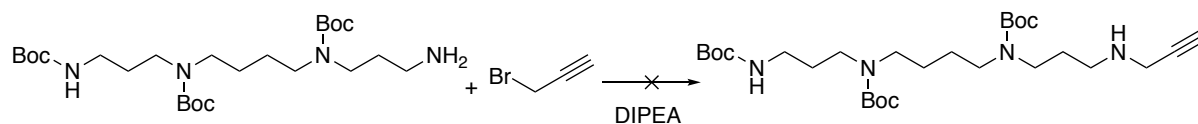
2.5.2 Synthesis of Putrescine Alkyne (9a)

Using the method published by Sund and Wilen,¹¹⁵ **9a** was synthesised by reacting mono Boc-protected putrescine with propargylbromide in presence of DIPEA (N,N-diisopropylethylamine) as a non-nucleophilic base (Scheme 2.14). The addition of propargylbromide was completed very slowly at 0°C in order to reduce the formation of the side product (double alkylation of the primary amine **9b**) as shown in scheme 2.14. The desired product was isolated as a yellow oil in 41% yield, comparable to the reported literature.



Scheme 2.14: Synthesis of putrescine alkyne **9a**.

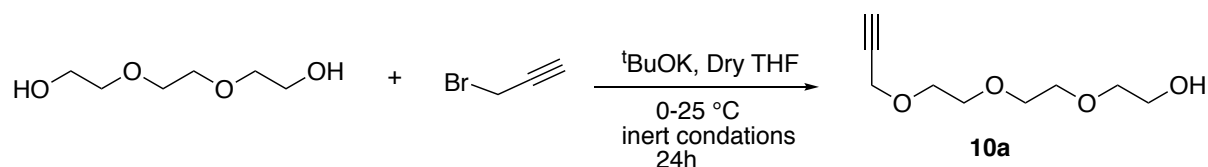
The attempt to apply the same conditions to synthesise a spermine functionalised alkyne was unsuccessful (Scheme 2.15) as the reaction produced a mixture of products which was difficult to isolate or purify due to the resulting products having either a high polarity or similar R_f in a range of different solvent systems. Therefore, an alternative route was adopted to prepare a spermine containing an alkyne that will be discussed in the Section 2.5.5.



Scheme 2.15: Unsuccessful reaction scheme for the synthesis of alkyne functionalised spermine.

2.5.3 Synthesis of PEG alkyne 10a

In an attempt to increase the solubility of the inherently water insoluble Pt(II) complexes, a proposed method of using a polyethylene glycol (PEG) linker was brought to light; in this case, triethylene glycol (TEG). PEG is a family of organic molecules which are soluble in water and many organic solvent systems because of their hydrocarbon chains, and their ether bonds which are able to hydrogen bond. PEG linkers have been used in the literature to increase the solubility and stability of molecules.¹¹⁶ Substituting one of the hydroxyl groups for an alkyne allow a route to potential coordination of the linker to the Pt(II) metal centre via a deprotonated cationic alkyne.¹¹⁷



Scheme 2.16: Synthesis route to PEG alkyne **10a**.

Using the method published by Z Li,¹¹⁸ **10a** was synthesised by the deprotonation of TEG followed by an $\text{S}_{\text{N}}2$ attack on the propargyl bromide, leading to the formation of the desired product (Scheme 2.16). Potassium *tert*-butoxide was used for the deprotonation of the alcohol for two reasons; TEG has a pK_{a} of 14.5 and so a strong base is required to remove the proton, and $t\text{BuO}^-$ is a bulky base and due to the steric hindrance, it is unlikely to undergo any competing substitution reactions.

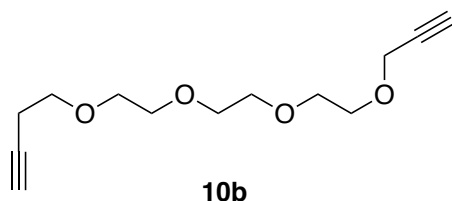


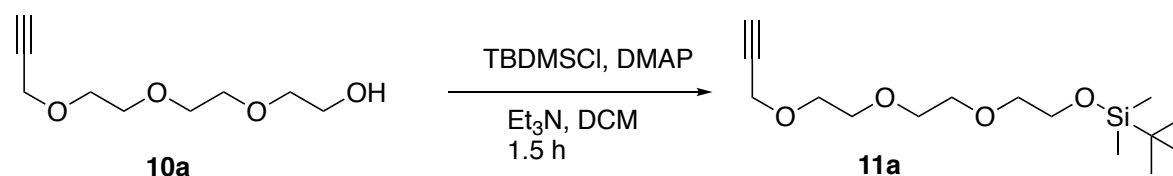
Figure 2.14: Bis-substituted side product **10b** (4,7,10,13-tetraoxahexadeca-1,15-diyne).

A side product of this reaction is the bis-substituted product, where the alkyne has substituted onto both of the alcohol groups (**10b**). Although precautions were taken to reduce this, such as dropwise addition of the propargyl bromide and decreased temperatures. The yield was still lower than that reported by Percec, 47% compared to 90%.¹¹⁸ The bis-substituted product was collected and purified for use in the future by another group member.

2.5.4 PEG Alkyne Hydroxyl Group Protection

Alcohols are very versatile functional groups that participate in a variety of reactions. They can be deprotonated with base which make them good nucleophiles in substitution reactions; they can be protonated, which also make them good leaving groups in substitution and elimination reactions. Alcohols can be oxidized to aldehydes or ketones, or transformed into better leaving groups (alkyl halides, or alkyl tosylates) allowing for a host of substitution and elimination reactions.

All this versatility comes with a drawback, as the alcohol group could get in the way of the intended reaction. This problem appears during the substitution of chloride on Pt(II) complexes, as the hydroxyl group (OH) coordinates to the Pt(II) metal centre leading to a bis-Pt(II) complex coordinating to one PEG alkyne ligand (discussed in more details in Chapter 3). Hence, the need to protect (OH) hydroxyl group on **10a** was essential for the successful synthesis of the desired Pt(II) complex.

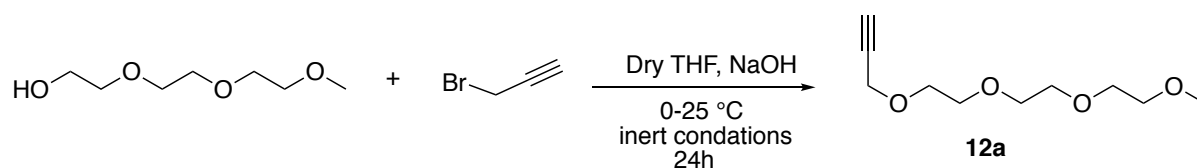


Scheme 2.17: **11a** alcohol group protection reaction with TBDMS.

The most frequent used protecting groups for hydroxyl group are organosilanes. The most common silyl ether used is trimethylsilyl (TMS) however for the aim of the project an acid

labile protecting group is needed. By varying the substituents attached to silicon, the steric and electronic characteristics of the protecting group can be finely tuned, allowing a wide variety of both reaction and deprotection conditions. Thus, *tert*-Butyldimethylsilyl ether (TBDMS) was selected as a suitable protecting group for this purpose due to its ease of installation, high stability under basic and neutral conditions at r.t. The terminal hydroxyl group on **10a** was protected with TBDMS upon the treatment with TBDMSCl in presence of dimethylaminopyridine (DMAP) accompanied by Et₃N in DCM to afford compound **11a** in excellent 93% yield (Scheme 2.17).

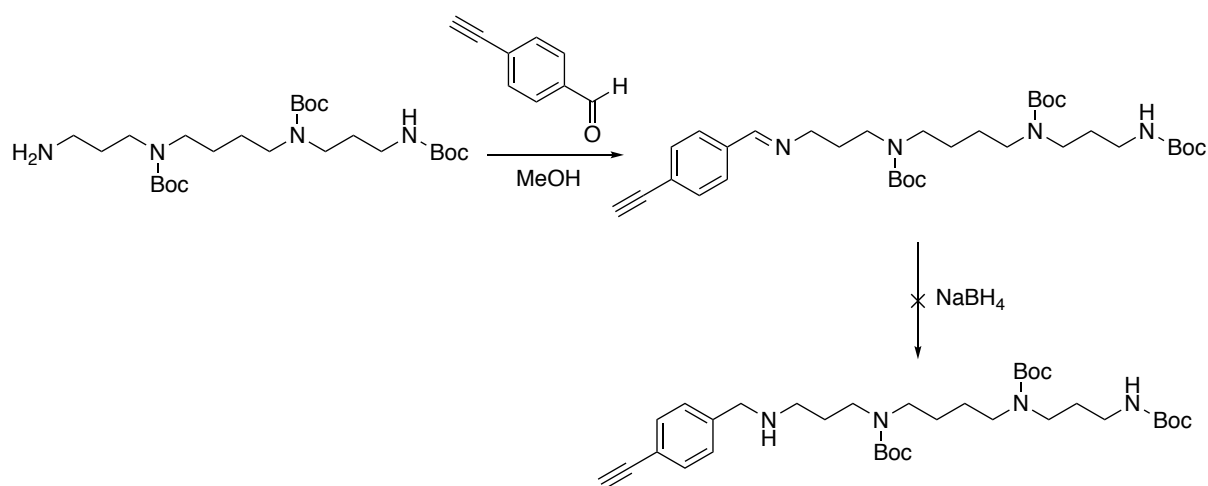
Another way to avoid hydroxyl group protection and deprotection steps was to use triethyleneglycol monomethyl ether which has similar solubility features. Following a literature method, **12a** was synthesised by the deprotonation of TEG followed by an S_N2 attack on the propargyl bromide, leading to the formation of the desired product in 82% yield (Scheme 2.18).¹¹⁹



Scheme 2.18: Synthesis of **12a** PEG alkyne.

2.5.5 Reductive Amination

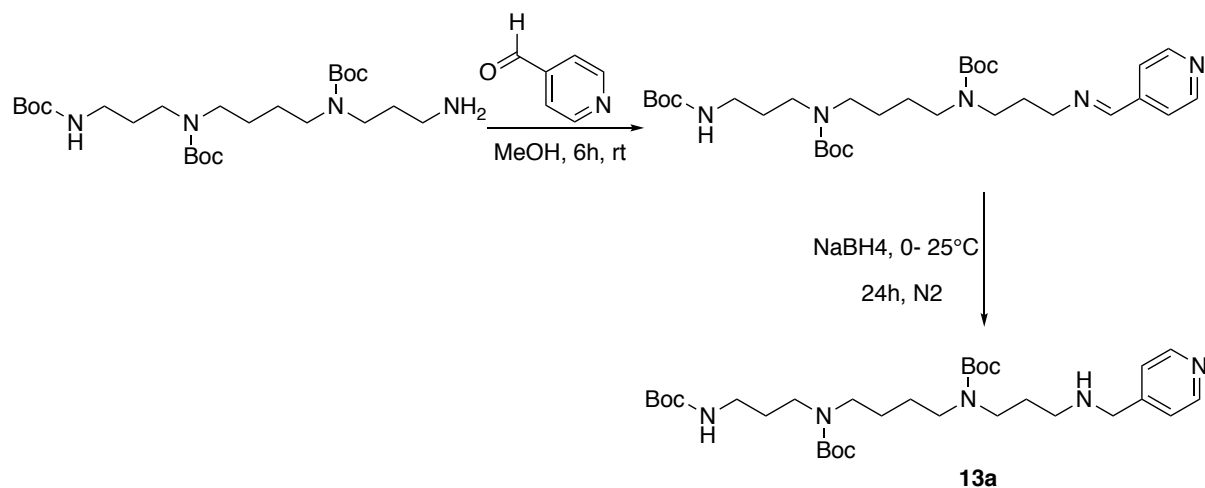
As previously discussed in Section 2.5.2, making amines through direct alkylation is generally not a good method to use. Starting with a carbonyl group that is then converted to an amine *via* an intermediate imine, this process is called a reductive amination.¹²⁰ The reduction can be performed *in situ*, starting with an aldehyde or ketone to form an imine, followed by reduction of the imine with a reducing agent such as sodium cyanoborohydride (NaBH_3CN), sodium borohydride (NaBH_4), or sodium tri-acetoxyborohydride ($\text{NaBH}(\text{OAc})_3$) giving a new amine. This method was attempted in the synthesis of a spermine bearing alkyne ligand (Scheme 2.19).



Scheme 2.19: Unsuccessful reductive amination reaction.

A reductive amination reaction was attempted *via* reacting a tri-Boc protected spermine with 4-ethynylbenzaldehyde in MeOH using NaBH_4 as a reductant. At the first step, full consumption of the aldehyde alongside imine formation was observed and confirmed by MS analysis and NMR spectroscopy. However, the reductive step to generate the desired product was unsuccessful, which may be due to a reduction of the terminal $\text{C}\equiv\text{C}$ triple bond alkyne or over alkylation of the tertiary amine. An alternative approach involves the use of weaker reducing agent like sodium cyanoborohydride (NaBH_3CN) was attempted in order to avoid reducing the alkyne. However, NaBH_3CN can only perform in acidic condition in order to ensure the formation of the iminium ion prior to the reduction. This was a problem because

Boc-protection groups can undergo cleavage under acidic conditions.¹²⁰ To overcome this limitation and avoid the reduction of the alkyne, tri-Boc protected spermine would be attached to an alkyne *via* amide coupling; this will be discussed in further detail in Section 2.5.6.

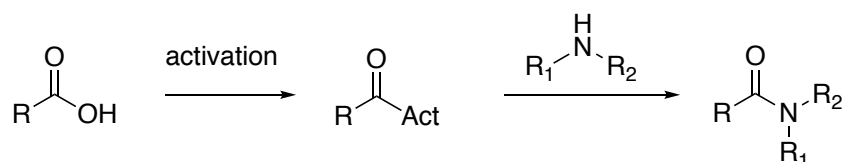


Scheme 2.20: Synthetic route of **13a**.

4-pyridine substituted with a polyamine (tri-Boc spermine) **13a** was also prepared *via* the above reductive amination route, with 4-pyridinecarboxaldehyde being used instead of 4-ethynylbenzaldehyde (Scheme 2.20). This reaction proceeded efficiently, affording **13a** in 76% yield without the need for further purification.

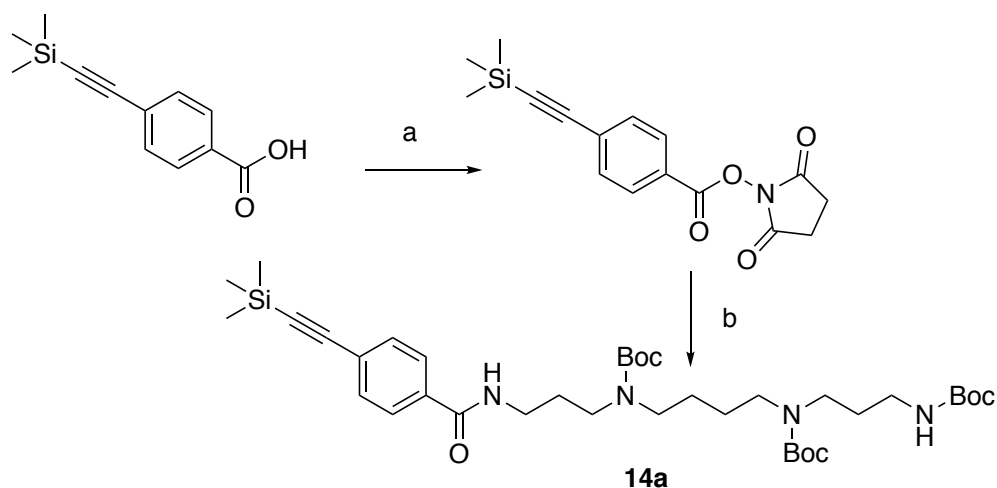
2.5.6 Amide Coupling Reaction

Amide bond formation is a powerful method of coupling two fragments of a molecule. Recent advances in this area offer a huge variety of reagents under very mild conditions with broad substrate tolerance which make it a good candidate for the conjugation of Boc-protected amines.



Scheme 2.21: Principle of the activation process for amide-bond formation.

Amide bonds are typically synthesised from the union of carboxylic acids and primary amines in the presence of a coupling reagents such as N-hydroxy succinimide (NHS) and carbodiimides such as di isopropyl carbodiimide (DIC). It is usually necessary to first activate the carboxylic acid, a process that usually take place by converting the -OH of the acid into a good leaving group prior to treatment with the amine (Scheme 2.21).

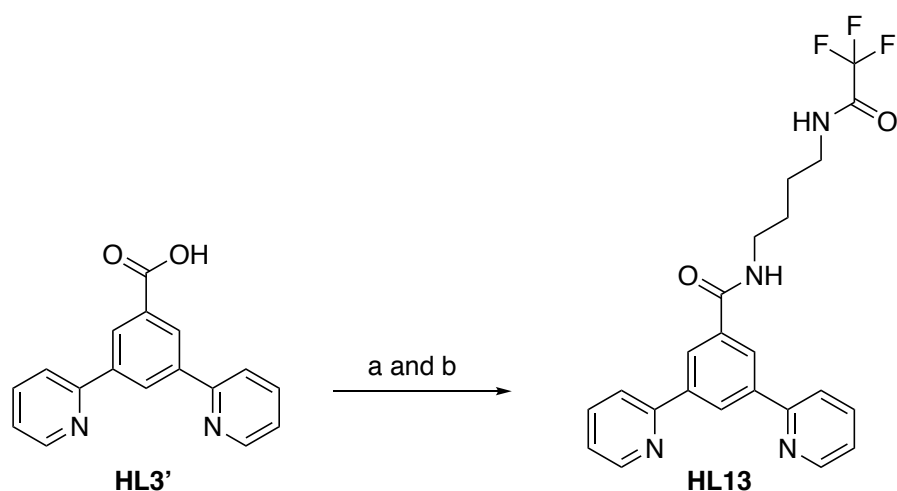


Scheme 2.22: Synthetic route to **14a**. **Reagents and conditions:** (a) DIC, NHS, Et_3N , dry DCM, r.t, 1h; (b) **4a**, dry DCM, MW 50°C, 1h, 35% over two steps.

14a was prepared following the aforementioned method (Scheme 2.22). 4-((trimethylsilyl)ethynyl) benzoic acid was dissolved in dry DCM and one equivalent of triethylamine was added to assist the solubility of the acid. NHS and N,N-diisopropylcarbodiimide (DIC) coupling reagents were added and the reaction mixture stirred

at r.t. for 1h. A white precipitate of diisopropylurea (DIC-urea) by product was filtered off using celite. A solution of **4a** in dry DCM was added and the reaction mixture was heated in microwave reactor to 50°C for 1 h. The desired product **14a** was obtained after a column purification using 100% EtOAc as an eluent in 35% yield over two steps. The yield could be improved by changing the solvent system. Recent literature surrounding amide bond formation have been to improve the solvent systems commonly used.¹²¹ Since the 1960s, DCM, DMF and N-methyl-2-pyrrolidone (NMP) have been the solvents of choice for such coupling reactions. Low peptide and amino acid solubility in DCM, as well as its potential reactivity with amines such as piperidine (commonly used to deprotect Fmoc functionalities), has meant that DMF is perhaps the most popular choice. Drawbacks of using DMF, such as its high boiling point (and therefore low evaporation rate) and decomposition to formaldehyde/dimethylamine, has meant that the development of new solvent systems has become increasingly more necessary. In 2014, Yahya E. Jad *et al.* published a study to compare the use of DMF, ACN and THF as coupling solvents.¹²¹ They concluded that ACN was a suitable alternative to DMF, reducing racemization in both solution-phase and solid-phase synthesis when compared with DMF, and in some cases, gave a greater coupling efficiency than DMF.

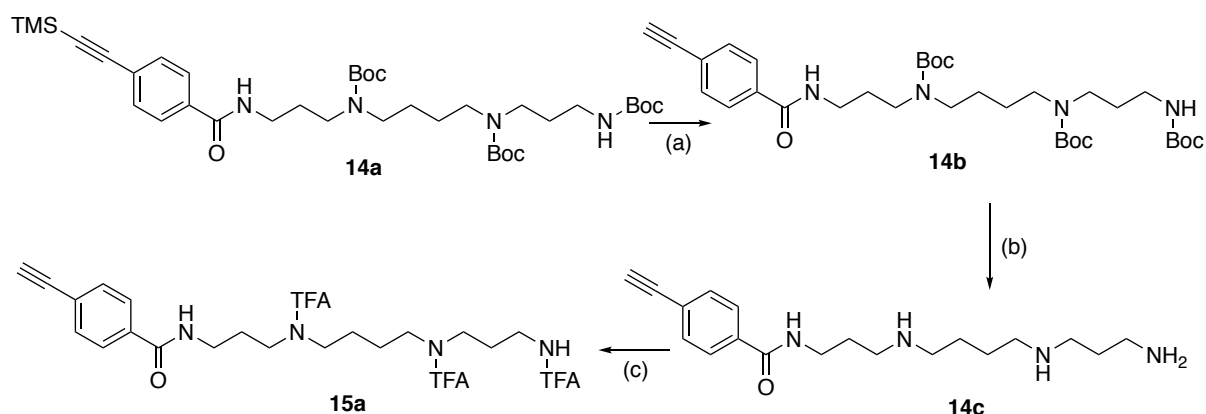
The TMS group on **14a** is deprotected prior to the coordination with Pt(II) using K₂CO₃, and the latter also enhances the basic conditions of the reaction mixture which are required for proceeding the reaction (see Section 3.3).



Scheme 2.23: Synthetic route of **HL13**. **Reagents and conditions:** (a) DIC, NHS, Et₃N, dry DMF, r.t, 1h; (b) **3a**, dry DMF, 18 h, r.t, 91% over two steps.

Amide coupling reaction was also used to synthesise the tridentate N^CN ligand **HL13** (Scheme 2.23). Dry DMF was used in this reaction, which increased the yield to 91% after a column purification in 0-5% MeOH in DCM to afford the product as a white solid. Furthermore, instead of using a microwave reactor in the second step, the reaction mixture was stirred at r.t. for 18 h after the addition of **3a**.

Following successful synthesis of the Boc-protected spermine conjugated alkyne ligand (**14a**), efforts to prepare the TFA-protected analogue were continued using **14a** as a synthetic precursor. A sequence of exchange reactions were proposed in which the Boc-protecting groups could be removed under anhydrous acidic conditions, and the resulting free-amine (**14c**) tri-TFA protected on addition of excess TFAA to afford **15a** (Scheme 2.24).



Scheme 2.24: Synthetic route of **15a**. **Reagents and Conditions:** (a) K₂CO₃, MeOH, 18h, r.t. (b) 4M HCl/dioxane, 0°C, 3 hours; (c) TFAA, Et₃N, 0°C – r.t., 3 hours, 93%.

First, the need to deprotect TMS group on **14a** was essential before incorporating TFA groups (**15a**) as the latter is a base-labile. The following reaction was found to proceed cleanly to intermediate (**14c**) upon treatment with 4 M HCl/ dioxane at 0°C. Complete conversion was observed after 3 hours (confirmed by ¹H NMR and MS(ESI+)) and the volatile Boc by-product was removed easily under high vacuum. The pH was adjusted to 7 by addition of 1 M NaOH solution to the reaction mixture upon formation of **14c** to ensure the deprotonation of the free amino groups in the intermediate (**14c**). This significantly increases the nucleophilicity of the nitrogen donor atoms and consequently increases the rate of nucleophilic attack, thus assuring product formation. Following removal of the volatiles under high vacuum, treatment with TFAA yielded the Tri-TFA protected product (**15a**) in excellent yield (93%).

2.6 Spectroscopic Characterisation of Ancillary Ligands

2.6.1 NMR Spectroscopy

The conjugated products were characterised as fully as possible by NMR spectroscopy (^1H , ^{13}C , ^{19}F , COSY and HSQC). The alkyne proton on all of PEG conjugated mono-ligands can be seen as a triplet with an integration of one proton at 2.48 ppm and was found to be coupling with the doublet at 4.21 ppm, as in accordance with previous recorded data. ^{13}C NMR spectra show a peak at 79.5 ppm, however this peak is not seen with DEPT135 data, meaning that the carbon in question must be quaternary, further confirming the presence of the alkyne.

Distinctive shifts in ^1H NMR spectra of the spermine conjugated ligands (**13a**, **14a**, **15a**) in comparison to the starting materials were observed, which confirmed the formation of the proposed products. Most notably the resonances corresponding to the methylene units neighbouring the free amino group experience an upfield shift (~ 1 ppm) upon conjugation in the **13a** ligand, which is consistent with the nuclei moving to a more deshielded environment neighbouring the heterocyclic pyridine ring. In contrast, the former proton resonances experience a higher field shift (~ 1.30 ppm) when neighbouring an amide on **14a**, and **15a** ligands (Figure 2.15). The NH amide proton peak appears at the highest shift (7.68 ppm) as a broad singlet. The amide proton assignment was also confirmed by HSQC as the proton shows no correlation to a carbon signal (Figure 2.16).

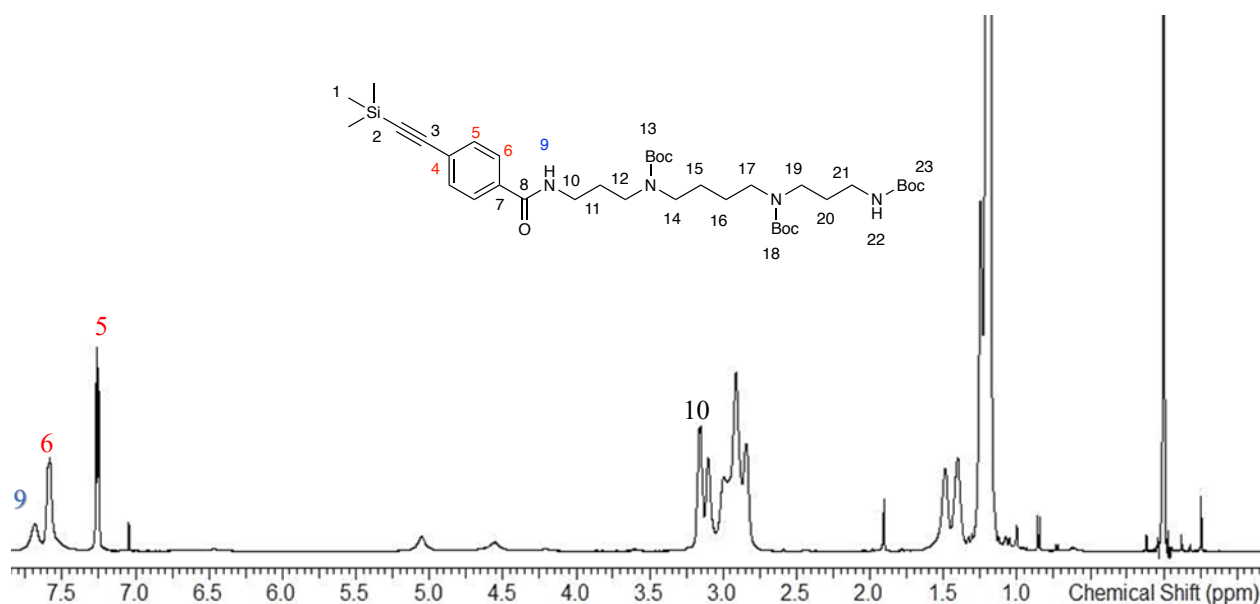


Figure 2.15: ^1H NMR spectra (CDCl_3 , 500 MHz) of **14a**.

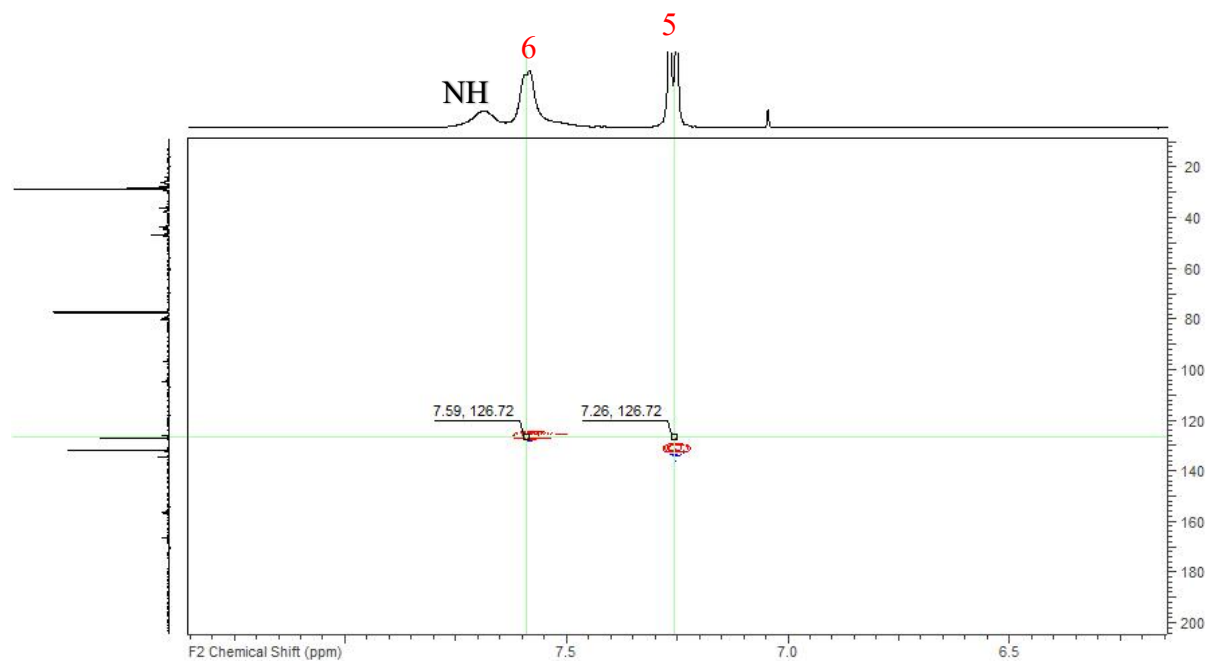


Figure 2.16: HSQC NMR spectra (CDCl_3 , 500 MHz) of **14a** ligand.

2.7 Conclusion

In conclusion, in this study two types of ligands were synthesized that will be able to cyclometalate or coordinate with Pt(II) metal centre to produce the desired complexes. The first type is the $\text{N}^{\wedge}\text{C}^{\wedge}\text{N}$ tridentate ligands which are prepared by a sequence of cross coupling reactions such as **HLn** ($n = 1-6$). **HL7** and **HL8** were synthesised *via* a click chemistry while **HL9** was synthesised using both previously mentioned reaction methods. The second type are monodentate ligands which were prepared by direct alkylation as seen in **9-12a**, reductive amination such as **13a**, or amide coupling reactions such as **14a** and **15a**. These ligands were purified by column chromatography and characterized by NMR spectroscopy and mass spectrometry.

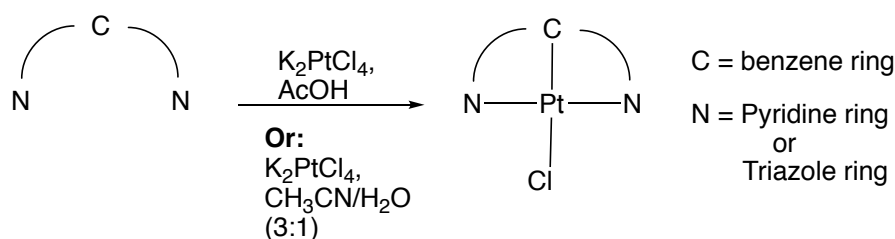
Chapter 3

3 Synthesis of Platinum Complexes

As discussed in the introduction, complexes of platinum have received much attention as luminescent reporters for a variety of applications due to their useful excited state properties. In particular, complexes related to 1,3-di(2-pyridyl)benzene platinum(II) chloride are highly emissive, with long phosphorescence lifetimes. In addition, complexes of Pt(II) are of particular interest due to their tendency to display square-planar geometries, allowing axial interactions with the metal centre leading to excited state modification through metal-metal or transient ligand-metal interactions. The utility of such compounds will therefore be explored, with the aim of producing novel luminescent probes for cellular imaging.

3.1 Complexation to Pt(II)

Two solvent systems are commonly reported in the literature for complexation of the tridentate N[^]C[^]N ligands: acetonitrile and water in a 3:1 ratio, as well as glacial acetic acid. The general reaction scheme for the complexation reaction shown in Scheme 3.1.⁹⁶ Both solvent systems involve heating to 120 °C in a sealed tube under nitrogen for 3 days and give cyclometalated complexes in comparable yield. Where possible, ligands were complexed with K₂PtCl₄ in glacial acetic acid. The acetonitrile/water system requires the aqueous solution of K₂PtCl₄ to be degassed separately from the solution of ligand in acetonitrile. However, this solvent system proves invaluable when ligands containing acid sensitive groups require complexation, such as **HL8**. During complexation, most complexes were observed to precipitate out of solution as bright yellow or orange solids; the process is further facilitated by cooling prior to the work-up. The complexes generally had low solubility, and the work-up involved a series of washings to remove any uncomplexed ligand and K₂PtCl₄.



Scheme 3.1: General procedure for complexation of the tridentate ligand to Pt(II).

With the exception of ligand **HL8**, complexation of the ligands *via* these routes was achieved in yields ranging from 10 to 48%. Ligands **HL4**, **HL5** and **HL6** underwent lower yielding complexations – these ligands generate complexes that possess unfavourable by-products (these will be discussed in detail later in this section), which hinder the complexation process and complicate the purification process.

Complexation of **HL8** was not successful when using acetonitrile and water (3:1) solvent system. After evaporation of the solvent mixture a yellow solid product was obtained which was characterised by ^1H NMR spectroscopy. An upfield shift of ^1H NMR signals was observed relative to the peaks of free ligand (Figure 3.1) suggesting that complexation had taken place. Unfortunately, the peak corresponding to H₇ present on CH activation site was still observed and hence concluded that monodentate N coordination could be the reason for shift of the peaks. Synthesis in acetic acid could not be applied to **HL8** because of the limitation of the Boc-protecting groups being unstable in acidic conditions.

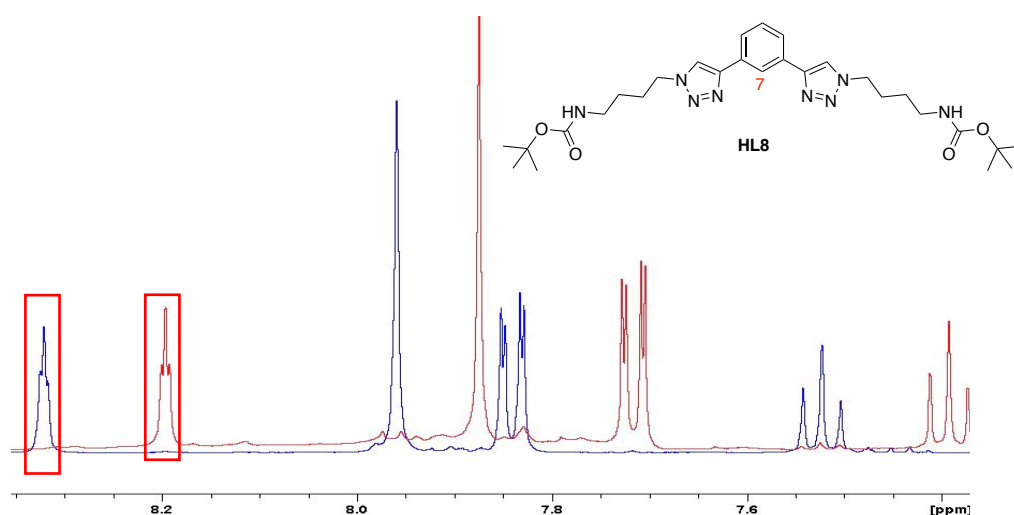


Figure 3.1: ^1H NMR spectra (CDCl_3 , 400 MHz) of up field peak shifting of **PtL8Cl** (Red) in compression with the free-ligand **HL8** (Blue).

Microwave heating is an ideal method for accelerating chemical reactions under conditions of increased pressure. It allows heating of a solvent at a much higher temperature than the conventional boiling point of the solvent. For example, ethanol has a conventional boiling point of 79°C , but microwave heating in a closed vessel can rapidly reach to 164°C .¹²² Moreover, microwave synthesis has other advantages over conventional heating such as generating products in high yields with high purity by reducing unwanted side reactions and it reduces reaction times.¹²² Hence, to overcome the problem of low yield, conventional heating method was replaced with microwave heating. Microwave cyclometallation was achieved in a reaction

analogous to the one described by Wang *et al.*,¹²³ using a mixture of acetic acid and water (9:1) as the solvent and heating for just 45 minutes. After cooling the reaction mixture to room temperature, a pale yellow solid **PtL7Cl** was obtained with high purity, which was collected by filtration. The yield was improved to 63%. The use of microwave heating allowed higher temperatures of reaction than the boiling point of the solvent (in this case 160°C) which, combined with the increased concentration of the reactants in solution, is thought to be the reason for the elevated rate of reaction.

Complexation of **HL4**, **HL5** and **HL6** led to a mixture of inseparable products (Figure 3.2). ¹H NMR spectroscopy indicated that complexation and cyclometallation had occurred, (two ¹⁹⁵Pt satellites were observed downfield, with the disappearance of H₇ proton peak of the ligand) (Figure 3.3). Also, the molecular ion peak for the desired complex was observed in the ASAP mass spectrum accompanied by another peak that has the same Pt isotope pattern with *m/z* 18 units higher than expected. This suggests that alkyne hydration of the ligand occurred upon complexation. As reported in the literature, the alkyne can be converted to a ketone by a catalyst in the presence of water and acid.¹²⁴ It is thought that during the reaction the resulting Pt(II) alkyne complex acts as a catalyst and causes the direct conversion of the alkyne on remaining unreacted ligands into the corresponding ketones in the presence of water and acetic acid (Figure 3.4). This conclusion was drawn after the repetition of the former reaction conditions with the hope that all of the alkyne Pt(II) complexes would be converted to their corresponding ketone Pt(II) complexes. However, the two resulting Pt(II) complexes remained in solution, and no further hydration was observed. This suggests that conversion of an alkyne to a keton occurs only on the proligand and not when complexed to Pt(II).

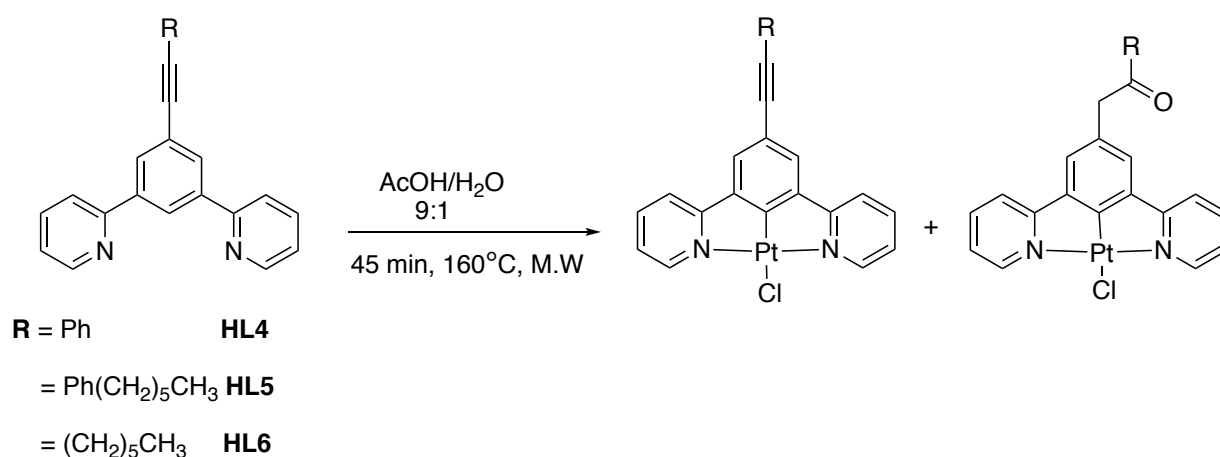


Figure 3.2: Microwave synthesis of **PtL4Cl**, **PtL5Cl** and **PtL6Cl** complexes led to a mixture of inseparable products.

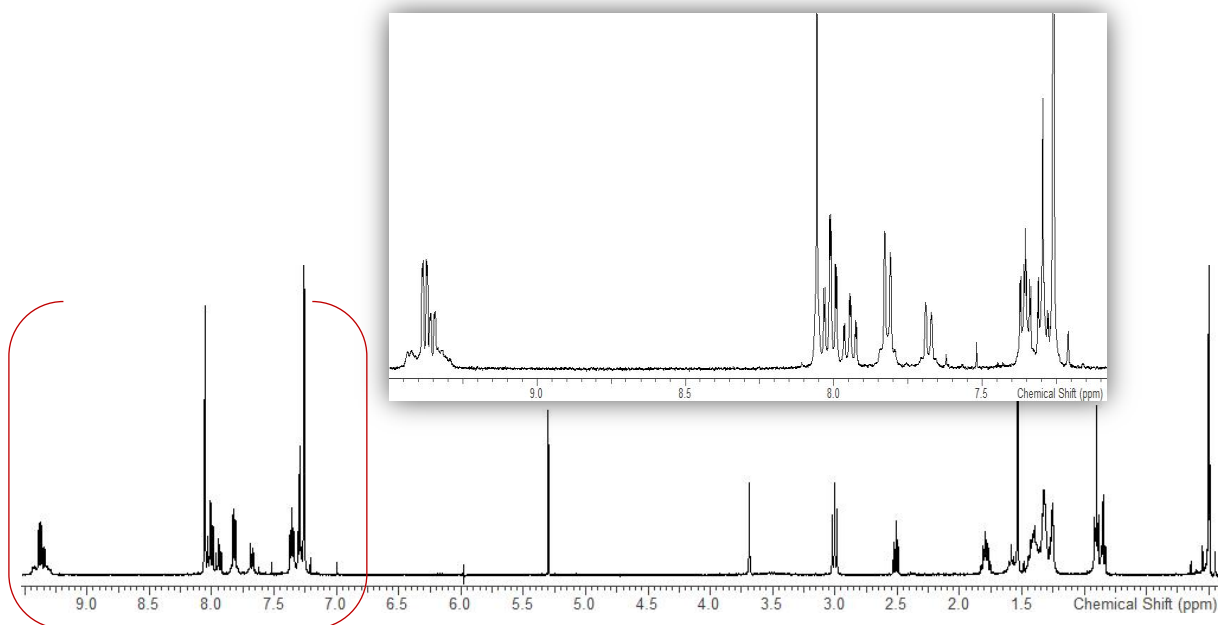


Figure 3.3: ^1H NMR spectra (CDCl_3 , 400 MHz) of a mixture of inseparable Pt(II) complexes of **PtL6Cl** and **PtL6^aCl**.

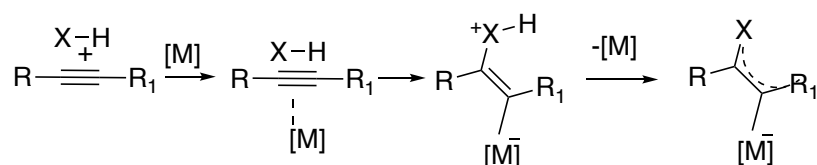
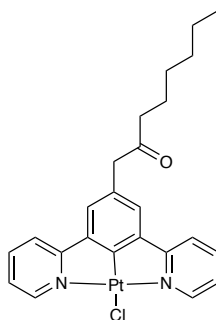


Figure 3.4: General metal-catalyzed addition to C-C triple bonds.¹²⁴

From all of the synthesised Pt(II) complexes, only a small amount of the ketone Pt(II) complex **PtL6^aCl** was successfully isolated from the crystallisation solution using DCM:Hexane solvents. **PtL6^aCl** was fully characterised by mass spectrometry and ^1H and ^{13}C NMR spectroscopy (Figure 3.5). An extra peak corresponding to CH_2 ketone H_{10} can be clearly seen at 3.65 ppm. Also, a triplet peak corresponding to H_8 was confirmed the hydrolysis of the neighbouring protons. ^{195}Pt satellites on one low field aromatic doublet are clearly seen for H_1 on the pyridine.



PtL6^aCl

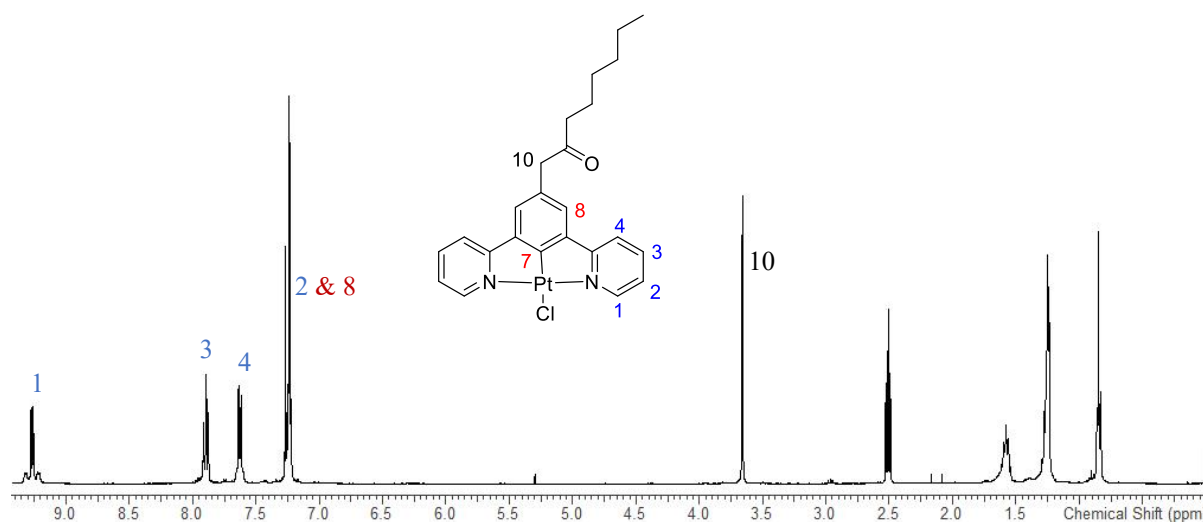
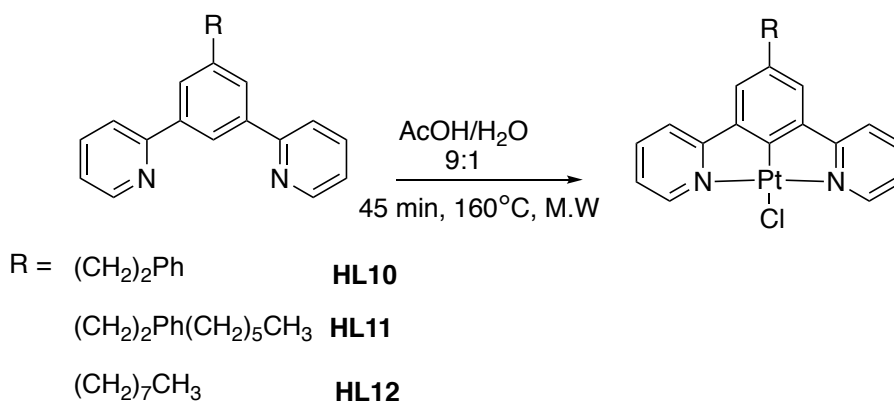


Figure 3.5: ^1H NMR spectra (CDCl_3 , 500 MHz) of **PtL6^aCl**.

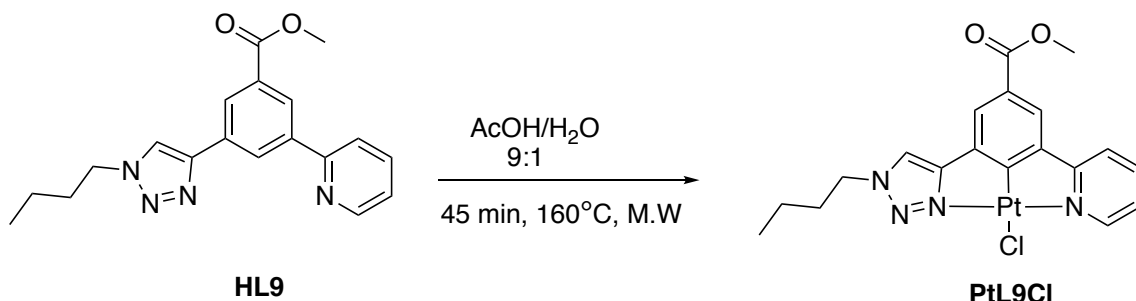
To overcome the issue of inseparable products, reduction of the alkyne on the $\text{N}^{\wedge}\text{C}^{\wedge}\text{N}$ proligand before cyclometallation with Pt(II) was thought to be the best solution. Cyclometallation of the hydrogenated ligands **HL10**, **HL11** and **HL12** was successfully achieved by direct reaction with K_2PtCl_4 using microwave reaction in a mixture of $\text{AcOH}/\text{H}_2\text{O}$ 9:1 for 45 min at 160°C (Scheme 3.2). The resulting Pt(II) complexes **PtL10Cl**, **PtL11Cl** and **PtL12Cl** precipitated from the reaction mixture as an orange or a yellow solid and the work up involved a series of washing to remove any impurities, to give the desired complexes in excellent yield (73 to 80%).



Scheme 3.2: Microwave synthesis of **PtL10Cl**, **PtL11Cl** and **PtL12Cl** complexes.

Another side product that was generated during the cyclometallation of the **HL12** is the Pt(IV) complex. This occurs when Pt(II) complexes are oxidised to their Pt(IV) analogues during microwave heating of the reaction. The Pt(IV) analogue was isolated from the reaction mixture containing the desired Pt(II) complex **PtL12Cl** by silica column chromatography using 100%

CH₂Cl₂ as an eluent ($R_f = 0.42$). The Pt(IV) complex of **HL12** was analysed by ¹H NMR spectroscopy and MS as well as X-ray crystallography which will be discussed in section 3.5.3.2. Also, the Pt(IV) photophysics was studied and compared with the Pt(II) precursor complex.



Scheme 3.3: Microwave synthesis of **PtL9Cl**.

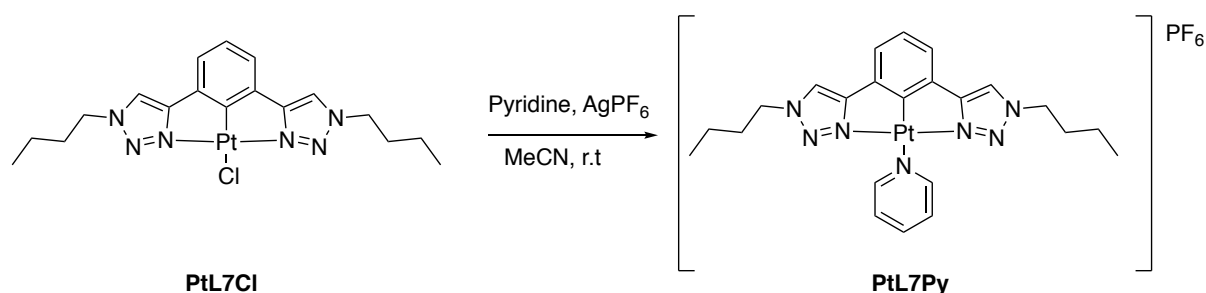
Asymmetric **PtL9Cl** complex, features both a pyridine and 1,2,3-triazole ring, was found to be accessible by the reaction between the corresponding **HL9** ligand and K₂PtCl₄ under the same previously mentioned microwave reaction conditions (Scheme 3.3). A simple purification procedure allows the isolation of the complex in yield of 43%. The resulting complex was found to be slightly soluble in methanol, so further quantities of product was extracted from the methanol washing, with careful purification by washing the complex with minimal quantities of methanol and diethyl ether.

3.2 Substitution of the Ancillary Chloride with Alkyne or Pyridine ligands

In addition to the synthesis of novel Pt(N[^]C[^]N) complexes with mixed nitrogen donors, the effects of the introduction of alkyne or pyridine ligands into the coordination sphere of platinum were explored. As discussed previously, this reaction was carried out to understand the ease of incorporation of alkyne or pyridine moieties bearing polyamines or lipophilic groups to the Pt(II) complexes and further to explore their photophysical properties.

3.2.1 Synthesis of Pyridine Substituted Pt(II) Complexes

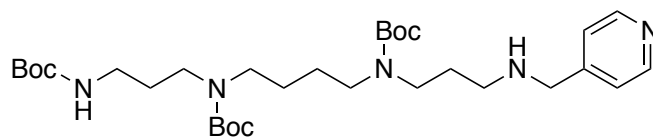
These reactions proceeded *via* two steps: removal of the chloride, followed by addition of the new ancillary ligand. Silver has a high affinity for chloride, so to remove the chloride, a slight excess of silver hexafluorophosphate or silver tetrafluoroborate was added to a suspension of a Pt(N[^]C[^]N)Cl complex in acetonitrile or DCM. The mixture was stirred at room temperature for 15 min, during which the new cationic solvent-ligated complex dissolved, and silver chloride precipitated. Upon removal of the silver chloride *via* centrifugation, a solution of the ancillary pyridine based ligand was added dropwise to the reaction mixture solution. Precipitation of the new complex was observed after 48 h stirring at room temperature, the precipitate was isolated and washed accordingly. The formation of the desired complex was monitored by MS and ¹H NMR spectroscopy.



Scheme 3.4: Synthesis of **PtL7Py**.

Pyridine was successfully incorporated to **PtL7Cl** complex in moderate 40% yield as an orange solid and no further purification was required (Scheme 3.4). This reaction was attempted to test the possibility and ease of synthesis of the reaction to study the stability and photophysics properties of the resulting complex and finally, to compare the result with the alkyne substituted complex.

Moreover, the incorporation of **13a** into **PtL1Cl** complex was also achieved and confirmed by MS and ¹H NMR spectroscopy. However, the desired complex decomposed during purification *via* a neutral alumina column (5% MeOH in DCM) to its starting material. Hence, care was required when isolating the required product not to expose the complex to Lewis bases, including CH₃CN. The pyridyl complexes decomposed readily when left standing, even in acetone solution, over as little as a few hours.

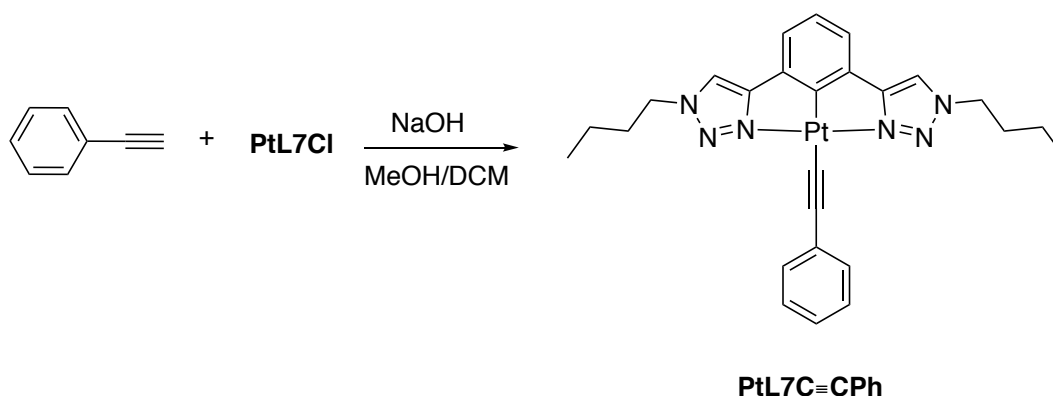


13a

These complexes did not exhibit intense emission and are prone to undergo self-quenching in aerated samples, hence can be challenging to be employed as a target for cellular imaging applications (see next chapter for more details). As a result of the lack of emission from these complexes, no further experiments were performed on these complexes.

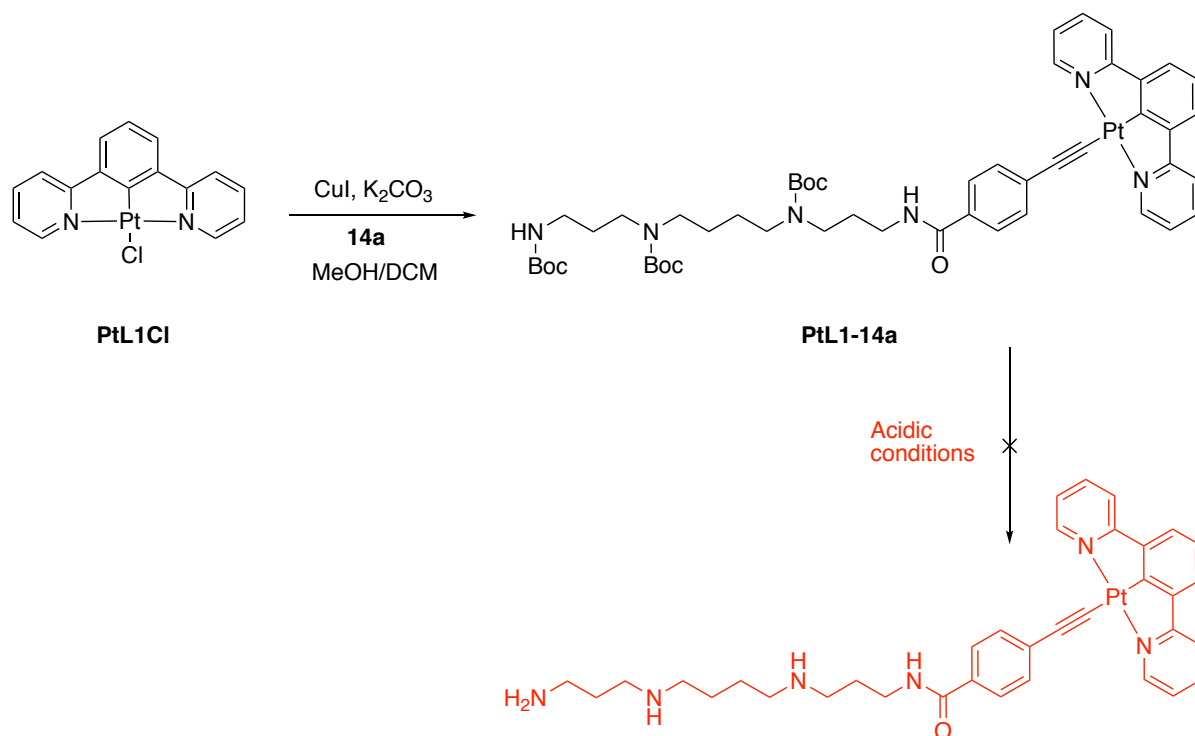
3.2.2 Synthesis of Alkyne Substituted Pt(II) Complexes

The chloride ligands for **PtL1Cl** and **PtL7Cl** were substituted for an alkyne ligand using different literature methods reported for similar platinum complexes. A technique similar to that of Chan *et al.* for other N[^]C[^]N-coordinated Pt(II) complexes was used to synthesise **PtL7C≡CPh** (Scheme 3.5).¹²⁵ The reaction proceeded under mild conditions at room temperature in a mixture of MeOH/DCM. Phenyl acetylene was deprotonated by sodium hydroxide, and then reacted with **PtL7Cl**, the product was retrieved from solution as a light-yellow precipitate. Purification was achieved by washing with water, methanol and diethyl ether. As mentioned previously, this complex was synthesised to study and understand the photophysical properties and compare the result with pyridine substituted **PtL7Py** complex.



Scheme 3.5: Synthesis of **PtL7C≡CPh**.

This method was also used for the synthesis of **PtL1-14a** however, a very low yield was achieved. To improve the yield, Sonogashira conditions were employed (terminal alkynes, CuI/ⁱPr₂NH/CH₂Cl₂), following a reported method by Lu W *et al.*,¹²⁶ which resulted in a simple workup and purification procedure (Scheme 3.6). **14a** was desilylated with K₂CO₃ in dry MeOH in the presence of CuI at room temperature after degassing the mixture three times (freeze – pump – thaw cycle). The resulting mixture was further treated with **PtL1Cl** in DCM to give the desired complex **PtL1-14a** as a dark orange precipitate in 54% yield. The resulting complex was characterised by MS and ¹H NMR spectroscopy. Further acid treatment with HCl in dioxane or TFA in DCM was required to deprotect the amino groups on the desired complex. Unfortunately, the complex was not stable under acidic conditions and decomposed. Additionally, due to the fact that the acetylide group displays a higher *trans*- influence than the phosphorus or pyridine donors, the desired product is appreciably more unstable.¹²⁷



Scheme 3.6: Synthetic route for **PtL1-14a**.

As discussed previously, a PEG alkyne linker was chosen based on their known ability to enhance the aqueous solubility and bio-compatibility of similar Pt(II) complexes.¹¹⁶ In an attempt to increase aqueous solubility of the complexes, integration a PEG alkyne moiety with an -OH group on the end was attempted. Upon insertion of the ancillary ligand **10a** into **PtL1Cl** complex, a *bis*-coordination was observed by ¹H NMR spectroscopy (Figure 3.5).

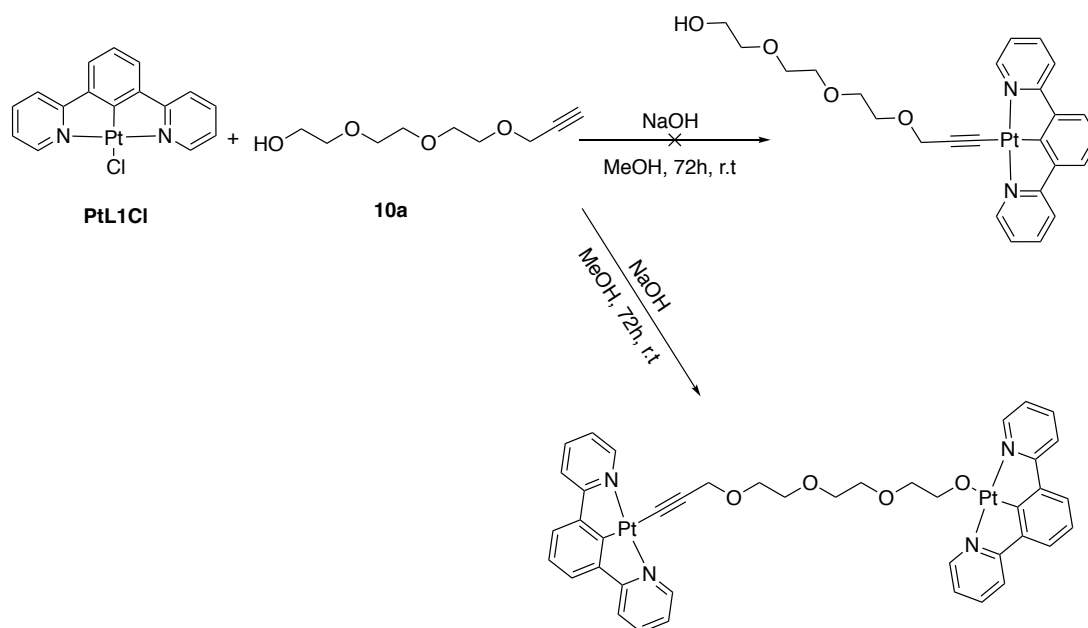
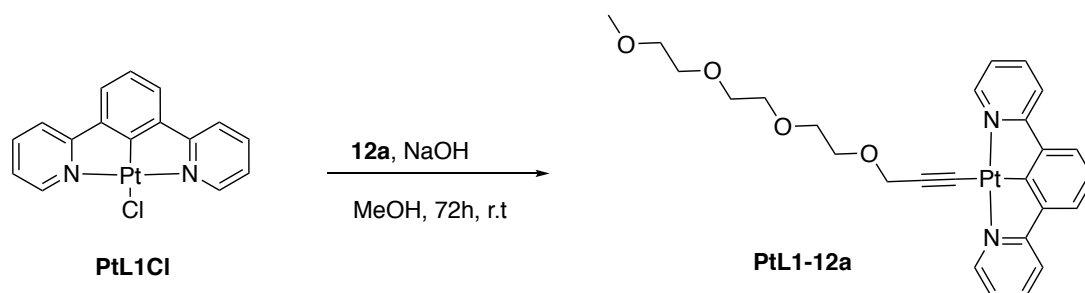


Figure 3.6: Proposed chemical scheme of the investigated *Bis*-Platinum complex.

In order to overcome this problem, the -OH group on **10a** was protected with the TBDMS group, which is stable under basic conditions. However, during the removal of the TBDMS protecting group on the complex, required treatment with acid, leading to decomposition of the complex. Another route was adopted, to avoid hydroxyl group protection and deprotection steps, by using triethyleneglycol monomethyl ether which has similar solubility features.

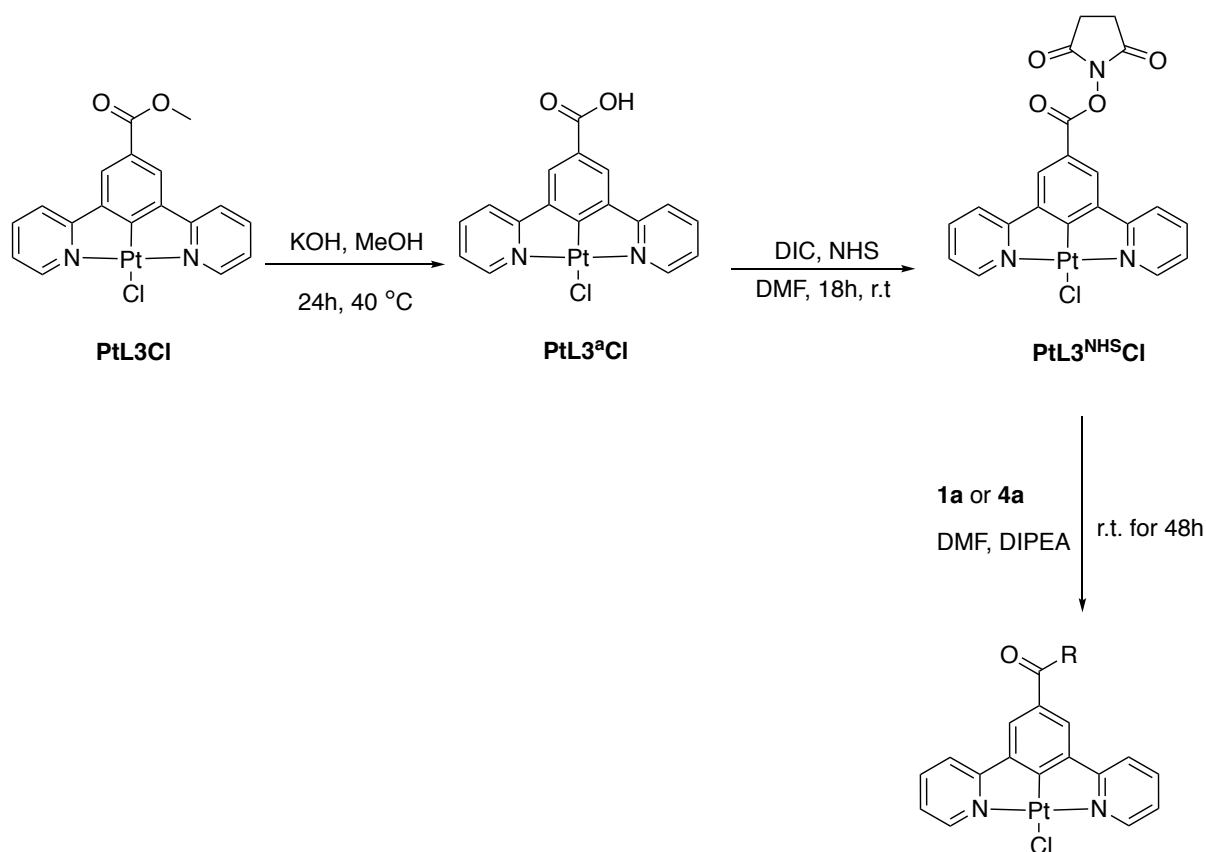
PEG alkyne ligand **12a** was incorporated successfully into the **PtL1** metal centre (Scheme 3.7). The reaction proceeded under inert conditions at room temperature in a mixture of MeOH/DCM, **12a** in the presence of sodium hydroxide reacted with **PtL1Cl**, the product precipitated from solution as a red solid by the addition of cold water. Purification was achieved by washing with water, and diethyl ether offering **PtL1-12a** in excellent yield (74%). **PtL1-12a** was found to be partially soluble in water, enough to study the photophysical properties of the complex in 100% water which will be discussed in detail in Chapter 4.



Scheme 3.7: Synthesis of **PtL1-12a**.

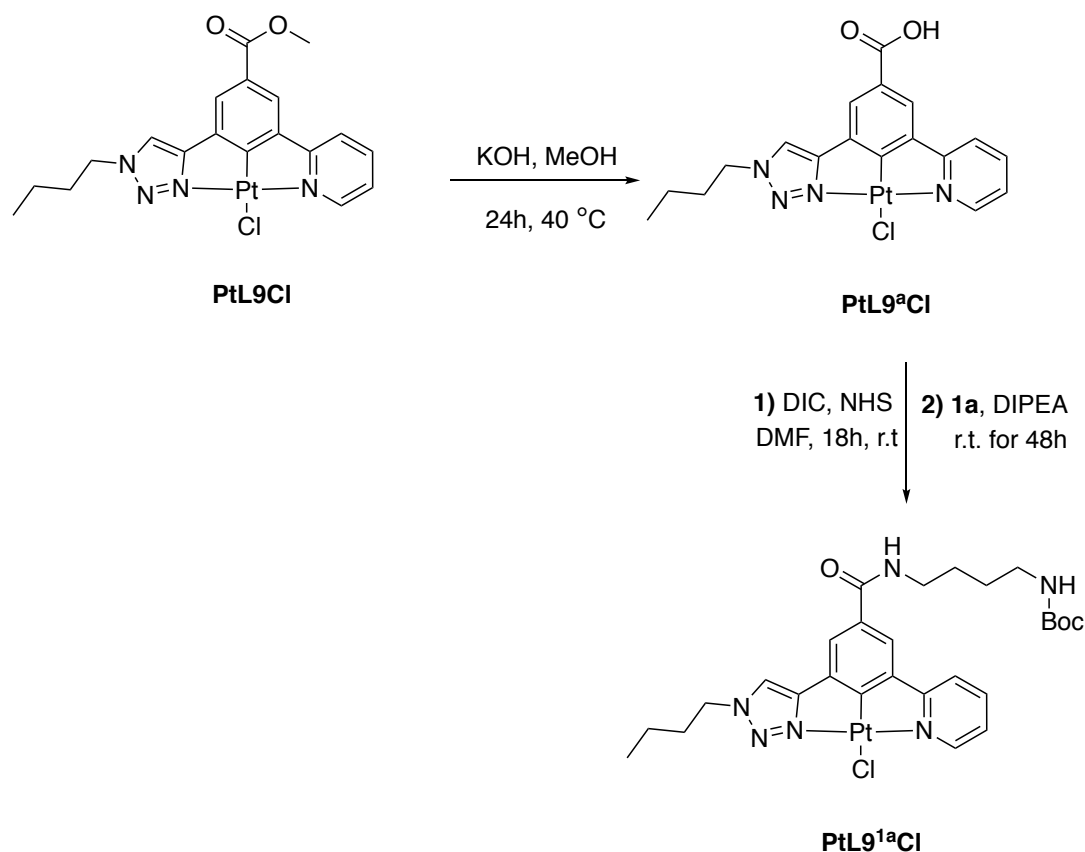
3.3 Amide Coupling on PtLnCl Complexes

Another chemical approach was adopted to introduce a polyamine chain onto Pt(II) complexes. This relied on amide coupling reactions. Starting from **PtL3Cl**, the methyl ester can be easily hydrolysed using KOH in MeOH at 40°C for 24 h, affording the desired acid complex **PtL3^aCl** in 80% yield. Subsequently, **PtL3^aCl** was activated using DIC and NHS in dry DMF and the resulting *N*-hydroxysuccinimidyl ester **PtL3^{NHS}Cl** was isolated in 95% yield and stored under inert atmosphere. **PtL3^{NHS}Cl** was then coupled with either boc putrescine **1a** or tri-Boc spermine **4a** amino group to give the anticipated complexes in excellent yields (Scheme 3.8).



Scheme 3.8: Synthesis of **PtL3RCl** complexes (R = **1a** or **4a**).

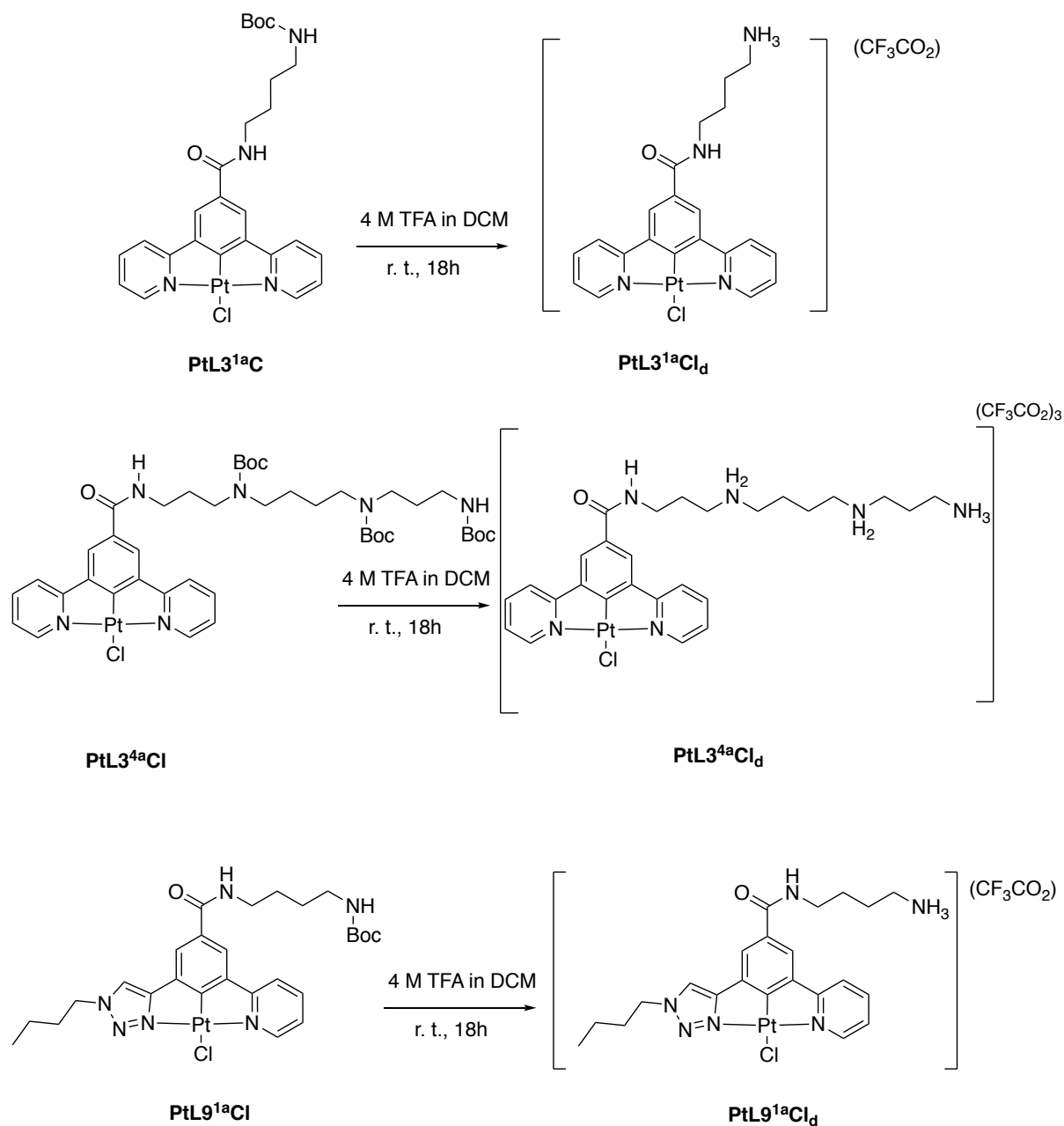
PtL9^{1a}Cl was also synthesised following the previously stated procedure but without the isolation of the NHS activated ester complex as **PtL9^{NHS}Cl** was more soluble in DMF and did not precipitate from the reaction solution like **PtL3^{NHS}Cl**. In this case a one pot reaction was performed for activation of **PtL9Cl** corresponding acid complex using NHS and DIC followed by amide coupling with **1a** amino group (Scheme 3.9).



Scheme 3.9: Synthesis of **PtL9^{1a}Cl**.

3.4 Deprotection of the Amino Groups on Pt(II) Complexes

Numerous strategies have been established in the literature for Boc-deprotection in the past.¹²⁰ A variety of reagents have been employed to effect this transformation, including strong acids, Lewis acids, and neutral conditions assisted by microwave heating. Here, Boc deprotection was successfully achieved by using acidic conditions such as trifluoroacetic acid (TFA) in CH_2Cl_2 and HCl in dioxane. **PtL3^{1a}Cl**, **PtL3^{4a}Cl** and **PtL9^{1a}Cl** were treated with 4 M TFA in DCM and the reaction was performed open to the air hence, tert-butyl cations are sequestered by adventitious moisture to form ${}^t\text{BuOH}$ (Scheme 3.10). CF_3CO_2^- was confirmed as a sole counter ion of the polyamine on the anticipated Pt(II) complexes by X-ray crystallography (will be discussed later in the chapter) and by ${}^{19}\text{F}$ NMR spectroscopy as CF_3CO_2^- group resonate observed at ~ -76.9 ppm.



Scheme 3.10: Deprotection reactions of $\text{PtL3}^{1a}\text{Cl}$, $\text{PtL3}^{4a}\text{Cl}$ and $\text{PtL9}^{1a}\text{Cl}$.

It was evident from these results that PtLnCl (where $n = 3^{1a}$ or 3^{4a} or 9^{1a}) complexes were found to be more stable under strong acidic condition required for Boc deprotection than PtLX (where $X = \text{alkyne}$ or pyridine substituted monodentate ligands). This may be as a result of weaker coordination between the platinum and the acetylide group, which displays a high *trans*-influence. Hence, the desired product is appreciably more unstable.

3.5 Spectroscopic Characterisation of Complexes

3.5.1 NMR Spectroscopy

In comparison with the pro-ligand spectra, ^1H NMR spectra of the Pt(II) (dipyridyl benzene) based complexes typically show some significant differences. Upon cyclometallation, there is always one less signal in the aromatic region of the ^1H NMR spectrum of a Pt(II) complex as the H_7 proton of the ligand is removed during cyclometallation. Furthermore, well-resolved ^{195}Pt satellites ($I = 1/2$, relative abundance 33.8%) are observed around the signal of H_1 ($J \approx 40$ Hz). Moreover, the signal assigned to H_1 moves to higher frequency (by approximately 0.5 ppm) upon cyclometallation. The latter effect is due to increased shielding within the phenyl ring, which is caused by an increase in electron density upon cyclometallation, and is consistent with reported results for similar systems.⁹⁶ Finally, H_2 stays at almost the same position, and H_3 and H_4 are sometimes observed to slightly change their relative positions. The chemical shifts of resonances in the pendant aryl groups were not greatly affected upon coordination. Example ^1H NMR spectra of the pro-ligand **HL11** and complex **PtL11Cl** are shown in (Figure 3.7).

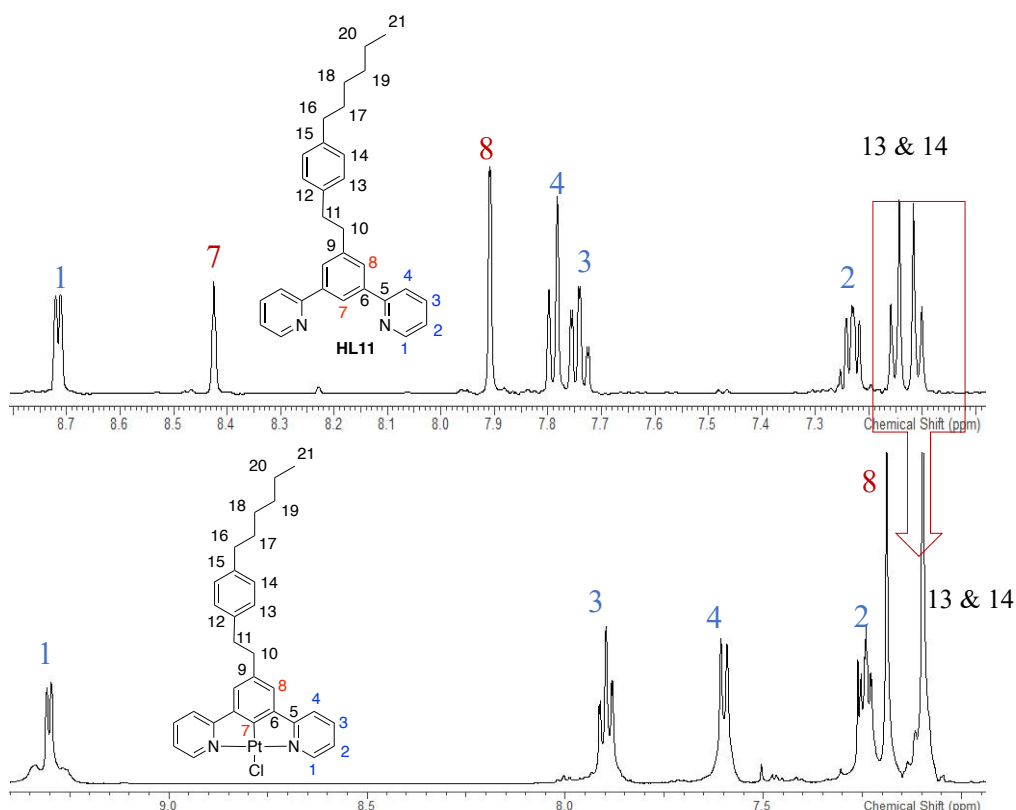


Figure 3.7: Aromatic region of the ^1H NMR spectra (CDCl_3 at 500 MHz) of the ligand **HL11** (top) and the corresponding complex **PtL11Cl** (bottom).

Di-triazole benzene based Pt(II) complex **PtL7Cl** also shows similar ^1H NMR spectroscopic trends in the aromatic region upon cyclometallation. The H_4 proton of the pro-ligand disappears upon complexation. The singlet on the triazole H_6 , the appeared triplet H_1 , and the appeared doublet H_2 corresponding to the hydrogen on the phenyl are shifted up field, typical sign of cyclometallation. On closer inspection, expansion of the appeared triplet and the doublet, shows a non-first order splitting pattern as ‘roofing’ is clearly visible (Figure 3.8).

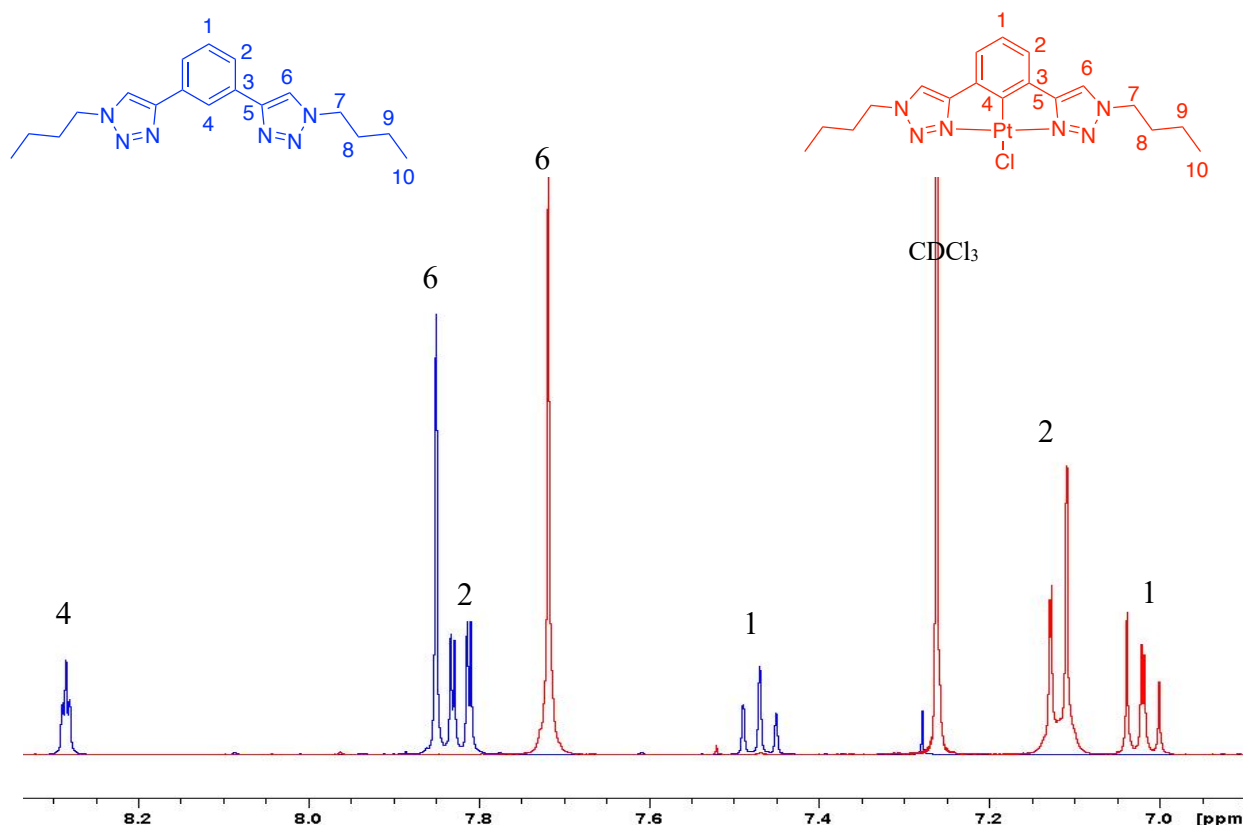


Figure 3.8: Aromatic region of the ^1H NMR spectra (CDCl_3 at 400 MHz) of **HL7** (blue) and **PtL7Cl** (red).

Second order spectra where chemical shift differences are comparable with J -values are observed for the phenyl protons and display complex spectral patterns. The accurate values of NMR parameters (δ and J) cannot be simply read from the spectrum and require simulation–iteration analysis (Figure 3.9). The phenyl protons in **PtL7Cl** are in an AB_2 system, the difference in chemical shift is ~ 0.1 ppm (at 400 MHz this is 40 Hz) and the coupling constant is ~ 7.6 Hz therefore $\Delta\nu/J = 40/7.6 = 5.3$, hence the non-first order nature. This is also referred to as strong coupling when the chemical shift difference in Hz approaches the value of the coupling constant; usually, when this ratio is < 6 the roofing becomes apparent.¹²⁸

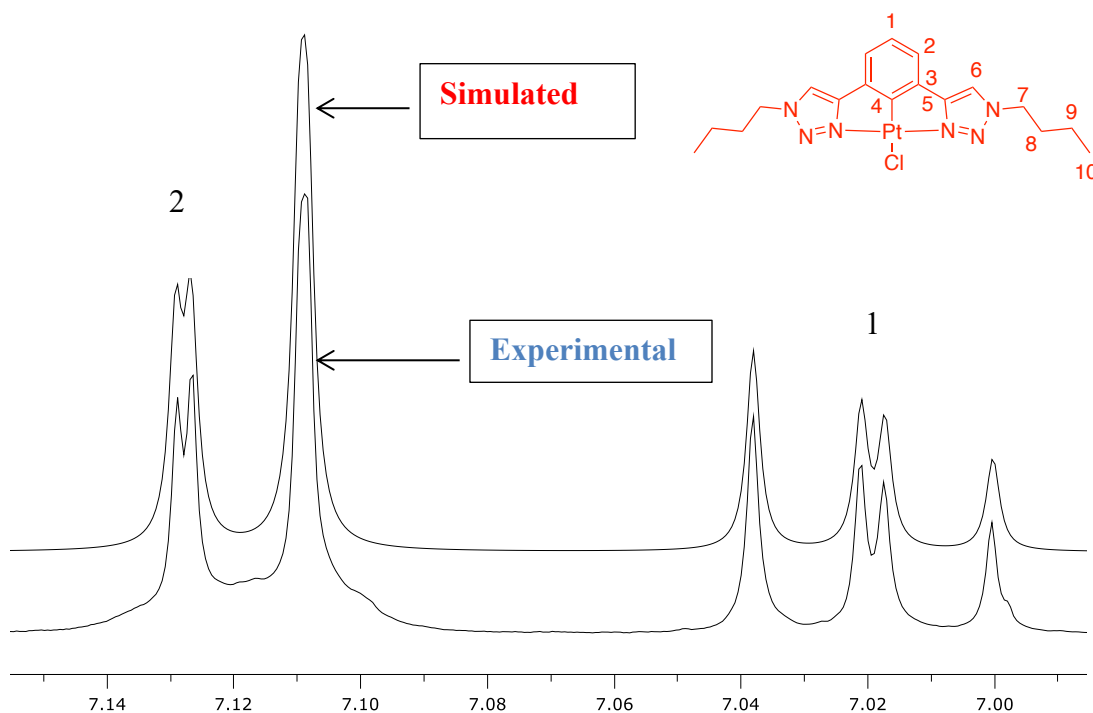


Figure 3.9: Simulated and experimental ^1H NMR spectra for **PtL7Cl**.

Changing the ancillary ligand led to slight changes in the ^1H NMR spectra. For instance, an up-field shift of all aromatic protons was seen upon substitution of the chloride ligand by pyridine. This indicates that all aromatic protons are becoming increasingly shielded.

The signal corresponding to H_1 on the halogenated series of **PtL1X** shifts to higher field as the halogen size increases.

Furthermore, the ^1H NMR spectrum of **PtL1-12a** (Cl substituted with PEG alkyne) showed a higher chemical shift corresponding to H_1 proton (at 9.48 ppm). This is due to proton H_1 is becoming less shielded as a result of increase electron density of the Pt. Also, as sign of successful ligand substitution, a proton peak corresponding to an alkyne proton **12a** was not seen and upon coordination an upfield shift of the H_{12} protons is noted (Figure 3.10).

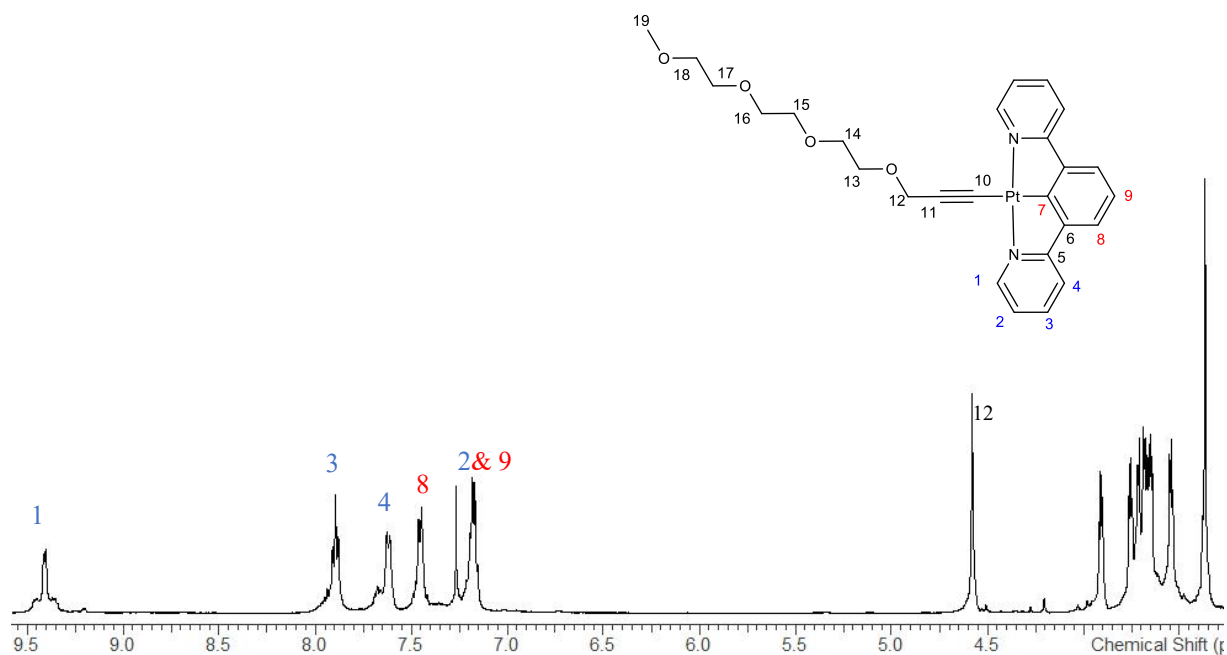


Figure 3.10: ^1H NMR spectra (CDCl_3 , 500 MHz) of **PtL1-12a**.

For the Pt(IV) complex **PtL12Cl₃**, all of the aromatic proton resonances of the ligand occur at higher chemical shift than for the respective Pt(II) complex **PtL12Cl**. This is consistent with the increasing positive charge on platinum, reducing electron density on the ligand. The ^{195}Pt satellites around H₁ proton show smaller J -coupling ($J \sim 20\text{--}25$ Hz), indicative of a poorer overlap with the contracted orbitals of the Pt(IV) centre.¹²⁹

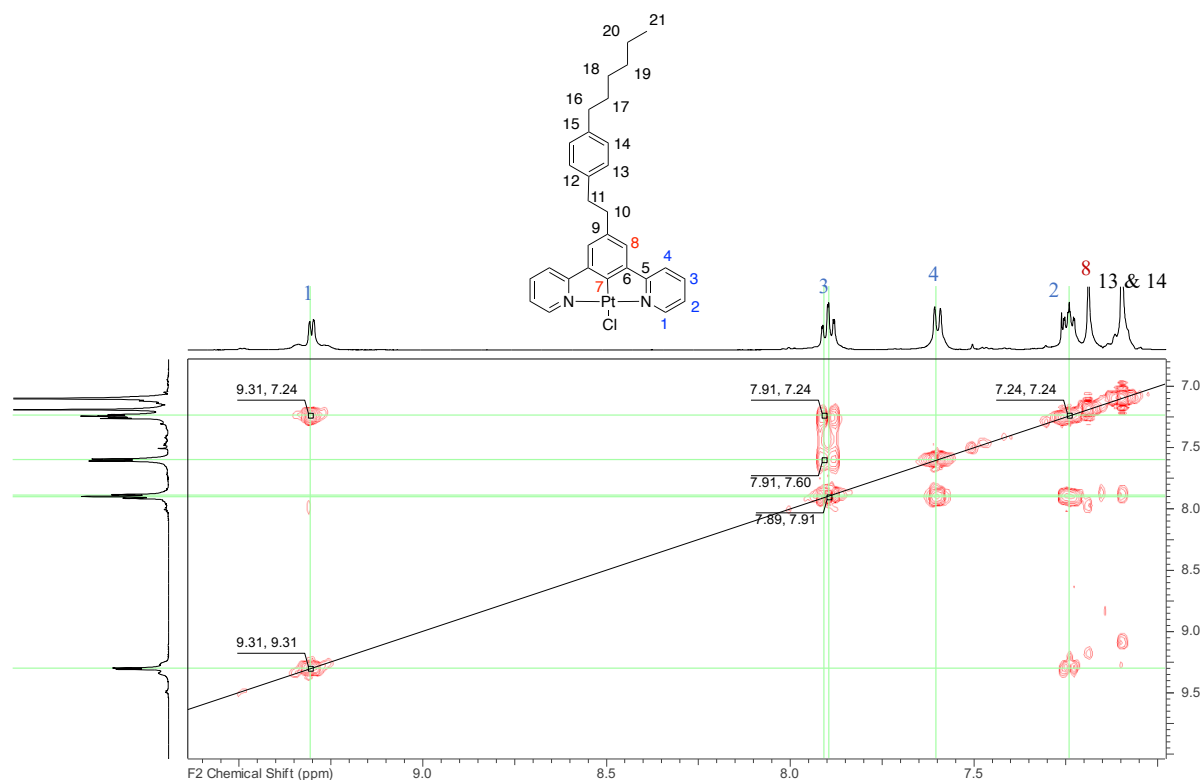


Figure 3.11: Aromatic region of the COSY spectra (CDCl_3 , 500 MHz) of **PtL11Cl** complex.

^1H - ^1H Correlation Spectroscopy (COSY) shows the correlation between hydrogens which are coupled to each other in the ^1H NMR spectrum. The total assignments of the ^1H NMR spectrum of the title complexes were confirmed by ^1H - ^1H COSY experiment, which offers a way to identify the spin-spin coupled pairs of protons that are three bonds apart. The COSY NMR spectrum of **PtL11Cl** is shown in Figure 3.11 as an example.

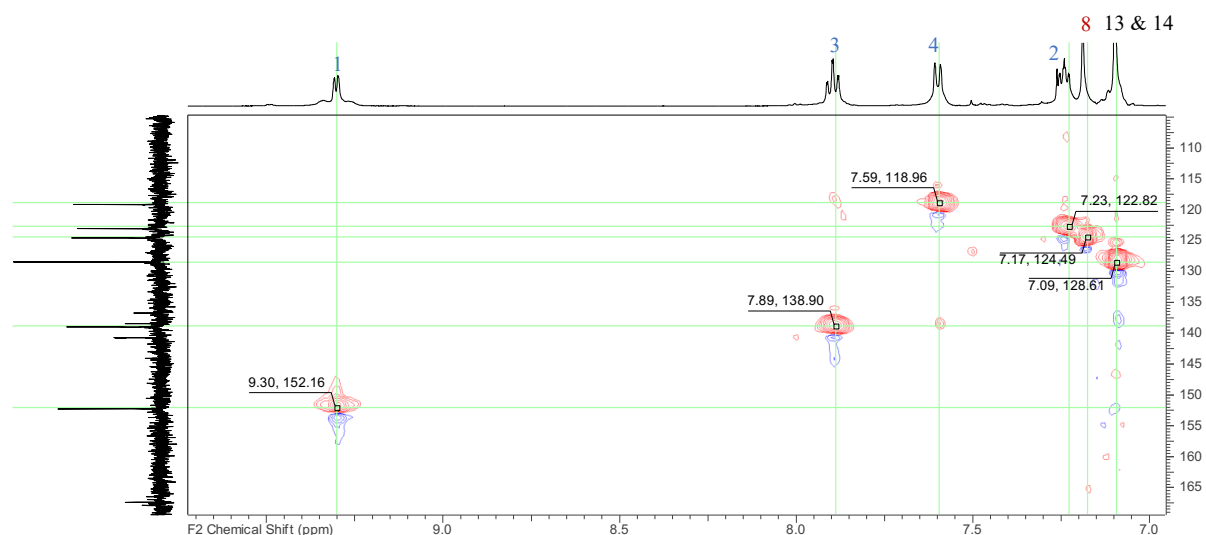


Figure 3.12: Aromatic region of the HSQC spectra (CDCl_3 , 500 MHz) of **PtL11Cl** complex.

After the full assignment of the ^1H NMR spectrum, HSQC and HMBC were used to confirm the assignments of ^{13}C NMR. For instance, HSQC shows which hydrogens are directly attached to which carbon atoms. The HSQC spectrum is most valuable when protons have already been assigned. For example, HSQC spectrum of **PtL11Cl** (Figure 3.12) shows a correlation between proton H_1 and the carbon at 152.16 ppm; this carbon is now assigned as C_1 . The DEPT experiments also confirm these assignments. HSQC was also used in confirming proton assignments of nitrogen or oxygen-bound protons; as no signal was shown by HSQC. The NH amide and NH_2 protons assignment for **PtL3^{1a}Cl_d** for instance, appears at (8.82 - 7.89) ppm respectively, were confirmed by HSQC as the protons show no correlation to a carbon signal (Figure 3.13).

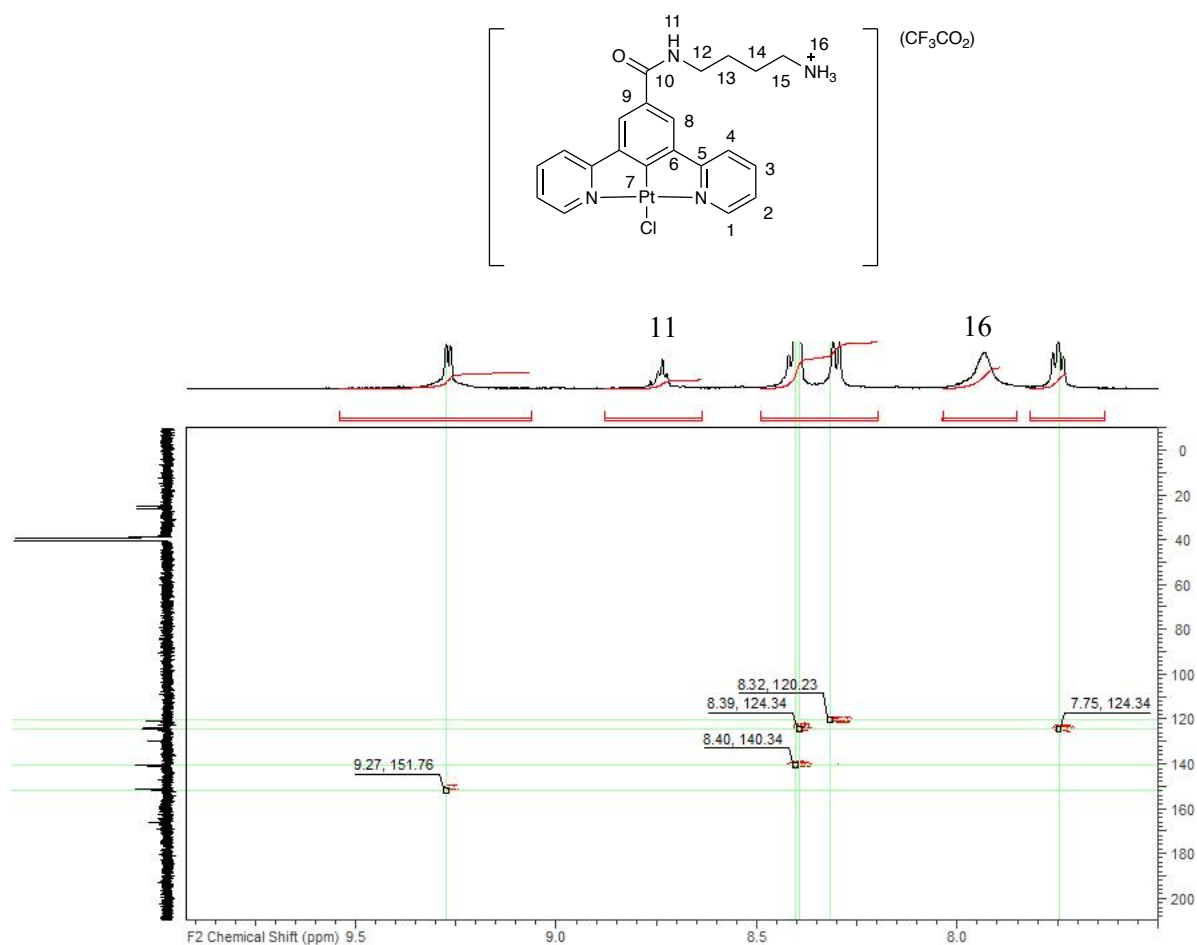


Figure 3.13: HSQC NMR spectra (DMSO at 500 MHz) of $\text{PtL3}^{1a}\text{Cl}_d$.

3.5.2 Mass Spectrometry

Unlike the proligands, most of the complexes do not contain any available sites for protonation. Mass peaks corresponding to the whole complex $[\text{M}]^+$ were difficult to detect using electrospray positive ion mass spectrometry (ESI)⁺. In the high resolution ESI experiment, the mass that was detected corresponded to the complex minus the ancillary ligand M-X , which hindered full characterisation of complexes resulting from ancillary ligand substitution. However, in the case of the cationic Pt(II) complexes the molecular ion peaks M^+ corresponding to the whole complex was easily observed which allow a full characterisation of the complexes. A low intensity peak at $[\text{2M-Cl}]$ is also commonly observed, which corresponds to a chlorobridged dimer. It is unclear whether this species forms during the HRMS experiment, or whether such species form during complexation. Hence, this phenomenon was also reported by William's and co-workers for similar Pt(II) complexes.⁹⁶

Furthermore, some of the masses correspond to the neutral Pt(II) complexes (where X = alkyne ligands) $[M+Na^+]$ was observed. Such species often appear in ESI⁺ experiments, and result from proton transfer during the experiment.

Atmospheric Solids Analysis Probe (ASAP) mass spectrometry has been successfully used for some of the complexes that were not soluble or air sensitive. ASAP uses an ambient ionization method, and can analyse a large array of substrates, including non-polar, high-melting point solids. This technique involves an atmospheric pressure ionization technique, where a hot desolvation gas is used to vaporise the sample, and the technique is ideally suited to analysis of the complexes. The complexes were input directly as solids, and the high resolution experiment returned peaks corresponding to the molecular ion and the molecular ion-minus-ancillary ligand. Sometimes however, the molecular ion peak is very weak, and the signal-to-noise ratio prevents accurate determination of this mass. When this was the case, the stronger peak corresponding to M-X (where X = ancillary ligand) has been reported

Typical platinum isotopic cluster pattern was observed in the mass spectra for all of the synthesised Pt(II) complexes demonstrating the presence of isotopes ¹⁹⁴Pt (32.9), ¹⁹⁵Pt (33.8), ¹⁹⁶Pt (25.3), ¹⁹⁸Pt (7.2) with the nuclide abundance in parentheses (A %). The *m/z* values recorded in the experimental section refer to the isotopic cluster corresponding to the ¹⁹⁵Pt.

3.5.3 X-ray Crystal Structures

3.5.3.1 Crystal Structures of Pt(II) Complexes

PtL10Cl, **PtL9Cl**, and **PtL3^{1a}Cl_d** complexes were successfully crystallized *via* either a slow evaporation of dichloromethane **PtL10Cl** or a slow vapor diffusion of diethyl ether into a concentrated dichloromethane solution (**PtL9Cl** and **PtL3^{1a}Cl_d**) (Figure 3.15). Important bond lengths and angles are given in Table 3.1. (Note: complete crystal data are given in Appendix 1). X-ray diffraction studies confirm the expected N²CN tridentate coordination, with binding of the anticipated ancillary ligand trans to the cyclometallating carbon.

Table 3.1: Selected bond lengths (Å) and angles (deg) of the Pt(II) complexes (All structures were acquired at 150 (2) K).

	PtL10Cl	PtL9Cl	PtL3^{1a}Cl_d
Pt-C ¹	1.914(8)	1.937(14)	1.892(11)
Pt-Cl	2.400(2)	2.403(4)	2.426(3)
Pt-N ¹	2.036(6)	2.044(12)	2.054(9)
Pt-N ²	2.035(6)	2.002(13)	2.034(9)
C ¹ -Pt-Cl	179.7(2)	179.2(4)	174.8(3)
N ² -Pt-N ¹	160.9(2)	160.2(5)	160.5(3)
N ² -Pt-Cl	99.67(18)	100.6(4)	100.0(2)
N ¹ -Pt-Cl	99.38(19)	99.3(3)	99.4(3)
C ¹ -Pt-N ²	80.2(3)	79.2(5)	78.9(4)
C ¹ -Pt-N ¹	80.7(3)	80.9(5)	81.5(5)

In all cases, approximately co-planar coordination could be confirmed, with C-Pt-Cl bond angles approaching 180 °. However, the N²-Pt-N¹ bond angles are distorted from linearity (but within the plane of the molecule), with angles approaching 160 °, and it is best to describe the Pt(II) centre as existing in a distorted square planar geometry. This distortion reflects the less-

than-optimum bite angle imposed by the tridentate ligand. Similar distortions are also found in Pt(II) (terpyridine, 1,3-dipyridylbenzene and 1-pyridyl-1,2,3 triazole benzene) complexes.¹³⁰ In the 1,3-dipyridylbenzene complexes, the Pt-C and Pt-N bond lengths are calculated as 1.91 Å and 2.03 Å respectively. These bonds are much shorter than corresponding bonds in related 6-phenyl-2,2'-bipyridine complexes (Figure 3.14) (where Pt-C and Pt-N are calculated as 2.04 Å and 2.14 Å),⁹⁶ reflecting the greater degree of orbital overlap, which results in the enhanced ligand field induced by N[^]C[^]N coordination.

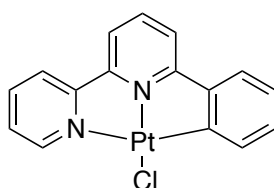


Figure 3.14: Chemical structure of 6-phenyl-2,2'-bipyridine Pt(II) complex.

Upon replacement of the outer pyridine ring by 1,2,3-triazole ring **PtL9Cl**, Pt-C distance increases to 1.937(14) Å. A similar observation was made on the parent structure of **PtL9Cl** by Schulze and co-workers.¹³¹ However, paying attention to the standard deviations given in these measurements, these distances may not be statistically relevant. The Pt-N distances are identical for pyridines when they are part of the same complex, namely for **PtL10Cl** (2.036(6) and 2.035(6) Å, respectively). However, the Pt-N² distance is shortened when replacing one pyridine with 1,2,3-triazole (2.002(13) Å), and this is opposite to what been observed in the related complex in the literature.¹³¹ The former findings may attribute to the more pronounced s-character of the triazole's N³ lone pair.¹³² The Pt-Cl bond is notably long (approximately 2.40 Å) in the case of the cyclometalated complexes as a result of the well-known *trans*-influence.^{133,134}

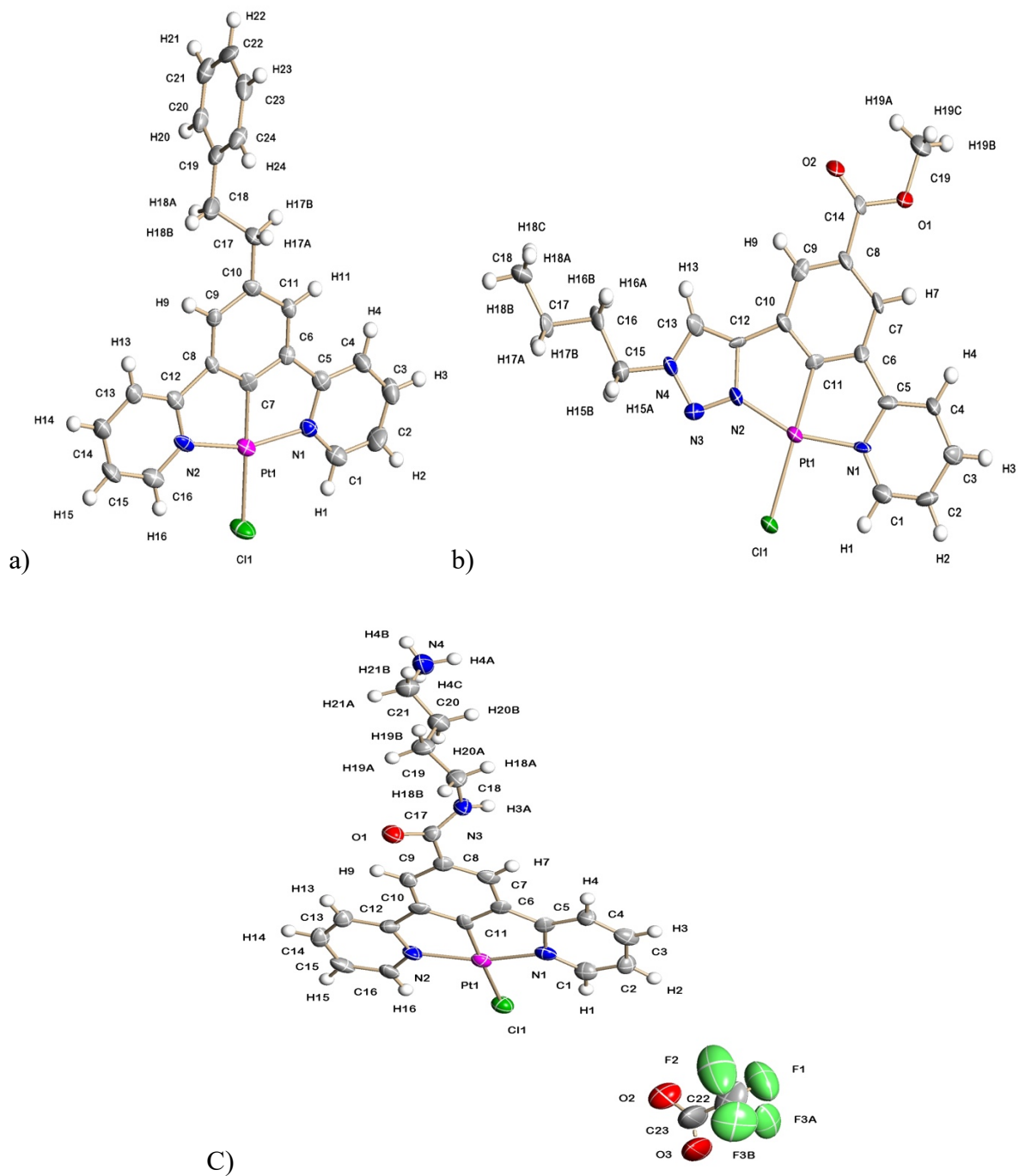


Figure 3.15: Molecular structures of a) PtL10Cl b) PtL9Cl c) PtL3^{1a}Cl_d.

3.5.3.2 Pt(IV) Complex Structure of PtL12Cl₃

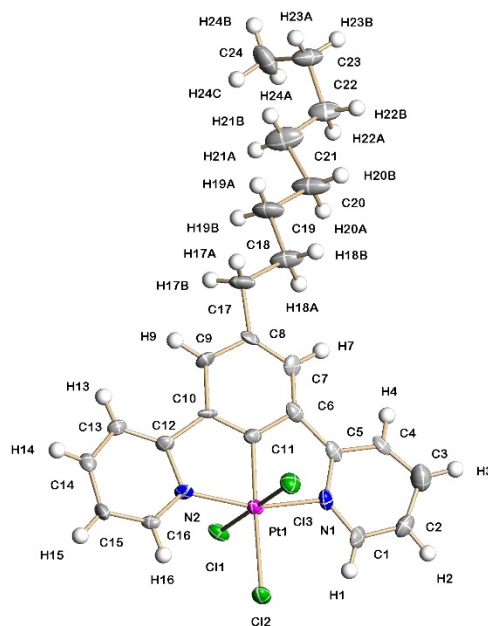


Figure 3.16: Crystal structure of PtL12Cl₃

Small crystals, suitable for X-ray diffraction, were obtained of PtL12Cl₃ via a slow evaporation from deuterated chloroform solvent. The complex adopts an approximately octahedral geometry, and important bond lengths are given in Table 3.2. The Pt-Cl bonds are non-equivalent within the complex, the longest Pt-Cl bond always corresponds to that which is trans to the cyclometallating carbon. The crystal structure of the substituted parent, PtL12Cl₃, which has been reported by William's and co-workers, also displays this behaviour.⁹⁶ This is consistent with a greater trans influence of an anionic carbon ligand compared to chloride. Compared to structures of the Pt(II) complexes, the Pt(IV) complex possess longer Pt-C bond (approximately 1.91 and 1.95 Å respectively). This elongation probably occurs to reduce steric interactions with the additional chloride ligands.

Table 3.2: Selected bond lengths (Å) and bond angles (deg) for PtL12Cl₃.

	PtL12Cl ₃		PtL12Cl ₃
Pt-C ¹	1.948(7)	C ¹ -Pt-Cl ¹	91.6(9)
Pt-N ¹	2.063(18)	C ¹ -Pt-Cl ²	177.8(9)
Pt-N ²	2.024(18)	C ¹ -Pt-Cl ³	89.1(9)

Pt-Cl ¹	2.323(6)	N ² -Pt-N ¹	161.6(2)
Pt-Cl ²	2.4361(18)	C ¹ -Pt-N ²	82.0(10)
Pt-Cl ³	2.307(6)	C ¹ -Pt-N ¹	79.8(10)

3.5.3.3 Crystal Packing

For all complexes, the molecules arrange themselves in one-dimensional stacking columns, similar to those reported for **PtL1Cl**. Within each stack, molecules adopt an antiparallel arrangement, effectively cancelling out the dipole moment of the nearest neighbour. The packing of **PtL9Cl** has somewhat different orientation, as it displays a close to head to tail orientation – it also adopts columnar packing (Figure 3.17).

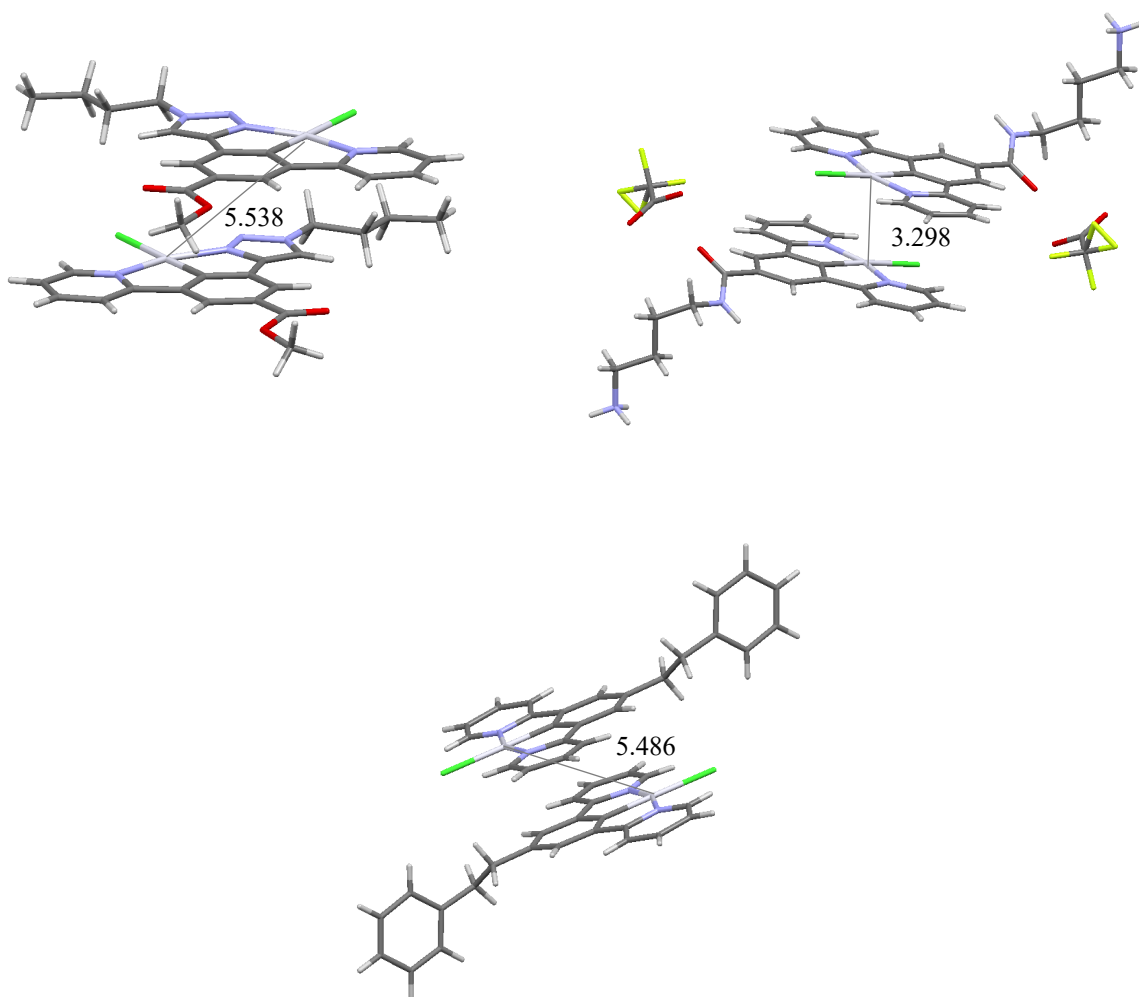


Figure 3.17: Packing of **PtL9Cl**, **PtL3^{1a}Cl_d** and **PtL10Cl** viewed along the a-axis.

To estimate whether any significant π - π or Pt-Pt interactions exist in the crystal packing, centroid-to-centroid distances were analysed. Distances of less than 3.7 Å were taken to indicate the presence of such interactions. Considering the aggregation tendency of the studied Pt(II) complexes, only one of the complexes displayed significant Pt-Pt interactions (**PtL3^{1a}Cl_d** (3.298 Å)) in their packing. In contrast, for complexes **PtL9Cl** and **PtL10Cl**, the central complex planes are well-separated from each other. This is probably due to steric interactions which prevent both complexes from being close in space.

3.6 Concluding remarks

A series of a novel platinum complexes were successfully synthesised these contained three types of a substituted N[^]C[^]N based tridentate ligands. **PtLnCl** (where n = **3^{1a}** or **3^{4a}** or **9^{1a}**) complexes were found to be more stable under strong acidic condition required for Boc deprotection than **PtL1X** (where X = alkyne or pyridine substituted monodentate ligands). These complexes were characterised *via* mass spectrometry, 1D and 2D ¹H and ¹³C NMR spectroscopy and results are further compared with the similar complexes quoted in literature. **PtL10Cl**, **PtL9Cl**, **PtL12Cl₃** and **PtL3^{1a}Cl_d** complexes were analysed further by X-ray crystallography. New methods have been explored to accelerate the overall synthetic route. These complexes are prepared in a similar manner to other examples of Pt(II) complexes in the literature⁹⁶ but the use of a microwave reactor has greatly reduced reaction times which enabled the complex to be prepared in 45 minutes instead of 3 days requirement for the conventional heating.

The substitution of the ancillary ligands with (alkyne or pyridine) substituted monodentate ligands was also investigated. It is believed that the strong destabilising nature of the cyclometalating bond generates a system disadvantageous to formation of new complexes with strongly donating ancillary ligands. Although, all blame cannot be attributed to the cyclometalating bond, since success incorporating *trans-carbanions* has been achieved in platinum(II) pincer complexes which contain softer donors than pyridine in the *cis*-positions.¹²⁷

Chapter 4

4 Photophysical Properties

Platinum(II) complexes incorporating a 1,3-di(2-pyridyl)benzene ligand are known to be highly luminescent, with lifetimes on the microsecond (μs) scale.⁹⁶ For example, the parent complex, **PtL1Cl**, exhibits a quantum yield (Φ) of 0.60 in degassed DCM at room temperature, and a lifetime at infinite dilution (τ_0) of 7.2 μs .⁹⁶ In order to evaluate the potential of the novel platinum(II) complexes as luminescent labels for bioimaging applications, the photophysical properties in solution were investigated. In this chapter, the photophysical properties including absorption and emission wavelengths, luminescent quantum yields, and lifetimes of a series of N[^]C[^]N-coordinated Pt(II) complexes will be discussed. The photochemistry of the complexes, on the whole, will be discussed together; however, the functional complexes incorporating a monodentate pyridine or alkyne ligands will be discussed separately with their own unique features.

4.1 Absorbance

Absorption spectra showing the lowest energy transitions of the complexes **PtLnCl** ($n = 1, 6a, 7, 9, 10, 11, 12$) recorded in dichloromethane at a concentration of 1×10^{-4} M at room temperature (Figure 4.1). All of these complexes display very intense absorption bands at ≤ 300 nm, assigned to $\pi - \pi^*$ transitions localised on the aromatic ligand, in accordance with previous literature on the parent complex **PtL1Cl**.⁹⁶ These transitions are followed by a second set of intense bands in the region 360 - 450 nm, assigned to metal-to-ligand charge transfer (¹MLCT). In the case of the complete replacement of the pyridine rings by 1,2,3-triazole rings in **PtL7Cl**, which is known to raise the energy of the π^* orbitals,^{132,135,136} a substantial hypochromic shift is observed in the absorption spectra. In comparison with the parent N[^]C[^]N Pt(II) complex **PL1Cl**, the second set of transitions consists of at least three bands, of which one, *ca.* 380 nm, is invariant within this series, and thus apparently independent of the 5-position substituent. The component of the lowest energy in this particular set of transitions is slightly red shifted through the range of complexes from 401- 417 nm. Hence, the electron-donating effects of the substituted group directly lead to a red shift in the ¹MLCT and a concomitant reduction in the oxidation potential when compared to the core structure **PtL1Cl**. This is primarily attributed to the effect that this substituent has upon the HOMO of this transition.¹³⁷ In **PtL7Cl**, the latter set of bands were also blue-shifted (308-370) relative to those in **PtL1Cl**. For **PtL9Cl** complex, bearing both a pyridine and a 1,2,3-triazole donor, the

absorption spectrum apparently combines absorption features of **PL1Cl** and **PtL7Cl** (Figure 4.1).

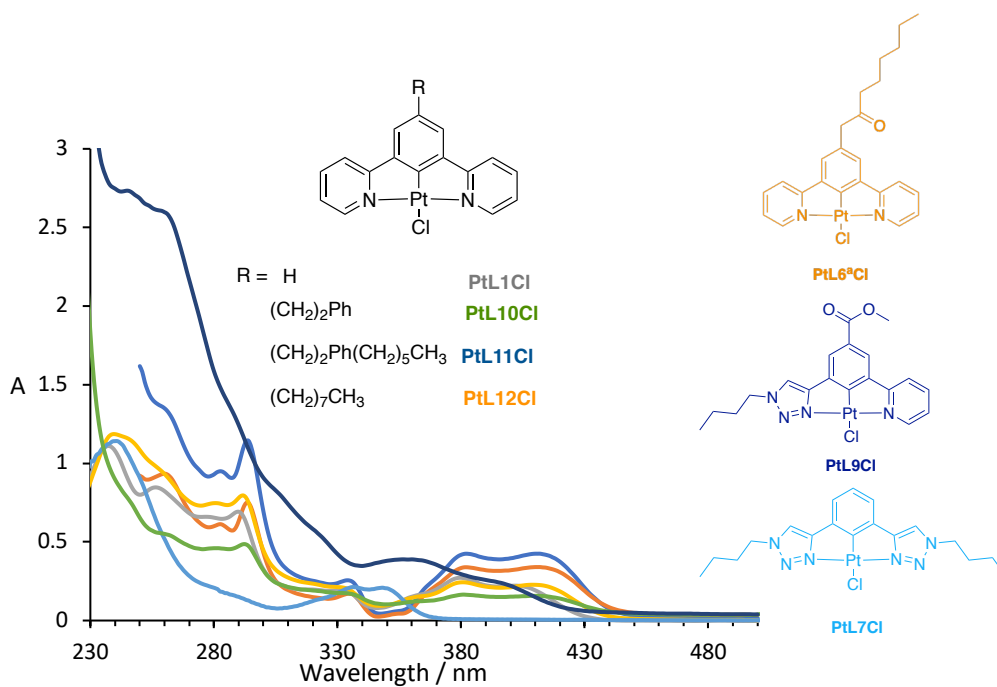


Figure 4.1: UV-vis absorption spectra of the Pt(II) complexes **PtLnCl** ($n = 1, 6a, 7, 9, 10, 11, 12$) 10μ M in DCM.

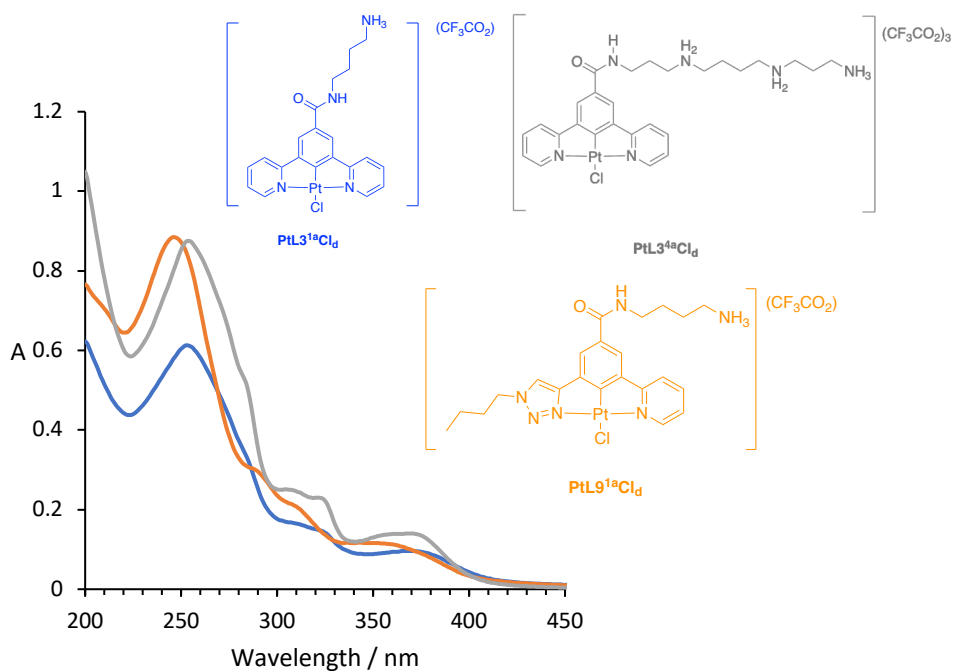


Figure 4.2: UV-vis absorption spectra of the Pt(II) complexes **PtLnCl** ($n = 3^{1a}, 3^{4a}, 9^{1a}$) 10μ M in deionised water.

In the highly water soluble complexes, **PtLnCl** ($n = 3^{1a}, 3^{4a}, 9^{1a}$), the absorption spectrum exhibits strong negative solvatochromic behaviour on going from the least polar solvent investigated, DCM, to the most polar solvent, deionised water (Figure 4.2). Strong solvatochromism is typical of transitions with an appreciable degree of charge transfer character, whilst the negative shift implies an excited-state with a lower dipole moment than the ground-state,¹³⁸ illustrated in (Figure 4.3). The absorption spectrum of these complexes showed two intense bands in the near UV region between 200 and 220 nm and between 225 and 300 nm corresponding to the $^1\pi-\pi^*$ transitions of the ligands. These are accompanied by a weaker, lower energy feature between 350-400 nm, assigned to the $^1\text{MLCT}$ bands.

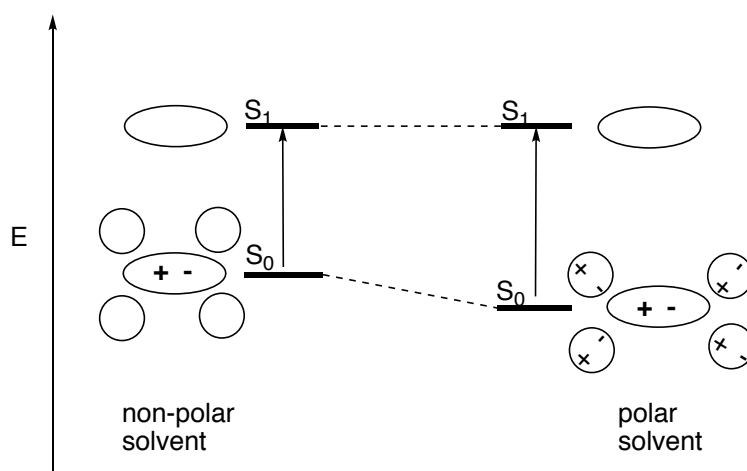


Figure 4.3: Diagram illustrates the solvent effect on the absorption shifts of a molecule with a large dipole moment in its ground than excited-state.¹ Hence, the transition on the right is higher in energy in polar media, observed as negative solvatochromism, due to the relative stabilisation effect of the solvent of the molecule's ground state.

4.2 Emission

In the case of N^CN 1,3-di(2-pyridyl)benzene based complexes, all complexes are intensely luminescent in dilute DCM at room temperature upon excitation at 410 nm (Figure 4.4). The emission maxima of the aryl-substituted complexes are slightly red shifted through the series in the order **PtL6^aCl** < **PtL1Cl** < **PtL12Cl** < **PtL10Cl** < **PtL11Cl**. As described in Section 4.1.1, the red shift is most likely a direct consequence of electron-donating groups raising the energy of the HOMO. In emission, the highest intensity vibrational band was typically the one of highest energy, which corresponds to the 0–0 vibrational origin of the T¹ to S⁰ transition. The bands at lower energy (and lower intensity) correspond to transitions to higher vibrational levels of the ground state. The shape and highly structured nature of the spectrum suggests that little geometric rearrangement occurs between the ground and excited states. Indeed, the emission characteristics compare well with those of the similar complexes.^{96,4,22,139}

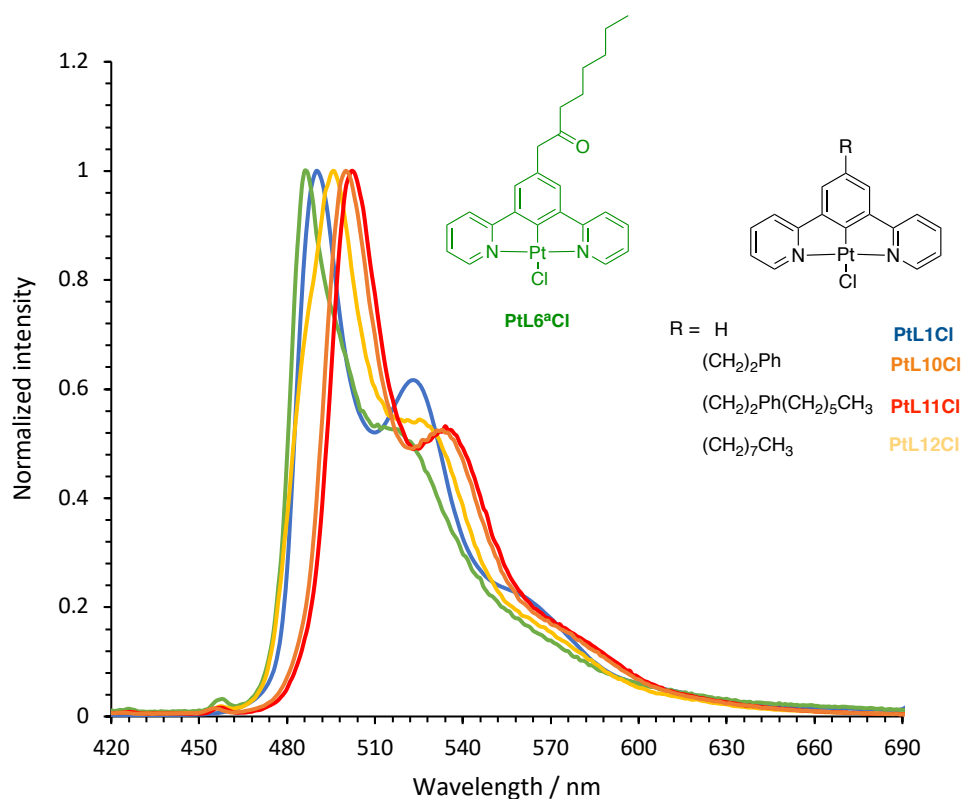


Figure 4.4: Emission spectra of the Pt(II) complexes **PtLnCl** (n = 1, 6a, 7, 11, 12) in DCM (10 μM).

In the case of the complete replacement of the pyridine rings on the cyclometalated N[^]C[^]N complex by 1,2,3 triazole rings, the emission was absent. This may be attributed to an additional lowering of the triplet metal-centred (³MC) energy and hence, more facilitated radiationless decay.¹³¹

For **PtL9Cl** complex, bearing both a pyridine and a 1,2,3-triazole donor, a highly intense green emission at λ_{max} 476 nm was observed. In contrast to what observed in the Uv-Visible spectrum, the emission spectrum of this complex is essentially identical in terms of the form and the structure of the spectrum to that of **PtL1Cl** (Figure 4.5), suggesting that the LUMO is localized on the pyridine ring.¹⁴⁰ Noticeably, the energetic separation between the emissive state and the ³MC is increased due to the energetically low-lying π^* orbitals of the pyridine moiety.¹³²

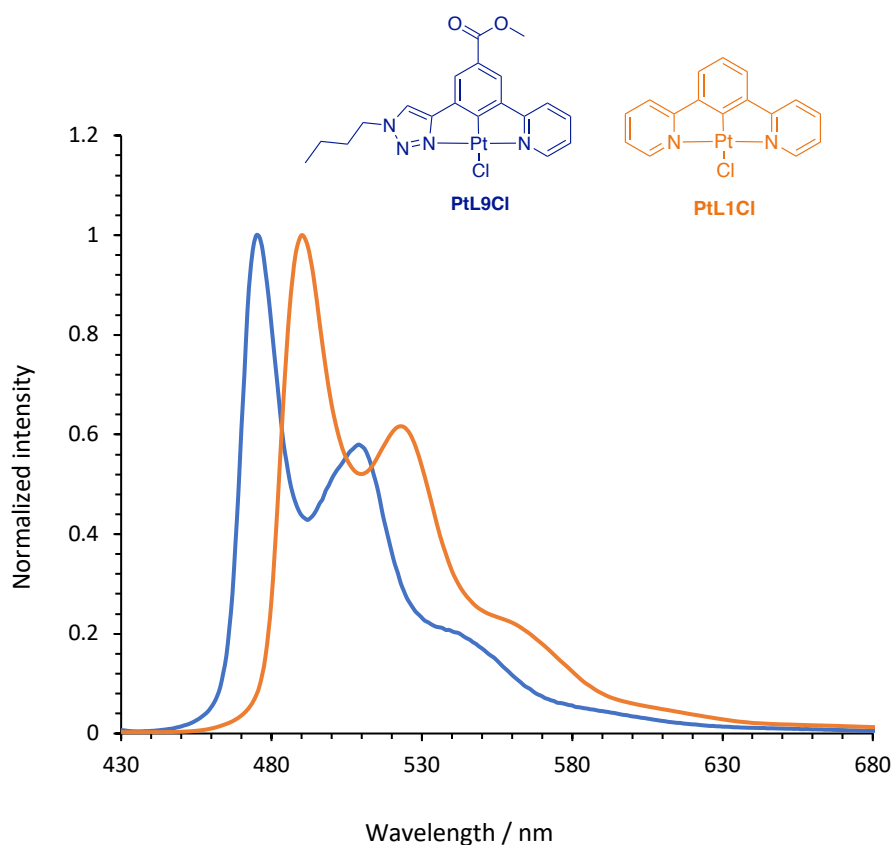


Figure 4.5: Emission spectra of **PtL9Cl** and **PtL1Cl** in DCM (10 μ M).

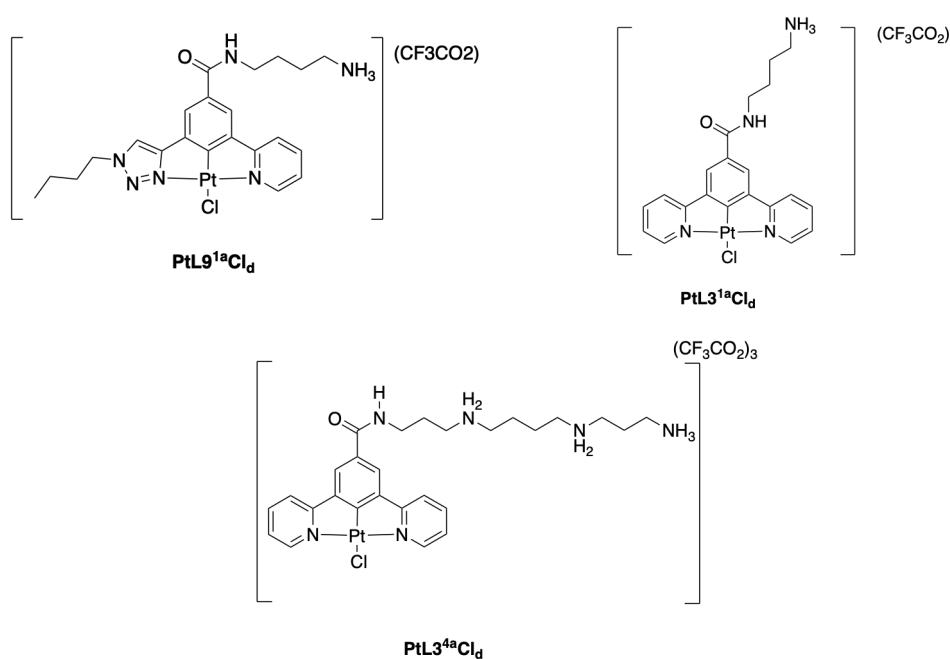
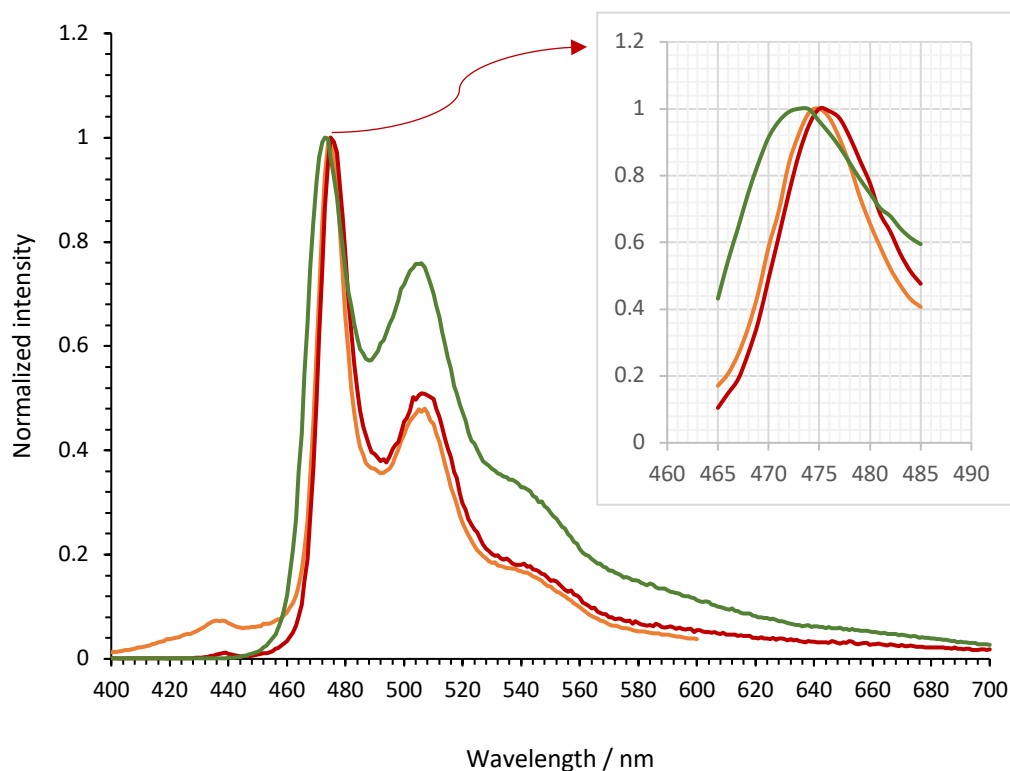


Figure 4.6: Emission spectra of the Pt(II) complexes (green **PtL9^{1a}Cl**, orange **PtL3^{4a}Cl**, and red **PtL3^{1a}Cl**) in deionised water (pH = 6.7) 10 μ M.

The emission spectra of the highly water soluble complexes **PtL9^{1a}Cl**, **PtL3^{4a}Cl** and **PtL3^{1a}Cl** showed structured bands corresponding to the phosphorescence from a ³MLCT state (Figure 4.6). The spectra show minimal effect of solvatochromism, *e.g.* shifting by only 20 nm from that of the core structure **PtL1Cl** in DCM, which is a feature typical of emission mostly from

a ligand-centred excited-state, where the polarity change accompanying this transition is localised toward the outer amine units.⁴ Such transitions are expected to display a minimal change in dipole moment, which then results in emission being largely unaffected by solvent polarity. The emission spectra of the complexes display a vibrationally highly structured resolved spectrum, typical of luminescence of ³LC character, therefore ³MLCT transition is too high in energy and not the lowest energy triplet transition. The component of highest intensity is the one of highest energy (*i.e.* 0-0 transition), indicating a minimal difference between ground- and excited-state geometry.

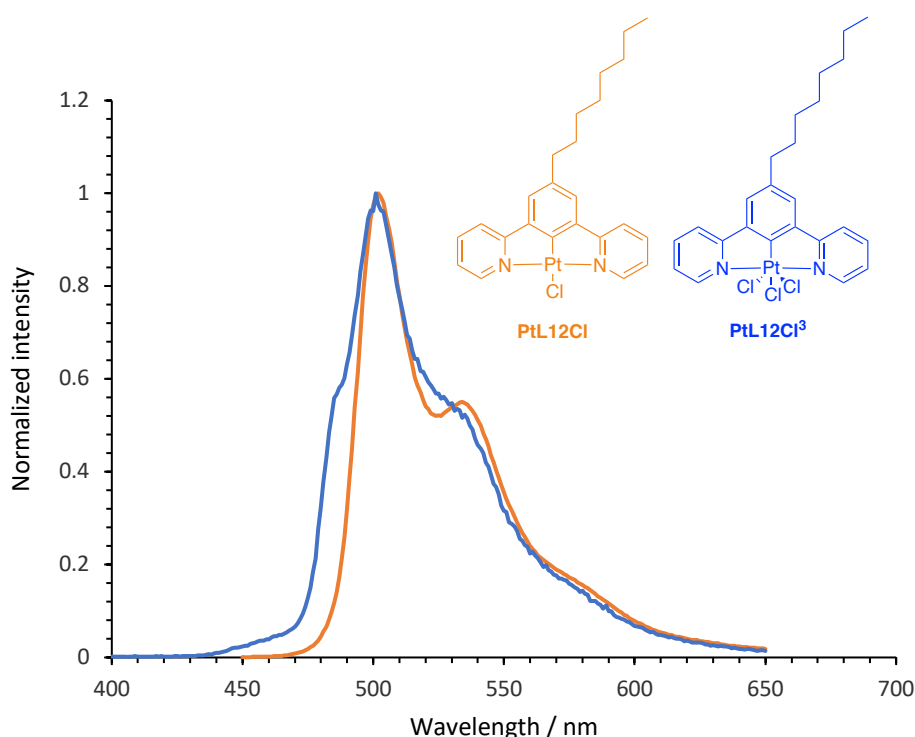


Figure 4.7: Normalized emission spectra of the Pt(II) complex (orange **PtL12Cl**), and Pt(IV) complex (blue **PtL12Cl³**) in DCM (10 μ M).

Comparison of the emission spectra of the tetradentate complexes **Pt(II)L12Cl** and **Pt(IV)L12Cl** showed that the luminescent emission in the green region had similar shape for both complexes (Figure 4.7). However, the lowest-energy emission bands corresponding to the ³MLCT transitions observed in the Pt(II) complexes almost disappear in the Pt(IV) analogues. This observation is consistent with the increase in the oxidation state of the metal, which should increase the energy associated with the ³MLCT transition, as it involves transient oxidation of the metal.

4.3 Excimeric Emission

For the complexes **PtLnCl** ($n = 1, 3^{1a}, 3^{4a}, 6a, 7, 11, 12$), increasing concentration leads to the appearance of a new, broad, structureless emission band centred at 690-700 nm, the progressive growth of which is accompanied by a concomitant reduction in the intensity of the aforementioned ^3LC emission. No significant differences were observed in the position or spectral profile of this low-energy band formed by the different substituted complexes. This behaviour is characteristic of excimer formation and emission, common to square-planar platinum(II) complexes.^{141,96}

This effect can be seen in Figure 4.8; the emission profile of a dilute sample in DCM was compared to emission profiles of solutions of increasing concentration for **PtL10Cl**. As the concentration was increased, the broad structureless excimeric emission grew in at lower energy at the expense of the monomeric emission. The overall colour of light observed was dependent on the ratio of the monomeric-to-excimeric emission, and hence colour can be controlled simply by controlling concentration.

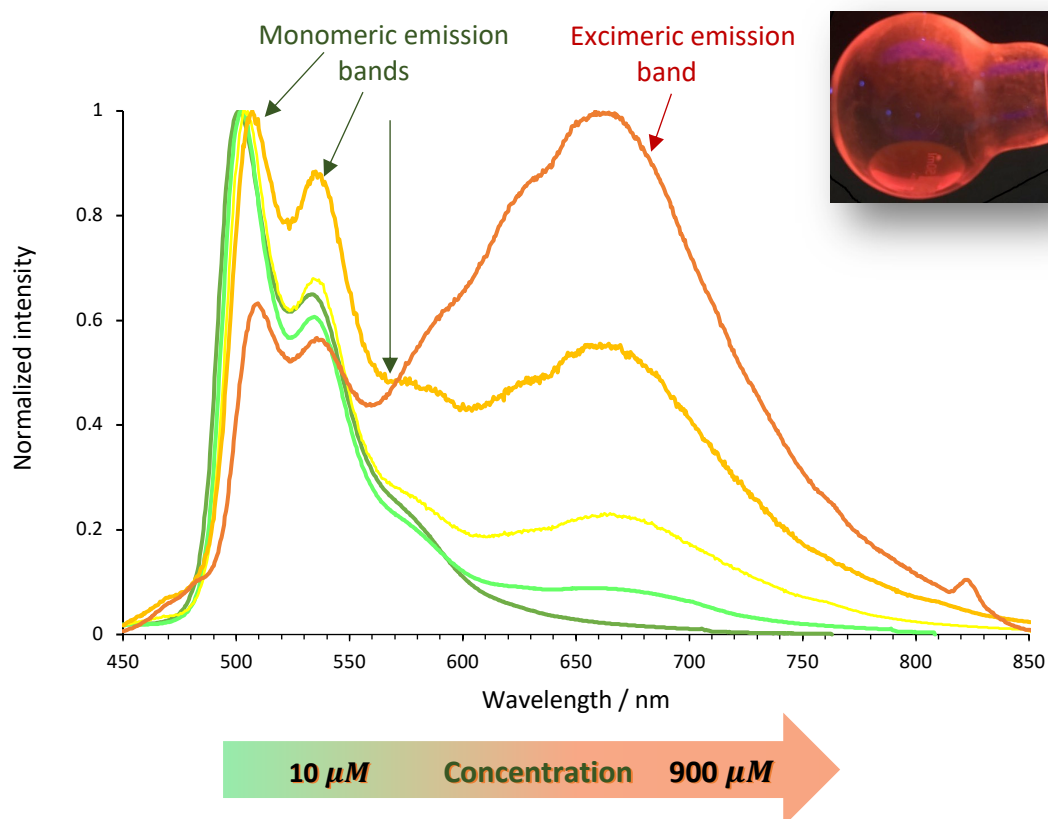


Figure 4.8: Emission spectra of various concentrations of **PtL10Cl** in DCM at room temperature. Note the increasing contribution from excimer emission with increasing concentration. A photograph of the emission under UV excitation (CH_2Cl_2 , $\lambda_{\text{ex}} = 365 \text{ nm}$).

Notably, in contrast to the previously mentioned complexes, no excimer emission was observed for **PtL9Cl**. It is suggested that, due to the presence of the bulky moieties, the aggregation tendency is lowered, in agreement with to what observed in the crystal structure (Section 3.5.3.3). Bulky, and sterically demanding systems, such as mesityl and tert-butyl groups are known to minimise solid-state intermolecular interactions between neighbouring planes of platinum complexes.¹³¹

4.4 Luminescence Quantum Yields and Lifetime Measurements

The fluorescence or phosphorescence quantum yield (Φ) is one of the most important photophysical parameters of emissive compounds and is defined as the ratio of the number of emitted photons relative to the number of photons absorbed. The luminescence quantum yield measurements vary depending on the experimental conditions, including solvent polarity, sample concentrations, quantity of dissolved oxygen in the solution, temperature and excitation wavelength.

There are two methods to calculate the quantum yield, including the gradient and single-point comparative methods. These involve comparing the analyte to a standard fluorophore of known quantum yield, as two fluorophores with the same absorbance at the same wavelength can be assumed to be absorbing the same number of photons. Thus, recording the emission spectrum of the two under identical conditions allows calculation to find a ratio of their quantum yields. Knowing the value of a standard allows the calculation of the quantum yield of an unknown. In this study $[\text{Ru}(\text{bpy})_3]\text{Cl}_2$ was chosen as the standard, with $\Phi = 0.028$ in aerated aqueous solution.⁶⁹

The single-point comparative method involves recording the electronic absorption spectrum with the fully corrected emission spectrum of the standard, and the analyte at the same molar concentration. The quantum yield can be calculated from Equation 4.1

$$\Phi_x = \Phi_s \left(\frac{A_s}{A_x}\right) \left(\frac{F_x}{F_s}\right) \left(\frac{\eta_x}{\eta_s}\right)^2 \quad \text{Equation 4.1}$$

x and s represent the analyte and the standard respectively, A is the absorbance at the excitation wavelength, F is the integrated fluorescence intensity and η is the refractive index of the solvent. The final term in this equation can be ignored, when all spectra are obtained in the same solvent.

The gradient method is slightly more accurate, and is the most reliable method of determining quantum yields. Plotting absorbance versus integrated fluorescence intensity over a range of concentrations gives a slope proportional to the quantum yield and absolute values can be calculated using Equation 4.2 through comparison to a standard. Again, the final term of the equation may be ignored if all measurements are conducted in the same solvent.

$$\Phi_x = \Phi_s \left(\frac{Grad_x}{Grad_s} \right) \left(\frac{\eta_x}{\eta_s} \right)^2 \quad \text{Equation 4.2}$$

The fluorescence quantum yield Φ in this study was measured via the gradient method, which gives more reliable Φ value of the Pt(II) complexes compared to that reported in the literature.

The luminescent lifetime (τ_0) can be defined as the average time a fluorophore remains in the excited state before emitting a photon and is a measure of the decay time of the fluorescent signal. It can be measured using time-correlated single photon counting (TCSPC). This is time-resolved measurement using a pulsed light source for excitation, which is adjusted so that less than one photon is detected per pulse and the time between the pulse and the photon detection is measured. Plotting the intensity versus time provides a curve representing the decay of the fluorescent signal that can be fitted with an exponential decay using the equation

$$I_t = I_0 e^{\frac{-t}{\tau}} \quad \text{Equation 4.3}$$

where I_t is the intensity at time = t , I_0 is the intensity at time = 0 and τ is the lifetime.

When calculating the quantum yield and lifetime, it is best to work using optically dilute solutions to minimise concentration effects such as self-quenching (*i.e.* conversion of the monomeric excited state to the excimer), the lifetime (τ_0) is observed to decrease with increasing concentration.¹⁴²

Quantum yields of metal complexes are generally highest in the green region: they decrease towards the blue region due to the energetic proximity of higher-lying deactivating states and decrease towards the red because of increased vibrational deactivation.¹⁴³

4.4.1 Quantum Yield and Lifetime of PtLnCl Complexes

Luminescence lifetime and quantum yields were recorded for all **PtLnCl** (**n = 6a, 9, 10, 11, 12**) complexes in aerated DCM at room temperature; quantum yield was calculated for all complexes by using the gradient method and lifetime of the complexes was measured by time-correlated single photon counting spectroscopy. The aerated quantum yields of **PtLnCl** (**n = 10, 11, 12**) 1,3-di(2-pyridyl)benzene based complexes were quite high relative to the reported parent complexes, in the range of 0.09-0.13 (Table 4.1). Whereas, the luminescence lifetimes were comparable in the microsecond range of 0.6-0.8 μs (Figure 4.9). This tells us something about the origin of the relative efficiencies of these complexes.

Φ and τ_0 are related to the radiative and non-radiative rate constants of the excited state. Relations between these radiative and non-radiative constants are given by Equations 4.4 and 4.5.

$$k_r = \frac{\Phi}{\tau} \quad \text{Equation 4.4}$$

$$k_{nr} = \frac{1}{\tau} - k_r \quad \text{Equation 4.5}$$

Thus, the larger Φ and comparable τ of these complexes relative to the parent complexes means that k_r is larger and k_{nr} is smaller for the former complexes, and these complexes are probably more efficient emitters.^{143,144}

Table 4.1: Luminescence lifetimes and emission quantum yields of **PtLnCl** (**n = 1, 3, 10, 9, 11, 12**) in aerated DCM.

Complex	τ_0 (aerated)/ μs	Φ_{lum} (aerated)
PtL1Cl ⁹⁶	0.50	0.039
PtL3Cl ⁹⁶	0.6	0.067
PtL10Cl	0.64	0.130
PtL11Cl	0.68	0.100
PtL12Cl	0.85	0.095
PtL9Cl	0.84	0.330

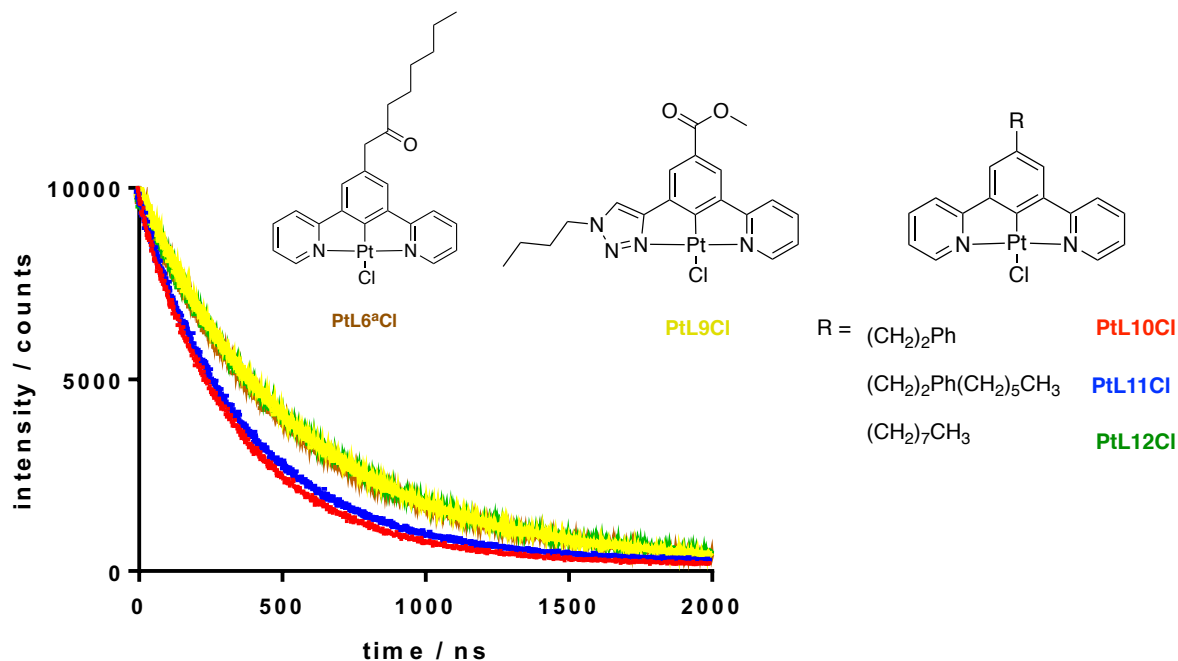


Figure 4.9: TCSPC luminescence exponential decay plots for **PtLnCl** ($n = 6a, 9, 10, 11, 12$) complexes at $\lambda_{\text{ex}} = 380 \text{ nm}$ $\lambda_{\text{em}} = 490 \text{ nm}$ ($100 \mu\text{M}$) in aerated DCM.

The quantum yield of **PtL6^aCl** ($\Phi = 0.03$) containing a ketone functionality on the para-position, is quite poor compared to **PtL12Cl** ($\Phi = 0.095$). This decrease in Φ could be because the excited state is becoming closer in energy to a higher lying non-radiative state, such as the $d-d^*$ state, so that there is an increased probability of non-radiative decay. This phenomenon is supported by the comparable lifetime ($\tau_0 = 0.83$ and 0.85) μs respectively, which indicates the increase in the k_{nr} .

The quantum yield for **PtL9Cl** complex, bearing both a pyridine and a 1,2,3-triazole donor, is ($\Phi = 0.33$) in aerated DCM, which is interestingly higher than the reference **PtL3Cl** ($\Phi = 0.067$). Moreover, the lifetime for this complex is ($\tau_0 = 0.84$), displaying a slightly higher timescale than the reference complex ($\tau_0 = 0.6$) in aerated DCM. As discussed earlier, large Φ and comparable τ of these two complexes could be attributed to large k_r .

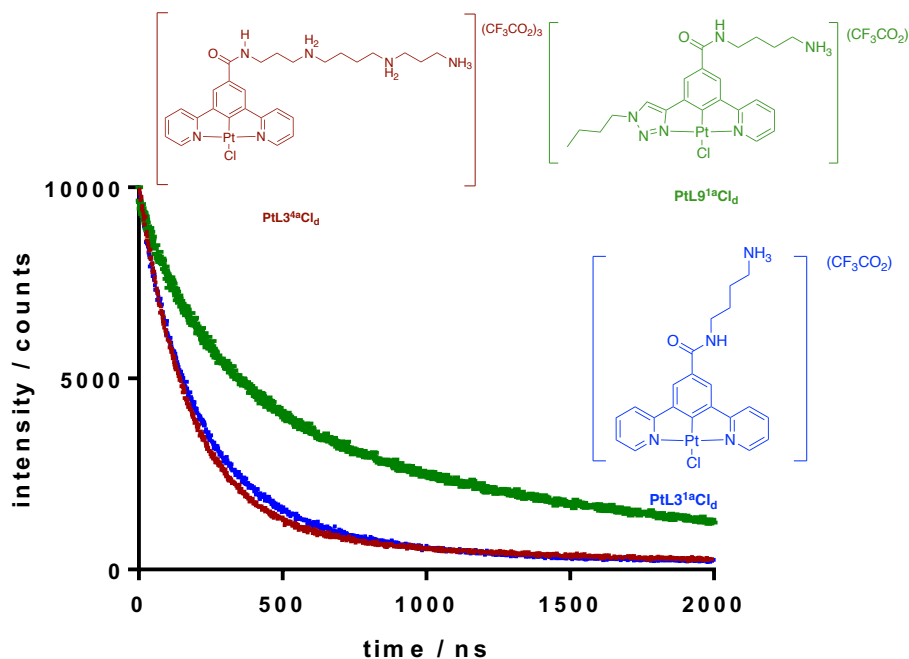


Figure 4.10: TCSPC luminescence exponential decay plot for **PtL9^{1a}Cl**, **PtL3^{4a}Cl** and **PtL3^{1a}Cl** complexes at $\lambda_{\text{ex}} = 380 \text{ nm}$ $\lambda_{\text{em}} = 490 \text{ nm}$ (100 μM) in aerated H₂O.

The quantum yields and luminescence lifetimes of **PtL9^{1a}Cl**, **PtL3^{4a}Cl** and **PtL3^{1a}Cl** complexes were recorded in aerated water solution (pH = 6.4). The quantum yields of these complexes in the range of 0.027-0.084 and the lifetimes are of the order of 0.62–1.31 μs (Table 4.2). It is difficult to draw reliable comparisons to similar complexes reported in the literature as the measurements are often recorded under different conditions, and the quantum yield is sensitive to changes in solvation and dissolved oxygen content. However, these complexes show a remarkable low sensitivity to quenching by oxygen compared to the parent complex **PtL3Cl** in aerated DCM, despite the fact that, complexes being dissolved in aqueous media may result in enhanced aggregation, unlike a chlorinated solvents. Furthermore, fluorescence lifetime tends to be shorter in more polar environment, because larger dipole moments of surrounding molecules can increase the efficiency of energy transfer.¹⁴⁵

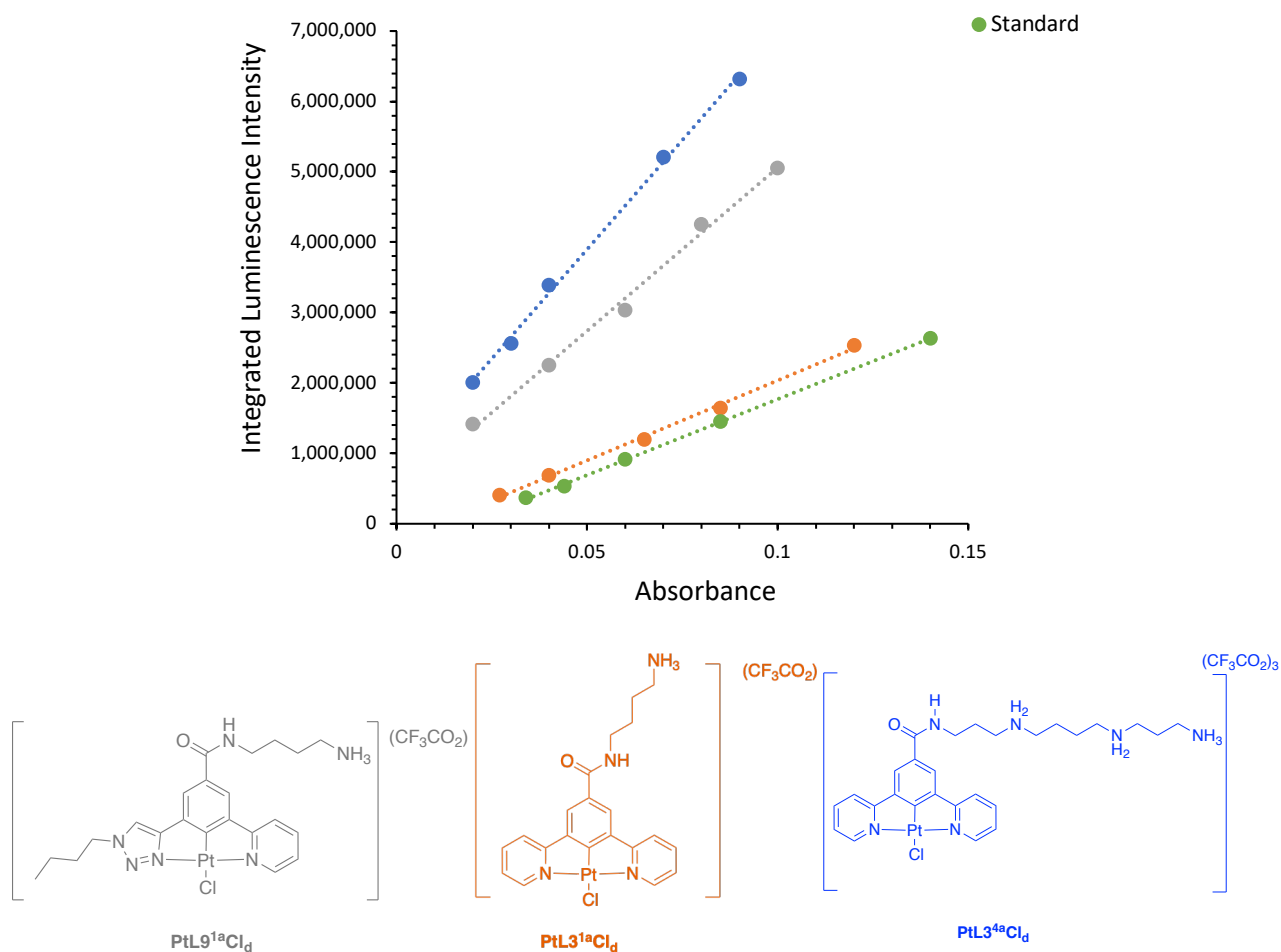


Figure 4.11: Integrated Fluorescence Intensity-Absorbance for **PtL3^{1a}Cl**, **PtL3^{4a}Cl** and **PtL9^{1a}Cl** and **[Ru(bpy)₃]Cl₂** as a standard in aerated H₂O at ($\lambda_{\text{ex}} = 380 \text{ nm}$ $\lambda_{\text{em}} = 490 \text{ nm}$).

Table 4.2: Luminescence lifetimes and emission quantum yields of **PtL3^{1a}Cl**, **PtL3^{4a}Cl** and **PtL9^{1a}Cl** in aerated H₂O.

Complex	τ_0 (aerated)/ μs	Φ_{lum} (aerated)
PtL3^{1a}Cl	1.08	0.027
PtL3^{4a}Cl	0.62	0.084
PtL9^{1a}Cl	1.31	0.06

In summary, the long luminescence lifetimes of **PtL9^{1a}Cl**, **PtL3^{4a}Cl** and **PtL3^{1a}Cl** complexes, makes these compounds promising candidates for use in time-resolved emission imaging microscopy, confocal microscopy and fluorescence lifetime imaging (FLIM) on the microsecond timescale.

4.5 Ancillary Ligand Substitution

Many examples may be found in the literature regarding substitution of the ancillary ligand(s) in related $N^{\wedge}N^{\wedge}N$, and $N^{\wedge}N^{\wedge}C$ complexes.^{126,146,147,25,148} Replacement of chloride ligand for stronger field ligands such as acetylides and cyanide often causes the $d-d^*$ state to shift to higher energy, decreasing its deactivating effect, which is observed as an increase in quantum yield. These substitutions are commonly accompanied by an increase in emission energy, which also results from the increased ligand field splitting energy.

During the last five years, there are a few reports concerning ancillary ligand substitution in $N^{\wedge}C^{\wedge}N$ complexes and their photophysical properties has been published to date.^{149,28,150,151} J. A. G. Williams *et al.* reported a series of $N^{\wedge}C^{\wedge}N$ complexes involving pyridine- or phosphine-based ancillary ligands.²⁸ These complexes had an overall charge of +1 and were unstable to decomposition in the presence of Lewis bases such as CH_3CN . The emission energies of phosphine-containing complexes are very similar to those of the analogous chloro-complexes, indicating that the 3LC excited state energy is not significantly affected by these ancillary ligands. Unfortunately, photophysical data for the pyridine complexes was not reported. Recently, Yam and co-workers have reported a series of alkynylplatinum(II) $N^{\wedge}C^{\wedge}N$ cyclometallated complexes which exhibited luminescent quantum yield up to 13%.¹⁵²

4.5.1 Cl Substitution for PtL7Cl

As discussed earlier, no emission was observed for **PtL7Cl**. However, upon substituting the Cl in **PtL7Cl** complex with an alkyne or pyridine, an emission band was observed at 534 and 428 nm respectively in degassed DCM (Figure 4.10). No sign of emission was detected in aerated DCM. This suggests that the excited states are a hybrid of singlet and triplet states, as discussed previously in the introduction, which allows the transfer of energy to the molecular oxygen in triplet state creating singlet oxygen, therefore leads to quenching of emission in the aerated samples. Notably, a red shift (106 nm) in the emission was observed for **PtL7C \equiv CPh** relative to **PtL7Py**. This may arise from the triplet excited state including metal to ligand charge transfer (MLCT) [$d\pi(\text{pt}) \rightarrow \pi^*(N^{\wedge}C^{\wedge}N)$] along with some ligand to ligand charge transfer (LLCT) [$\pi(C\equiv C) \rightarrow \pi^*(N^{\wedge}C^{\wedge}N)$] character.

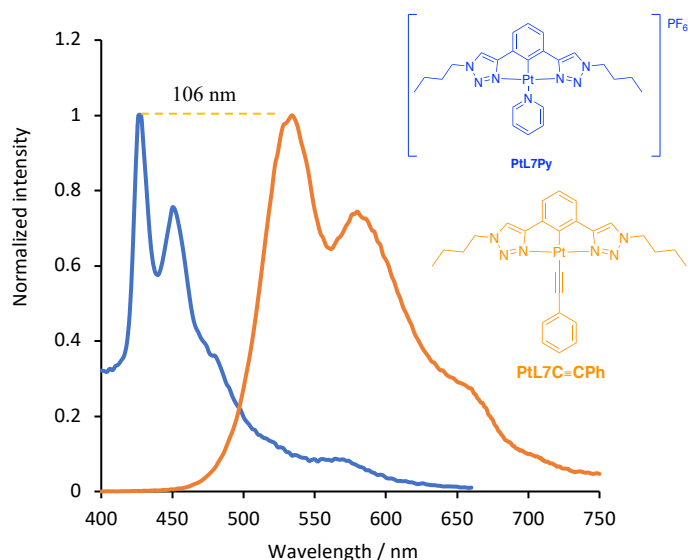


Figure 4.10: Normalized emission spectra of **PtL7Py** (blue) $\lambda_{\text{max}} = 428$, and **PtL7C≡CPh** (orange) $\lambda_{\text{max}} = 534$ in degassed DCM.

In summary, it is concluded that as these complexes do not show an intense emission and are prone to undergo self-quenching in aerated samples, meaning that it would be challenging to employ these fluorescent probes in cellular imaging applications.

4.5.2 Cl Substitution for PtL1Cl

As discussed previously in section 2.5.3 (PEG) alkyne linker was chosen based on their known ability to enhance the aqueous solubility and bio-compatibility of similar Pt(II) complexes. The resultant **PtL1-12a** complex was found to be partially soluble in water; however, it was sufficiently soluble to study the photophysical properties in aqueous media. The effect of solvent (DCM and water) on the absorption and emission properties of **PtL1-12a** (Figures 4.11 and Figure 4.12) was investigated.

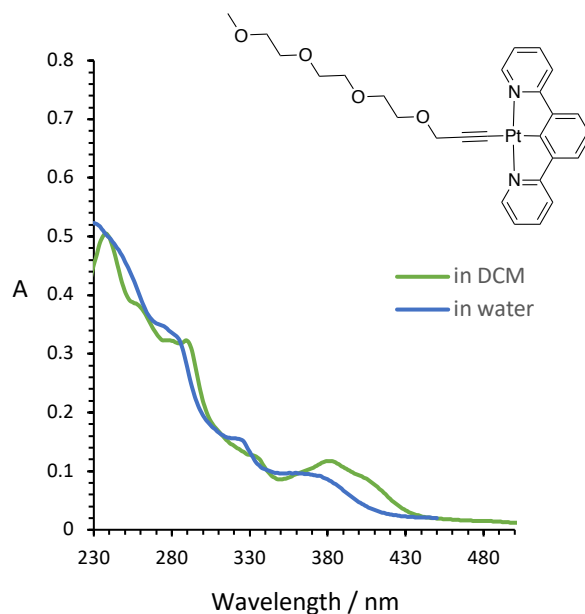


Figure 4.11: UV-vis. absorption spectra of **PtL1-12a** in (green) DCM solution and (blue) deionized water.

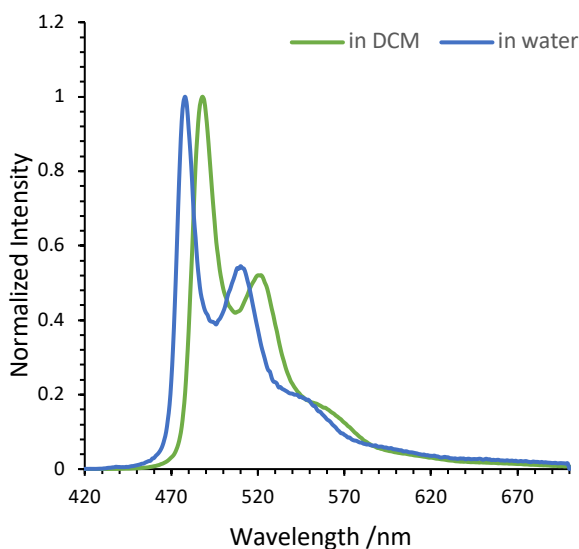


Figure 4.12: Emission spectra of **PtL1-12a** in (green) DCM solution and (blue) deionized water.

PtL1-12a displays negative minimal effect of solvatochromism in the low energy absorption band (Figure 4.11): the λ_{max} shifts from 401 nm in DCM, to 387 nm in H₂O. A similar effect was observed at the emission maxima of this complex (*i.e.* shifting by only 10 nm). The emission band of **PtL1-12a** remains highly structured, relative to the chloro analogue. The quantum yield of the complex ($\Phi = 0.211$) in aerated DCM is higher than the analogous chloro complex **PtL1Cl** ($\Phi = 0.039$). In contrast, a decrease in the lifetime of **PtL1-12a** complex was observed compared to chloro analogous complex ($\tau_0 = 0.25$ and $0.5 \mu\text{s}$ respectively).

4.6 Concluding Remarks

All of the synthesised Pt(II) 1,3-di(2-pyridyl)benzene based complexes were found to be highly emissive from DCM solution at r.t, with quantum yields reaching as high as 0.13 in aerated DCM. The quantum yields of these complexes were found to be significantly higher than the parent complex **PtL1Cl** in aerated DCM.

The emission for **PtL7Cl** was absent in the case of the complete replacement of the pyridine rings on the cyclometalated N[^]C[^]N complex by 1,2,3 triazole ones. However, for complex **PtL9Cl**, bearing both a pyridine and a 1,2,3-triazole donor, an intense green emission was observed, with the photoluminescence quantum yield being even higher than for reference complex in aerated DCM.

The emission profiles of the highly water soluble complexes **PtL9^{1a}Cl**, **PtL3^{4a}Cl** and **PtL3^{1a}Cl** showed structured bands corresponding to the phosphorescence from a ³MLCT state. The quantum yields of these complexes in the range of 0.027-0.083 and the lifetimes are of the order of 0.62–1.32 microseconds. The long luminescence lifetimes of these complexes make these compounds promising candidates for use in time-resolved emission imaging microscopy, confocal microscopy and fluorescence lifetime imaging (FLIM) on the microsecond timescale.

For the complexes **PtLnCl** (n = **1**, **3^{1a}**, **3^{4a}**, **6a**, **7**, **11**, **12**), increasing concentration leads to emissive excimeric emission. No excimeric emission was observed for **PtL9Cl**, presumably, due to the presence of the bulky moieties, the aggregation tendency is lowered, in agreement to what observed in the crystal structure.

Substituting the ancillary chloride for stronger field ligands such as acetylides and PEG alkyne often causes the *d-d** state to shift to higher energy, decreasing its deactivating effect, which is observed as an increase in quantum yield, with a further red-shift in emission. Comparatively, substitution of chloride with pyridine led to a further blue-shift in emission.

Chapter 5

5 Conclusions and Scope for Future Work

5.1 General Conclusions

The overall synthetic objective of the project - to create new platinum(II) complexes incorporating variously functionalised N[^]C[^]N ligands in order to be used in the future as a potential probe for synaptic imaging – has been achieved. This approach allows for the incorporation of two individual fragments; a polyamine tail and a lipophilic group in order to allow for more selective delivery and enhance interaction with the surface of the neuronal cells. A series of novel Pt(II) complexes featuring three types of a substituted N[^]C[^]N based tridentate ligands has been prepared and fully characterised. The project began with the intention of investigating if such metal complexes can be made followed by considering the ease of synthesis *via* comparing conventional heating *vs* microwave heating.

In the first step of the project, lipophilic alkyl chains or a polyamine was introduced *via* three types of a substituted N[^]C[^]N based ligands system. A number of synthetic strategies have been employed in the synthesis of such ligands, for which the main strategies involve either one of or a combination of metal catalysed cross-coupling and click reactions. Each strategy has its own merits and disadvantages, which have been discussed in turn. A second approach by which a polyamine or a lipophilic group was incorporated into Pt(II) complexes *via* the substitution of the monodentate chloride with an ancillary ligand containing one of these functionalities was also investigated. A series of monodentate ligands with an alkyne functionality were synthesised *via* different methods such as amine or PEG alkylation, amide coupling and reductive amination of a Schiff base. All the ligands and intermediates were characterised by ¹H and ¹³C NMR spectroscopy and mass spectrometry and X-ray analysis.

In Chapter 3, the experimental procedures involved in the synthesis of diversely substituted platinum(II) complexes were explained. The structural characterisation of all synthesised complexes was discussed. These complexes have been characterised *via* mass spectrometry, 1D and 2D ¹H and ¹³C NMR spectroscopy and results are further compared with the similar complexes quoted in literature. Four complexes were analysed further by X-ray crystallography. **PtLnCl** (where n = **3^{1a}** or **3^{4a}** or **9^{1a}**) complexes were found to be more stable under strong acidic condition required for Boc deprotection than **PtL1X** (where X = alkyne or pyridine substituted monodentate ligands). The substitution of the ancillary ligands with (alkyne or pyridine) substituted monodentate ligands was also investigated. It is believed that

the strong destabilising nature of the cyclometalating bond generates a system disadvantageous to formation of new complexes with strongly donating ancillary ligands.

Chapter 4 was dedicated to the analysis of the photophysical properties including absorption, emission wavelengths, luminescent quantum yields and lifetimes of the generated platinum(II) complexes. All of the synthesised Pt(II) 1,3-di(2-pyridyl)benzene based complexes were found to be highly emissive, with quantum yields reaching as high as 0.13 in aerated DCM. The quantum yields of these complexes were found to be significantly higher than the parent complex reported in the literature. The emission for triazole based Pt(II) complexes was absent in the case of the complete replacement of the pyridine rings on the cyclometalated N[^]C[^]N complex by 1,2,3 triazole ones. However, when formally replacing only one pyridine ring in Pt(II) complexes of 1,3-di(2-pyridyl)benzene ligands by a 1,2,3-triazole, an intense green emission was observed, with the photoluminescence quantum yield being even higher than for reference complex in aerated DCM. The emission profiles of the highly water soluble Pt(II) complexes showed structured bands corresponding to the phosphorescence from a ³MLCT state. The quantum yields of these complexes in the range of 0.027 - 0.082 and the lifetimes are of the order of 0.6 – 1.3 μs. Substituting the ancillary chloride for stronger field ligands such as acetylides and PEG alkyne often causes the *d-d*^{*} state to shift to higher energy, decreasing its deactivating effect, which is observed as an increase in quantum yield and a further red-shift in emission. On the contrary, substitution of chloride with pyridine led to a further blue-shift in emission.

The work described in this thesis represents significant progress not only towards the overall goal of synthesising a potential probe for cellular imaging but also has opened up numerous and diverse opportunities to further advance the chemistry developed in this project for diverse bioimaging applications.

5.2 Future Direction

5.2.1 Cytotoxicity

As discussed in the introduction, intracellular probes should be of low toxicity to the biological system under study – it is therefore important to determine the cytotoxicity of these synthesised Pt(II) complexes. The toxicity of compounds can be represented by the half maximal inhibitory concentration value (IC_{50}) which represents the concentration causing 50% cell death over the length of the dose.

5.2.2 Cellular Studies

The platinum(II) conjugates synthesised were proposed as candidate compounds to perhaps improve upon the existing synthetic protocol. As well as the inherent benefit of increased resistance to photobleaching, the polyamine tail should adhere to the cell membrane through electrostatic interactions as well as providing good water solubility, therefore excess dye enabling to be washed away easily. Moreover, platinum(II) was chosen for the study owing to its adequately electron rich density and anticipated to provide contrast in electron microscopy images. Electron dense Pt(II) allows the accumulation of the complex and hence eliminates the need for treatment with DAB before performing the electron microscopy, as well as avoiding the use OsO_4 which is toxic in nature.

Further studies of the platinum(II) compounds in synaptic imaging are required to determine how successful they are in entering synaptic vesicles. It would be of great interest to explore the intracellular localisation of these compounds as well as to better determine their uptake properties, so as to develop similar conjugates as fluorescent probes of synaptic function.

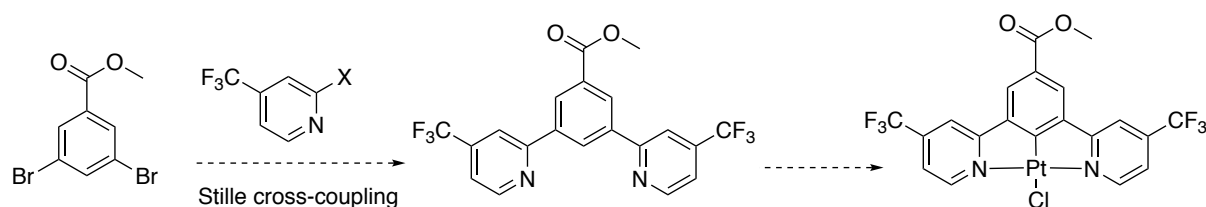
5.2.3 Modification of the Tridentate N[^]C[^]N Ligand

The synthetic route to the core structure had been established, so it remains to build around the core to investigate the effects of altering or adding to the tridentate N[^]C[^]N ligand.

For the N[^]C[^]N pyridyl benzene based complex, it would interesting to establish the effects of substitution of electron withdrawing *e.g.* trifluoromethyl groups into the pyridyl rings of the

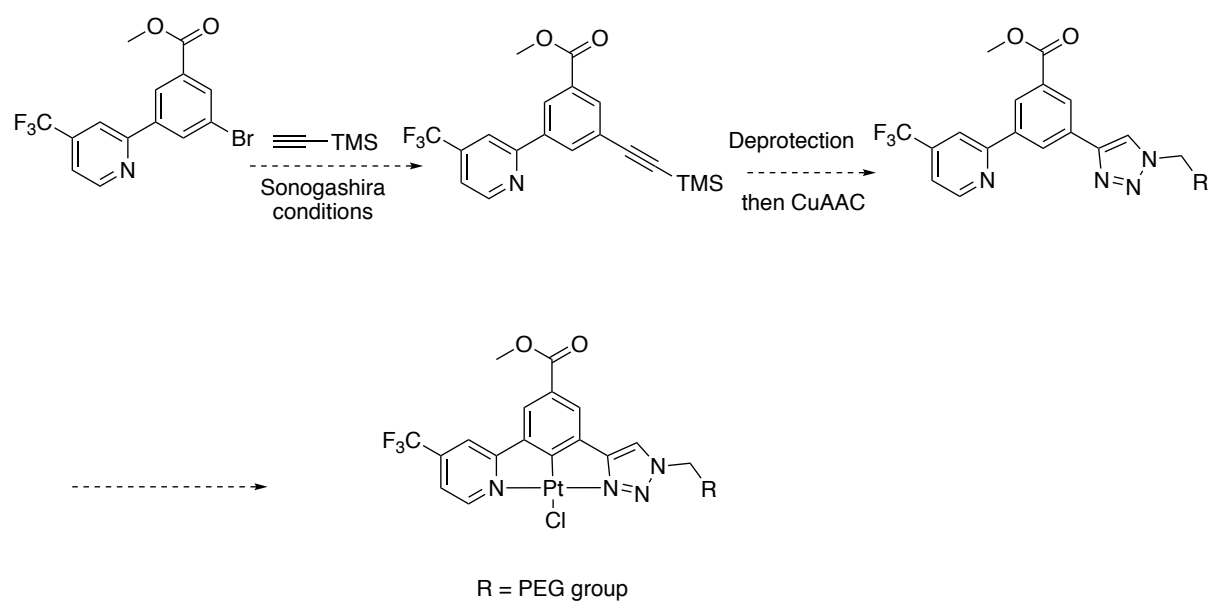
ligands. Williams and co-workers reported a range of Pt(II) complexes bearing CF₃ groups into either the 4- or 5-position of the pyridyl rings of the ligand.¹³⁷ The effect on emission is greatest for the 4-position, a result which can be understood, for the monomeric excited state, in terms of the significant contribution of this position to the LUMO but not to the HOMO, such that the LUMO is stabilised and the HOMO–LUMO gap decreased. An interesting feature of CF₃-containing complexes is that they were relatively insensitive to diffusional quenching by dissolved molecular oxygen. Thus, the lifetimes and quantum yields were reduced by a factor of only 3 to 4 upon aeration, compared to factors of 10 to 30 times for other members of the Pt(N[^]C[^]N)Cl class of complexes. This result will be useful in the context of bio-imaging applications, that require an aerated aqueous environment.

The new proligand based on the 1,3-di(2-pyridyl)benzoate skeleton, incorporating CF₃ groups in the pyridyl rings at the 4-position, could be prepared by a procedure similar to that used previously in the synthesis of **HL3**, involving a palladium-catalysed Stille cross-coupling as shown by Scheme 5.1. Subsequent reaction of the proligands with K₂PtCl₄ will give the corresponding complex.



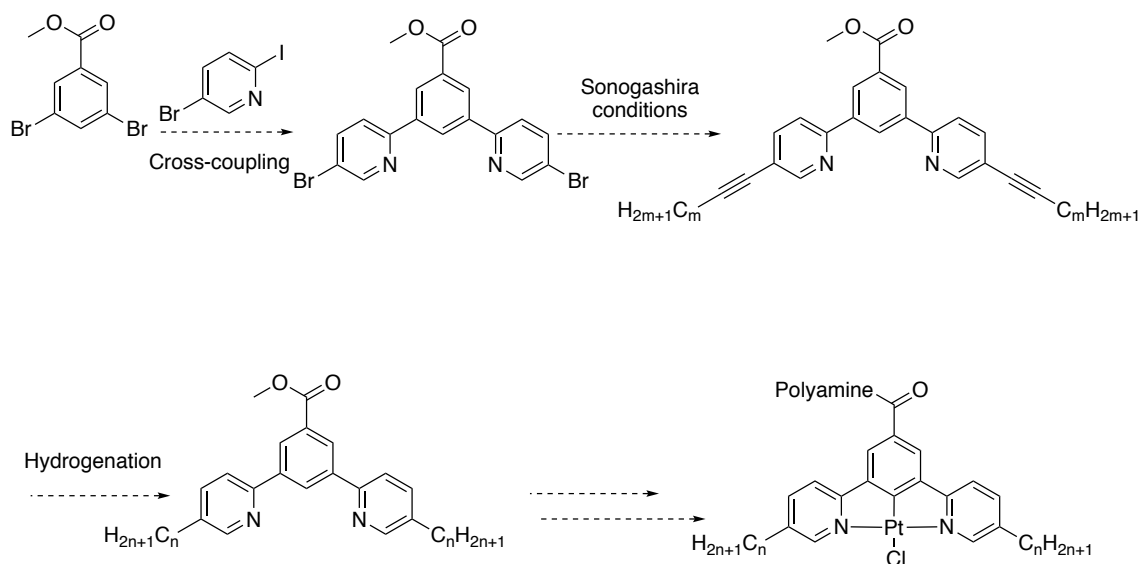
Scheme 5.1: Potential synthetic routes to the substituted N[^]C[^]N ligands and its complex.

To make the chemistry more efficient, the side-product generated from the previously mentioned reaction of the N[^]C[^]N ligands could be used further for producing asymmetric new ligands feature both a pyridine and 1,2,3-triazole ring (Scheme 5.2). This could be achieved by Sonogashira coupling reaction, followed by the cleavage of the trimethylsilyl TMS group, yielding the pyridine-function alised alkyne building block, which will readily convert into the N[^]C[^]N- ligand *via* a CuAAC reaction. This will give a useful handle for functionalization on the triazole ring, including hydrophilic group such as PEG group, potentially leading to a more water soluble platinum(II) complex.



Scheme 5.2: Potential synthetic routes to asymmetric N^CN ligands and its complex.

Another possibility would be to incorporate a lipophilic moiety into the pyridyl rings and a cationic tail (amine chain) into the benzene ring (Scheme 5.3). A lipophilic cyclometallating ligand can be synthesised using a palladium-catalysed cross-coupling of the methyl-3,5-dibromobenzoate with 2-iodo-5-bromopyridine. The dibromo derivative will react with terminal alkynes under Sonogashira conditions to give the alkynyl derivatives, which will then reduce to the alkyl derivatives. After generating the platinum(II) complex, polyamine chain could be easily introduced via amide coupling following a procedure previously used for **PtL3^aCl** complex. Combining the lipophilic and the hydrophilic polyamine ligand with Pt(II) 1,3-di(2-pyridyl)benzene based complex would yield a platinum(II) compound that would hopefully exhibit amphiphilic behaviour and possibly offer an improvement over FM-143FX in synaptic imaging.



Scheme 5.3: Potential synthetic routes to an ambiphilic platinum(II) complex.

5.2.4 Potential Applications

Looking at longer term aims of this research, the versatility of the N[^]C[^]N ligands opens up the possibility of tailor-made probes for specific assays, diagnostics or treatments. Almost any biomarker for disease could potentially be assayed by introducing the correct functionality into the N[^]C[^]N ligand: amine or thiol-reactive groups for labelling proteins or antibodies; substrates for upregulated receptors; hormones; and peptides for recognition (Figure 5.1).

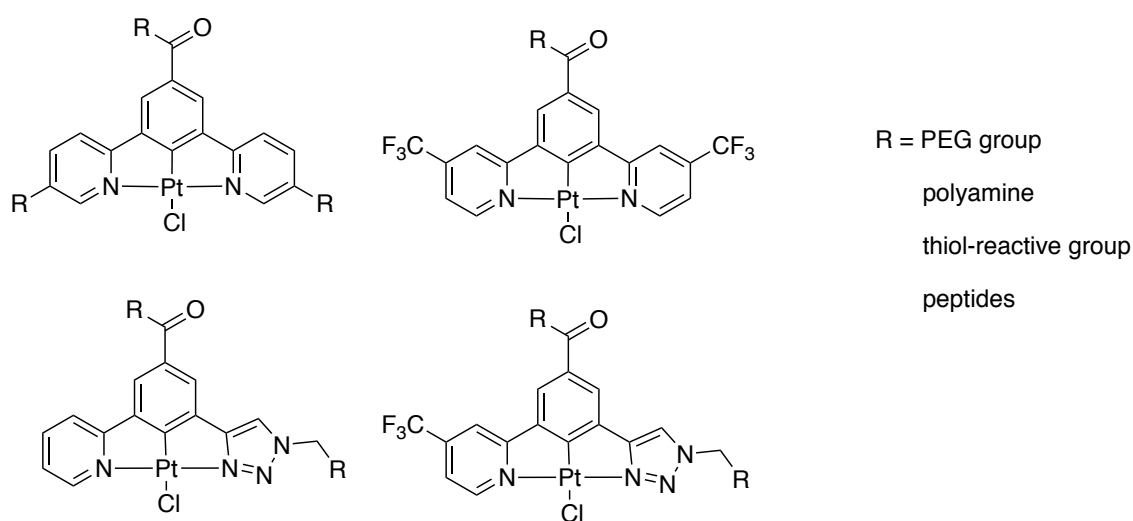


Figure 5.1: proposed targeting platinum(II) complexes.

This also opens up the potential to not only diagnose and learn about diseases more effectively but to treat them more efficiently, as the route to cytotoxic platinum(II) conjugates using the versatile chemistry discussed in this thesis can be extended to incorporate other biologically relevant molecules or biomarkers of cancer. Examples do exist, including compounds by Lai *et al.*, which exhibit higher cytotoxicity upon irradiation than in dark studies, suggestive of a high efficacy for $^1\text{O}_2$ generation.¹⁵³ Moreover, Wieczorek *et al.* expanded on the development of protein labelling probes in the synthesis of a series of N[^]C[^]N Pt(II) complexes (Figure 5.2).¹⁵⁴ They found that organometallic pincer–platinum complexes can be used for diagnostic targeting of proteins, which in combination with a serine hydrolase reactive phosphonate inhibitor opens up new activity-based protein profiling possibilities. It has been found that these complexes have a limited solubility in common organic solvents and complete insolubility in water or buffer solutions. DMF appeared to be the only solvent in which all complexes dissolved readily. Since DMF is a strongly coordinating solvent, it is not the ideal solvent for performing the spectroscopic studies; the use of coordinating solvents renders the studied compounds less emissive.

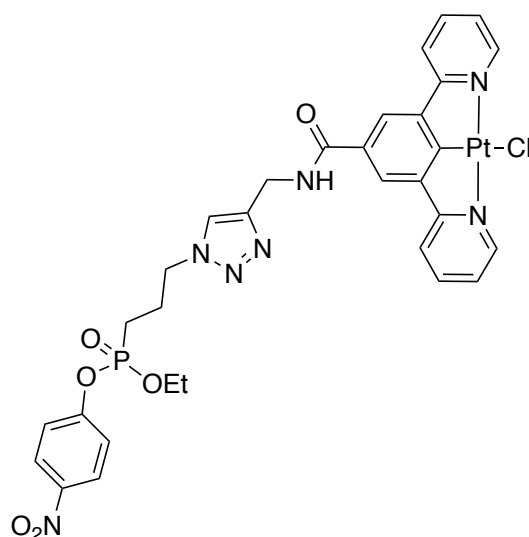


Figure 5.2: Luminescent pincer platinum(II) phosphonate inhibitor.¹⁵⁴

An interesting project stemming from this would be to use the chemistry developed in this research to synthesise a hydrophilic Pt(II) complex that has the capacity to overcome the solubility issue and used as protein labelling probe. This could be achieved by incorporating a

PEG group through the 1,2,3-triazole ring in the N^CN cyclometalated Pt(II) complex (Figure 5.3). Combining the reactive phosphonate inhibitor and the hydrophilic group yield an Pt(II) compound that would hopefully exhibit ambiphilic behaviour and possibly offer an improvement in the protein labelling.

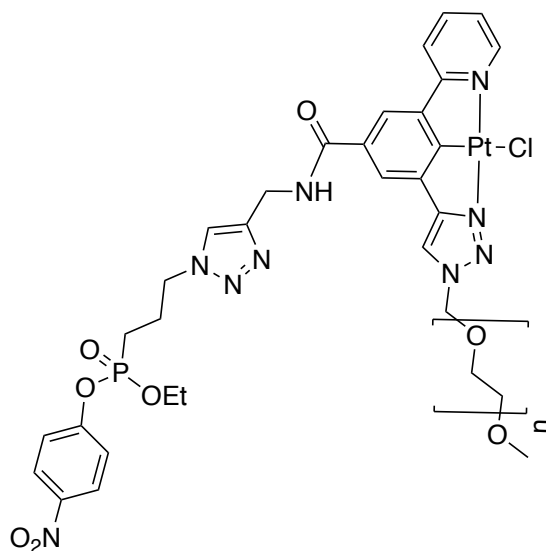


Figure 5.3: Proposed platinum(II) phosphonate inhibitor.

Chapter 6

6 Experimental

6.1 Material and instrument

All reagents and solvents were obtained commercially from Aldrich or Alfa Aesar and used without further purification with the exception of: triethylamine which was distilled, and stored over potassium hydroxide, dichloromethane, tetrahydrofuran, toluene and acetonitrile were dried using a PureSolve solvent drying system from Innovative Technologies; imidazole 1-sulfonyl azide hydrogensulfate was prepared by a previous worker in the Lowe group.⁹⁰

Analytical TLC was run on aluminum-backed silica or neutral alumina plates with a fluorescence indicator at 254 nm, preparative flash column chromatography was performed with silica gel 60 (230-400 mesh) or neutral activated Brockmann I grade alumina (150 mesh). NMR spectra were recorded on Bruker AV500, DRX400 or AV400 spectrometers at 298 K unless otherwise stated. Chemical shifts are quoted in ppm relative to tetramethylsilane (TMS). All coupling constants are quoted in Hz and were calculated from spectra directly with TOPSPIN v3.5 or ACDLabs.

Electronic absorption spectra were recorded on a Shimadzu UV 180 spectrometer using a 10 × 10 mm quartz Hellma cuvette with 2 nm slit width and are recorded in nm. Luminescence data was recorded using a Jobin Yvon Horiba FluoroMax-P spectrometer in a 10 × 10 mm quartz Hellma cuvette. Excitation and emission maxima are limited in accuracy to the monochromator slit width of 3 nm and are recorded in nm.

Quantum yield was measured following comparative methods.¹⁴² 0.1 M [Ru(bpy)₃Cl₂] was used as a standard for photoluminescence quantum yield. Five dilute solutions from both the standard and the sample were prepared depending on the absorbance wavelengths (0.1, 0.08, 0.06, 0.04 and 0.02). After determining the integrated fluorescence intensity at the same λ_{ex} and solvent for all samples, a graph of the integrated fluorescence intensity vs. absorbance was plotted.

Lifetimes were measured using a Jobin Yvon Horiba FluoroLog 3 exciting at 370 nm monitoring the emission 400-700 nm with a bandwidth of 1.5 nm. The bandwidth of the excitation laser was determined by Rayleigh scattered light from a suspension of Ludox. The data was binned into channels of 1.95 ns/ch and 0.24 ns/ch. All plots were created and analysed using GraphPad Prism 7. The numbering of compounds is arbitrary from left to right and is purely to aid the assignment of spectra; it does not reflect any IUPAC nomenclature or

substitution pattern. Primes indicate the same atom in a different ligand. All methods reported are for the best yield obtained. Infra-red spectra were recorded on a Perkin Elmer Spectrum one FTRIR instrument and stretches are quoted in reciprocal centimeters (cm^{-1}).

A Micromass Quatro LC Spectrometer was used to record mass spectra, measured in m/z , with analytes in methanol. High resolution mass spectra were recorded on a Water Aquity XEVO Q ToF machine and also measured in m/z .

All Pt(II)LCl complexes and some ligand synthesis were carried out using microwave irradiation using a CEM by using vial size 10 mL or 50/35 mL with septum.

CAUTION:

This thesis describes the syntheses of azides: all synthesis of azides should be performed behind a blast shield.

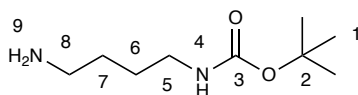
$$\frac{(\text{Number of C atoms} + \text{Number of O atoms})}{\text{Number N atoms}}$$

Equation 6.1

If the ratio for an organic azide compound accord to Equation 6.1 is less than 3, these low molecular weight organic azides should not be stored in pure form and avoid isolating if possible. If the ratio is less than 1, the azide must not be isolated. All waste from metal azide reactions should be treated as follows: dilute to give no more than 5 wt% of azide, add 150 wt% NaNO_2 with respect to azide; the solution was cooled to 0°C and 20% sulfuric acid added dropwise until the azide spot is negative – dilute a couple of drops of azide waste with 1 mL of 1 M HCl add 1 drop of 1 M FeCl_3 . A bright red precipitate indicates the presence of azide ions. Organic azide waste can be treated by reducing the azide to an amine by dissolving the azide in at less than 5wt% solution in 6 M HCl and adding excess granular tin, then stirring at room temperature for 1 hr.

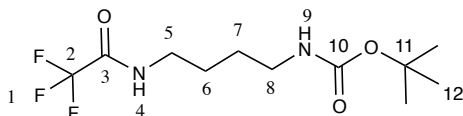
6.2 Synthesis of Pre-ligands;

6.2.1 Tert-butyl (4-aminobutyl)carbamate (**1a**).⁹²



Following a modified literature procedure, a solution of (Di-tertbutyl dicarbonate) Boc_2O (0.764 g, 3.50 mmol) in 1,4-dioxane (30 ml) was added dropwise by an addition funnel to a stirring solution of 1,4-diaminobutane (0.882 g, 10.0 mmol) in dioxane (20 ml) under N_2 at r.t. and left to stir for 18 h. The solvent was removed *in vacuo* and H_2O (20 ml) was added to the residue. The white insoluble bis-substituted by-product was isolated by filtration. The filtrate was then extracted with DCM (3 x 20 ml), dried over Na_2SO_4 , and the solvent removed under reduced pressure to afford a pale yellow oil (0.399 g, 60%) which was used without further purification. ^1H NMR (400 MHz, CDCl_3): δ 4.66 (br s, 1H, 4-NHBoc), 3.16-3.10 (m, 2H, 5- CH_2), 2.71 (t, 2H, $J = 6.1$, 8- CH_2), 1.57-1.46 (m, 4H, 6- and 7- CH_2), 1.44 (s, 9H, (1- CH_3)₃), 1.24 (br s, 2H, 9- NH_2); ^{13}C NMR (100 MHz, CDCl_3): δ 154.5 (3-C), 77.5 (2-C), 40.3 (5-C), 38.9 (8-C), 29.4 (6-C or 7-C), 27.0 (1-C), 26.0 (6-C or 7-C); MS (ES+) 189 $[\text{M}+\text{H}]^+$; 133 $[(\text{M}-\text{tBu})+2\text{H}]^+$; 89 $[(\text{M}-\text{Boc})+2\text{H}]^+$; HRMS (ES+) $\text{C}_9\text{H}_{21}\text{N}_2\text{O}_2$ $[\text{M}+\text{H}]^+$ requires 189.1603 found 189.1612.

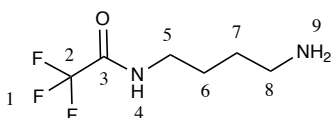
6.2.2 Tert-butyl (4-(2,2,2-trifluoroacetamido)butyl)carbamate (**2a**).⁹³



Following a modified literature procedure, Ethyltrifluoroacetate (0.792 g, 5.58 mmol) was added to a solution of **1a** (0.148 g, 0.79 mmol) in chloroform (2 ml) and the resulting solution stirred for 24 h at r.t. The reaction mixture was washed with water (15 ml) and extracted into chloroform (3 x 10 ml). The combined organic extracts were evaporated under reduced pressure and dried under high vacuum to yield a white solid (0.217 g, 95%). ^1H NMR (400 MHz; CDCl_3): δ 6.88 (br s, 1H, 4-NH), 4.57 (br s, 1H, 9-NH), 3.34 (q, 2H, $J = 6.4$, 5- CH_2),

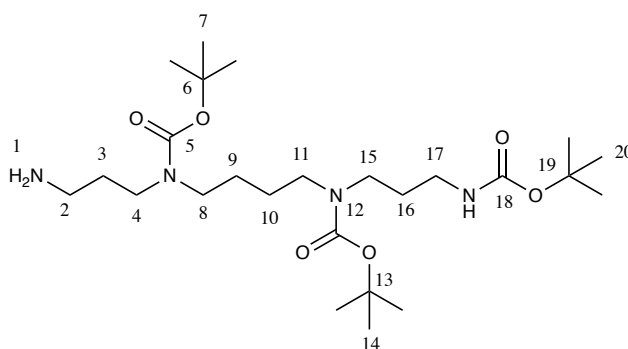
3.07 (q, 2H, $J = 6.3$, 8-CH₂), 1.65-1.55 (m, 2H, 6-CH₂), 1.50-1.45 (m, 2H, 7-CH₂), 1.40 (s, 9H, 12-(CH₃)₃); ¹³C NMR (100 MHz; CDCl₃): δ 156.3 (3- and 10-C), 117.4 (2-C) 79.6 (11-C), 39.5 (5- and 8-C), 28.4 (12-C), 27.6 (6-C), 25.7 (7-C); ¹⁹F NMR (400 MHz; CDCl₃): δ -76.1(s, 3F, 1-CF₃); MS (ESI+) 307 [M+Na]⁺, 185 [M-Boc+2H]⁺; HRMS (ESI+) C₁₁H₂₀F₃N₂O₃ [M+H]⁺ requires 285.1426 found at 285.1438.

6.2.3 N-(4-aminobutyl)-2,2,2-trifluoroacetamide (3a).⁹³



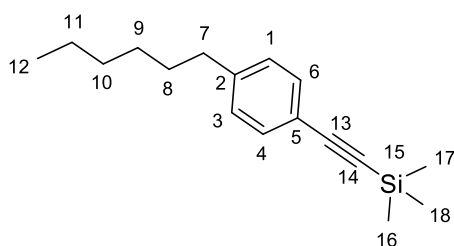
Following a modified literature procedure, **2a** (0.644 g, 2.27 mmol) was dissolved in 4 M HCl in dioxane (10 ml) under an inert atmosphere of N₂ at 0 °C and allowed to stir for 3 h. The product was isolated by addition of diethyl ether (10 ml) and the precipitate collected by filtration. The crude product was recrystallised in hot diethylether, collected by filtration, and washed with cold diethyl ether. The resulting solid was dried under vacuum to yield the product as a pale yellow solid (0.285 g, 69%). ¹H NMR(400 MHz; D₂O): δ 3.33 (t, 2H, $J = 6.3$, 5-CH₂), 3.00 (t, 2H, $J = 7.2$, 8-CH₂), 1.69–1.61 (m, 4H, 6- and 7-CH₂); ¹³C NMR (100 MHz; D₂O): δ 117.3 (2-C), 39.0 (5- and 8-C), 24.9 (6-C), 24.1 (7-C); ¹⁹F NMR (400 MHz; D₂O): δ -75.8 (s, 3F, 1-CF₃); MS (ESI+) 185 [M+H]⁺; HRMS (ESI+) C₆H₁₁N₂OF₃ [M+H]⁺ requires 185.0902 found at 185.0974.

6.2.4 Tert-butyl(4-((3-aminopropyl)(tert-butoxycarbonyl)amino)butyl)(3-((tert-butoxycarbonyl)amino)propyl) carbamate (4a).¹⁵⁵



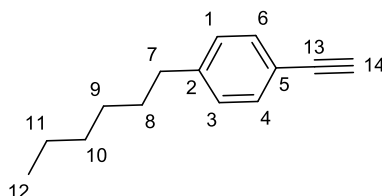
Following a modified literature procedure, to a stirring solution of N₁, N_{1'}-(butane-1, 4-diyl)bis(propane-1,3-diamine) (1.00 g, 5.10 mmol) in 25% MeOH in DCM (200 ml), 2-hydroxybenzaldehyde (0.630 g, 5.10 mmol) was added dropwise. Anhydrous Na₂SO₄ (5.70 g, 40.20 mmol) was added and the reaction was stirred overnight at r.t. The produced amine was used in the next step without isolation or purification. The reaction mixture was cooled to 0 °C, and Boc₂O (3.40 g, 15.60 mmol) was added. After stirring for 18 h at r.t., the solvent was removed *in vacuo* to provide the tri-Boc protected amine. The amine was cleaved by addition of CH₃ONH₂ (1.60 g, 18.70 mmol) and Na₂CO₃ (2.00 g, 18.70 mmol). The reaction solution changed from a yellow to a cloudy white solution in which was stirred for 2 h. The solvent was removed *in vacuo* and the residue dissolved in DCM (50 ml). The organic layer was washed with an aqueous solution of Na₂CO₃ (10 wt%), separated, filtered and concentrated to yield 5.080 g of crude product. The product was purified by column chromatography (SiO₂), with initial solvent system of (75% DCM: 25% hexane) to remove the oxime side product (R_f = 0.4). The solvent system was then changed to 1% NH₄OH: 5% MeOH in DCM to elute the product (R_f = 0.3). The product was obtained as a sticky oil (1.0 g, 41%); ¹H NMR (400 MHz, CDCl₃): δ 3.41-3.09 (m, 10H, 4-, 8-, 11-, 15-, 17-CH₂), 2.71(t, 2H, J = 6.1, 2-CH₂), 2.09-2.06 (m, 4H, 3- and 16-CH₂), 1.52-1.41 (m, 31H, 9-, 10-CH₂ and 7-, 14-, 20-CH₃); ¹³C NMR (100 MHz, CDCl₃): δ 156 (5-, 12-, 18-C), 79.5 (6-C), 79.3 (12-C), 78.9 (18-C), 46.7 (8-C), 43.9 (11-C), 39.3 (4-C), 37.4 (15-C), 28.5 (2-C), 28.4 (7-, 14-, 20-C), 26.0 (3- and 16-C), 25.6 (9- and 10-C); MS (ES⁺) 504 [M+H]⁺, 404 [M-Boc +2H]⁺; HRMS (ES⁺) C₂₅H₅₁N₄O₆ [M]⁺ requires 503.3805 found 503.3809.

6.2.5 2-(4-Hexylphenyl)ethynyl) trimethylsilane (**5a**).¹⁰²



Following a modified literature procedure, CuI (0.095 g, 0.50 mmol), PPh₃ (0.131 g, 0.50 mmol), and PdCl₂(PPh₃)₂ (0.175 g, 0.25 mmol) were added in a Schlenk tube. The system was evacuated and backfilled with N₂ three times, followed by the addition of toluene (5 ml), Et₃N (5 ml), and 1-bromo-4-hexylbenzene (1.20 g, 5.0 mmol). The reaction mixture was stirred at r.t. for 15 mins, and then trimethylsilylacetylene (2.12 ml, 15.0 mmol) was added via the septum. The reaction was stirred for 18 h at 70 °C. The volatile compounds were removed *in vacuo*, and the resulting solid was extracted into diethyl ether (10 ml). The organic extract was washed brine solution (3 x 10 ml) and dried over anhydrous MgSO₄. The solvent was removed under reduced pressure and the residue was purified by silica gel chromatography with hexane only to afford **6a** (0.830 g, 70%) as a colourless oil. ¹H NMR (400 MHz, CDCl₃): δ 7.36 (d, 2H, *J* = 8.1, 4- and 6-CH), 7.20 (d, 2H, *J* = 8.1, 1- and 3-CH), 2.55 (t, 2H, *J* = 7.6, 7-CH₂), 1.38-1.25 (m, 2 H, 11-CH₂), 1.16-1.12 (m, 6H, 8-, 9- and 10-CH₂), 0.86 (t, 3H, *J* = 6.7, 12-CH₃), 0.24 (s, 9 H, 16-, 17- and 18-CH₃). ¹³C NMR (100 MHz, CDCl₃): δ 143.6 (5-C), 132.0 (4- and 6-C), 128.5 (1- and 3-C), 120.5 (2-C), 105.6 (14-C), 93.2 (13-C), 35.8 (7-C), 31.8 (11-C), 31.3 (10-C), 29.0 (9-C), 22.7 (8-C), 14.4 (12-C). HRMS (ES+) C₁₇H₂₇Si [M+H] requires 259.1882 found 259.1877.

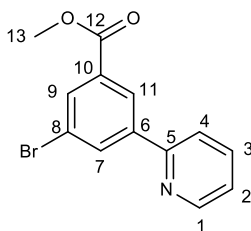
6.2.6 1-Ethynyl-4-hexylbenzene (**6a**).¹⁰²



Following a modified literature procedure, **5a** (0.762 g, 2.95 mmol) was added to a solution of K₂CO₃ (2.0 g, 14.78 mmol) in dry CH₃OH/ THF (6 ml each) under nitrogen. The reaction

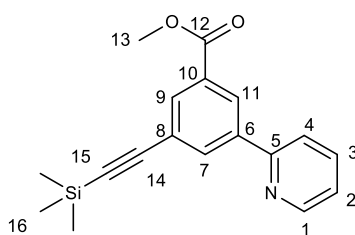
mixture was stirred 18 h at r.t. Solvent was removed under reduced pressure. The residue was purified through silica gel chromatography with hexane, affording (**6a**) as a yellow oil. Yield: 0.478 g (87%). ¹H NMR (400 MHz, CDCl₃): δ 7.36 (d, 2H, *J* = 8.1, 4- and 6-CH), 7.20 (d, 2H, *J* = 8.1, 1- and 3-CH), 3.03 (s, 1H, 14-CH), 2.55 (t, 2H, *J* = 7.6, 7-CH₂), 1.35-1.28 (m, 2 H, 11-CH₂), 1.12-1.09 (m, 6H, 8-, 9- and 10-CH₂), 0.86 (t, 3H, *J* = 6.7, 12-CH₃). ¹³C NMR (100 MHz, CDCl₃): δ 143.6 (5-C), 132.0 (4- and 6-C), 128.5 (1- and 3-C), 120.5 (2-C), 83.8 (13-C), 76.4 (14-C), 35.8 (7-C), 31.8 (11-C), 31.3 (10-C), 28.9 (9-C), 22.7 (8-C), 14.4 (12-C). HRMS (ES+) C₁₄H₁₈ [M+H] requires 187.1487 found 187.1486.

6.2.7 Methyl 3-bromo-5-(pyridin-2-yl)benzoate (**7a**)



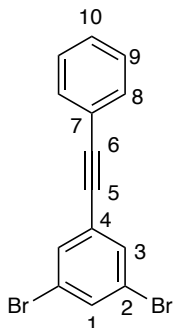
7a was isolated as a by-product from **HL25** stille coupling reaction with (*R_f* = 0.75) as a white solid (0.600 g, 51%). ¹H NMR (500 MHz, CDCl₃): δ 8.66 (d, 1H, *J* = 4.5, 1-CH), 8.51 (t, 1H, *J* = 1.8, 7-CH), 8.36 (t, 1H, *J* = 1.8, 9-CH), 8.14 (t, 1H, *J* = 1.8, 11-CH), 7.72 (m, 2H, 3- and 4-CH), 7.25 (ddd, *J* = 7.2, 4.8, 1.2, 1H, 2-CH), 3.92 (s, 3H, 13-CH₃). ¹³C (500 MHz, 125 MHz, CDCl₃): δ 165.3 (C=O, 12-C), 154.3 (quat), 149.6 (1-C), 141.5 (quat), 137.1 (3-C or 4-C), 133.9 (9-C), 132.4 (11-C), 131.3 (quat), 126.1 (7-C), 122.9 (2-C), 120.3 (3-C or 4-C), 51.2 (13-C). MS (ES+) 293 [M+H]; HRMS (ES+) C₁₃H₁₀BrNO₂ [M+H] requires 293.9961 found 293.9953.

6.2.8 Methyl 3-(pyridin-2-yl)-5-((trimethylsilyl)ethynyl)benzoate (8a)



7a (0.550 g, 1.80 mmol), was dissolved in 10 ml dry THF and charged into a dry Schlenk tube followed by Et₃N (1 ml), CuI (0.017 g, 0.09 mmol), Pd(PPh₃)₂Cl₂ (0.063 g, 0.09 mmol), and PPh₃ (0.052 g, 0.36 mmol). The entire system was evacuated and backfilled with N₂ three times and stirred for 15 mins. under N₂ at r.t. Trimethylsilyl acetylene (0.529 g, 5.40 mmol), was added to the reaction mixture under N₂ and let to react for 48 h at r.t. A volatile compounds were removed under reduced pressure, and the resulting solid was extracted into diethyl ether (5 ml). The organic extract was washed with brine solution (3 x 10 ml) and dried over anhydrous MgSO₄. The solvent was removed reduced pressure and the residue was purified by silica gel chromatography (20% EtAOc, 80% hexane) to afford product (R_f = 0.43) as orange oil (0.497 g, 89%). ¹H NMR (500 MHz, CDCl₃): δ 8.66 (d, 1H, *J* = 4.5, 1-CH), 8.51 (t, 1H, *J* = 1.8, 7-CH), 8.36 (t, 1H, *J* = 1.8, 9-CH), 8.14 (t, 1H, *J* = 1.8, 11-CH), 7.72 (m, 2H, 3- and 4-CH), 7.25 (ddd, 1H, *J* = 7.2, 4.8, 1.2, 2-CH), 3.92 (s, 3H, 13-CH₃), 0.24 (s, 9H, 16-CH₃); ¹³C (500 MHz, 125 MHz, CDCl₃): δ 166.2 (C=O, 12-C), 155.3 (quat), 149.8 (1-C), 139.7 (quat), 136.9 (3-C or 4-C), 134.4 (9-C), 132.8 (11-C), 130.9 (quat), 127.4 (7-C), 124.3 (quat), 121.9 (2-C), 120.3 (3-C or 4-C), 103.7 (quat), 95.1 (quat), 51.2 (C-13). MS (ES⁺) 310 [M+H]; HRMS (ES⁺) C₁₈H₁₉NO₂Si [M+H] requires 310.1265 found 310.1263.

6.2.9 1,3-dibromo-5-(phenylethynyl)benzene (2).¹⁵⁶

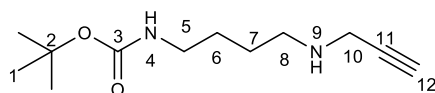


Following a modified literature procedure, to a solution of ethynylbenzene (0.196 g, 0.58 mmol) and 1,3,5-tribromobenzene (0.253 g, 0.80 mmol) in degassed Et₃N (7.5 ml) were added

PdCl₂(PPh₃)₂ (0.030 g, 0.04 mmol), CuI (0.009 g, 0.04 mmol) and PPh₃ (0.005 g, 0.036 mmol) under N₂. The reaction mixture was stirred at 70 °C for 18 h. The solvent was removed under reduced pressure and the residue was purified by column chromatography (hexane:DCM, 9:1) to give a pale yellow solid (0.120 g, 61%). ¹H NMR (400 MHz, CDCl₃): δ 7.61 (t, 1H, *J* = 1.8, 1-CH), 7.59 (d, 2H, *J* = 1.8, 3-CH), 7.46 (d, 2H, *J* = 8.8, 8-CH), 7.38-7.32 (m, 3H, 9- and 10-CH). ¹³CNMR (100 MHz, CDCl₃): δ 133.8 (1-C), 132.9 (8-C), 131.7 (3-C), 128.9 (9- and 10-C), 128.4 (quat), 126.7 (quat), 122.6 (quat), 91.9 (5-C), 86.3 (6-C). MS (ES⁺) 334 [M+H]⁺

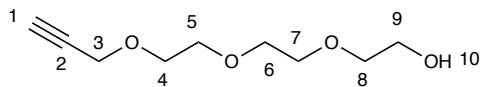
6.3 Synthesis of Mono-ligands

6.3.1 Tert-butyl (4-(prop-2-yn-1-ylamino)butyl)carbamate (**9a**).¹¹⁵



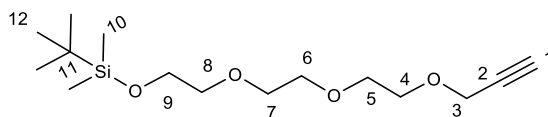
Following a modified literature procedure, **1a** (3.92 g, 20.80 mmol) was dissolved in 50 ml chloroform. DIPEA (N,N-diisopropylethylamine), 2.9 ml, and propargylbromide (1.66 ml, 80% in toluene, 15.40 mmol) was added, and the mixture was stirred at r.t. for 18 h. The mixture to 40 °C for 2 h, then diluted with chloroform (100 ml), washed twice with 40 ml 0.2 M NaOH solution and dried over Na₂SO₄. The solvent was removed under reduced pressure, yielding a yellow oil that was purified by column chromatography (5% MeOH: 94% DCM and 1% NH₄OH). The product was isolated as a yellow oil (1.920 g, 41%). ¹H NMR (300 MHz, CDCl₃): δ 4.71 (br s, 1H, 4-NH), 3.43 (d, 2H, *J* = 2.4, 10-CH₂), 3.13 (q, 2H, *J* = 6.3, 5-CH₂), 2.71 (t, 2H, *J* = 6.6, 8-CH₂), 2.17 (t, 1H, *J* = 2.4, 12-CH), 1.60 (br s, 1H, 9-NH), 1.58-1.48 (m, 4H, 6- and 7-CH₂), 1.39 (s, 9H, 1-(CH₃)₃).

6.3.2 2-(2-(2-(prop-2-yn-1-yloxy)ethoxy)ethoxy)ethan-1-ol (**10a**).¹¹⁹



Following a modified literature procedure, to an oven dry flask under N₂, potassium *tert*-butoxide (3.820 g, 33.00 mmol) was suspended in dry THF (150 ml) at 0 °C and stirred for 10 mins. Triethylene glycol (8.73 ml, 65.40 mmol) was added to the solution *via* the septum, and the solution was left to warm to r.t. whilst stirring for 30 mins. Propargyl bromide (3.67 ml, 80 wt. % in toluene, 32.70 mmol) in dry THF (25 ml) was added dropwise, *via* septum, to the solution. The mixture was left to stir at r.t. for 16 h, and the reaction monitored by TLC (EtOAc, KMnO₄ stain, R_f = 0.38). Once complete, reaction mixture was taken up in THF and filtered over celite, and solvent removed *in vacuo* to yield a dark yellow oil as the crude product. The crude product was purified using silica column chromatography (50-100% EtOAc in DCM) to give the product as a pale-yellow oil (2.90 g, 47%). ¹H NMR (400 MHz; CDCl₃): δ 4.21 (d, 2H, *J* = 2.5, 3-CH₂), 3.76-3.65 (m, 10H, 4-, 5-, 6-, 7- and 8-CH₂), 3.64-3.59 (m, 2H, 9-CH₂), 2.50 (br s, 1H, 10-OH), 2.48 (t, 1H, *J* = 2.4, 1-CH); ¹³C (100 MHz; CDCl₃): δ 79.5 (2-C), 74.6 (1-C), 72.5 (6-C), 70.6 (7-C), 70.3 (5- and 8-C), 69.0 (4-C), 61.6 (9-C), 58.4 (3-C), MS(ESI+) 211 [M+Na]⁺; HRMS (ESI+) C₉H₁₇O₄ [M+H]⁺ requires 189.1127 found at 189.1129.

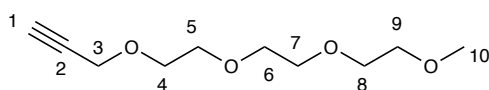
6.3.3 2,2,3,3-tetramethyl-4,7,10,13-tetraoxa-3-silahexadec-15-yne (**11a**)



Triethylamine (1.280 g, 12.70 mmol), DMAP (0.192 g, 1.60 mmol) and TBDMSCl (1.740 g, 11.60 mmol) were dissolved in DCM (60 ml). **10a** (2.00 g, 10.60 mmol) was added dropwise over 5 mins, then the mixture was stirred at r.t. for 90 mins. The reaction mixture was poured into H₂O and extracted into EtOAc, and the combined organic layers were washed with brine, dried over anhydrous MgSO₄, filtered and concentrated *in vacuo* to give an off white oil which was passed through a short column (9:1 Hexane:EtOAc) to give the product as a colourless oil (3.00 g, 93%). ¹H NMR (500 MHz; CDCl₃): δ 4.14 (d, 2H, *J* = 2.5, 3-CH₂), 3.68 (t, 2H, *J* =

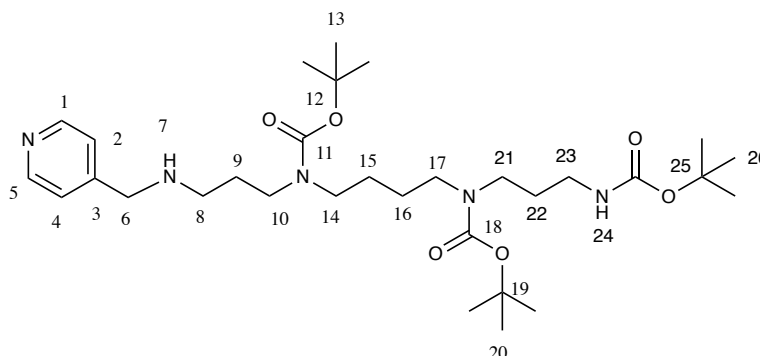
5.3, 9-CH₂), 3.66-3.61 (m, 8H, 4-, 5-, 6-, and 7-CH₂), 3.49 (t, 2H, *J* = 5.3, 8-CH₂), 2.36 (t, 1H, *J* = 2.4, 1-CH), 0.82 (s, 9H, 12-(CH₃)₃), 0.02 (s, 6H, 10-(CH₃)₂); ¹³C (125 MHz; CDCl₃): δ 79.7 (2-C), 74.5 (1-C), 72.8 (8-C), 70.6 (7-C), 70.3 (5-, 6-C), 69.0 (4-C), 62.7 (9-C), 58.0 (3-C), 26.5 (12-C), 18.3 (11-C), 0.05 (10-C); MS(ESI+) 325 [M+Na]⁺; HRMS (ESI+) C₁₅H₃₁O₄ [M+H]⁺ requires 303.1996 found at 303.1992.

6.3.4 2,5,8,11-tetraoxatetradec-13-yne (12a).¹¹⁹



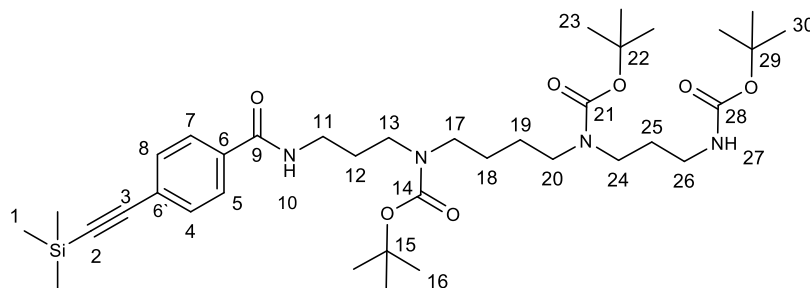
Following a modified literature procedure, an oven dry flask was charged with dry THF (15 ml), NaOH pellets (2.40 g, 60.0 mmol), and triethyleneglycol monomethyl ether (2.460 g, 15.0 mmol). The flask was cooled to 0 °C and stirred for 10 mins, before propargyl bromide (2.510 ml, 22.50 mmol) was added dropwise. The reaction mixture was allowed to warm to r.t. and stirred for 24 h. The reaction mixture was poured into Et₂O (20 ml) and washed with water (50 ml). The aqueous layer was further extracted with Et₂O (2 × 20 ml), and the combined organic extracts were washed with 10% aq. HCl, followed by sat. NaHCO₃ solution and brine, then dried over anhydrous MgSO₄. Column chromatography (silica gel, Et₂O/hexane, 10:90) gave the product as a colourless oil (2.480 g, 82%). ¹H NMR (400 MHz, CDCl₃): δ 4.18 (d, 2H, *J* = 2.4, 3-CH₂) 3.76- 3.65 (m, 10H, 4-, 5-, 6-, 7- and 8-CH₂), 3.63-3.54 (m, 2H, 9-CH₂), 3.36 (s, 3H, 10-CH₃), 2.49 (t, 1H, *J* = 2.4, 1-CH); ¹³C NMR (100 MHz, CDCl₃): δ 79.5 (2-C), 74.4 (1-C), 71.8 (6-C), 70.5 (7-C), 70.4 (5- and 8-C), 70.3 (4-C), 69.0 (9-C), 58.9 (10-C), 58.3 (3-C), MS (ESI+) 226 [M+H+Na]⁺, 225 [M+Na]⁺, HRMS (ESI+) C₁₀H₁₉O₄ [M+H]⁺ requires 203.1127 found at 203.1129.

6.3.5 Tert-butyl(4-((tert-butoxycarbonyl)(3-((pyridinylmethyl)amino)propyl)amino)butyl)(3-((tert-butoxycarbonyl)amino)propyl)carbamate (13a).



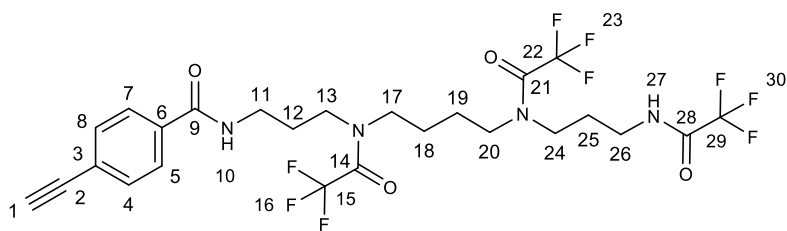
A solution of 4-pyridincarboxaldehyde (0.050 g, 0.49 mmol) in MeOH (10 ml) was added to a stirred solution of **4a** (0.250 g, 0.49 mmol). The reaction was then stirred at r.t. under N₂ for 4 h. TLC (5% MeOH in DCM) was used to monitor the reaction. Upon completion of the reaction, the solution was cooled to 0 °C and NaBH₄ (0.020 g, 0.49 mmol) was added in small portions; the reaction mixture was stirred at r.t. under N₂ for overnight. The volatiles were then removed under reduced pressure, and the resulting residue was re-dissolved (15ml) in water. 1N HCl was added dropwise to alter the pH of the solution to 8 and the product was extracted into DCM (3 x 15ml). The organic layer was isolated, dried over Na₂SO₄, filtered, and concentrated to yield a colorless oil (0.220 g, 76%); ¹H NMR (400MHz, CDCl₃): δ 8.53 (d, 2H, *J* = 4.6 Hz, 1-, 5-CH), 7.20 (d, 2H, *J* = 7.04 Hz, 2-, 4-CH), 3.70 (s, 2H, 6-CH₂), 3.30-3.10 (m, 10H, 10-, 14-, 17-, 21-, 23-CH₂), 2.59 (t, 2H, *J* = 6.1 Hz, 8-CH₂), 1.90 (m, 2H, 9-CH₂), 1.70 (m, 4H, 15- and 16-CH₂), 1.51 (s, 27H, 13-, 20- and 26-(CH₃)₃); ¹³C NMR (100MHz, CDCl₃): δ 206.9 (11, 18, 24-C), 149.6 (1-, 5-C), 121 (2-, 4-C), 63.2 (6-C), 30.8 (8-C), 28.4 (13, 20, 26-C); MS(ESI⁺): 595 [M+H]⁺, 495 [M-BOC+2H]⁺; HRMS (ES⁺) C₃₁H₅₆N₅ requires 594.4246 found 594.4231.

6.3.6 Tert-butyl(4-(tert-butoxycarbonyl)(3-(tert-butoxycarbonyl)amin)propyl)amino)butyl)(3-(4-(trimethylsilyl)ethynyl)benzamido) propyl)carbamate (14a).



4-((trimethylsilyl)ethynyl)benzoic acid (0.109 g, 0.50 mmol) was dissolved in dry DCM (2.50 ml) and Et₃N (70 μL, 0.5 mmol) was added. DIC (0.063 g, 0.50 mmol) and NHS (0.057 g, 0.50 mmol) were added and the mixture was left to stir at r.t. for 1 h under N₂. The white precipitate was removed by celite filtration and the filtrate diluted with dry DCM (2.5 ml). A solution of **4a** (0.276 g, 0.55 mmol) in dry DCM (2 ml) was added with Et₃N (76 μL, 0.55 mmol) and the solution was heated in a microwave reactor to 50 °C for 1 h. The reaction mixture was diluted with DCM (10 ml) and washed with water (10 ml). The aqueous layers were combined and extracted with DCM (2 x 10 ml). The organic layers were combined, washed with saturated NaHCO₃, (20 ml) and brine (20 ml) then dried over anhydrous MgSO₄. The drying agent was filtered off and the filtrate concentrated *in vacuo*. The crude mixture was purified by column chromatography, eluting with EtOAc to give the title compound (R_f = 0.6) as a pale yellow oil (0.125 g, 35%). ¹H NMR (500 MHz, CDCl₃): δ 7.68 (br s, 1H, 10-NH), 7.58 (m, 2H, 7- and 5-CH), 7.25 (br d, 2H, *J* = 7.9, 4- and 8-CH), 4.78 (s br, 1H, 27-NH), 3.15 (q, 2H, *J* = 6.1, 11-CH₂), 3.15-3.05 (m, 2H, 24-CH₂), 3.04-2.95 (m, 2H, 13-CH₂), 2.93-2.88 (m, 4H, 17- and 20-CH₂), 2.87-2.78 (m, 2H, 26-CH₂), 1.58-1.47 (m, 2H, 12-CH₂), 1.45-1.35 (m, 2H, 25-CH₂), 1.28-1.23 (m, 4H, 18- and 19-CH₂) 1.22-1.15 (m, 27H, 16-, 23- and 30-(CH₃)₃) 0.02 (s, 9H, 1-(CH₃)₃); ¹³C NMR (125 MHz, CDCl₃): δ 166.1 (9-C), 165.1 (14-C), 156.2 (21-C), 155.9 (28-C), 150.1 (6-C), 147.3 (6'-C), 132.5 (4- and 8-C), 127.3 (5- and 7-C), 104.5 (3-C), 96.7 (2-C), 80.1 (29-C), 79.7 (15-C), 79.1 (22-C), 46.9 (17-C), 46.1 (20-C), 44.5 (13-C), 43.0 (24-C), 37.6 (26-C), 35.5 (11-C), 29.2 (25-C), 28.2 (16-, 23- and 30-C), 27.2 (12-C), 25.1 (12-C), 25.8 (18- and 19-C) 0.1 (1-C). MS(ES⁺) 725 [M+Na]⁺, 703 [M+H]⁺, 603 [M-Boc+2H]⁺, HRMS (ES⁺) C₃₇H₆₃N₄O₇²⁸Si[M+H]⁺ requires 703.4466 found 703.4490. C₃₇H₆₃N₄O₇ Na ²⁸Si[M+Na]⁺ requires 725.4285 found 725.4304.

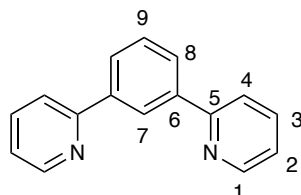
6.3.7 4-ethynyl-N-(3-(2,2,2-trifluoro-N-(4-(2,2,2-trifluoro-N-(3-(2,2,2-trifluoroacetamido)propyl)acetamido)butyl)acetamido)propyl)acetamido)benzamide (15a)



14a (0.125 g, 0.17 mmol) was taken up in 4M HCl/dioxane (2 ml) at 0 °C and allowed to stir at r.t. for 18 h. Upon reaction completion (as confirmed by MS) the reaction mixture was neutralised by dropwise addition of 1M NaOH and the volatiles removed under reduced pressure. The reaction mixture was subsequently co-evaporated with Et₃N (3 x 2 ml) and residue re-dissolved in Et₃N (2 ml) and DCM (1 ml). A solution of trifluoroacetic anhydride (249.90 mg, 1.19 mmol) in DCM (1 ml) was added dropwise to the reaction mixture at 0 °C over 30 mins, ensuring the temperature was maintained below 5 °C. The resulting solution was warmed to r.t. and left to stir for a further 20 h. The reaction was quenched by addition of H₂O (4 ml) and the aqueous phase extracted with EtOAc (3 x 10 ml), dried over MgSO₄ and evaporated under high vacuum to give a yellow oil. The residue was purified by column chromatography (50-100 % EtOAc/Hexane) to give the title product as a yellow oil (0.040 g, 93%). ¹H NMR (400 MHz; CDCl₃): δ 7.80-7.74 (m, 2H, 7- and 5-CH), 7.70 (br s, 1H, 10-NH), 7.57-7.50 (m, 2H, 4- and 8-CH), 3.59-3.36 (m, 10H, 11-, 24-, 13-, 17- and 20-CH₂), 3.34-3.25 (m, 2H, 26-CH₂), 3.21 (s, 1H, 1-CH), 1.93-1.81 (m, 4H, 12-, 25-CH₂), 1.69-1.58 (m, 4H, 18- and 19-CH₂); ¹³C NMR (100 MHz, CDCl₃): δ 166.1 (9-C), 165.1 (14-C), 156.2 (21-C), 155.9 (28-C), 150.1 (6-C), 147.3 (3-C), 132.5 (4- and 8-C), 127.3 (5- and 7-C), 104.5 (2-C), 96.7 (1-C), 80.1 (29-C), 79.7 (15-C), 79.1 (22-C), 46.9 (17-C), 46.1 (20-C), 44.5 (13-C), 43.0 (24-C), 37.6 (26-C), 35.5 (11-C), 29.2 (25-C), 27.2 (12-C), 25.1 (12-C), 25.8 (18- and 19-C); ¹⁹F NMR (400 MHz; CDCl₃): δ -76.9 (s, 9F, 16-, 23- and 30-F); MS (ESI+) 619 [M+H]⁺, 641 [M+Na]⁺; HRMS (ESI+) C₂₅H₂₈F₉N₄O₄ [M+H]⁺ requires 619.1967 found 619.1990, C₂₅H₂₈F₉N₄O₄Na [M+Na]⁺ requires 641.1786 found 641.1815.

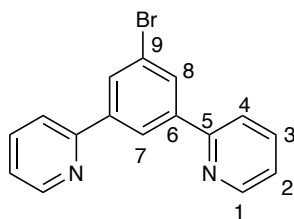
6.4 Synthesis of Tridentate-ligands

6.4.1 1,3-Di(2-pyridyl)benzene (HL1).¹⁵⁷



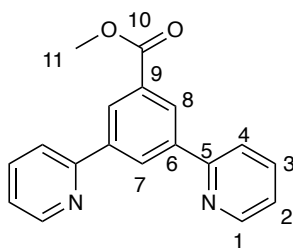
Following a modified literature procedure, a mixture of 1,3-dibromobenzene (1.070 g, 4.55 mmol), 2-tri-*n*-butylstannylpyridine (4.280 g, of 92% purity, 10.90 mmol), lithium chloride (1.550 g, 36.60 mmol), and bis(triphenylphosphine) palladium(II) chloride (0.202 g, 0.29 mmol) were all suspended in toluene (15 ml). The mixture was stirred at reflux for 24 h. The completion of the reaction was monitored by Ms and TLC (20% hexane/80% diethyl ether; $R_f = 0.6$). After cooling to room temperature, the insoluble residue was separated from the solution by filtration and washed with more toluene. The toluene was removed under reduced pressure, and the residue taken up into a mixture of dichloromethane (150 ml) and aqueous NaHCO_3 (5% w/v, 100 ml). The organic phase was separated, washed a second time with the same volume of NaHCO_3 , then dried over anhydrous MgSO_4 and solvent removed under reduced pressure. The product was purified by column chromatography on silica gel, using elution gradient of hexane in diethyl ether (20% to 80%), yielding **HL1** as a brown oil (0.649 g, 61%). ^1H NMR (500 MHz, CDCl_3): δ 8.73 (ddd, 2H, $J = 4.8, 1.8, 0.9$, 1-CH), 8.64 (t, 1 H, $J = 1.7$, 7-CH), 8.07 (dd, 2H, $J = 7.6, 1.8$, 8-CH), 7.85 (d, 2H, $J = 7.9$, 4-CH), 7.78 (td, 2H, $J = 7.7, 1.9$, 3-CH), 7.60 (t, 1H, $J = 7.7$, 9-CH), 7.26 (ddd, 2H, $J = 7.2, 4.6, 1.0$, 2-CH). ^{13}C NMR (126 MHz, CDCl_3): δ 157.4 (quat), 149.8 (1-C), 140.0 (quat), 136.9 (3-C), 129.4 (9-C), 127.6 (8-C), 125.7 (7-C), 122.4 (2-C), 120.9 (4-C). MS (ESI⁺): m/z 232 $[\text{M}]^+$.

6.4.2 1-Bromo-3,5-bis(2-pyridinyl)benzene (HL2).⁹⁶



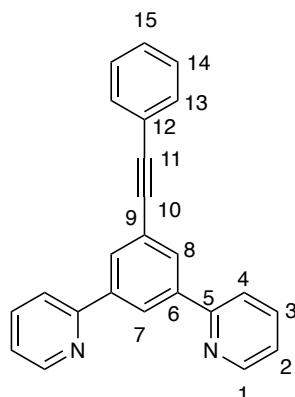
Following a modified literature procedure, a 1.6 M of n-butyl lithium solution in hexane (15.0 ml) was added to the stirred solution of 2-bromopyridine (3.770 g, 23.85 mmol) in THF (75 ml) at $-86\text{ }^{\circ}\text{C}$ and stirred for 2 h. To this solution was added a solution of ZnCl_2 (3.250 g, 23.85 mmol) in THF (32 ml) at $-86\text{ }^{\circ}\text{C}$ and the resulting mixture was stirred for 2 h at r.t. Then, a solution of 1, 3, 5- tribromobenzene (3.750 g, 11.90 mmol) and $\text{Pd}(\text{PPh}_3)_4$ (0.820 g, 0.70 mmol) in THF (15 ml) was added to the solution and the mixture was stirred at r.t. for 24 h. Brine (75 ml) was added and the organic phase was extracted into EtOAc (3 x 200 ml) and the combined organic phase was washed one time with brine (200 ml). The organic phase was dried over anhydrous MgSO_4 , concentrated *in vacuo* to give 4.700 g of white solid. The resulting crude product was purified by silica gel column chromatography with hexane/EtOAc (2:1 in v/v), affording 2.400 g (61%). ^1H NMR (400 MHz, CDCl_3): δ 8.72 (ddd, 2H, $J = 5.6, 1.8, 0.9$, 1-CH), 8.55 (t, 1H, $J = 1.5$, 7-CH), 8.22 (d, 2H, $J = 1.8$, 8-CH), 7.85–7.75 (m, 4H, 4- and 3-CH), 7.29 (ddd, 2H, $J = 6.7, 4.8, 1.8$, 2-C). ^{13}C NMR (100MHz, CDCl_3): δ 159.0 (5-C), 149.4 (1-C), 143.4 (9-C), 140.0 (6-C), 136.7 (3-C), 130.4 (8-C), 125.0 (7-C), 122.4 (2-C), 120.3 (4-C); HRMS: $[\text{M}+\text{H}]^+$ calcd for $\text{C}_{16}\text{H}_{12}\text{BrN}_2$, 311.0184; found, 311.0181.

6.4.3 Methyl-3,5-di(2-pyridyl)benzoate (HL3).⁹⁶



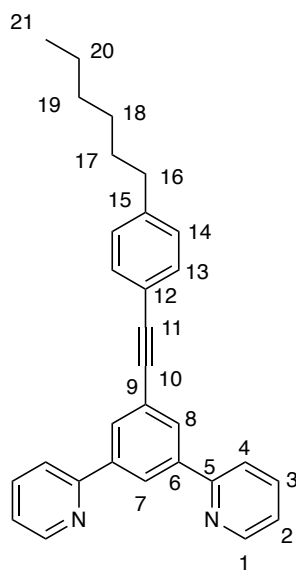
Following a modified literature procedure, a mixture of methyl-3,5-dibromobenzoate (1.180 g, 4.01 mmol), 2-tri-*n*-butylstannylpyridine (5.0 g of 95% purity, equivalent to 9.68 mmol, remainder mostly tetra-*n*-butyltin), bis(triphenylphosphine)palladium dichloride (0.176 g, 0.25 mmol), and lithium chloride (1.390 g, 32.70 mmol) were added in a Schlenk tube. The whole system was evacuated and backfilled with N₂ three times, then dry toluene (15 ml) was added. The mixture was degassed via five freeze-pump-thaw cycles, and then heated at reflux under a nitrogen atmosphere for 24 h. The completion of the reaction was monitored by MS and TLC (20% hexane/80% diethyl ether; R_f = 0.42). After cooling to room temperature, the insoluble residue was separated from the solution by filtration and washed with more toluene. The toluene was removed under reduced pressure, and the residue taken up into a mixture of dichloromethane (150 ml) and aqueous NaHCO₃ (5% w/v, 100 ml). The organic phase was separated, washed a second time with the same volume of NaHCO₃, then dried over anhydrous MgSO₄ and solvent removed under reduced pressure. The product was purified by column chromatography on silica gel, using elution gradient of hexane in diethyl ether (20% to 80%), yielding **HL3** as a white solid (0.525 g, 45%). ¹H NMR (500 MHz, CDCl₃): δ 8.91 (t, 1H, *J* = 1.8, 7-CH), 8.74 (d, 2H, *J* = 4.5, 1-CH), 8.71 (d, 2H, *J* = 1.8, 8-CH), 7.91 (d, 2H, *J* = 7.8, 4-CH), 7.79 (td, 2H, *J* = 7.8, 1.8, 3-CH), 7.28 (ddd, 2H, *J* = 7.2, 4.8, 1.2, 2-CH), 3.99 (s, 3H, 11-CH₃). ¹³C NMR (125 MHz, CDCl₃): δ 166.9 (C=O C-10), 156.1 (quat), 149.8 (1-C), 140.3 (quat), 137.0 (3-C), 131.3 (quat), 129.8 (7-C), 128.3 (8-C), 122.7 (2-C), 120.8 (4-C), 52.3 (11-C). MS (ESI⁺): *m/z* 290 [M+H].

6.4.4 2,2'-(5-(phenylethynyl)-1,3-phenylene)dipyridine (HL4)



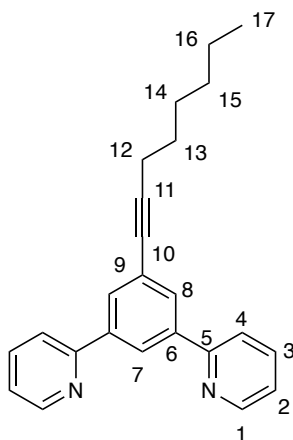
HL2 (0.500 g, 1.60 mmol), Pd(PPh₃)₄ (0.092 g, 0.05 mmol), and CuI (0.015 g, 0.05 mmol) were charged into a Schlenk tube and degassed with N₂ three times. Ethynylbenzene (0.326 g, 3.20 mmol) was dissolved in dry toluene (10 ml) and added to the reaction mixture under N₂ with DIPEA (2 ml). The reaction mixture was stirred for 18 h at 80 °C, and the reaction was monitored by TLC (EtOAc:hexane, 50:50), product (R_f = 0.62). After cooling to r.t. the solvent was removed under reduced pressure, and the residue was purified by column chromatography on silica gel (EtOAc:hexane, 50:50) to afford the title product as brown oil (0.399 g, 80%). ¹H NMR (400 MHz, CDCl₃): δ 8.72 (ddd, 2H, *J* = 4.8, 2.1, 0.9, 1-CH), 8.61 (t, 1H, *J* = 1.7, 7-CH), 8.24 (d, 2H, *J* = 1.7, 8-CH), 7.86 (d, 2H, *J* = 7.8, 4-CH), 7.78 (ddd, 2H, *J* = 1.7, 5.6, 7.7, 3-CH) 7.57 (d, 2H, *J* = 8.1, 13-CH), 7.46-7.36 (m, 3H, 15- and 14-CH), 7.26 (ddd, 2H, *J* = 1.2, 4.9, 7.9, 2-CH); ¹³C NMR (100 MHz, CDCl₃): δ 159.0 (5-C), 149.4 (1-C), 143.4 (9-C), 140.0 (6-C), 136.7 (3-C), 131.4 (13-C), 130.4 (8-C), 127.9 (15- and 14-C), 125.0 (7-C), 124.6 (12-C), 122.4 (2-C), 120.3 (4-C), 89.9 (10-C), 89.3 (11-C); MS (ES⁺) 333 [M+H]; HRMS (ES⁺) C₂₄H₁₆N₂ [M+H] requires 333.2327 found 333.2331.

6.4.5 2,2'-(5-((4-hexylphenyl)ethynyl)-1,3-phenylene)dipyridine (HL5).



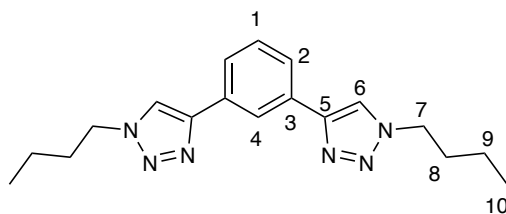
Synthesized according to a procedure similar to that of **HL4** except 1-Ethynyl-4-hexylbenzene (0.435 g, 2.34 mmol) was used in place of ethynylbenzene, yielding an orange oil of **HL5** (0.308 g, 94%). ^1H NMR (400 MHz, CDCl_3): δ 8.72 (ddd, 2H, $J = 4.8, 2.1, 0.9$, 1-CH), 8.61 (t, 1H, $J = 1.6$, 7-CH), 8.22 (d, 2H, $J = 1.6$, 8-CH), 7.85 (d, 2H, $J = 7.8$, 4-CH), 7.76 (ddd, 2H, $J = 1.7, 5.6, 7.7$, 3-CH) 7.47 (d, 2H, $J = 8.1$, 13-CH), 7.26 (ddd, 2H, $J = 1.2, 4.9, 7.9$, 2-CH), 7.17 (d, 2H, $J = 8.2$, 14-CH), 2.61 (t, 2H, $J = 8.1$, 16- CH_2), 1.61 (quint, 2H, $J = 7.8$, 17- CH_2) 1.45-1.31 (m, 6H, 20-, 19- and 18- CH_2), 0.88 (t, 3H, $J = 6.8$, 21- CH_3), ^{13}C NMR (100 MHz, CDCl_3): δ 159.0 (5-C), 149.6 (1-C), 143.4 (9-C), 140.0 (6-C), 136.7 (3-C), 131.4 (13-C), 130.4 (8-C), 128.3 (14-C), 125.0 (7-C), 124.6 (12-C), 122.4 (4-C), 120.2 (15-C), 120.3 (2-C), 90.2 (10-C), 88.6 (11-C), 36.0 (16-C), 31.8 (18-C), 31.0 (17-C), 28.4 (19-C), 22.4 (20-C), 13.8 (21-C); MS (ES⁺) 417 [M+H]; HRMS (ES⁺) $\text{C}_{30}\text{H}_{29}\text{N}_2$ [M+H] requires 417.2327 found 417.2331.

6.4.6 2,2'-(5-(oct-1-yn-1-yl)-1,3-phenylene)dipyridine (HL6)



Synthesized according to a procedure similar to that of **HL4** except 1-Octyne (0.209 g, 1.90 mmol) was used in place of ethynylbenzene, yielding a sticky brown oil of **HL6** (0.295 g, 91%). ^1H NMR (400 MHz, CDCl_3): δ 8.74 (ddd, 2H, $J = 4.8, 2.1, 0.9$, 1-CH), 8.67 (t, 1H, $J = 1.7$, 7-CH), 8.12 (d, 2H, $J = 1.7$, 8-CH), 7.88 (d, 2H, $J = 7.8$, 4-CH), 7.83 (ddd, 2H, $J = 1.7, 5.6, 7.7$, 3-CH), 7.31 (ddd, 2H, $J = 1.1, 4.7, 7.3$, 2-CH), 2.50 (t, 2H, $J = 7.0$, 12- CH_2), 1.69 (quint, 2H, $J = 7.8$, 13- CH_2) 1.51-1.48 (m, 2H, 14- CH_2), 1.39-1.27 (m, 4H, 15- and 16- CH_2), 0.96 (t, 3H, $J = 6.8$, 17- CH_3); ^{13}C NMR (100 MHz, CDCl_3): δ 156.5 (5-C), 149.3 (1-C), 139.9 (9-C), 136.7 (3-C), 130.4 (8-C), 125.1 (6-C), 124.6 (7-C), 122.4 (2-C), 120.6 (4-C), 91.0 (10-C), 80.3 (11-C), 31.4 (15-C), 28.7 (13-C), 28.4 (14-C), 22.5 (16-C), 19.4 (12-C), 14.0 (17-C); MS (ES⁺) 341 [M+H]; HRMS (ES⁺) $\text{C}_{24}\text{H}_{24}\text{N}_2$ [M+H] requires 341.2014 found 341.2930.

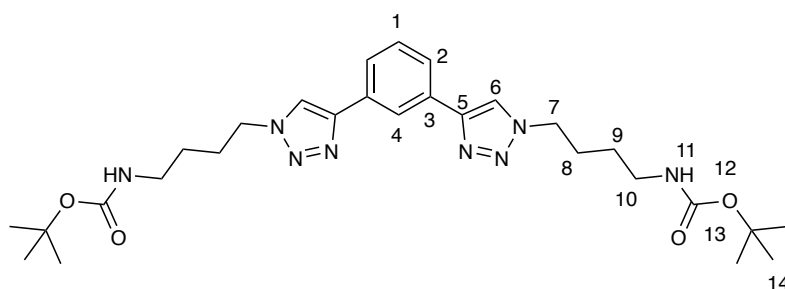
6.4.7 1,3-bis(1-butyl-1H-1,2,3-triazol-4-yl)benzene (HL7)



Sodium azide (0.286 g, 4.40 mmol) was added to a solution of 1-bromobutane (0.575 g, 4.20 mmol) in ethanol/ H_2O (7:3, 25 ml). The solution was heated to 80 $^\circ\text{C}$ under N_2 for overnight. After cooling to r.t., 1,3-diethynylbenzene (0.302 g, 2.40 mmol) was added with sodium ascorbate (0.140 g, 0.70 mmol) and $\text{CuSO}_4 \cdot 5\text{H}_2\text{O}$ (0.120 g, 0.48 mmol). The resulting mixture

was stirred for 6 h at 60 °C. On cooling to r.t., the reaction mixture was washed with saturated EDTA solution (adjusted to pH 10 with NH₄OH) and the aqueous mixture was extracted with EtOAc (3 x 30 ml). The combined organics were dried MgSO₄, filtered and concentrated. The crude residue was crystallised from EtOAc/Hexane to yield the title compound as a white solid (0.352 g, 54%); ¹H NMR (400 MHz, CDCl₃): δ 8.27 (t, 1H, *J* = 1.4, 4-CH), 7.87 (s, 2H, 6-CH), 7.82 (dd, 2H, *J* = 7.7, 1.4, 2-CH), 7.48 (t, 1H, *J* = 7.7, 1-CH), 4.34 (t, 4H, *J* = 7.1, 7-CH₂), 1.86 (q, 4H, *J* = 6.3, 8-CH₂), 1.43-1.36 (m, 4H, 9-CH₂), 0.97 (t, 3H, *J* = 7.4, 10-CH₃); ¹³C NMR (100 MHz, CDCl₃): δ 147.0 (5-C), 131.5 (3-C), 129.4 (2-C), 128.1 (6-C), 125.6 (1-C), 122.8 (4-C), 50.1 (7-C), 32.3 (9-C), 19.7 (8-C), 13.5 (10-C); MS (ES⁺) 348 [M+Na]⁺, 325 [M+H]⁺, HRMS (ES⁺) C₁₈H₂₄N₆ [M+H]⁺ requires 325.2136 found 325.2141.

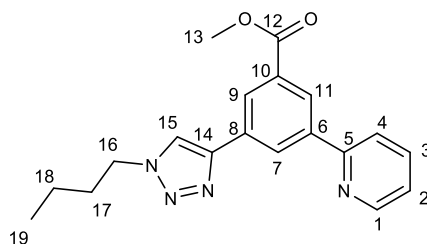
6.4.8 di-tert-butyl(1,3-phenylenebis(1H-1,2,3-triazole-4,1-diyl))bis(butane-4,1-diyl)dicarbamate (HL8)



1a (0.377 g, 2 mmol) was dissolved in MeOH/H₂O (3:1, 8 ml), with NaHCO₃ (0.588 g, 7.0 mmol) and 2 M CuSO₄ aqueous solution (240 μL, 0.20 mmol). ISA*H₂SO₄ (0.650 g, 2.40 mmol) was added and the reaction mixture was stirred at r.t. whilst maintaining the pH above 8 with saturated NaHCO₃. After 1 h, sodium ascorbate (0.080 g, 0.40 mmol) was added followed by 1,3- diethynylbenzene (0.126 g, 1.0 mmol) and the mixture was heated to 60°C for 18 hr. NH₄OH (2 ml) was added to the reaction mixture and the methanol removed under reduced pressure. The residue was partitioned between EtOAc (30 ml) and water (30 ml), and separated. The organic layer was washed with water (30 ml), saturated NaHCO₃ (30 ml), saturated brine (30 ml), dried over MgSO₄, filtered, and concentrated. The crude residue was crystallised from EtOAc/hexane to give the title compound as an off-white solid (0.628 g, 57%). ¹H NMR (400 MHz, CDCl₃): δ 8.27 (t, 1H, *J* = 1.4, 4-CH), 7.87 (s, 2H, 6-CH), 7.82 (dd, 2H, *J* = 7.7, 1.4, 2-CH), 7.48 (t, 1H, *J* = 7.7, 1-CH), 4.59 (br s, 2H, 11-NH), 4.45 (t, 4H, *J* = 7.1, 7-CH₂), 3.18 (q, 4H, *J* = 6.3, 10-CH₂), 1.92-2.09 (m, 4H, 9-CH₂), 1.54-1.50 (m, 4H,

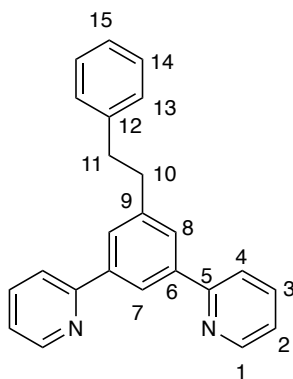
8-CH₂), 1.44 (s, 18H, 13-CH₃); ¹³C NMR (100 MHz, CDCl₃): δ 156 (12-C), 147 (5-C), 131 (6-C), 129.4 (3-C), 125 (2-C), 122.8 (4-C), 120 (1-C), 49.9 (7-C), 39.6 (10-C), 28.4 (13-C), 27.5 (8-C), 27.1 (9-C); MS (ES⁺) 577 [M+Na]⁺, 555 [M+H]⁺, 355 [M-2Boc+3H]⁺, HRMS (ES⁺) C₂₈H₄₂N₈O₄[M+H]⁺ requires 555.3480 found 555.3405. m.p 107 °C.

6.4.9 Methyl 3-(1-butyl-1H-1,2,3-triazol-4-yl)-5-(pyridin-2-yl)benzoate (HL9)



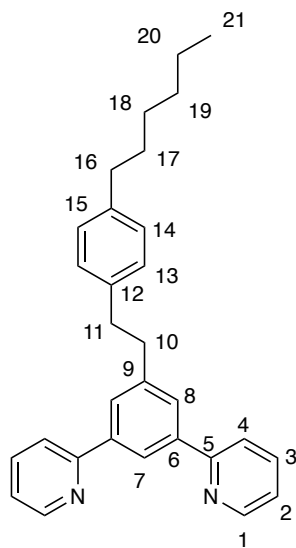
1-Bromobutane (0.270 g, 2.0 mmol) and sodium azide (0.156 g, 2.40 mmol) were dissolved in 5 ml (4:1, THF:H₂O) and refluxed for 18 h. After cooling to r.t., **9a** (0.497 g, 1.60 mmol), K₂CO₃ (0.300 g), sodium ascorbate (0.040 g, 0.20 mmol), and CuSO₄ · 5H₂O (0.039 g, 0.16 mmol), were added, and the solution was heated at 60 °C for 72 h under N₂. Once the reaction mixture was cooled to r.t., TLC (50:50, EtOAc:hexane) confirmed the reaction completion (R_f = 0.4), and the product was identified by MS. Water was added to the reaction mixture and product extracted into EtOAc. The organic layer was washed with aqueous solution of EDTA, brine and water then dried over MgSO₄, and concentrated yielding a sticky brown oil. The crude product was purified by column chromatography on silica gel (20% Et₂O in DCM) to afford the title product as a sticky yellow (oil 0.160 g, 30%). ¹H NMR (500 MHz, CDCl₃): δ 8.53-8.48 (m, 2H, 1- and 7-CH), 8.42 (t, 1H, *J* = 1.6, 9-CH), 8.34 (t, 1H, *J* = 1.5, 11-CH), 7.78 (s, 1H, 15-CH), 7.66 (d, 1H, *J* = 7.9, 4-CH), 7.59 (dd, 1H, *J* = 7.5, 1.8, 3-CH), 7.08 (ddd, 1H, *J* = 7.2, 4.8, 1.2, 2-CH), 4.23 (t, 2H, *J* = 7.2, 16-CH₂), 3.76 (s, 3H, 13-CH₃), 1.75 (quint, 2H, *J* = 7.5, 17-CH₂), 1.20-1.09 (m, 2H, 18-CH₂), 0.78 (t, *J* = 7.8, 3H, 19-CH₃); ¹³C NMR (125 MHz, CDCl₃): δ 167.4 (C=O, 12-C), 156.4 (quat), 150.4 (1-C), 147.3 (quat), 140.9 (quat), 137.1 (3-C), 132.5 (quat), 131.9 (quat), 129.1 (7-C), 128.1 (9-C), 127.6 (11-C), 123.3 (2-C), 121.4 (15-C), 120.9 (4-C), 52.9 (13-C), 51.0 (16-C), 33.0 (17-C), 20.2 (18-C), 14.2 (19-C). MS (ES⁺) 337 [M+H]; HRMS (ES⁺) C₁₉H₂₀N₄O₂ [M+H] requires 337.1667 found 337.1665.

6.4.10 2,2'-(5-phenethyl-1,3-phenylene)dipyridine (HL10)



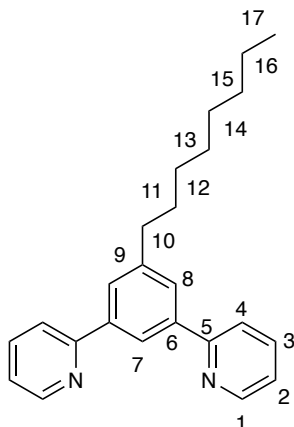
A suspension of **HL4** (0.399 g, 1.20 mmol) and 10% Pd/C (0.300 g, 1.88 mmol) in EtOAc (100 ml) was stirred under a balloon of hydrogen for 48 h at 30 °C and reaction completion was monitored by MS. The reaction mixture was diluted with EtOAc and filtered through celite. The filtrate was concentrated, and give **HL10** (0.403 g, 100%) as a pale brown oil. ¹H NMR (400 MHz, CDCl₃): δ 8.59 (ddd, 2H, *J* = 4.8, 2.1, 0.9, CH), 8.32 (t, 1H, *J* = 1.7, 7-CH), 7.80 (d, 2H, *J* = 1.6, 8-CH), 7.65 (d, 2H, *J* = 7.8, 4-CH), 7.59 (ddd, 2H, *J* = 1.7, 5.6, 7.7, 3-CH) 7.16 (d, 2H, *J* = 8.1, 13-CH), 7.14-7.12 (m, 2H, 14-CH), 7.09-6.95 (m, 3H, 2- and 15-CH), 3.06-3.00 (m, 4H, 10- and 11-CH₂); ¹³C NMR (100 MHz, CDCl₃): δ 156.2 (5-C), 148.5 (1-C), 141.8 (9-C), 140.6 (6-C), 138.9 (12-C), 135.7 (3-C), 135.3 (4-C), 127.4 (8-C), 127.3 (2-C), 124.9 (14-C), 122.2 (7-C), 121.1 (13-C), 119.7 (15-C), 37.2 (10- and 11-C); MS (ES⁺) 337 [M+H]; HRMS (ES⁺) C₂₄H₂₁N₂ [M+H] requires 337.1702 found 337.1713.

6.4.11 2,2'-(5-(4-hexylphenethyl)-1,3-phenylene)dipyridine (HL11)



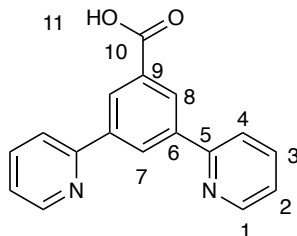
Synthesized according to a procedure similar to that of **HL10** except **HL5** (0.307 g, 0.73 mmol) was used in place of **HL4**. Pale yellow oil (0.306 g, 0.73 mmol) was obtained in 100% yield. ^1H NMR (500 MHz, CDCl_3): δ 8.71 (d, 2H, $J = 4.7$, 1-CH), 8.42 (t, 1H, $J = 1.5$, 7-CH), 7.90 (d, 2H, $J = 1.5$, 8-CH), 7.78 (d, 2H, $J = 7.8$, 4-CH), 7.73 (ddd, 2H, $J = 1.7$, 5.6, 7.7, 3-CH), 7.22 (ddd, 2H, $J = 1.2$, 4.9, 7.9, 2-CH), 7.15 (d, 2H, $J = 7.9$, 14-CH), 7.10 (d, 2H, $J = 7.9$, 13-CH) 3.06- 3.00 (m, 4H, 10- and 11- CH_2), 2.57 (t, 2H, $J = 7.8$, 16- CH_2), 1.59 (quint, 2H, $J = 7.5$, 17- CH_2) 1.28-1.32 (m, 6H, 20-, 19- and 18- CH_2), 0.88 (t, 3H, $J = 6.8$, 21- CH_3); ^{13}C NMR (125 MHz, CDCl_3): δ 157.4 (5-C), 149.6 (1-C), 143.4 (9-C), 140.0 (6-C), 139.9 (15-C), 138.9 (12-C), 136.7 (3-C), 128.2 (13- and 14-C), 127.6 (8-C), 123.2 (4-C), 122.4 (7-C), 120.2 (2-C), 38.4 (10-C), 37.7 (11-C), 35.5 (16-C), 31.6 (18-C), 31.0 (17-C), 28.4 (19-C), 22.4 (20-C), 14.1 (21-C); MS (ES⁺) 421 [M+H]; HRMS (ES⁺) $\text{C}_{30}\text{H}_{33}\text{N}_2$ [M+H] requires 421.2639 found 421.2644.

6.4.12 2,2'-(5-octyl-1,3-phenylene)dipyridine (HL12)



Synthesized according to a procedure similar to that of **HL10** except **HL6** (0.290 g, 0.85 mmol) was used in place of **HL4**. Pale yellow oil (0.293 g, 0.85 mmol) was obtained in 100% yield. ^1H NMR (500 MHz, CDCl_3): δ 8.73 (d, 2H, $J = 4.7$, 1-CH), 8.41 (app s, 1H, 7-CH), 7.93 (app s, 2H, 8-CH), 7.85 (d, 2H, $J = 7.8$, 4-CH), 7.77 (ddd, 2H, $J = 1.7, 5.6, 7.7$, 3-CH), 7.25 (ddd, 2H, $J = 1.2, 4.9, 7.9$, 2-CH), 2.79 (t, 2H, $J = 7.8$, 10- CH_2), 1.74 (quint, 2H, $J = 7.5$, 11- CH_2), 1.41-1.38 (m, 2H, 12- CH_2), 1.29-1.16 (m, 8H, 13-, 14-, 15- and 16- CH_2), 0.89 (t, 3H, $J = 6.8$, 17- CH_3); ^{13}C NMR (125 MHz, CDCl_3): δ 157.5 (5-C), 149.6 (1-C), 144.1 (9-C), 139.8 (6-C), 136.7 (3-C), 127.6 (8-C), 123.3 (7-C), 122.1 (4-C), 120.8 (2-C), 36.2 (10-C), 31.9 (11- or 12-C), 31.6 (11- or 12-C), 29.5 (13- and 14-C), 29.2 (15-C), 22.6 (16-C), 14.1 (17-C); MS (ES+) 345 [M+H]; HRMS (ES+) $\text{C}_{24}\text{H}_{28}\text{N}_2$ [M+H] requires 345.2327 found 345.2345.

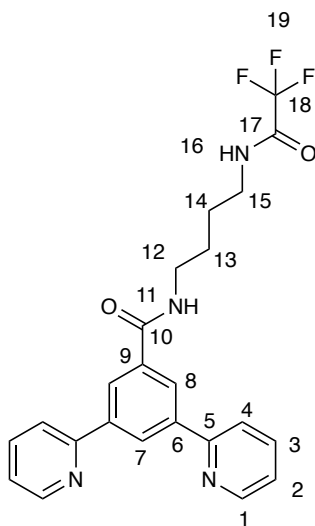
6.4.13 3,5-di(pyridin-2-yl)benzoic acid (HL3).



A mixture of **HL3** (0.378 g, 1.30 mmol) and KOH (0.446 g, 11.15 mmol) in MeOH (15 ml) and water (5 ml) was refluxed for 4 h under N_2 . After removing the solvent under reduced pressure, the resulting residue was added to water and neutralized with aqueous HCl (4N, 9.60 ml, 38.40 mmol) to obtain a precipitate. The precipitate was filtered off and washed with water (3 x 10 ml). The product was directly used in the next reaction. ^1H NMR (400 MHz, DMSO-

d^6): δ 8.85 (d, 2H, $J = 6.0$, 1-CH), 8.57 (s, 1H, 7-CH), 8.49 (d, 2H, $J = 1.6$, 8-CH), 8.28-8.08 (m, 4H, 3- and 4-CH), 7.60 (ddd, 2H, $J = 5.8, 7.4$, 2-CH). ^{13}C NMR (100 MHz, DMSO- d^6): δ 167.2 (10-C), 167.8 (1-C), 166.3 (3-C), 156.1 (7-C), 152.0 (quat), 141.3 (quat), 130.3 (8-C), 126.7 (4-C), 125.5 (quat), 121.5 (2-C). MS (ESI+): m/z 277 $[\text{M}+\text{H}]^+$.

6.4.14 3,5-di(2pyridine-2-yl)-N-(4-(2,2,2-trifluoroacetamido)butyl)benzamide (HL13)



HL3' (0.109 g, 0.50 mmol) was dissolved in dry DMF (2.5 ml) and Et_3N (70 μL , 0.50 mmol) was added. DIC (0.630 g, 0.50 mmol) and NHS (0.570 g, 0.50 mmol) were added and the mixture was left to stir at r.t. for 1 hr under N_2 . A solution of amine **3a** (0.276 g, 0.55 mmol) in dry DMF (2 ml) was added and the reaction mixture was stirred for 18 h at r.t. The white precipitate was filtered off through celite and the filtrate was diluted with DCM (10 ml) and water (10 ml), separated and the aqueous extracted with DCM (2 x 10 ml). The organic layers were combined and dried over MgSO_4 and isolated under reduced pressure. The crude product was then purified by column chromatography on silica gel (DCM to 5% MeOH in DCM) to afford the title product ($R_f = 0.7$) as a white solid (0.295 g, 91%). Remaining di-isopropanol urea (DIU) was removed by dissolving in DCM (10 ml) and washing with 5% HCl solution (20 ml). ^1H NMR (500 MHz, D_2O): δ 8.76 (d, 2H, $J = 5.3$, 1-CH), 8.53 (t, 2H, $J = 7.7$, 3-CH), 8.42 (s, 1H, 7-CH), 8.34 (s, 2H, 8-CH), 8.25 (br d, 2H, $J = 8.1$, 4-CH), 7.94 (t, 2H, $J = 6.6$, 2-CH) 3.40 (app br s, 2H, 12- CH_2), 3.32 (app br s, 2H, 15- CH_2), 1.63 (app br m, 4H, 13- and 14- CH_2); ^{13}C NMR (125 MHz, D_2O): δ 168.4 (10-C), 151.2 (17-C), 145.9 (3-C), 143.2 (1-C), 136.9 (9-C), 134.3 (6-C), 130.5 (7-C), 128.6 (8-C), 126.0 (2-C), 125.9 (4-C), 39.7 (12-C), 39.4 (15-C), 25.5 (13-C), 25.2 (14-C); ^{19}F NMR (400 MHz; D_2O): δ -75.8 (s, 3F, 1- CF_3); MS (ES+) 443 $[\text{M}+\text{H}]$; HRMS (ES+) $\text{C}_{23}\text{H}_{21}\text{F}_3\text{N}_4\text{O}_2$ $[\text{M}+\text{H}]$ requires 443.1695 found 443.1677.

6.5 Synthesis of PtLCl Complexes

6.5.1 General Procedures

- **Method A**¹⁵⁸

Under a nitrogen atmosphere, a solution of K_2PtCl_4 (1 equiv.) and the appropriate tridentate ligand (1 equiv.) in AcOH-H₂O (9:1, 4 ml), was placed in a microwave reactor at 150 °C (250 W) for 45 minutes. After cooling to room temperature, the reaction mixture was filtered. The precipitate was washed successively with methanol, water, ethanol and diethyl ether, then dried under high vacuum.

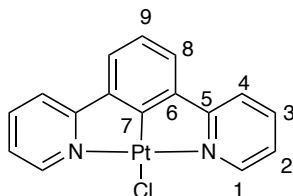
- **Method B**⁴

The appropriate tridentate ligand (1 equiv.) was dissolved in MeCN (15 ml), and a solution of K_2PtCl_4 (1 equiv.) in H₂O (5 ml) was added, giving a yellow-orange solution. The mixture was heated at vigorous reflux for 3 days, and then allowed to cool, giving a yellow precipitate. The precipitate was isolated by filtration, washed with water (4 x 5 ml), ethanol (4 x 5 ml), acetonitrile (4 x 5 ml), and diethylether (2 x 5 ml), and then dried *in vacuo*.

- **Method C**¹⁵³

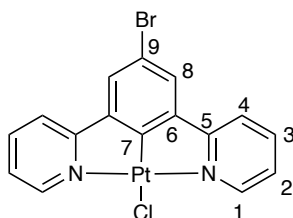
To a solution of amine (3 equiv.) in dry DMF (2 ml), DIPEA was added (3 equiv.), following the addition of the activated ester (1 equiv.). The reaction was left stirring at r.t. for 48 h under N₂ and monitored by MS. The solvent was removed under reduced pressure and the dark orange solid was dissolved in DCM and then purified by column chromatography on silica gel (0 to 5% MeOH in DCM) to afford the title product.

6.5.2 Synthesis of PtL1Cl Complex.⁹⁶



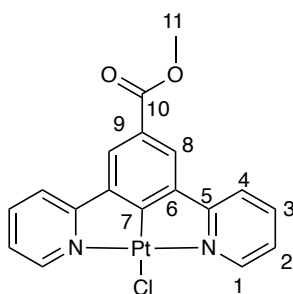
PtL1Cl was prepared by method A. K_2PtCl_4 (62.0 mg, 150 μ mol) and **HL1** (27.0 mg, 100 μ mol) in AcOH-H₂O (9:1, 4 ml). The product was obtained as a bright yellow solid (41.0 mg, 76%). ¹H NMR (500 MHz, CDCl₃): δ 9.36 (d, 2H, $J = 5.7, 1.5, J_{Pt195} = 41.5$, 1-CH), 7.95 (ddd, 2H, $J = 1.5, 7.7, 8.7$, 3-CH), 7.70 (dd, 2H, $J = 8.7, 1.4$, 4-CH), 7.47 (d, 2H, $J = 7.7$, 8-CH), 7.30 (ddd, 2H, $J = 7.7, 5.7, 1.4$, 2-CH), 7.24 (t, 1H, $J = 7.7$, 9-CH). ¹³C NMR (126 MHz, CDCl₃): 167.3 (7-C), 159.0 (5-C), 152.3 (1-C), 140.7 (6-C), 139.0 (3-C), 124.5 (8-C), 123.4 (9-C), 123.0 (2-C), 119.4 (4-C); MS (ES⁺) 426 [M-Cl]⁺; HRMS (ES⁺) C₁₆H₁₁N₂¹⁹⁵Pt [M-Cl]⁺ requires 426.3646 found 426.3649.

6.5.3 Synthesis of PtL2Cl Complex.⁹⁶



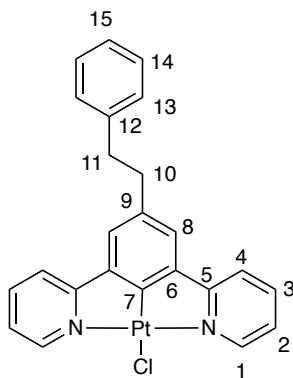
PtL2Cl was prepared by method A. K_2PtCl_4 (83.0 mg, 200 μ mol) and **HL2** (61.0 mg, 190 μ mol) in AcOH-H₂O (9:1, 4 ml). The product was obtained as a yellow/orange solid (55.0 mg, 52%). ¹H NMR (400 MHz, CDCl₃): δ 9.22 (d, 2H, $J = 5.7, 1.6, J_{Pt195} = 42.0$, 1-CH), 7.95 (ddd, 2H, $J = 1.6, 7.8, 8.7$, 3-CH), 7.61 (d, 2H, $J = 8.7$, 4-CH), 7.44 (s, 2H, 8-CH), 7.28 (ddd, 2H, $J = 7.8, 5.7, 1.6$, 2-CH). ¹³C NMR (100 MHz, CDCl₃): 167.3 (7-C), 159.0 (5-C), 152.3 (1-C), 140.7 (6-C), 139.0 (3-C), 138.4 (9-C), 124.5 (8-C), 123.0 (2-C), 119.4 (4-C); MS (ES⁺) 505 [M-Cl]⁺; HRMS (ES⁺) C₁₆H₁₀BrN₂¹⁹⁵Pt [M-Cl]⁺ requires 505.2646 found 505.2649.

6.5.4 Synthesis of PtL3Cl Complex.⁹⁶



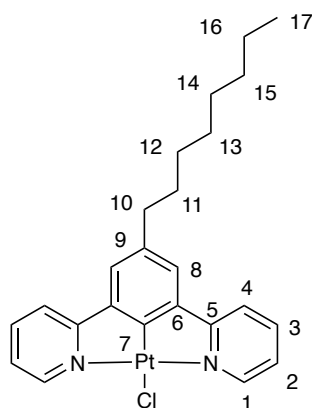
PtL3Cl was prepared by **method B**. K_2PtCl_4 (0.500 g, 1.5 mmol) and **HL3** (0.300 g, 1 mmol) in acetonitrile (15 ml). The product was obtained as a yellow solid (410.0 g, 79%). 1H NMR (500 MHz, $CDCl_3$): δ 9.39 (d, 2H, $J = 5.7, 1.8, J_{Pt195} = 41.3$, 1-CH), 8.15 (s, 2H, 8-CH), 8.00 (td, 2H, $J = 8.1, 1.8$, 3-CH), 7.82 (d, 2H, $J = 8.1$, 4-CH), 7.34 (ddd, 2H, $J = 9.0, 5.7, 1.8$, 2-CH), 3.94 (s, 3H, 11- CH_3). ^{13}C NMR (125 MHz, $CDCl_3$): δ 167.2 (10-C), 167.2 (quat), 157.1 (quat), 152.3 (1-C), 139.4 (3-C), 125.4 (8-C), 123.7 (quat), 123.2 (2-C), 119.7 (4-C), 52.3 (11-C). HRMS (ESI+) $C_{18}H_{13}N_2O_2^{195}Pt [M-Cl]^+$ requires 484.0627 found at 484.0630.

6.5.5 Synthesis of PtL10Cl Complex.



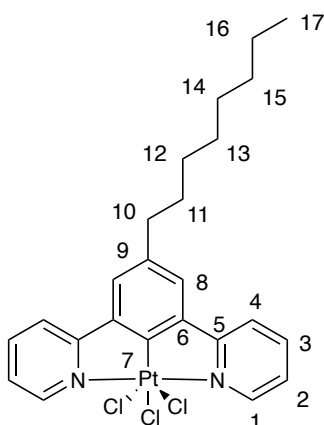
PtL10Cl was prepared by **method A**. K_2PtCl_4 (62.0 mg, 150 μ mol) and **HL10** (34.0 mg, 100 μ mol) in AcOH- H_2O (9:1, 4 ml). The product was obtained as yellow solid (48.0 mg, 85%). 1H NMR (400 MHz, $CDCl_3$): δ 9.33 (d, 2H, $J = 5.0, 1.5, J_{Pt195} = 36.5$, 1-CH), 7.91 (ddd, 2H, $J = 1.5, 7.1, 8.7$, 3-CH), 7.61 (d, 2H, $J = 7.1$, 4-CH), 7.29-7.22 (m, 4H, 2- and 8-CH), 7.20-7.15 (m, 5H, 13-, 14-, and 15-CH), 2.95 (m, 4H, 10- and 11- CH_2); ^{13}C NMR (100 MHz, $CDCl_3$): 167.3 (7-C), 159.0 (5-C), 152.3 (1-C), 140.7 (6-C), 139.0 (3-C), 138.4 (9-C), 136.7 (12-C), 128.6 (13-C), 128.4 (14-C), 126.1 (15-C), 124.5 (8-C), 123.0 (2-C), 119.1 (4-C), 38.6 (10-C), 38.1 (11-C); MS (ES+) 530 $[M-Cl]^+$; HRMS (ES+) $C_{24}H_{19}N_2^{195}Pt [M-Cl]^+$ requires 530.2346 found 530.1199, $[(M-Cl) + MeCN]^+$ found 571.1464.

6.5.6 Synthesis of PtL12Cl Complex.



PtL12Cl was prepared by **method A**. K_2PtCl_4 (50.0 mg, 120 μmol) and **HL12** (37.0 mg, 110 μmol) in AcOH:H₂O (9:1, 4 ml). The pure product was obtained as orange solid (52.0 mg, 83%). ¹H NMR (500 MHz, CDCl₃): δ 9.26 (d, 2H, $J = 5.3, 1.5, J_{Pt195} = 36.5$, 1-CH), 7.90 (ddd, 2H, $J = 1.5, 7.7, 8.7$, 3-CH), 7.63 (d, 2H, $J = 7.7$, 4-CH), 7.18-7.27 (m, 4H, 2- and 8-CH), 2.55 (t, 2H, $J = 7.6$, 10-CH₂), 1.63 (quin, 2H, $J = 7.6$, 11-CH₂) 1.38-1.29 (m, 10H, 12-, 13-, 14-, 15- and 16-CH₂), 0.87 (t, 3H, $J = 6.8$, 17-CH₃); ¹³C NMR (125 MHz, CDCl₃): 167.7 (7-C), 159.0 (5-C), 152.2 (1-C), 141.2 (6-C), 138.9 (3-C), 137.5 (9-C), 124.7 (2-C), 123.0 (8-C), 118.4 (4-C), 36.6 (10-C), 31.5 (11-C), 29.2 (12-C), 29.3 (13-C), 28.6 (14-C), 23.4 (15-C), 22.5 (16-C), 13.7 (17-C); MS (ES⁺) 538 [M-Cl]⁺; HRMS (ES⁺) C₃₀H₃₁N₂¹⁹⁵Pt [M-Cl]⁺ requires 538.1822 found 538.1846, [(M-Cl)+MeCN]⁺ requires 579.2088 found 579.2122.

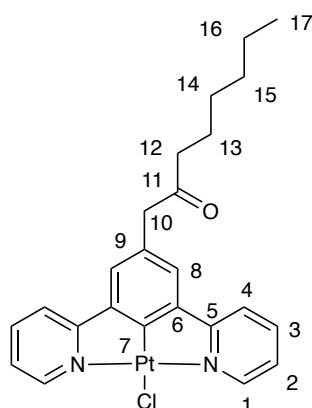
6.5.7 Synthesis of PtL12Cl₃ Complex.



PtL12Cl₃ was isolated as a side product from the reaction to synthesis **PtL12Cl** and the complex structure was confirmed by X-ray crystallography as yellow crystal. ¹H NMR (500

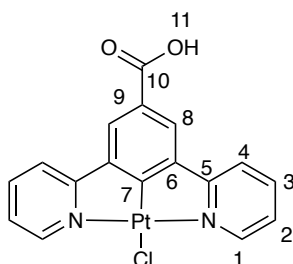
MHz, CDCl₃): δ 9.50 (ddd, 2H, $J = 5.7, 1.5, J_{Pt195} = 30.5$, 1-CH), 8.03 (ddd, 2H, $J = 1.5, 7.7, 8.7$, 3-CH), 7.93 (d, 2H, $J = 7.7$, 4-CH), 7.57 (s, 2H, 8-CH), 7.48-7.37 (m, 2H, 2-CH) 2.84 (t, 2H, $J = 7.6$, 10-CH₂), 1.73 (quin, 2H, $J = 7.6$, 11-CH₂) 1.38-1.29 (m, 10H, 12-, 13-, 14-, 15- and 16-CH₂), 0.87 (t, 3H, $J = 6.8$, 17-CH₃); HRMS (ES⁺) C₃₀H₃₁N₂¹⁹⁵Pt [M-Cl]⁺ requires 609.1148 found 609.1196.

6.5.8 Synthesis of PtL6^aCl Complex.



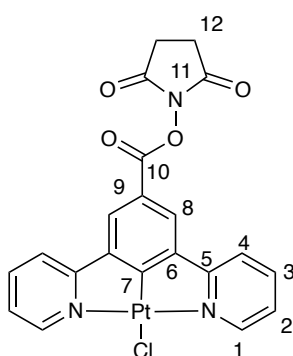
PtL6^aCl was prepared by **method A**. K₂PtCl₄ (50.0 mg, 120 μ mol) and **HL6** (35.0 mg, 110 μ mol) in AcOH:H₂O (9:1, 4 ml). In the crude product two different signals for proton NMR were observed and one of the complexes was successfully isolated by washing the solid with acetone yielding a yellow solid **PtL6^aCl**. ¹H NMR (500 MHz, CDCl₃): δ 9.24 (d, 2H, $J = 5.3, 1.5, J_{Pt195} = 36.5$, 1-CH), 7.88 (ddd, 2H, $J = 1.5, 7.7, 8.7$, 3-CH), 7.61 (d, 2H, $J = 7.7$, 4-CH), 7.21-7.15 (m, 4H, 2- and 8-CH), 3.65 (s, 2H, 10-CH₂) 2.51 (t, 2H, $J = 7.4$, 12-CH₂), 1.57 (quin, 2H, $J = 7.4$, 13-CH₂) 1.25 (m, 6H, 14-, 15- and 16-CH₂), 0.84 (t, 3H, $J = 6.8$, 17-CH₃), ¹³C NMR (125 MHz, CDCl₃): δ 208.8 (11-C), 166.8 (7-C), 159.9 (5-C), 152.2 (1-C), 141.2 (6-C), 138.5 (3-C), 128.9 (9-C), 125.5 (2- or 8-C), 123.1 (2- or 8-C), 119.2 (4-C), 50.1 (10-C), 42.0 (12-C), 31.5 (14-C), 28.9 (15-C), 22.2 (16-C), 23.9 (13-C), 14.0 (17-C); MS (ES⁺) 552 [M-Cl]⁺; HRMS (ES⁺) C₃₀H₃₁N₂¹⁹⁵Pt [M-Cl]⁺ requires 552.1615 found 552.1635, [(M-Cl)+MeCN]⁺ requires 593.1802 found 593.1911.

6.5.9 Synthesis of PtL3^aCl Complex.¹⁵⁴



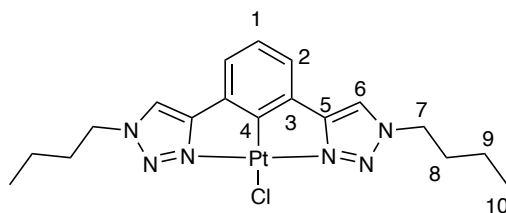
KOH (1.08 g, 19.24 mmol) was dissolved in MeOH (5ml), with **PtL3^aCl** (0.100 g, 0.192 mmol) was added into this solution. The reaction mixture was stirred at 40 °C for 24 h. Aqueous HCl (4N, 9.6 ml, 38.4 mmol) was added to the reaction mixture. The resulting yellow precipitate was collected by filtration and washed with water (3 × 20 ml) and MeOH (2 × 20 ml) and dried *in vacuo*. A yellow solid was obtained (0.078.3 g, 80%). ¹H NMR (500 MHz, DMSO-*d*⁶): δ 9.12 (d, 2H, *J* = 5.8, *J*_{Pt195} = 34.0, 1-CH), 8.35 (s, 2H, 8-CH), 8.28-8.08 (m, 4 H, 4- and 3-CH), 7.60 (ddd, 2 H, *J* = 5.8, 7.4, 2-CH). ¹³C NMR (125 MHz, DMSO-*d*⁶): δ 168.4 (10-C), 167.8 (1-C), 166.3 (3-C), 156.1 (7-C), 152.0 (5-C), 141.3 (6-C), 141.3 (8-C), 126.7 (4-C), 125.5 (9-C), 121.52 (2-C). HRMS (ES⁺): C₂₀H₁₄N₃O¹⁹⁵Pt [M-Cl]⁺ requires 470.0468 found 469.8722, [(M-Cl) + MeCN]⁺ 511.0736.

6.5.10 Synthesis of PtL3^{NHS}Cl Complex.¹⁵⁴



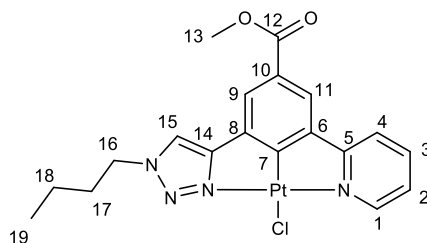
To a solution of **PtL3^aCl** (0.110 g, 0.20 mmol) in dry DMF (0.6 ml), DIC (0.027 g, 0.24 mmol) and NHS (0.027 g, 0.24 mmol) were added then reaction mixture was left to stir for 18 h. A yellow precipitate was collected by filtration then washed with dry DMF (3 × 0.5 ml) and dried *in vacuo* to give **PtL3^{NHS}Cl** (0.115 g, 95%). ¹H NMR (500 MHz, DMSO-*d*⁶): δ 9.18 (d, 2H, *J*

6.5.13 Synthesis of PtL7Cl Complex.



PtL7Cl was prepared by **method A**. K_2PtCl_4 (41.0 mg, 100 μmol) and **HL7** (32.0 mg, 100 μmol) in $\text{AcOH}:\text{H}_2\text{O}$ (9:1, 4 ml). The product was obtained as a pale-yellow solid (0.035 g, 63%). ^1H NMR (400 MHz, CDCl_3): δ 7.72 (s, 2H, 6-CH), 7.10 (d, 2H, $J = 7.6$, 2-CH), 7.01 (app t, 1H, $J = 7.6$, 1-CH), 4.42 (t, 4H, $J = 7.3$, 7- CH_2), 1.97 (quin, 4H, $J = 5.6$, 8- CH_2), 1.44-1.62 (m, 4H, 9- CH_2), 0.97 (t, 6H, $J = 7.3$, 10- CH_3); ^{13}C NMR (100 MHz, CDCl_3): δ 147.7 (5-C), 132.6 (4-C), 131.5 (3-C), 123.5 (1-C), 120.4 (2-C), 118.3 (6-C), 52.2 (7-C), 31.7 (8-C), 19.7 (9-C), 13.5 (10-C); HRMS (ES+) $\text{C}_{18}\text{H}_{23}\text{N}_6^{195}\text{Pt}$ $[\text{M}-\text{Cl}]^+$ requires 518.1633 found 518.1645.

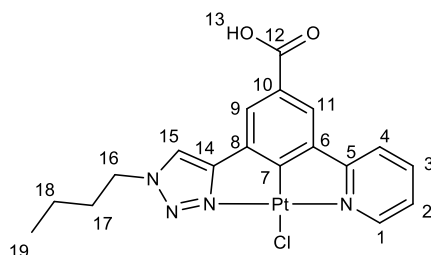
6.5.14 Synthesis of PtL9Cl Complex.



PtL9Cl was prepared by **method A**. K_2PtCl_4 (124 mg, 300 μmol) and **HL9** (82.0 mg, 240 μmol) in $\text{AcOH}:\text{H}_2\text{O}$ (9:1, 4 ml). **PtL9Cl** was obtained as a yellow solid (58.0 mg, 43%). ^1H NMR (500 MHz, CD_2Cl_2): δ 9.21 (d, 1H, $J = 5.0, 1.5$, $J_{\text{Pt}195} = 36.5$, 1-CH), 7.91 (ddd, 1H, $J = 1.5, 7.7, 8.7$, 3-CH), 7.79 (d, 2H, $J = 7.1$, 9- and 11-CH), 7.65 (s, 1H, 15-CH), 7.62 (br d, 1H, $J = 7.7$, 4-CH) 7.27 (br t, 1H, $J = 5.0$, 2-CH), 4.42 (t, 2H, $J = 7.2$, 16- CH_2), 3.76 (s, 3H, 13- CH_3) 1.92 (quint, 2H, $J = 7.5$, 17- CH_2), 1.36-1.31 (m, 2H, 18- CH_2), 0.92 (3H, t, $J = 7.2$, 19- CH_3), ^{13}C NMR (125 MHz, CD_2Cl_2): δ 167.4 (C=O, 12-C), 166.7 (quat), 166.2 (quat), 157.0 (quat), 152.2 (1-C), 141.2 (quat), 139.8 (3-C), 133.0 (quat), 125.5 (quat), 123.9 (9- or 11-C), 123.7 (15-C), 123.4 (2-C), 120.2 (4-C), 120.0 (9- or 11-C), 120.9 (4-C), 52.9 (13-C), 52.4 (16-C), 32.2 (17-C), 20.2 (18-C), 13.5 (19-C); MS (ES+) 530 $[\text{M}-\text{Cl}]^+$; HRMS (ES+) $\text{C}_{19}\text{H}_{19}\text{N}_4$

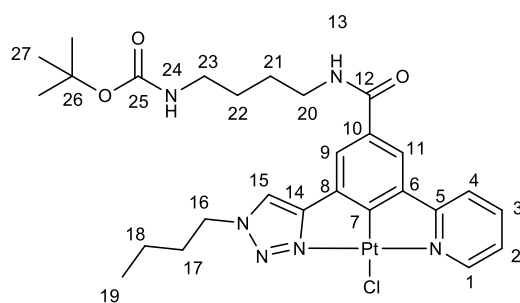
$\text{O}_2^{195}\text{Pt} [\text{M}-\text{Cl}]^+$ requires 530.1161 found 530.1156, $[\text{2M}-\text{Cl}]^+$ requires 1095.1989 found 1095.2010.

6.5.15 Synthesis of $\text{PtL9}^{\text{a}}\text{Cl}$ Complex.



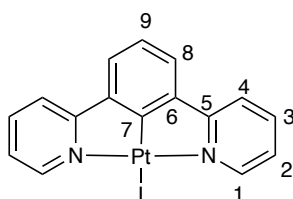
KOH (1.08 g, 19.24 mmol) was dissolved in MeOH (5ml). PtL9Cl (0.057 g, 0.10 mmol) was added into this solution. The reaction mixture was stirred at 40 °C for 24 h. Aqueous HCl (4N, 9.6 ml, 38.40 mmol) was added to the reaction mixture. The resulting yellow precipitate was collected by filtration and washed with water (3×20 ml) and MeOH (2×20 ml) and dried *in vacuo*. A pale-yellow solid was obtained (0.045 g, 81%). ^1H NMR (500 MHz, DMSO-*d*₆): δ 9.34 (d, 1H, $J = 5.9, 1.5, J_{\text{pt}195} = 36.5$, 1-CH), 9.01 (s, 1H, 15-CH), 8.41 (d, 1H, $J = 7.1$, 9-CH), 8.33-8.26 (m, 2H, 3- and 4-CH), 8.24 (d, 2H, $J = 0.9$, 11-CH), 7.74 (br t, 1H, $J = 5.9$, 2-CH), 4.67 (t, 2H, $J = 7.3$, 16-CH₂), 2.03 (quint, 2H, $J = 7.3$, 17-CH₂), 1.46-1.56 (m, 2H, 18-CH₂), 1.06 (t, 3H, $J = 7.3$, 19-CH₃), ^{13}C NMR (125 MHz, DMSO-*d*₆): δ 167.4 (C=O, 12-C), 166.7 (quat), 166.2 (quat), 157.0 (quat), 150.9 (1-C), 141.2 (quat), 139.8 (3-C), 133.0 (quat), 125.5 (quat), 124.9 (11-C), 123.7 (15-C), 123.4 (2-C), 121.9 (9-C), 120.2 (4-C), 120.9 (4-C), 52.4 (16-C), 32.2 (17-C), 20.2 (18-C), 13.5 (19-C); MS (ES⁺) 530 $[\text{M}-\text{Cl}]^+$; HRMS (ES⁺) C₁₈H₁₇N₄ O₂¹⁹⁵Pt $[\text{M}-\text{Cl}]^+$ requires 516.1001, found 516.0999, $[(\text{M}-\text{Cl})+\text{MeCN}]^+$ requires 557.1266, found 557.1271.

6.5.16 Synthesis of PtL9^aCl Complex.



To a solution of PtL9^aCl (0.200 g, 0.36 mmol) in dry DMF (2 ml), DIC (0.045 g, 0.40 mmol) and NHS (0.046 g, 0.40 mmol,) were added then reaction mixture was left to stir for 18 h. A white precipitate was filtered off and the filtrate was collected and used in the next step. To the resulting filtrate solution **1a** (0.075 g, 0.40 mmol), and DIPEA (0.030 g) were added and reaction mixture stirred for 48 h at r.t. under N₂ and monitored by MS. The solvent was removed under reduced pressure and the resulting orange solid was dissolved in DCM and then purified by column chromatography on silica gel (0-5% MeOH in DCM) to afford product (R_f = 0.7) as an orange solid (0.220 g, 84%). ¹H NMR (500 MHz, CDCl₃): δ 8.87 (d, 1H, *J* = 6.1, 1.5, *J*_{pt195} = 36.5, 1-CH), 7.74 (s, 1H, 15-CH), 7.71 (d, 1H, *J* = 7.5, 3-CH), 7.67 (t, 1H, *J* = 5.2, 13-NH), 7.50 (br d, 1H, *J* = 7.5, 4-CH), 7.45 (s, 1H, 9-CH), 7.22 (s, 1H, 11-CH), 7.06 (t, 1H, *J* = 6.1, 2-CH), 4.96 (br s, 1H, 24-NH), 4.34 (br t, 2H, *J* = 7.4, 16-CH₂), 3.42 (m, 2H, 20-CH₂), 3.20-3.15 (m, 2H, 23-CH₂), 1.89 (quint, 2H, *J* = 7.3, 17-CH₂), 1.74-1.69 (m, 2H, 21-CH₂), 1.66-1.56 (m, 2H, 22-CH₂), 1.42 (s, 9H, 27-CH₃) 1.36-1.25 (m, 2H, 18-CH₂), 0.95 (t, 3H, *J* = 7.3, 19-CH₃); ¹³C NMR (125 MHz, CDCl₃): δ 168.4 (quat), 165.7 (quat), 161.5 (quat), 162.3 (quat), 157.4 (quat), 154.9 (quat), 150.6 (1-C), 139.7 (quat), 138.9 (3-C), 131.6 (quat), 130.3 (quat), 123.0 (2-C), 121.5 (11- and 9-C), 119.6 (4-C), 117.8 (15-C), 79.1 (quat), 52.6 (16-C), 40.3 (20-C), 39.7 (23-C), 32.2 (17-C), 28.4 (27-C), 27.6 (22-C), 26.6 (21-C), 20.2 (18-C), 13.5 (19-C); HRMS (ES⁺) C₂₇H₃₅N₆ O₃¹⁹⁵Pt [M-Cl]⁺ requires 686.2418 found 686.2421, [2M-Cl]⁺ found 1408.4486.

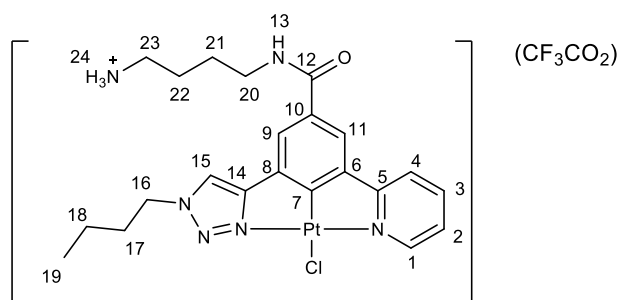
6.6 Synthesis of PtL1I Complex.



A mixture of chloroplatinum complex **PtL1Cl** (40.00 mg, 90 μmol) and KI (149.00 mg, 900 μmol) was stirred in MeOH:DCM (1:1, 20 ml) at r.t. for 18 h. The resulting solution was filtered through celite, and solvent was removed under reduced pressure. Then the residue was purified by silica gel column chromatography (100% DCM) to give the iodoplatinum complex **PtL1I** as bright yellow solid. ^1H NMR (500 MHz, CDCl_3): δ 9.89 (d, 2H, $J = 5.0, 1.5$, $J_{\text{PtI}95} = 37.9$, 1-CH), 7.92 (ddd, 2H, $J = 1.5, 7.7, 8.7$, 3-CH), 7.68 (d, 2H, $J = 7.7$, 4-CH), 7.45 (d, 2H, $J = 7.5$, 8-CH), 7.2-7.3 (m, 3H, 2- and 9-CH), MS (ES $^+$) 425 $[\text{M-I}]^+$; HRMS (ES $^+$) $\text{C}_{16}\text{H}_{11}\text{IN}_2$ ^{194}Pt requires 551.9593 found $[\text{M-I}]^+$ 425.0549.

6.7 Synthesis of Cationic Complexes

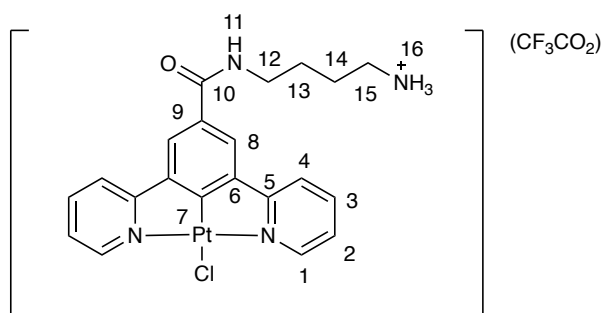
6.7.1 Synthesis of PtL9 $^{1a}\text{Cl}_d$



PtL9 $^{1a}\text{Cl}_d$ (0.200 g, 0.27 mmol) was dissolved in 4M TFA in DCM (2 ml) and stirred at r.t. for 18 h. The volatiles were removed under reduced pressure to produce the title product (0.123 g) as an orange solid without further purification. ^1H NMR (500 MHz, MeOD): δ 8.59 (br d, 1H, $J = 5.0$, 1-CH), 8.08 (s, 1H, 15-CH), 7.77-7.65 (m, 1H, 3-CH), 7.38 (br s, 2H, 9- and 11-CH), 7.12-7.09 (m, 2H, 2- and 4-CH), 4.34 (br t, 2H, $J = 7.4$, 16- CH_2), 3.43-3.36 (m, 2H, 20- CH_2), 3.08-2.98 (m, 2H, 23- CH_2), 1.91-1.87 (m, 2H, 17- CH_2), 1.85-1.80 (m, 2H, 21- CH_2), 1.78-1.64

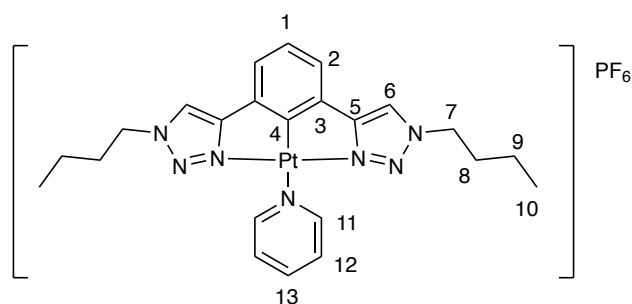
(m, 2H, 22-CH₂), 1.42-1.36 (m, 2H, 18-CH₂), 1.02-0.98 (m, 3H, 19-CH₃); ¹³C NMR (125 MHz, MeOD): δ 169.9 (q, *J* = 34.1, CF₃CO₂), 167.0 (quat), 165.7 (quat), 164.0 (quat), 163.0 (quat), 162.2 (quat), 157.8 (quat), 150.9 (1-C), 141.5 (quat), 140.4 (3-C), 133.6 (quat), 130.6 (quat), 124.0 (2-C and 4-C), 122.4 (11- and 9-C), 121.2 (15-C), 53.5 (16-C), 40.3 (20-C), 37.9 (23-C), 31.7 (17-C), 27.0 (22-C), 23.8 (21-C), 20.3 (18-C), 13.8 (19-C); ¹⁹F NMR (400MHz, MeOD): δ -76.4 (s, 3F-CF₃CO₂); HRMS (ES+) C₂₂H₂₈N₆ O¹⁹⁵Pt [M-Cl]⁺ requires 586.1894 found 586.1896, [2M-Cl]⁺ found 1207.3490.

6.7.2 Synthesis of PtL3^{1a}Cl_d



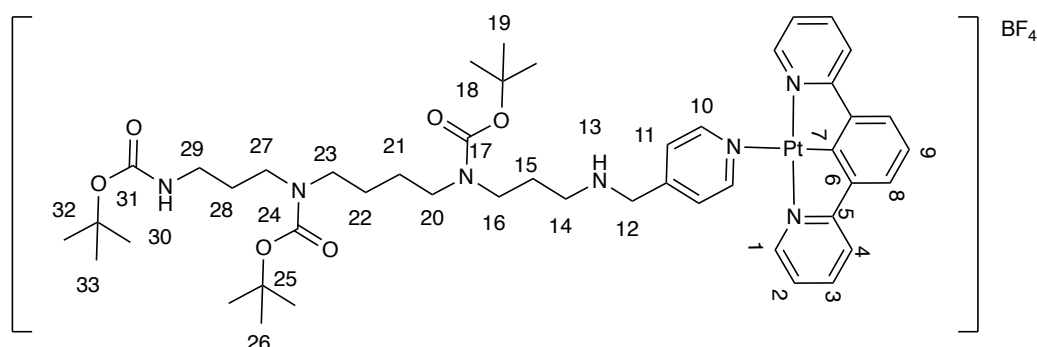
PtL3^{1a}Cl (0.295 g, 0.43 mmol) was dissolved in 4M TFA in DCM (2 ml) and stirred at r.t. for 18 h. The volatiles were removed under reduced pressure to produce the product (0.096 g) as a bright orange solid without further purification. ¹H NMR (500 MHz, DMSO-*d*⁶): δ 9.29 (2H, br d, *J* = 6.1, 1-CH), 8.74 (t, 1 H, *J* = 5.4, 11-NH), 8.51-8.43 (m, 4H, 3- and 4-CH) 8.38 (br d, 2H, *J* = 7.7, 8-CH), 7.94 (br s, 2H, 16-NH), 7.75 (t, 2H, *J* = 6.1, 2-CH), 3.49-3.37 (m, 2H, 12-CH₂), 2.99-2.87 (m, 2H, 15-CH₂), 1.77-1.68 (m, 4H, 13- and 14-CH₂); ¹³C NMR (125 MHz, DMSO-*d*⁶): δ 169.9 (q, *J* = 34.1, CF₃CO₂), 165.8 (quat), 157.8 (quat), 151.3 (1-C), 142.5 (quat), 141.6 (3-C), 133.6 (quat), 129.8 (quat), 124.7 (2-C), 122.6 (4-C), 120.2 (8-C), 39.2 (12-C), 38.8 (15-C), 24.7 (13- and 14-C); ¹⁹F NMR (400MHz, DMSO-*d*⁶): δ -73.8 (s, 3F-CF₃CO₂); HRMS (ES+) C₂₁H₂₁N₄ O¹⁹⁵Pt [M-Cl]⁺ requires 540.1363 found 540.1368.

6.7.4 Synthesis of PtL7Py



PtL7Cl (10.0 mg, 18.0 μmol) was dissolved in 5 ml MeCN and AgPF_6 (7.0 mg, 20 μmol) in MeCN (2 ml) was added. The reaction mixture was stirred for 15 mins, at r.t. and white precipitate was filtered off. Pyridine (1.6 μL , 20 μmol) was added dropwise to the reaction mixture and stirred for 48 h. The formation of the desired complex was monitored by MS and ^1H NMR. The solvent was removed under a reduced pressure to give an orange solid (5.0 mg, 50%). ^1H NMR (400 MHz, CDCl_3): δ 8.52 (d, 2H, $J = 6.4$, 11-CH), 7.73 (s, 2H, 6-CH), 7.24 (t, 1H, $J = 7.6$, 13-CH) 7.14 (d, 2H, $J = 7.4$, 2-CH), 7.18 (app dd, 2H, $J = 7.6$, 6.4, 12-CH), 7.01 (t, 1H, $J = 7.4$, 1-CH), 4.43 (t, 4H, $J = 7.3$, 7-CH₂), 1.97 (q, 4H, $J = 5.6$, 8-CH₂), 1.42-1.56 (m, 4H, 9-CH₂), 0.97 (t, 6H, $J = 7.2$, 10-CH₃); MS (ESI+) 597 [M]⁺; HRMS (ESI+) $\text{C}_{23}\text{H}_{28}\text{N}_7$ $^{195}\text{Pt}[\text{M}]^+$ requires 597.2128 found 597.2122.

6.7.5 Synthesis of PtL1-13a

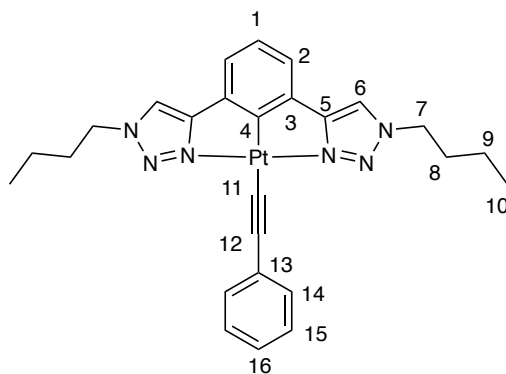


PtL1Cl (20.0 mg, 45.0 μmol) was dissolved in 5 ml, DCM and AgBF_4 (11.0 mg, 50.0 μmol) in MeOH (2 ml) was added. The reaction mixture stirred for 15 mins at r.t. and white precipitate

was filtered off. **13a** (55.0 mg, 90.0 μmol) in 2ml of DCM was added dropwise to the reaction mixture and stirred for 48 h. The formation of the desired complex was monitored by MS. The solvent was removed under a reduced pressure to give a yellow solid. Crude yield was passed through a neutral alumina column (5% MeOH in DCM) and the desired complex decomposed to its starting material during purification process (see Section 3.2.1). MS (ESI+) 1019 $[\text{M}]^+$; HRMS (ESI+) $\text{C}_{47}\text{H}_{66}\text{N}_7\text{O}_6^{195}\text{Pt} [\text{M}]^+$ requires 1019.4828 found 1019.4722.

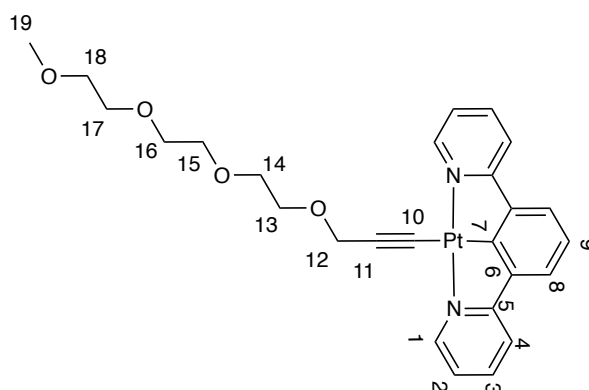
6.8 Neutral Pt(II) complexes

6.8.1 Synthesis of $\text{PtL7C}\equiv\text{CPh}$



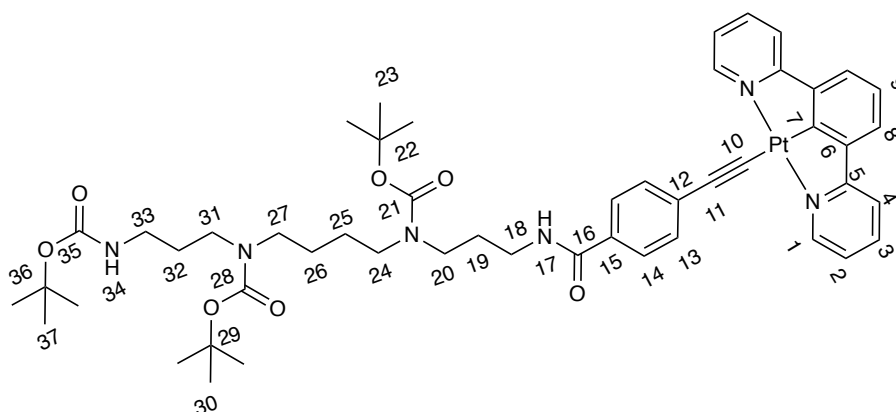
A mixture of phenylacetylene (30.0 mg, 300 μmol) and NaOH (12.0 mg, 300 μmol) in MeOH was stirred for 30 mins at r.t. A solution of **PtL7Cl** (55.0 mg, 100 μmol) in DCM was added dropwise to the reaction mixture and stirred for a further 24 h. After filtration, the resulting solid was washed with deionized water (3×10 ml), MeOH (3×10 ml), and diethyl ether (3×10 ml) to yield a yellow solid (28.0 mg, 48%). ^1H NMR (400 MHz, CDCl_3): δ 7.75 (s, 2H, 6-CH), 7.64 (d, 2H, $J = 7.6$, 14-CH) 7.24 (t, 2H, $J = 7.6$, 15-CH) 7.15 (d, 2H, $J = 7.4$, 2-CH), 7.18 (t, 1H, $J = 7.3$, 16-CH) 7.01 (app t, $J = 7.4$, 1H, 1-CH), 4.4 (t, 4H, $J = 7.3$, 7- CH_2), 1.97 (quin, 4H, $J = 5.6$, 8- CH_2), 1.42-1.56 (m, 4H, 9- CH_2), 0.97 (t, 6H, $J = 7.3$, 10- CH_3); ^{13}C NMR (100 MHz, CDCl_3): δ 147.7 (5-C), 139.2 (16-C), 132.6 (4-C), 132.0 (13-C), 131.5 (3-C), 127.4 (14-C), 124.6 (15-C) 123.5 (1-C), 120.4 (2-C), 118.3 (6-C), 52.2 (7-C), 31.7 (8-C), 19.7 (9-C), 13.5 (10'- and 10-C); HRMS (ES+) $\text{C}_{26}\text{H}_{28}\text{N}_6^{195}\text{Pt} [\text{M}+\text{H}]^+$ requires 620.2103 found 620.2139.

6.8.2 Synthesis of PtL1-12a



12a (48.0 mg, 240 μ ml), and NaOH (10.0 mg, 0.24 ml) were dissolved in 2 ml MeOH and degassed with N_2 *via* (freeze – pump – thaw) cycle 3 times then stirred at r.t. for 15 mins. **PtL1Cl** (66.0 mg, 120 μ ml) was dissolved in 2 ml MeOH (note: the complex is only partially soluble in MeOH) and added to the reaction mixture. The resulting clear orange solution was stirred at r.t. for 72 h. Reaction completion was monitored by MS. Water (4 ml) was poured into the reaction mixture and the resulting red precipitate was collected by filtration, then washed with water and diethyl ether (3×10 ml), to give **PtL-12a** as a red solid (56.0 mg, 74%). 1H NMR (500 MHz, $CDCl_3$): δ 9.41 (d, 2H, $J = 5.0, 1.5$, $J_{Pt195} = 37.9$, 1-CH), 7.89 (t, 2H, $J = 7.3$, 3-CH), 7.61 (d, 2H, $J = 7.3$, 4-CH), 7.45 (d, 2H, $J = 7.5$, 8-CH), 7.21-7.34 (m, 3H, 2- and 9-CH), 4.57 (s, 2H, 12- CH_2), 3.97 (t, 2H, $J = 4.3$, 13- CH_2), 3.75 (t, 2H, $J = 4.3$, 14- CH_2), 3.73-3.63 (m, 6H, 15-, 16-, 17- CH_2), 3.54 (t, 2H, $J = 4.3$, 18- CH_2), 3.37 (s, 3H, 19- CH_3); ^{13}C NMR (125 MHz, $CDCl_3$): δ 152.4 (1-C), 138.9 (3-C), 123.8 (4-C), 121.1 (2-C), 118.4 (8-C), 72.2 (18-C), 69.9 (14-, 15-, 16-, 17-C), 67.6 (13-C), 59.9 (12-C), the low solubility of this complex did not allow the detection of the quaternary carbons; HRMS (ES+) $C_{26}H_{28}IN_2 O_4 Na^{195}Pt$ requires 650.1609 found 650.1595.

6.8.3 Synthesis of PtL1-14a



14a (120.0 mg, 170.0 μmol), CuI (5.0 mg) and K_2CO_3 (500.0 mg) were dissolved in 5 ml dry MeOH and degassed with N_2 *via* (freeze – pump – thaw) cycle 3 times, then stirred at r.t. for 15 mins. **PtL1Cl** (36.0 mg, 80.0 μmol) was dissolved in 2 ml dry DCM and added into the reaction mixture slowly under N_2 in absent of light and stirred at r.t. for 72 h. Reaction completion was monitored by MS. Water (4 ml) was poured into the reaction mixture and dark orange precipitate was collected by filtration and washed with water, MeOH and diethyl ether (3×10 ml), to give **PtL-14a** (46.0 mg, 54%) as an orange solid. ^1H NMR (500 MHz, CDCl_3): δ 9.47 (d, 2H, $J = 5.0$, $J_{Pt195} = 37.9$, 1-CH), 7.93 (t, 2H, $J = 7.3$, 3-CH), 7.83 (br d, 2H, $J = 7.9$, 13-CH), 7.69 (d, 2H, $J = 7.9$, 14-CH), 7.61 (d, 2H, $J = 7.3$, 4-CH), 7.52 (d, 2H, $J = 7.5$, 8-CH), 7.23-7.35 (m, 3H, 2- and 9-CH), 4.78 (s br, 1H, 34-NH), 3.50-3.31 (m, 6H, 18-, 20- and 27- CH_2), 2.93-2.88 (m, 4H, 24- and 33- CH_2), 2.87-2.78 (m, 2H, 32- CH_2), 1.58-1.47 (m, 2H, 19- CH_2), 1.28-1.23 (m, 4H, 26- and 25- CH_2) 1.22-1.15 (m, 27H, 23-, 30- and 37-(CH_3)₃); HRMS (ES+) $\text{C}_{50}\text{H}_{65}\text{N}_6 \text{O}_7^{195}\text{Pt}$ requires 1056.4532 found 1056.4563; $\text{C}_{50}\text{H}_{65}\text{N}_6 \text{O}_7\text{Na}^{195}\text{Pt}$ requires 1078.4382 found 1078.4340.

7 References

- 1 A. P. de Silva, H. Q. N. Gunaratne, T. Gunnlaugsson, A. J. M. Huxley, C. P. McCoy, J. T. Rademacher and T. E. Rice, *Chem. Rev.*, 1997, **97**, 1515-1566.
- 2 L. Basabe-Desmonts, D. N. Reinhoudt and M. Crego-Calama, *Chem. Soc. Rev.*, 2007, **36**, 993-1017.
- 3 J. G. Vos and J. M. Kelly, *Dalt. Trans.*, 2006, 4869-4883.
- 4 D. L. Rochester, S. Develay, S. Zális and J. A. G. Williams, *J. Chem. Soc. Dalt. Trans.*, 2009, 1728-1741.
- 5 E. C. Constable, *Chem. Soc. Rev.*, 2007, **36**, 246-253.
- 6 V. Fernandez-Moreira, F. L. Thorp-Greenwood and M. P. Coogan, *Chem. Commun.*, 2010, **46**, 186-202.
- 7 Q. Zhao, C. Huang and F. Li, *Chem. Soc. Rev.*, 2011, **40**, 2508-2524.
- 8 S. K. Chakraborty, *On disturbances produced in an elastic medium by twists applied on the inner surface of a spherical cavity*, 1956, vol. 33.
- 9 E. M. Goldys, *Fluorescence applications in biotechnology and life science*, Wiley, New York, 2009.
- 10 A. Jablonski, *Phys. A Stat. Mech. its Appl.*, 1985, **129**, 439-454.
- 11 L. Prodi, M. T. Gandolfi and F. Group, *Handbook of Photochemistry*, 3rd ed., 2006.
- 12 M. Y. Berezin and S. Achilefu, *Chem. Rev.*, 2010, **110**, 2641-2684.
- 13 G. Di Marco, M. Lanza, A. Mamo, I. Stefio, C. Di Pietro, G. Romeo and S. Campagna, *Anal. Chem.*, 1998, **70**, 5019-5023.
- 14 K. K.-W. Lo, K. Y. Zhang, S.-K. Leung and M.-C. Tang, *Angew. Chem. Int. Ed.*, 2008, **47**, 2213-2216.
- 15 K. K.-W. Lo, C.-K. Chung, T. K.-M. Lee, L.-H. Lui, K. H.-K. Tsang and N. Zhu, *Inorg. Chem.*, 2003, **42**, 6886-6897.
- 16 J.-M. Hsieh, M.-L. Ho, P.-W. Wu, P.-T. Chou, T.-T. Tsai and Y. Chi, *Chem. Commun.*, 2006, 615-617.
- 17 J. A. Cowan, *J. Med. Chem.*, 1996, **39**, 4346.
- 18 H. C. Gerritsen, R. Sanders, A. Draaijer, C. Ince and Y. K. Levine, *J. Fluoresc.*, 1997, **7**, 11-15.
- 19 Y. Y. Chia and M. G. Tay, *Dalt. Trans.*, 2014, **43**, 13159-13168.
- 20 I. Eryazici, C. N. Moorefield and G. R. Newkome, *Chem. Rev.*, 2008, **108**, 1834-1895.
- 21 J. A. Gareth Williams, S. Develay, D. L. Rochester and L. Murphy, *Coord. Chem. Rev.*, 2008, **252**, 2596-2611.
- 22 J. A. G. Williams, in *Photochemistry and Photophysics of Coordination Compounds II*, eds. V. Balzani and S. Campagna, Springer Berlin Heidelberg, 2007, pp. 205-268.

- 23 C.-K. Koo, K.-L. Wong, C. W.-Y. Man, H.-L. Tam, S.-W. Tsao, K.-W. Cheah and M. H.-W. Lam, *Inorg. Chem.*, 2009, **48**, 7501-7503.
- 24 C. K. Koo, K. L. Wong, C. W. Y. Man, Y. W. Lam, L. K. Y. So, H. L. Tam, S. W. Tsao, K. W. Cheah, K. C. Lau, Y. Y. Yang, J. C. Chen and M. H. W. Lam, *Inorg. Chem.*, 2009, **48**, 872-878.
- 26 S. Logothetidis, *Introduction in Clinical Nanomedicine*, 2003, vol. 1.
- 27 E. Baggaley, J. A. Weinstein and J. A. G. Williams, *Coord. Chem. Rev.*, 2012, **256**, 1762-1785.
- 28 W. A. Tarran, G. R. Freeman, L. Murphy, A. M. Benham, R. Katakly and J. A. G. Williams, *Inorg. Chem.*, 2014, **53**, 5738-5749.
- 29 S. W. Botchway, M. Charnley, J. W. Haycock, A. W. Parker, D. L. Rochester, J. A. Weinstein and J. A. G. Williams, *Proc. Natl. Acad. Sci. U. S. A.*, 2008, **105**, 16071-16076.
- 30 E. Baggaley, S. W. Botchway, J. W. Haycock, H. Morris, I. V. Sazanovich, J. A. G. Williams and J. A. Weinstein, *Chem. Sci.*, 2014, **5**, 879-886.
- 31 R. McGuire, M. C. McGuire and D. R. McMillin, *Coord. Chem. Rev.*, 2010, **254**, 2574-2583.
- 32 G. S. Ming and C.-M. Che, *Chem. – A Eur. J.*, **15**, 7225-7237.
- 33 W. H.-T. Law, L. C.-C. Lee, M.-W. Louie, H.-W. Liu, T. W.-H. Ang and K. K.-W. Lo, *Inorg. Chem.*, 2013, **52**, 13029-13041.
- 34 N. K. Allampally, C.-G. Daniliuc, C. A. Strassert and L. De Cola, *Inorg. Chem.*, 2015, **54**, 1588-1596.
- 35 Y. Li, L. Zhao, A. Y.-Y. Tam, K. M.-C. Wong, L. Wu and V. W.-W. Yam, *Chemistry*, 2013, **19**, 14496-14505.
- 36 U. Bachrach, *Plant Physiol. Biochem.*, 2010, **48**, 490-495.
- 37 A. E. Pegg and P. P. McCann, *Am. J. Physiol.*, 1982, **243**, C212-21.
- 38 R. A. J. Casero and L. J. Marton, *Nat. Rev. Drug Discov.*, 2007, **6**, 373-390.
- 39 A. E. Pegg, *Biochem. J.*, 1986, **234**, 249-262.
- 40 H. M. Wallace, A. V Fraser and A. Hughes, *Biochem. J.*, 2003, **376**, 1-14.
- 41 J. Jänne, L. Alhonen, M. Pietilä and T. A. Keinänen, *Eur. J. Biochem.*, **271**, 877-894.
- 42 K. Igarashi and K. Kashiwagi, *Plant Physiol. Biochem.*, 2010, **48**, 506-512.
- 43 O. Perez-Leal and S. Merali, *Amino Acids*, 2012, **42**, 611-617.
- 44 N. Minois, D. Carmona-Gutierrez and F. Madeo, *Aging (Albany. NY)*, 2011, **3**, 716-732.
- 45 M. Atiya Ali, E. Poortvliet, R. Strömberg and A. Yngve, *Food Nutr. Res.*
- 46 G. D. Luk, G. Goodwin, L. J. Marton and S. B. Baylin, *Proc. Natl. Acad. Sci. U. S. A.*, 1981, **78**, 2355-2358.

- 47 A. E. Pegg, *IUBMB Life*, 2009, **61**, 880-894.
- 48 T. Rossi, A. Coppi, E. Bruni, A. Ruberto, S. Giudice and G. Baggio, *Anticancer Res.*, 2008, **28**, 2765-2768.
- 49 I. Wyatt, A. R. Soames, M. F. Clay and L. L. Smith, *Biochem. Pharmacol.*, 1988, **37**, 1909-1918.
- 50 N. Kaur, J.-G. Delcros, J. Imran, A. Khaled, M. Chehtane, N. Tschammer, B. Martin and O. Phanstiel, *J. Med. Chem.*, 2008, **51**, 1393-1401.
- 51 D. Soulet, B. Gagnon, S. Rivest, M. Audette and R. Poulin, *J. Biol. Chem.*, 2004, **279**, 49355-49366.
- 52 P. M. Cullis, R. E. Green, L. Merson-Davies and N. Travis, *Chem. Biol.*, 1999, **6**, 717-729.
- 53 O. Phanstiel, N. Kaur and J.-G. Delcros, *Amino Acids*, 2007, **33**, 305-313.
- 54 Z. Tian, S. Xie, Y. Du, Y. Ma, J. Zhao, W. Gao and C. Wang, *Eur. J. Med. Chem.*, 2009, **44**, 393-399.
- 55 R. A. Gardner, J.-G. Delcros, F. Konate, F. Breitbeil, B. Martin, M. Sigman, M. Huang and Phanstiel, *J. Med. Chem.*, 2004, **47**, 6055-6069.
- 56 C. Wang, J.-G. Delcros, J. Biggerstaff and Phanstiel, *J. Med. Chem.*, 2003, **46**, 2663-2671.
- 57 A. J. Palmer, R. A. Ghani, N. Kaur, O. Phanstiel and H. M. Wallace, *Biochem. J.*, 2009, **424**, 431-438.
- 58 N. Seiler and F. Dezeure, *Int. J. Biochem.*, 1990, **22**, 211-218.
- 59 A. J. Palmer and H. M. Wallace, *Amino Acids*, 2010, **38**, 415-422.
- 60 M. Belting, K. Mani, M. Jönsson, F. Cheng, S. Sandgren, S. Jonsson, K. Ding, J.-G. Delcros and L.-A. Fransson, *J. Biol. Chem.*, 2003, **278**, 47181-47189.
- 61 M. R. Burns, G. F. Graminski, R. S. Weeks, Y. Chen and T. G. O'Brien, *J. Med. Chem.*, 2009, **52**, 1983-1993.
- 62 U. K. B. Roy, N. S. Rial, K. L. Kachel and E. W. Gerner, *Mol. Carcinog.*, 2008, **47**, 538-553.
- 63 M. P. M. Marques, 2013, **2013**, 1-29.
- 64 O. Heby and L. Persson, *Trends Biochem. Sci.*, 1990, **15**, 153-158.
- 65 A. Bonetti, T. Franceschi, P. Apostoli, A. Messori, L. Sperotto, G. L. Cetto, A. Molino and R. Leone, *Ther. Drug Monit.*, 1995, **17**, 25-32.
- 66 S. Hector, C. W. Porter, D. L. Kramer, K. Clark, J. Prey, N. Kisiel, P. Diegelman, Y. Chen and L. Pendyala, *Mol. Cancer Ther.*, 2004, **3**, 813 LP-822.
- 67 R. Tummala, P. Diegelman, S. Hector, D. L. Kramer, K. Clark, P. Zagst, G. Fetterly, C. W. Porter and L. Pendyala, *Cancer Chemother. Pharmacol.*, 2011, **67**, 401-414.
- 68 A. J. Kraker, J. D. Hoeschele, W. L. Elliott, H. D. Showalter, A. D. Sercel and N. P.

- Farrell, *J. Med. Chem.*, 1992, **35**, 4526-4532.
- 69 J. L. Holley, A. Mather, R. T. Wheelhouse, P. M. Cullis, J. A. Hartley, J. P. Bingham and G. M. Cohen, *Cancer Res.*, 1992, **52**, 4190-4195.
- 70 J. L. Pelley, A. S. Daar and M. A. Saner, *Toxicol. Sci.*, 2009, **112**, 276-296.
- 71 A. J. Amoroso, R. J. Arthur, M. P. Coogan, J. B. Court, V. Fernández-Moreira, A. J. Hayes, D. Lloyd, C. Millet and S. J. A. Pope, *New J. Chem.*, 2008, **32**, 1097-1102.
- 72 V. Fernández-Moreira, F. L. Thorp-Greenwood, A. J. Amoroso, J. Cable, J. B. Court, V. Gray, A. J. Hayes, R. L. Jenkins, B. M. Kariuki, D. Lloyd, C. O. Millet, C. F. Williams and M. P. Coogan, *Org. Biomol. Chem.*, 2010, **8**, 3888-3901.
- 73 K. K.-W. Lo, M.-W. Louie, K.-S. Sze and J. S.-Y. Lau, *Inorg. Chem.*, 2008, **47**, 602-611.
- 74 K. K.-W. Lo, T. K.-M. Lee, J. S.-Y. Lau, W.-L. Poon and S.-H. Cheng, *Inorg. Chem.*, 2008, **47**, 200-208.
- 75 T. Edition, *Neuroscience*, Sinauer Associates, Inc., Sunderland, MA USA, 2004.
- 76 J. Jackson, A. Papadopulos, F. A. Meunier, A. McCluskey, P. J. Robinson and D. J. Keating, *Mol. Psychiatry*, 2015, **20**, 810-819.
- 77 S. T. Brady and L. Tai, in *Basic Neurochemistry*, eds. S. T. Brady, G. J. Siegel, R. W. Albers and D. L. Price, Academic Press, New York, 8th ed., 2012, pp. 3-25.
- 78 J. R. Morgan, G. J. Augustine and E. M. Lafer, *Neuromolecular Med.*, 2002, **2**, 101-114.
- 79 N. C. Harata, S. Choi, J. L. Pyle, A. M. Aravanis and R. W. Tsien, *Neuron*, 2006, **49**, 243-256.
- 80 T. A. Ryan, *Proc. Natl. Acad. Sci.*, 2003, **100**, 2171-2173.
- 81 L.-G. Wu, T. A. Ryan and L. Lagnado, *J. Neurosci.*, 2007, **27**, 11793-11802.
- 82 K. M. Buckley, H. E. Melikian, C. J. Provoda and M. T. Waring, *J. Physiol.*, 2000, **525 Pt 1**, 11-19.
- 83 H. Zhong, G.-M. Sia, T. R. Sato, N. W. Gray, T. Mao, Z. Khuchua, R. L. Huganir and K. Svoboda, *Neuron*, 2009, **62**, 363-374.
- 84 A. C. Ashton and Y. A. Ushkaryov, *J. Biol. Chem.*, 2005, **280**, 37278-37288.
- 85 Y. Saheki and P. De Camilli, *Cold Spring Harb. Perspect. Biol.*, 2012, **4**, a005645.
- 86 P. Hoopmann, S. O. Rizzoli and W. J. Betz, *Cold Spring Harb. Protoc.*, 2012, **2012**, 77-83.
- 87 K. M. Harris and R. J. Weinberg, *Cold Spring Harb. Perspect. Biol.*
- 88 V. Marra, J. J. Burden, F. Crawford and K. Staras, *Nat. Protoc.*, 2014, **9**, 1337-1347.
- 89 P. Verstreken, T. Ohyama and H. J. Bellen, *Methods Mol. Biol.*, 2008, **440**, 349-369.
- 90 S. Phillips, University of Leicester, 2014.
- 91 P. G. M. Wuts and T. W. Greene, *Greene's Protective Groups in Organic Synthesis*,

- Wiley, Hoboken, New Jersey, 2007.
- 92 J. Chadwick, J. Chadwick, M. Jones, A. E. Mercer, P. A. Stocks, S. A. Ward, B. K. Park and P. M. O'Neill, *Bioorg. Med. Chem.*, 2010, **18**, 2586-2597.
- 93 X. Wu, J. Chen, M. Ji, J. Varady, B. Levant and S. Wang, *Bioorg. Med. Chem. Lett.*, 2004, **14**, 5813-5816.
- 94 A. Muth, M. Madan, J. J. Archer, N. Ocampo, L. Rodriguez and O. Phanstiel, *J. Med. Chem.*, 2014, **57**, 348-363.
- 95 M. Chavarot and Z. Pikramenou, *Tetrahedron Lett.*, 1999, **40**, 6865-6868.
- 96 J. A. G. Williams, A. Beeby, E. S. Davies, J. A. Weinstein and C. Wilson, *Inorg. Chem.*, 2003, **42**, 8609-8611.
- 97 S. J. Farley, D. L. Rochester, A. L. Thompson, J. A. K. Howard and J. A. G. Williams, *Inorg. Chem.*, 2005, **44**, 9690-9703.
- 98 N. Miyaura, ed. L. S. B. T.-A. in M.-O. C. Liebeskind, JAI, 1998, vol. 6, pp. 187-243.
- 99 T. N. Y. Hoang, M. Humbert-Droz, T. Dutronc, L. Guénée, C. Besnard and C. Piguet, *Inorg. Chem.*, 2013, **52**, 5570-5580.
- 100 R. Chinchilla and C. Nájera, *Chem. Soc. Rev.*, 2011, **40**, 5084-5121.
- 101 A. Elangovan, Y.-H. Wang and T.-I. Ho, *Org. Lett.*, 2003, **5**, 1841-1844.
- 102 Q. Meng, L. Jiang, Z. Wei, C. Wang, H. Zhao, H. Li, W. Xu and W. Hu, *J. Mater. Chem.*, 2010, **20**, 10931-10935.
- 103 H. C. Kolb, M. G. Finn and K. B. Sharpless, *Angew. Chem. Int. Ed. Engl.*, 2001, **40**, 2004-2021.
- 104 R. A. Evans, *Aust. J. Chem.*, 2007, **60**, 384-395.
- 105 I. Grenthe, *J. Am. Chem. Soc.*, 1961, **83**, 360-364.
- 106 V. V Rostovtsev, L. G. Green, V. V Fokin and K. B. Sharpless, *Angew. Chem. Int. Ed. Engl.*, 2002, **41**, 2596-2599.
- 107 C. W. Tornøe, C. Christensen and M. Meldal, *J. Org. Chem.*, 2002, **67**, 3057-3064.
- 108 V. O. Rodionov, V. V Fokin and M. G. Finn, *Angew. Chem. Int. Ed. Engl.*, 2005, **44**, 2210-2215.
- 109 F. Amblard, J. H. Cho and R. F. Schinazi, *Chem. Rev.*, 2009, **109**, 4207-4220.
- 110 C. Creutz, *Inorg. Chem.*, 1981, **20**, 4449-4452.
- 111 R. van Geel, M. F. Debets, D. W. P. M. Löwik, G. J. M. Pruijn and W. C. Boelens, *Amino Acids*, 2012, **43**, 1251-1263.
- 112 H. Huang and J. S. Panek, *Org. Lett.*, 2003, **5**, 1991-1993.
- 113 F. Friscourt, 2010, **12**, 4936-4939.
- 114 T. Otani, K. Ueki, K. Cho, K. Kanai, K. Tateno and T. Saito, *Chem. Commun.*, 2015, **51**, 7895-7898.

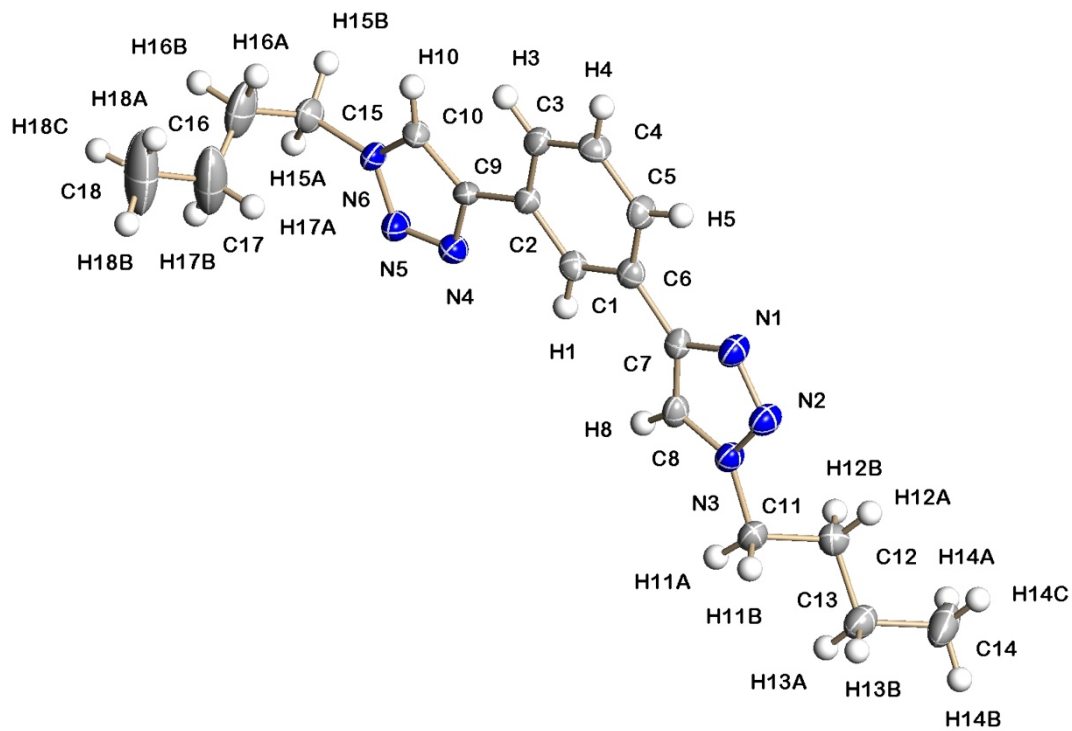
- 115 P. Sund and C. E. Wilén, *React. Funct. Polym.*, 2015, **89**, 24-30.
- 116 M. E. Robinson, D. J. Lunn, A. Nazemi, G. R. Whittell, L. De Cola and I. Manners, *Chem. Commun.*, 2015, **51**, 15921-15924.
- 117 B. Fuss, M. Dede, B. Weibert and H. Fischer, *Organometallics*, 2002, **21**, 4425-4431.
- 118 Z. Li and Y. Chau, *Polym. Chem.*, 2010, **1**, 1599-1601.
- 119 A. Garofalo, A. Parat, C. Bordeianu, C. Ghobril, M. Kueny-Stotz, A. Walter, J. Jouhannaud, S. Begin-Colin and D. Felder-Flesch, *New J. Chem.*, 2014, **38**, 5226-5239.
- 120 J. J. Clayden, N. Greeves and S. Warren, *Oxford Univ. Press*, 2001, **40**, 1990-1992.
- 121 Y. E. Jad, G. A. Acosta, S. N. Khattab, B. G. de la Torre, T. Govender, H. G. Kruger, A. El-Faham and F. Albericio, *Org. Biomol. Chem.*, 2015, **13**, 2393-2398.
- 122 D. Koziej, C. Floryan, R. A. Sperling, A. J. Ehrlicher, D. Issadore, R. Westervelt and D. A. Weitz, *Nanoscale*, 2013, **5**, 5468-5475.
- 123 Z. Wang, E. Turner, V. Mahoney, S. Madakuni, T. Groy and J. Li, *Inorg. Chem.*, 2010, **49**, 11276-11286.
- 124 J. A. Goodwin and A. Aponick, *Chem. Commun.*, 2015, **51**, 8730-8741.
- 125 A. K. W. Chan, E. S. H. Lam, A. Y. Y. Tam, D. P. K. Tsang, W. H. Lam, M. Y. Chan, W. T. Wong and V. W. W. Yam, *Chem. - A Eur. J.*, 2013, **19**, 13910-13924.
- 126 W. Lu, B. X. Mi, M. C. W. Chan, Z. Hui, C. M. Che, N. Zhu and S. T. Lee, *J. Am. Chem. Soc.*, 2004, **126**, 4958-4971.
- 127 T. R. Papo and D. Jaganyi, *J. Coord. Chem.*, 2015, **68**, 794-807.
- 128 F. A. Perras and D. L. Bryce, *J. Magn. Reson.*, 2014, **242**, 23-32.
- 129 B. M. Still, P. G. A. Kumar, J. R. Aldrich-Wright and W. S. Price, *Chem. Soc. Rev.*, 2007, **36**, 665-686.
- 130 S.-W. Lai, M. C. W. Chan, K.-K. Cheung and C.-M. Che, *Inorg. Chem.*, 1999, **38**, 4262-4267.
- 131 B. Schulze, C. Friebe, M. Jäger, H. Görls, E. Birekner, A. Winter and U. S. Schubert, *Organometallics*, 2018, **37**, 145-155.
- 132 B. Schulze and U. S. Schubert, *Chem. Soc. Rev.*, 2014, **43**, 2522-2571.
- 133 B. Pinter, V. Van Speybroeck, M. Waroquier, P. Geerlings and F. De Proft, *Phys. Chem. Chem. Phys.*, 2013, **15**, 17354-17365.
- 134 A. Hofmann, L. Dahlenburg and R. van Eldik, *Inorg. Chem.*, 2003, **42**, 6528-6538.
- 135 D. Schweinfurth, R. Pattacini, S. Strobel and B. Sarkar, *Dalt. Trans.*, 2009, 9291-9297.
- 136 C. E. Welby, S. Grkinic, A. Zahid, B. S. Uppal, E. A. Gibson, C. R. Rice and P. I. P. Elliott, *Dalt. Trans.*, 2012, **41**, 7637-7646.
- 137 E. Rossi, L. Murphy, P. L. Brothwood, A. Colombo, C. Dragonetti, D. Roberto, R. Ugo, M. Cocchi and J. A. G. Williams, *J. Mater. Chem.*, 2011, **21**, 15501-15510.

- 138 B. Tzeng, W. Fu, C. Che, H. Chao and K. Cheung, 1999, 1017-1023.
- 139 P. I. P. Elliott, *Organomet. Chem.*, 2014, **39**, 1-25.
- 140 S. Develay, O. Blackburn, A. L. Thompson and J. A. G. Williams, *Inorg. Chem.*, 2008, **47**, 11129-11142.
- 141 W. B. Connick, D. Geiger and R. Eisenberg, *Inorg. Chem.*, 1999, **38**, 3264-3265.
- 142 K. Suzuki, A. Kobayashi, S. Kaneko, K. Takehira, T. Yoshihara, H. Ishida, Y. Shiina, S. Oishi and S. Tobita, *Phys. Chem. Chem. Phys.*, 2009, **11**, 9850-9860.
- 143 C.-K. Li, X.-X. Lu, K. M.-C. Wong, C.-L. Chan, N. Zhu and V. W.-W. Yam, *Inorg. Chem.*, 2004, **43**, 7421-7430.
- 144 S. Lamansky, P. Djurovich, D. Murphy, F. Abdel-Razzaq, H. E. Lee, C. Adachi, P. E. Burrows, S. R. Forrest and M. E. Thompson, *J. Am. Chem. Soc.*, 2001, **123**, 4304-4312.
- 145 S. C. F. Kui, Y. C. Law, G. S. M. Tong, W. Lu, M. Y. Yuen and C. M. Che, *Chem. Sci.*, 2011, **2**, 221-228.
- 146 I. C. Khoo, S. Webster, S. Kubo, W. J. Youngblood, J. D. Liou, T. E. Mallouk, P. Lin, D. J. Hagan and E. W. Van Stryland, *J. Mater. Chem.*, 2009, **19**, 7525-7531.
- 147 D. Qiu, J. Wu, Z. Xie, Y. Cheng and L. Wang, *J. Organomet. Chem.*, 2009, **694**, 737-746.
- 148 Y. Li, L. Zhao, A. Y. Y. Tam, K. M. C. Wong, L. Wu and V. W. W. Yam, *Chem. - A Eur. J.*, 2013, **19**, 14496-14505.
- 149 U. Siemeling, F. Bretthauer, C. Bruhn, T. P. Fellingner, W. L. Tong and M. C. W. Chan, *Zeitschrift fur Naturforsch. - Sect. B J. Chem. Sci.*, 2010, **65**, 1089-1096.
- 150 V. Rani, H. B. Singh and R. J. Butcher, *J. Organomet. Chem.*, 2018, **859**, 33-43.
- 151 Z. Wang, Z. Sun, X. Q. Hao, J. L. Niu, D. Wei, T. Tu, J. F. Gong and M. P. Song, *Organometallics*, 2014, **33**, 1563-1573.
- 152 M. H.-Y. Chan, H.-L. Wong and V. W.-W. Yam, *Inorg. Chem.*, 2016, **55**, 5570-5577.
- 153 T. Chatzisideri, S. Thysiadis, S. Katsamakos, P. Dalezis, I. Sigala, T. Lazarides, E. Nikolakaki, D. Trafalis, O. A. Gederaas, M. Lindgren and V. Sarli, *Eur. J. Med. Chem.*, 2017, **141**, 221-231.
- 154 B. Wiczorek, B. Lemcke, H. P. Dijkstra, M. R. Egmond, R. J. M. Klein Gebbink and G. Van Koten, *Eur. J. Inorg. Chem.*, 2010, 1929-1938.
- 155 A. Muth, M. Madan, J. J. Archer, N. Ocampo, L. Rodriguez and O. Phanstiel, *J. Med. Chem.*, 2014, **57**, 348-363.
- 156 F. Nisic, A. Colombo, C. Dragonetti, D. Roberto, A. Valore, J. M. Malicka, M. Cocchi, G. R. Freeman and J. A. G. Williams, *J. Mater. Chem. C*, 2014, **2**, 1791-1800.
- 157 D. J. Cárdenas, A. M. Echavarren and M. C. Ramírez de Arellano, *Organometallics*, 1999, **18**, 3337-3341.

8 Appendix

Crystal data and structure refinements
Additional figures

8.1 X-ray Crystallography Data

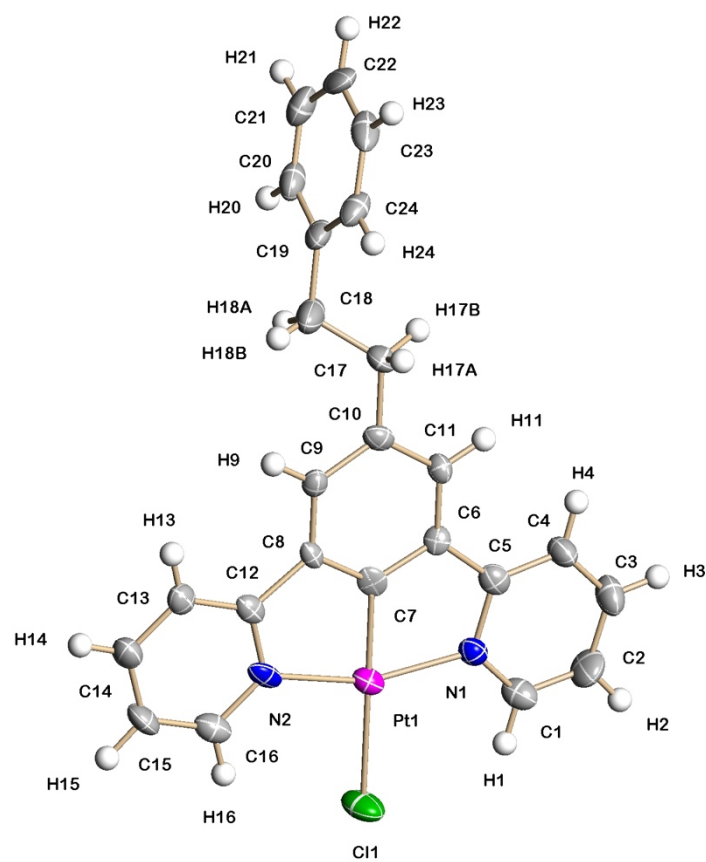


Figures show 50% displacement ellipsoids. $R1 = 0.0662$, $wR2 = 0.1367$.

Figure 8.1: X-Ray structure of **HL7**.

Table 8.1: Crystal data and structure refinement for **HL7**.

Identification code	15107	
Empirical formula	C18 H24 N6	
Formula weight	324.43	
Temperature	150(2) K	
Wavelength	0.71073 Å	
Crystal system	Monoclinic	
Space group	P2(1)/c	
Unit cell dimensions	a = 16.176(4) Å	$\alpha = 90^\circ$.
	b = 10.622(3) Å	$\beta = 90.279(5)^\circ$.
	c = 10.412(3) Å	$\gamma = 90^\circ$.
Volume	1788.9(7) Å ³	
Z	4	
Density (calculated)	1.205 Mg/m ³	
Absorption coefficient	0.076 mm ⁻¹	
F(000)	696	
Crystal size	0.35 x 0.34 x 0.02 mm ³	
Theta range for data collection	2.29 to 25.00°.	
Index ranges	-19<=h<=19, -12<=k<=12, -12<=l<=12	
Reflections collected	12597	
Independent reflections	3151 [R(int) = 0.1225]	
Completeness to theta = 25.00°	99.9 %	
Absorption correction	Empirical	
Max. and min. transmission	0.969 and 0.282	
Refinement method	Full-matrix least-squares on F ²	
Data / restraints / parameters	3151 / 0 / 219	
Goodness-of-fit on F ²	0.920	
Final R indices [I>2sigma(I)]	R1 = 0.0662, wR2 = 0.1367	
R indices (all data)	R1 = 0.1310, wR2 = 0.1566	
Largest diff. peak and hole	0.373 and -0.263 e.Å ⁻³	

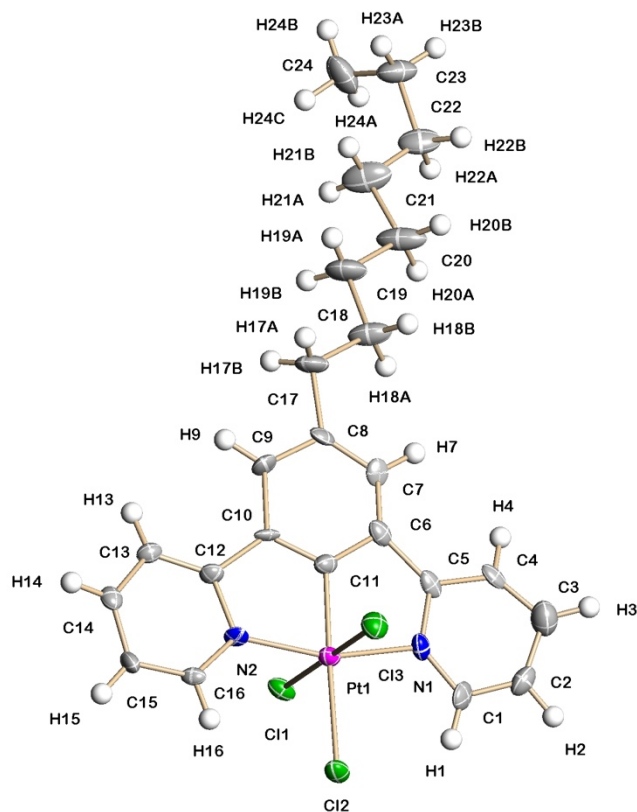


Figures show 50% displacement ellipsoids. $R_1 = 0.0429$, $wR_2 = 0.0731$.

Figure 8.2: X-Ray structure of **PtL10Cl**.

Table 8.2: Crystal data and structure refinement for **PtL10Cl**.

Identification code	17002	
Empirical formula	C ₂₄ H ₁₉ Cl N ₂ Pt	
Formula weight	565.95	
Temperature	150(2) K	
Wavelength	0.71073 Å	
Crystal system	Orthorhombic	
Space group	Pbca	
Unit cell dimensions	a = 14.092(3) Å	α = 90°.
	b = 10.553(3) Å	β = 90°.
	c = 26.670(6) Å	γ = 90°.
Volume	3966.2(16) Å ³	
Z	8	
Density (calculated)	1.896 Mg/m ³	
Absorption coefficient	7.222 mm ⁻¹	
F(000)	2176	
Crystal size	0.44 x 0.08 x 0.04 mm ³	
Theta range for data collection	1.53 to 26.00°.	
Index ranges	-17 ≤ h ≤ 17, -13 ≤ k ≤ 12, -32 ≤ l ≤ 32	
Reflections collected	29113	
Independent reflections	3892 [R(int) = 0.1195]	
Completeness to theta = 26.00°	99.9 %	
Absorption correction	Empirical	
Max. and min. transmission	0.831 and 0.452	
Refinement method	Full-matrix least-squares on F ²	
Data / restraints / parameters	3892 / 0 / 253	
Goodness-of-fit on F ²	0.925	
Final R indices [I > 2σ(I)]	R1 = 0.0429, wR2 = 0.0731	
R indices (all data)	R1 = 0.0788, wR2 = 0.0813	
Largest diff. peak and hole	1.398 and -0.909 e.Å ⁻³	

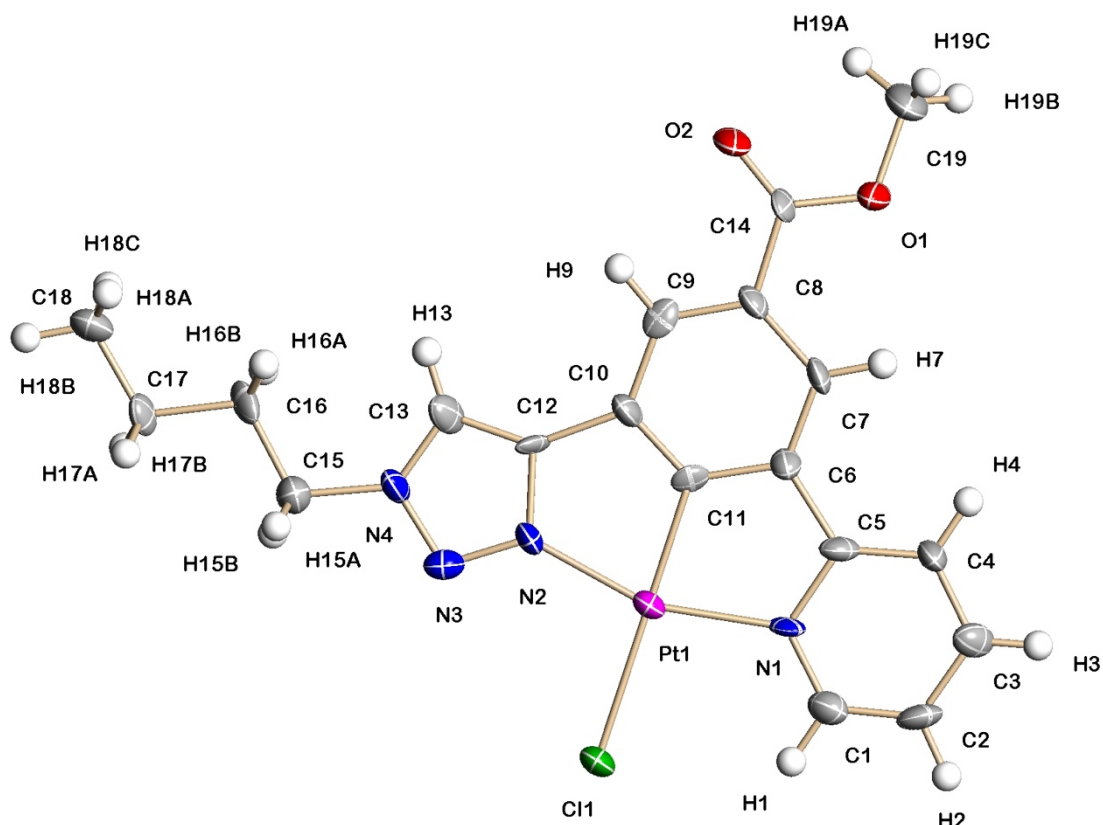


Figures show 50% displacement ellipsoids. The structure has been solved in the lower symmetry space group CC (*ie* the wrong space group). $R1 = 0.0419$, $wR2 = 0.0836$.

Figure 8.2: X-Ray structure of $PtL12Cl_3$.

Table 8.2: Crystal data and structure refinement for **PtL12Cl₃**.

Identification code	17071	
Empirical formula	C ₂₄ H ₂₇ Cl ₃ N ₂ Pt	
Formula weight	644.92	
Temperature	150(2) K	
Wavelength	0.71073 Å	
Crystal system	Monoclinic	
Space group	Cc	
Unit cell dimensions	a = 12.0415(18) Å	α = 90°.
	b = 17.173(3) Å	β = 108.100(3)°.
	c = 11.8145(18) Å	γ = 90°.
Volume	2322.3(6) Å ³	
Z	4	
Density (calculated)	1.845 Mg/m ³	
Absorption coefficient	6.402 mm ⁻¹	
F(000)	1256	
Crystal size	0.20 x 0.11 x 0.04 mm ³	
Theta range for data collection	2.14 to 25.99°.	
Index ranges	-14 ≤ h ≤ 14, -21 ≤ k ≤ 21, -14 ≤ l ≤ 14	
Reflections collected	8985	
Independent reflections	4433 [R(int) = 0.0600]	
Completeness to theta = 25.99°	99.9 %	
Absorption correction	Empirical	
Max. and min. transmission	0.831 and 0.452	
Refinement method	Full-matrix least-squares on F ²	
Data / restraints / parameters	4433 / 261 / 272	
Goodness-of-fit on F ²	0.970	
Final R indices [I > 2σ(I)]	R1 = 0.0419, wR2 = 0.0836	
R indices (all data)	R1 = 0.0529, wR2 = 0.0872	
Absolute structure parameter	?	
Largest diff. peak and hole	1.815 and -0.725 e.Å ⁻³	

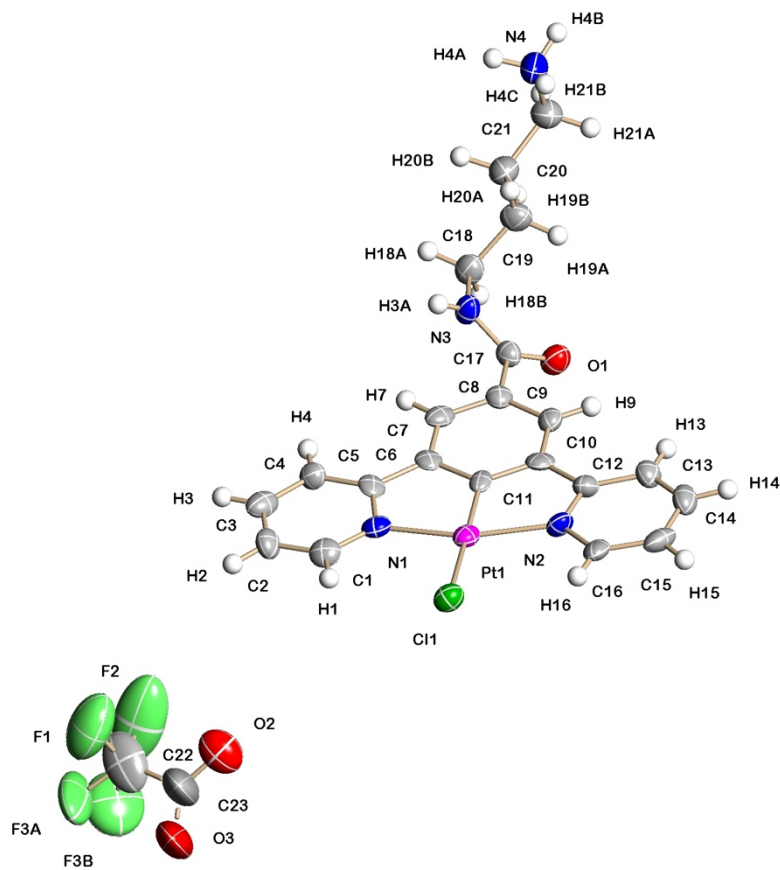


Figures show 50% displacement ellipsoids. $R_1 = 0.0747$, $wR_2 = 0.1451$.

Figure 8.3: X-Ray structure of PtL9Cl.

Table 8.3: Crystal data and structure refinement for **PtL9Cl**.

Identification code	18027	
Empirical formula	C ₁₉ H ₁₉ Cl N ₄ O ₂ Pt	
Formula weight	565.92	
Temperature	150(2) K	
Wavelength	0.71073 Å	
Crystal system	Monoclinic	
Space group	P2(1)/c	
Unit cell dimensions	a = 11.316(6) Å	α = 90°.
	b = 22.337(12) Å	β = 94.742(11)°.
	c = 7.322(4) Å	γ = 90°.
Volume	1844.5(17) Å ³	
Z	4	
Density (calculated)	2.038 Mg/m ³	
Absorption coefficient	7.775 mm ⁻¹	
F(000)	1088	
Crystal size	0.22 x 0.19 x 0.12 mm ³	
Theta range for data collection	1.81 to 26.00°.	
Index ranges	-13 ≤ h ≤ 13, -27 ≤ k ≤ 27, -9 ≤ l ≤ 9	
Reflections collected	14132	
Independent reflections	3613 [R(int) = 0.1654]	
Completeness to theta = 26.00°	100.0 %	
Absorption correction	Empirical	
Max. and min. transmission	0.831 and 0.356	
Refinement method	Full-matrix least-squares on F ²	
Data / restraints / parameters	3613 / 12 / 246	
Goodness-of-fit on F ²	0.958	
Final R indices [I > 2σ(I)]	R1 = 0.0747, wR2 = 0.1451	
R indices (all data)	R1 = 0.1342, wR2 = 0.1625	
Largest diff. peak and hole	4.735 and -1.207 e.Å ⁻³	



Figures show 50% displacement ellipsoids. Shown is the cat-ion and anion.

Figure 8.4: X-Ray structure of $\text{PtL9}^{1a}\text{Cl}_d$.

Table 8.4: Crystal data and structure refinement for **PtL9^{1a}Cl_d**.

Identification code	18048	
Empirical formula	C ₂₅ H ₃₀ Cl F ₃ N ₄ O ₅ Pt	
Formula weight	754.07	
Temperature	150(2) K	
Wavelength	0.71073 Å	
Crystal system	Triclinic	
Space group	P-1	
Unit cell dimensions	a = 7.7127(14) Å	α = 92.620(4)°.
	b = 9.1484(17) Å	β = 101.725(4)°.
	c = 18.711(3) Å	γ = 101.313(4)°.
Volume	1262.5(4) Å ³	
Z	2	
Density (calculated)	1.984 Mg/m ³	
Absorption coefficient	5.731 mm ⁻¹	
F(000)	740	
Crystal size	0.19 x 0.16 x 0.04 mm ³	
Theta range for data collection	2.23 to 26.00°.	
Index ranges	-9 ≤ h ≤ 9, -11 ≤ k ≤ 11, -23 ≤ l ≤ 23	
Reflections collected	9956	
Independent reflections	4900 [R(int) = 0.0881]	
Completeness to theta = 26.00°	98.7 %	
Absorption correction	Empirical	
Max. and min. transmission	0.831 and 0.381	
Refinement method	Full-matrix least-squares on F ²	
Data / restraints / parameters	4900 / 6 / 326	
Goodness-of-fit on F ²	0.939	
Final R indices [I > 2σ(I)]	R1 = 0.0632, wR2 = 0.1303	
R indices (all data)	R1 = 0.0850, wR2 = 0.1384	
Largest diff. peak and hole	2.432 and -2.486 e.Å ⁻³	